U.S. Department of Commerce
National Technical Information Service

N74 75522

LONGITUDINAL AND LATERAL STABILITY AND CONTROL CHARACTERISTICS OF A LARGE-SCALE MODEL WITH A SWEPT WING AND AUGMENTED JET FLAP

U.S. ARMY AIR MOBILITY R&D LABORATORY
MOFFETT FIELD, CA

APR 72

NASA TECHNICAL
MEMORANDUM

NASA TM X-62,145

NASA TM X-62,145

LONGITUDINAL AND LATERAL STABILITY AND CONTROL CHARACTERISTICS OF A LARGE–SCALE MODEL WITH A SWEPT WING AND AUGMENTED JET FLAP

Michael D. Falarski and David G. Koenig

Ames Research Center
and
U.S. Army Air Mobility R&D Laboratory
Moffett Field, Calif. 94035

April 1972

NOTATION

A	thrust augmentation ratio of jet augmentor, J_A/J_I
b	wing span, m(ft)
BLC	boundary layer control
c	chord, m(ft)
$\bar{c}$	mean aerodynamic chord, m(ft)
C_D	drag coefficient, $\frac{\text{drag}}{qS}$
C_{D_m}	total momentum drag coefficient due to gas generator and compressor gas flow
$C_{J_{AI}}$	isentropic augmentor jet force coefficient, (see text) $\frac{\text{isentropic force}}{qS}$
C_{J_I}	total isentropic jet thrust coefficient, $C_{J_{AI}} + C_{\mu_{aI}} + C_{\mu_{FI}}$
C_{ℓ}, C_R	rolling moment coefficient, $\frac{\text{rolling moment}}{qSb}$
C_L	lift coefficient, $\frac{\text{lift}}{qS}$
C_m	pitching moment coefficient, $\frac{\text{pitching moment}}{qS\bar{c}}$
C_n	yawing moment coefficient, $\frac{\text{yawing moment}}{qSb}$
$C_{T_{JP}}$	jet pipe thrust coefficient, $\frac{\text{thrust}}{qS}$
C_Y	side force coefficient, $\frac{\text{side force}}{qS}$
$C_{\mu_{aI}}$	isentropic aileron BLC coefficient, $\frac{\text{isentropic BLC force}}{qS}$
$C_{\mu_{FI}}$	isentropic fuselage BLC coefficient, $\frac{\text{isentropic BLC force}}{qS}$
d	distance between trailing edge of flap and shroud, m(ft) (see fig. 2(e))
i_t	horizontal tail incidence, positive with trailing edge down, deg

J_A	augmentor jet force at q = 0, n/m^2(psf)
J_I	isentropic jet force at q = 0, n/m^2(psf)
q	free-stream dynamic pressure, n/m^2(psf)
S	wing area, sq m(sq ft)
t	airfoil thickness, m(ft)
x	chordwise station, m(ft)
y	airfoil ordinate, m(ft)
Z_{JP}	distance between moment center and line of action of jet-pipe residual thrust, m(ft)
α,AL	model angle of attack, deg
β	angle of sideslip of plane of symmetry, deg
δ_a	aileron deflection (δ_a = 45/60 means left aileron at 45°, right aileron at 60°) positive with trailing edge down, deg
δ_e	elevator deflection, positive with trailing edge down, deg
δ_f	augmentor flap deflection, positive with trailing edge down, deg (see figure 2(e))
δ_{ID}	augmentor intake door deflection, positive with leading edge down, deg (see figure 2(e))
δ_{JP}	deflection of jet pipes relative to fuselage datum plane, deg
δ_s	slat deflection, positive with leading edge down, deg (see figure 2(c))
δ_{SP}	spoiler deflection, trailing edge up, deg (see figure 2(k))
Δ_d	augmentor throttling, reduction in distance between trailing edge of flap and shorud in percent of d.
θ	augmentor jet angle relative to wing chord plane, deg

SUBSCRIPTS

a	aileron
A	augmentor
f	flap
F	fuselage
JP	jet-pipe
I	isentropic
L	left
R	right
s	slat
u	uncorrected
V	Viper
w	wing
1	forward elevator element
2	aft elevator element

3<

SUMMARY

This report presents data of an investigation of the lateral-directional stability and control characteristics of large-scale swept augmentor wing model in the Ames 40-by 80- foot wind tunnel. Also included are the results of a study to determine the static efficiency of the augmentor flap. As a preliminary investigation of engine nacelle interferences, flow-through nacelles were mounted on the model for a short series of tests. The results of the investigation are included in this report. Studies were made for augmentor primary thrust coefficient of 0 to 1.50. The Reynolds Numbers range based on the wing mean aerodynamic chord was 2.43×10^6 to 4.1×10^6.

INTRODUCTION

The augmentor wing concept is being studied as one means of attaining STOL performance in turbofan powered aircraft. Wind tunnel tests on a large-scale unswept augmentor wing model are reported in references 1 and 2. An initial investigation of a swept augmentor wing model was reported in reference 3. These tests indicate that the lift and drag characteristics were comparable to those of the unswept wing. The investigation also indicated no serious longitudinal or lateral stability and control problems.

The aerodynamics of the swept wing were subsequently investigated more extensively and these results are reported herein. The primary emphasis of the test program was on the longitudinal and lateral stability and control characteristics. Also included are the results of tests to determine the static augmentation of this configuration. As a preliminary study of engine nacelle interferences, flow-through nacelles were mounted under the wing for a short series of runs. The results of this study are also presented in this report.

This research program was undertaken in cooperation with the Defense Research Board of Canada and DeHavilland Aircraft of Canada, Limited.

MODEL AND APPARATUS

Basic Model

The model is shown installed in the wind tunnel in figures 1(a) and 1(b). Figure 1(c) shows the model mounted on the static test support. The basic geometric details of the model are shown in figure 2 and the model reference dimensions and airfoil coordinates are listed in Tables I to III. The air for the augmentor and BLC systems was supplied by a pump consisting of a J-85 coupled pneumatically to two turbocompressors, which are modified Viper engines. The turbocompressor supplied air for the augmentor and aileron BLC(see figure 3).

The wing planform and leading edge slat geometry are shown in figures 4(a) and 4(b). Slat gaps of .5% c_w, 1.0% c_w and 1.5% c_w were investigated.

The horizontal tail planform geometry is described in figure 5(a) and Table II. For this series of tests the tail was equipped with the leading edge slat shown in figure 5(b). The slotted, double-hinged elevator, shown in figure 5(c), provided longitudinal control. The horizontal tail was mounted in either a high or low position as shown in figures 2 and 5(d). When the tail was in the high position it was set at an incidence of -8.7°. The incidence of the tail in the low position was 0.3°.

Augmentor Flap

The geometry of the augmentor flap cross section is shown in figure 6(a). The augmentor is an ejector system consisting of a trailing edge primary nozzle (figure 6(b)) through which the compressed air is delivered, (lower) flap, (upper) shroud, and intake door. The secondary air is entrained from the wing upper surface, the slot between the intake door and shroud, and the tertiary gap between the wing lower surface and flap. The mixed jet is ejected downward between the flap and the shroud. The angle of the intake door was optimized for each flap deflection. The diffusion angle for this report is $4^\circ 50'$; for the investigation of reference 3, it was $6^\circ 37'$.

The ducting for the primary air and aileron BLC is shown in figures 6(c) and 6(d). Figure 6(d) shows the variation of duct diameter with wing span which was designed to maintain a duct Mach number of .36.

Fuselage BLC

The fuselage BLC installation is shown in figure 7. It was located just aft of the wing leading edge in the part of the wing spanning the fuselage for the purpose of preventing airflow separation at the wing fuselage juncture by energizing the fuselage boundary layer. The BLC air was provided by J-85 compressor bleed air.

Aileron BLC

The geometry of the aileron BLC system is shown in figure 8. The system was fed through an extension of the augmentor primary air duct. Aileron blowing was therefore coupled with the augmentor output. Airflow to the aileron was approximately 5% of the total turbo-compressor output.

A short series of tests were made with a slotted aileron as shown in figure 9. For these tests the aileron BLC duct and nozzle were removed. The augmentor duct was sealed at its tip and the augmentor primary nozzle area was increased over the outer 25% span to maintain the same nozzle area. In an attempt to improve the slotted aileron performance, a few tests were made with the lower slot inlet radius removed and the slot overlap increased.

Lateral Control System

The model was equipped with several methods for lateral control: Ailerons.- Lift requirements for landing and take-off resulted in symmetrical drooping of the BLC aileron by as much as 45°. They were normally drooped to 30°. Lateral control was obtained by differentially deflecting the ailerons.

Spoilers.- Upper wing panel type spoilers were installed on the left wing for lateral control as shown in figure 8. The spoilers were 11.2% of wing chord, located ahead of the aileron.

Augmentor Throttling.- A flat plate was installed on the lower portion of the flap of the outer 50% of the port wing augmentor as shown in figure 6(a). This simulates a deflected aft portion of the flap to reduce the augmentor exit area and affect a local throttling of the augmentor eflux to create a rolling moment.

Flow-Through Nacelles

The flow-through nacelle used for the engine nacelle interference study is shown in figure 10(a). The flow through the left inboard nacelle was measured with a pressure rake mounted vertically at the duct exit. A typical exit pressure distribution is presented in figure 10(b). Unless otherwise specified, the flow-through nacelles were not mounted on the wing.

TESTS

Wind Tunnel

The test procedure consisted primarily of varying either angle of attack or sideslip at constant thrust coefficient. The angle of attack range was -8° to 30° and the sideslip range was -19° to 8°. Thrust coefficient was varied from 0 to 1.5. The dynamic pressure and augmentor plenum total pressure for each nominal C_{J_I} are listed below.

C_{J_I} nominal	q n/m² (psf)	PT_{AUG} cm. of Hg(in. of Hg)
1.5	201(4.2)	61.0(24)
1.1	240(5)	53.4(21)
0.8	383(8)	61.0(24)
0.4	383(8)	25.4(10)
0.2	670(14)	20.3(8)
0.0	383(8)	00.0(0)

The position of the augmentor intake door was set at its optimum angle for each flap deflection, as determined in reference 3. Longitudinal characteristics of the model with the slotted aileron were investigated during the first several runs of the program. For the duration of the program the aileron BLC was installed. The ailerons were symmetrically deflected to 30° unless otherwise specified. The effect of wing leading edge slot gap on longitudinal characteristics was also investigated during the first part of the test program. For the remainder of the investigation the slat gap was set at 1.0% c_w.

The longitudinal characteristics of the wing with intake door-shroud assembly removed, simulating a slotted jet flap, were studied. The tertiary slot was sealed for part of the investigation to simulate a plain jet flap. The slot was sealed with a flat plate attached from the bottom surface of the wing to the bottom surface of the flap. Longitudinal characteristics with flow-through nacelles were measured with the complete augmentor flap and the shroud removed.

Static Augmentor Performance

The static performance of the model was obtained outside the wind tunnel with the model installed on the test stand shown in figure 1(c). The forces were measured by three 2-axis load cells. The following augmentor configurations were investigated:

Configuration	Augmentor Diffuser Angle	Aileron
1	6° 37′	BLC
2	6° 37′	Slotted
3	4° 50′	Slotted

Configuration 1 is the augmentor arrangement reported in reference 3, while arrangement 3 was studied in the present investigation.

DATA REDUCTION

For all force and moment data, the effects of compressor residual jet thrust, and the intake momentum drag of the fuselage mounted J85 and Viper engines, have been subtracted from the measured values. Forces and moments are referred to the stability axes. The corrections made for thrust and ram drag are as follows:

$$C_L = C_{L_u} - C_{T_{JP}} \sin(\alpha_u - \delta_{JP})$$

$$C_{D_{net}} = C_{D_u} + C_{T_{JP}} \cos(\alpha_u - \delta_{JP}) - C_{D_{mJ85}} - C_{D_{MV}}$$

$$C_{m_{net}} = C_{m_u} - C_{T_{JP}} \frac{Z_{JP}}{\bar{c}}$$

Wind tunnel boundary corrections were based upon the "aerodynamic C_L", computed as follows:

$$C_{L_{AERO}} = C_{L_U} - C_{J_A} (A_{net}) \sin(\theta + \alpha_u) \qquad \text{(Augmentor)}$$

$$- C_{\mu aL} \sin(\delta_{aL} + \alpha_u) \frac{S_a}{S} \qquad \text{(Aileron BLC, left)}$$

$$- C_{\mu aR} \sin(\delta_{aR} + \alpha_u) \frac{S_a}{S} \qquad \text{(Aileron BLC, right)}$$

$$- C_{\mu F} \sin\alpha_u \left(\frac{S_F}{S}\right) \qquad \text{(Fuselage BLC)}$$

Thus the following boundary corrections were made:

$$\alpha = \alpha_u + .458\ C_{L_{AERO}}$$

$$C_D = C_{D_u} + .00799\ C_{L_{AERO}}^2$$

$$C_m = C_{m_u} + .023\ C_{L_{AERO}} \qquad \text{(tail on only)}$$

The moment center used for data computation was located longitudinally at 0.25 $\bar{c}$ and vertically 0.20 $\bar{c}$ below the wing chord datum.

The $C_{J_{AI}}$ is the force coefficient computed on the basis of the measured mass flow and total pressure in the duct prior to discharge.

DATA PRESENTATION

Results of the static tests are presented in figure 11. The longitudinal aerodynamic characteristics of the model are presented in figures 12 to 23. This data is summarized in figures 24 to 26. An index to the longitudinal data figures is presented in Table IV. The lateral stability and control characteristics are presented in figures 27 to 37. Table V is an index to these figures.

Table VI is presented as a run by run index of the wind tunnel tests.

REFERENCES

1. Koenig, D. G.; Corsiglia, V. R.; Morelli, J. P.; Aerodynamic Characteristics of a Large Scale Model with an Unswept Wing and Augmented Jet Flap. NASA TN D-4610, 1968.
2. Cook, A. M.; Aiken, T. N.: Low Speed Aerodynamic Characteristics of a Large Scale STOL Transport Model with an Augmented Jet Flap. NASA TM X-62017, 1971.
3. Falarski, M. D.; Koenig, D. G.: Aerodynamic Characteristics of a Large Scale Model with a Swept Wing and Augmented Jet Flap. NASA TM X-62029, 1971.

TABLE I. - WING REFERENCE DIMENSIONS

Wing area, sq m(sq ft)	21.36(230.0)
Aspect ratio	8.0
Span, m(ft)	13.08(42.895)
Taper ratio	0.30
Sweep at 1/4 chord, deg	27.5
Airfoil section	RAE 104
Root chord, m(ft)	2.515(8.25)
Tip chord, m(ft)	0.755(2.475)
Root thickness, percent	12 1/2
Tip thickness, percent	10 1/2
Augmentor span limits, Inner, m(ft) (percent)	1.111(3.645)(12.34)
Augmentor span limits, Outer, m(ft) (percent)	4.575(15.01)(70.0)
Wing area spanned by one augmentor, sq m(sq ft)	6.75(72.62)
Wing area spanned by one aileron, sq m(sq ft)	1.997(21.50)
Wing area spanned by fuselage, sq m(sq ft)	3.88(41.77)
Flap hinge axis, percent chord	68.543
Aileron hinge axis, percent chord	68.0
Incidence, camber, twist	0
Mean aerodynamic chord, m(ft)	1.793(5.880)

NOTE: All chords are measured in streamwise direction.

TABLE II. - TAIL REFERENCE DIMENSION

Horizontal Tail

Gross area, sq m(sq ft)	55.77(60.0)
Aspect ratio	4.5
Span, m(ft)	5.005(16.432)
Taper ratio	0.40
Sweep at 1/4 chord, deg	25
Airfoil section	RAE 104 with modified l.e.
Thickness/Chord ratio, percent	10
Root chord, m(ft)	1.591(5.22)
Tip chord, m(ft)	0.635(2.082)
Elevator hinge axis, percent chord	[redacted] see fig. 5c
Elevator travel, deg	±30
Tailplane incidence, deg	±12
Tailplane arm, m(ft)	6.804(22.32)
Tailplane volume coefficient, HIGH POS.	0.990
" " " , LOW POS.	0.816
Mean aerodynamic chord, m(ft)	1.114(3.654)

Vertical Fin

Fin arm, m(ft)	5.361(17.603)
Fin volume coefficient	0.07476

TABLE III. - COORDINATES OF R.A.E. 104 AIRFOIL(t/c max.=.10)

X/C	Y/C 100	X/C	Y/C 100
0	0	0.35	4.9300
0.001	0.3441	0.36	4.9488
0.002	0.4863	0.38	4.9775
0.003	0.5953	0.4	4.9946
0.004	0.6870	0.42	5.0000
0.005	0.7676	0.44	4.9937
0.006	0.8404	0.45	4.9862
0.007	0.9072	0.46	4.9756
0.0075	0.9387	0.48	4.9454
0.008	0.9692	0.5	4.9027
0.009	1.0274	0.52	4.8468
0.01	1.0824	0.54	4.7769
0.012	1.1842	0.55	4.7363
0.0125	1.2083	0.56	4.6917
0.014	1.2776	0.58	4.5802
0.016	1.3642	0.6	4.4650
0.018	1.4452	0.62	4.3113
0.02	1.5215	0.64	4.1370
0.025	1.6960	0.65	4.0438
0.03	1.8522	0.66	3.9473
0.035	1.9945	0.68	3.7452
0.04	2.1256	0.7	3.5331
0.05	2.3617	0.72	3.3128
0.06	2.5709	0.74	3.0861
0.07	2.7592	0.75	2.9708
0.075	2.8468	0.76	2.8545
0.08	2.9307	0.78	2.6103
0.09	3.0881	0.8	2.3819
0.1	3.2336	0.82	2.1437
0.12	3.4945	0.84	1.9055
0.14	3.7222	0.85	1.7864
0.15	3.8254	0.86	1.6673
0.16	3.9224	0.88	1.4202
0.18	4.0992	0.9	1.1910
0.2	4.2556	0.92	0.9528
0.22	4.3936	0.925	0.8932
0.24	4.5149	0.94	0.7146
0.25	4.5697	0.95	0.5955
0.26	4.6208	0.96	0.4764
0.28	4.7124	0.975	0.2977
0.3	4.7905	0.98	0.2382
0.32	4.8556	0.9875	0.1489
0.34	4.9082	1.0	0

TABLE IV.– INDEX TO LONGITUDINAL DATA FIGURES

FIGURE	EFFECTS	δ_f	AILERON	HORIZ. TAIL	VERTICAL TAIL	NACELLES	SHROUD	REMARKS
12 a	δ_a	70	SLOT	OFF	OFF	OFF	ON	SLOTTED AILERON
b	C_{J_I}	↓						$\delta_a = 4$, SLOT SEALED
c	↓	40						↓
d	δ_{a_R}	70						
e	δ_{a_L}							
f	δ_{a_R}		↓					↓
13 a	SLAT GAP		BLC					SLAT GAP STUDY
b	↓							↓
14	δ_{ID}							
15 a	FUS. BLC							
b	↓	↓			↓			
16 a	C_{J_I}	30			ON			
b							↓	
c		↓			↓		OFF	
17 a		40			OFF		ON	
b				↓	ON			
c				HIGH		↓		
d				OFF		ON		
e	↓			LOW				
f	δ_{e_1}			↓		↓	↓	
g	C_{J_I}			OFF		OFF	OFF	
h						↓		TERITARY SLOT SEALED
i		↓			↓	ON	↓	
18		60			OFF	OFF	ON	
19 a		70						
b	↓							$\delta_a = 4°$
c	δ_a				↓	↓		
d	C_{J_I}				ON	UN		
e						↓	↓	INB'D NACELLES ONLY
f						OFF	OFF	
g				↓		ON	↓	
20 a	↓			LOW		OFF	ON	
b	δ_e							
c	↓							$\delta_{e_L} = 0$
d	↓							$\delta_{e_L} = -15$
21 a	C_{J_I}			HIGH				
b	↓							
c	δ_e	↓	↓	↓	↓	↓	↓	$\delta_{e_2} = 0$

TABLE IV.- CONCLUDED

FIGURE	EFFECTS	δ_f	AILERON	HORIZ. TAIL	VERTICAL TAIL	NACELLES	SHROUDS	REMARKS
21d	δ_{e_1}	70	BLC	HIGH	ON	OFF	ON	$\delta_{e_2} = -16$
e								$\delta_{e_2} = -21$
f	δ_{e_2}							
22a	C_{J_I}			LOW		ON		
b	δ_e							
c	δ_e							
23a	$C_{D_{C_L = CONST}}$	30-70		OFF	ON	OFF		SUMMARY FIGURES
b	$C_{L_{\alpha=0}}$							
c	$C_{D_{\alpha=0}}$							
d	$C_{L_{max}}$							
24a	$C_{D_{C_L = CONST}}$						OFF	
b	$C_{L_{\alpha=0}}$							
c	$C_{D_{\alpha=0}}$							
d	$C_{L_{MAX}}$							
25a	$C_{D^t_{C_L = CONST}}$					ON & OFF	ON & OFF	
b	$C_{L^t_{\alpha=0}}$							
c	$C_{D^t_{\alpha=0}}$							
d	$C_{L_{MAX}}$							

Table V. – Index to Lateral Stability and Control Figures.

Figure	Effects	δ_f	Aileron	Horiz. Tail	Vertical Tail	Nacelles	Shroud	α, deg	β, deg	Nom. C_{J_I}	
26a	C_{J_I}	70	BLC	OFF	OFF	OFF	ON	0	~	~	
b	C_{J_I}	↓		↓	↓			12		0	
27a		40		HIGH	ON			0		~	
b		↓						12			
28a		70						12			
b	↓			↓		↓		0		↓	
29a	α			LOW		ON		0,12		.77	
b	-	↓		↓		↓		0	↓	↓	
30a	δ_a	40		HIGH		OFF		~	[illegible]	~	
b	↓							~	-8	1.1	
c	C_{J_I}							0	~	~	$\delta_a = 15/45$
d	↓							12	↓	~	↓
e	δ_{a_L}							0,4,12	0	1.1	
f	δ_{a_R}	↓						↓			
31a	δ_a	70						~	↓	~	
b	C_{J_I}							0	~	~	$\delta_a = 15/45$
c	↓							12	↓	~	↓
d	δ_a							~	0	1.12	
e	δ_a							4	0	1.1	
f	δ_a	↓						0	0	1.1	
32a	THROTTLING	40						~	0	1.1	
b										1.09	
c										.36	
d	↓							↓	↓	↓	
e	β							~	-8,0	1.1	$\Delta\delta = 60\%$
f								↓	↓	.36	
g	↓	↓						4	~	1.1	↓
33a	THROTTLING	70						~	0	1.09	
b										↓	
c										.36	
d	↓								↓		
e	β								0,-8	↓	$\Delta\delta = 60\%$
f	↓	↓						↓	↓	1.1	↓
34a	δ_{SP}	70						~	0	1.1	.01 cw Vent
b	↓							↓		.36	
c	δ_{SP}, δ_{a_L}							4		1.1	
d	↓	↓	↓	↓	↓	↓	↓	↓	↓	.4	↓

TABLE V. - CONCLUDED.

FIGURE	EFFECTS	δ_f	AILERON	HORIZ. TAIL	VERTICAL TAIL	NACELLES	SHROUD	α, deg	β, deg	NOM. C_{J_T}	
35a	δ_{sp}	40	BLC	HIGH	ON	OFF	ON	~	0	1.1	.016 CN VENT
b	↓								↓	.36	
c	β							↓	0,-8	1.06	δ_{sp}=36°
d	δ_{sp}, δ_{a_L}	↓						4	0	~	
36a	δ_{sp}	70						~		1.1	
b	↓							↓	↓	.36	
c	β							4	~	1.1	δ_{sp}=50°
d	δ_{sp}, δ_{a_L}							4	0	1.1	
e	↓									.4	
37a	δ_{sp}									~	
b	↓	↓	↓	↓	↓	↓	↓	↓	↓	↓	↓ δ = 4/50

TABLE VI. - SWEPT AUGMENTOR WING RUN INDEX

NOTE: VERTICAL FIN OFF RUNS 7–55

RUN		TUNNEL			POWER			WING					TAIL				
RUN NO		q, psf	α, deg	β, deg	AUGP, "Hg	FUS BLC, psig	C_J	δ_f, deg	δ_{ID}, deg	δ_a deg	δ_s deg.	SLAT GAP, %	POS.	i_t, deg	δ_e/δ_a	REMARKS	FIG NO
7		8	~	0	0	0	0	70	50	4	60	1.0	OFF	–	–	SLOTTED AILERON	12a
8										15							
9										30							
10		5			21		1.1			15							
11										30							
12			0,~12							~							12d,e,f
13			0							~						AIL. SLOT FAIRING OFF	,e
14			0,~							~						AIL. SLOT FAIRING OFF AND OVERLAP EXTENDED	,f
15		4.2	~		24		1.5			4						AILERON SLOT SEALED	12b
16		8					.8										
17							.8	40									12c
18		4.2					1.5										
19		8			0		0										
20		4.2			24		1.5	70								BLOWN AILERON INSTALLED	19b
21		8					.8										
22		5			21		1.1										
23										30		1.5				SLAT OPTIMIZATION	13a
24										15		1.5					13b
25										30		1.0					13a,14,19a
26										45							19c
27										15							13b,19c
28			0							4/~							31f

TABLE VI. - SWEPT AUGMENTOR WING RUN INDEX

RUN		TUNNEL			POWER			WING					TAIL				
Run No		q, psf	α, deg	β, deg	AUGP, "Hg	FUS BLC, psig	C_J	δ_f, deg	δ_{TD}, deg	δ_a, deg	δ_s, deg	SLAT GAP, %	POS.	i_t, deg	δ_e/δ_s	REMARKS	FIG NO
29		8	~	0	0	0	0	70		30	60	1.0	OFF	–	–		19a
30		4.2	↓		24		1.5										19a
31		5	0,12		↓		1.25		~								
32		5	~				1.25		45								
33		5			21		1.1		45								14
34		8			24		8										15b, 19a
35		8			10		.4										
36		14			8		.2										
37		5			21	30	1.1										15a
38		8			24	20	.8										15b
39		8			10	0	.4					.5					13a
40		5			21	30	1.1					.5					
41		4.2			24	0	1.55	60				1.0					18
42		5			21		1.1										
43		8			24		.8										
44		8			10		.4										
45		8			0		0										
46		4.2			24		1.5	40									
47		5			21		1.1										17a
48		8			24		.8										
49		8			10		.4										
50		14			8		.2										

TABLE VI. - SWEPT AUGMENTOR WING RUN INDEX

RUN		TUNNEL			POWER			WING					TAIL				
RUN NO		q, psf	α, deg	β, deg	AUGP, "Hg	FUS BLC, psig	C_{J_T}	δ_f, deg	δ_{TO}, deg	δ_a deg	δ_s deg	SLAT GAP, %	POS.	i_t, deg	δ_e/δ_a	REMARKS	FIG NO
51		8	∼	0	0	0	0	40		30	60	1.0	OFF	-	-		17a
52		8	0	∼	24		.8	70								VERTICAL TAIL OFF	27a
53		8	12		24		.8										
54		8	↓		0		0										27b
55		8	0	↓	0		0									↓	27a
56		4.2	∼	0	24		1.5						LOW	-3	0		20a
57		5	-8, 0, 12 ∼		21		1.1								∼, 0		↓ , b, c
58		5	∼		21		1.1								-25		20 b
59		8			24		.8								0		20a
60		8	↓		10		.4								0		↓
61		5	-8, 0		21		1.1								∼/15		20d
62		5	∼		21		1.1								∼, -25	4 NACELLES ON	22b, c
63		4.2			24		1.5								0		22a
64		4.2			24		1.5										
65		5			21		1.1										, b
66		8	↓	↓	24		.8										↓
67		8	0	∼													29a
68		8	12	↓	↓		↓										29a
69		8	∼	0	10		.4										22a
70		8			0		0	↓							↓		22a
71		5			21		1.1	40							∼, -25		17e, f
72		4.2	↓	↓	24		1.5	↓		↓	↓	↓	↓	↓	0	↓	↓

TABLE VI. - SWEPT AUGMENTOR WING RUN INDEX

Run: Run No		Tunnel: q, psf	α, deg	β, deg	Power: Augp, "Hg	Fus BLC, psig	C_J	Wing: δ_f, deg	δ_{fo}, deg	δ_a, deg	δ_s, deg	Slat gap, %	Tail: Pos.	i_t, deg	δ_e/δ_{es}	Remarks	Fig No
73		5	~	0	21	0	1.1	40		30	60	1.0	Low	.5	0	4 Nacelles on	17e
74		8	↓	0	24	↓	.8	↓		↓	↓	↓	↓	↓	↓	↓	↓
75		↓	0	~	↓		↓										
76		↓	12	~	↓		↓	↓					↓	↓	↓	↓	
77		4.2	~	0	24		1.5	70					OFF	-	-	Vertical Fin off - 4 Nacelles on	19c
78		5	↓	0	21		1.1	↓					↓			↓	↓
79		8	0	~	24		.8										29b
80		8	12	~	24		↓	↓									
81		4.2	~	0	24		1.5	40									17d
82		5	↓	↓	21		1.1	↓									↓
83		8			24		.8										
84		8			0		0	↓								↓	↓
85		4.2			24		1.5	70								- Two Nacelles on	19d
86		5			21		1.1	↓								↓	↓
87		8			24		.8										
88		8			0		0						↓			↓	↓
89		5	↓		21		1.1						High	-8.7	0		21a, 31a
90		↓	-8,0,12		↓		↓						↓	↓	~		21c
91			~												-25		21b
92			~												-25/16		21b
93			-8,0,12												~/-16		21d
94		↓	~	↓	↓	↓	↓	↓		↓	↓	↓	↓	↓	-25/-21		21b

TABLE VI. - SWEPT AUGMENTOR WING RUN INDEX

RUN		TUNNEL			POWER			WING					TAIL				
RUN NO		q, psf	α, deg	β, deg	AUGP, "Hg	FUS BLC, psig	C_J	δ_f, deg	δ_{SD}, deg	δ_a deg	δ_s deg.	SLAT GAP, %	POS.	i_t, deg	$\epsilon_e/\epsilon_{e_2}$	REMARKS	FIG NO
95		5	0,12	0	21	0	1.1	70		30	60	1.0	HIGH	-8.7	~/-21		21e
96		5	~		21		1.1								-25/17.[illegible]		21b
97		4.2			24		1.5								0		21a
98		5			21		1.1										
99		8			24		.8										
100		8			10		.4										, 31a
101		8	↓	↓	0		0										↓
102		5	0	~	21		1.1										28d
103		5	12		21		1.1										28c
104		8	0		10		.4										28d
105		8	12	↓	10		.4										28c
106		4.2	~	0	24		1.5	40									17c
107		5			21		1.1										, 30a
108		8			24		.8										
109		8	↓	↓	10		.4										↓, 30a
110		↓	0	~	↓		↓										28a
111			12														28b
112		5	12		21		1.1										28b
113		5	0	↓	21		1.1										28a
114		8	~	0	10		.4			15/45							30a
115		5	↓	↓	21		1.1										30a
116		5	0	~	21		1.1			↓							30c

TABLE VI. - SWEPT AUGMENTOR WING RUN INDEX

RUN		TUNNEL			POWER			WING					TAIL				
RUN NO		q, psf	α, deg	β, deg	AUGP, "Hg	FUS BLC, psig	C_J	δ_f, deg	δ_{TD}, deg	δ_a, deg	δ_s, deg	SLAT GAP, %	POS.	i_t, deg	δ_e/δ_a	REMARKS	FIG NO
117		8	~	0	0	0	0	40		30	60	1.0	HIGH	-8.7	0		17c
118		5	0	↓	21	↓	1.1	↓		~/~	↓	↓	↓				31e,f
119		↓	4		↓		↓			↓							↓ ,35d
120			12	↓													
121			12	~						15/45							30d
122			~	-8						↓							30b
123		↓	↓	-8	↓		↓			30							30b
124		8	0	~	10		.4			15/45							30c
125		↓	12	↓	↓		↓	↓		↓							30d
126		5	~	0	21		1.1	70									31a
127		8	↓	↓	10		.4	↓		↓							↓
128		5	↓	↓	21		1.1			45/15							↓ ,36d
129		↓	4	↓	↓		↓			~/~							31e,34c
130			0	~						15/45							31b
131		↓	12	↓	↓		↓			↓							31c
132		8	12		10		.4										31c
133		↓	0	↓	↓		↓										31b
134		5	~	-8	21		1.1			↓							31d
135		↓	↓	-8	↓		↓			30							31d
136		↓		0	↓		↓			↓						20% THROTTLING	33a,b
137		8		↓	10		.4									↓	33c,d
138		5	↓	↓	21	↓	1.1	↓		↓	↓	↓	↓			60% THROTTLING	33a,b,f

TABLE VI. - SWEPT AUGMENTOR WING RUN INDEX

RUN		TUNNEL			POWER			WING					TAIL				
RUN NO		q, psf	α, deg	β, deg	AUGP, "Hg	FUS BLC, psig	C_J	δ_f, deg	δ_{ID}, deg	δ_a deg	δ_s deg	SLAT GAP, %	POS.	i_t, deg	δ_e/δ_{e_2}	REMARKS	FIG NO
139		8	~	0	10	0	.4	70		30	60	1.0	HIGH	-8.7	0	60% THROTTLING	33c,d,e
140		↓	↓	-8	↓	↓	.4	↓		↓	↓	↓	↓			↓	33e
141		5	↓	-8	21		1.1										33f
142		↓	4	~	↓		↓										
143		↓	~	0	↓		↓									40% THROTTLING	
144		8	↓	↓	10		.4	↓								↓	
145		5			21		1.1	40									32a,b
146		8			10		.4	↓									32c,d
147		5			21		1.1									60% THROTTLING	32a,b,e
148		8		↓	10		.4									↓	32c,d,f
149		↓		-8	↓		↓										32f
150		5	↓	-8	21		1.1										32e
151		↓	4	~	↓		↓										32g
152		↓	~	0	↓		↓									20% THROTTLING	32a,b
153		8	↓	↓	10		.4									↓	32c,d
154		5			21		1.1										32a,b,35a
155		8			10		.4	↓									32c,d,35b
156		5			21		1.1	70									34a,36a
157		8			10		.4	↓									34b,36b
158		5	↓		21		1.1			↓						δ_{ID}=22° (___) VENT	34a
159		↓	4		↓		↓			~/30						↓	34c
160		8	~	↓	10	↓	.4	↓		30	↓	↓	↓				34b

TABLE VI. - SWEPT AUGMENTOR WING RUN INDEX

RUN		TUNNEL			POWER			WING					TAIL				
RUN NO		q psf	α, deg	β, deg	AUG P, "Hg	FUS BLC, psig	C_J	δ_f, deg	δ_{ID}, deg	δ_a deg	δ_s deg	SLAT GAP, %	POS.	i_t, deg	δ_e/δ_s	REMARKS	FIG NO
161		8	~	0	10	0	.4	70		~/30	60	1.0	HIGH	-8.7	0	δ_{sp} = 22° ( ) VENT	34d
162		5	4	↓	21		1.1	↓		↓	↓	↓	↓			δ_{sp} = 38° ↓	34c
163		↓	↓		↓		↓									↓ ( ) VENT	36d
164																δ_{sp} = 10° ↓	36d
165		8	↓		10		.4			↓						↓	36e
166		5	~		21		1.1			30							36a
167		8	↓		10		.4			30						↓	36b
168		5	4		21		1.1			~/30						δ_{sp} = 20°	36d
169		8	↓		10		.4	↓		↓						↓	36e
170		5	↓		21		1.1	40		↓							35d
171		↓	~		↓		↓	↓		30							35a
172		8	↓		10		.4			30							35b
173		↓	4		↓		↓			~/30						↓	35d
174		5	~		21		1.1			↓						δ_{sp} = 36°	35a,c
175		↓	4	↓	↓		↓									↓	35d
176			↓	-8				↓		↓							35c
177			~	0				70		30						δ_{sp} = 50°	36a
178		↓	4	↓	↓		↓	↓		~/30						↓	36d
179		8	~		10		.4			30							36b
180		↓	4	↓	↓		↓			~/30							36e
181		5	↓	~	21		1.1			30						↓ ↓	36c
182		8	↓	0	10		4	↓		~/30	↓	↓	↓				34d

TABLE VI. - SWEPT AUGMENTOR WING RUN INDEX

RUN		TUNNEL			POWER			WING					TAIL				
RUN NO		q, psf	α, deg	β, deg	AUGP, "Hg	FUS BLC, psig	C_{J_T}	δ_f, deg	δ_{TD}, deg	δ_a, deg	δ_s, deg	SLAT GAP, %	POS.	i_t, deg	δ_e/δ_{e_2}	REMARKS	FIG NO
183		0	−8	0	21	0	∞	70		4	60	1.0	OFF	–	–		
184		5	~				1.1	↓		30							19a
185		0					∞	30		4							
186		5			↓		1.1			30							16a
187		8			10		.4										
188		8			24		.8										
189		14			8		.2										↓
190		16			24		.4										16b
191		25			24		.3										16b
192		4.2			24		1.5										16a
193		8	↓		0		0	↓									16a
194		0	−8		21		∞	40									
195		8	~		24		.8										17b
196		16					.4										
197		25	↓		↓		.3			↓							↓
198		0	−8		21		∞			4						SHROUD & INTAKE DOOR OFF	
199		4.2	~		24		1.5			30							17g
200		5			21		1.1										
201		8			24		.8										
202		8			10		.4										
203		14	↓		8		.2										↓
204		14	14	↓	~	↓	~	↓		↓	↓	↓	↓			↓	

TABLE VI. - SWEPT AUGMENTOR WING RUN INDEX

RUN		TUNNEL			POWER			WING					TAIL				
RUN NO		q, psf	α, deg	β, deg	AUGP, "Hg	FUS BLC, psig	C_J	δ_f, deg	δ_{TD}, deg	δ_a deg	δ_s deg	SLAT GAP, %	POS.	i_t, deg	ε_e/δ_e	REMARKS	FIG NO
205		25	14	0	~	0	~	40		30	60	1.0	OFF	—	—	SHROUD & INTAKE DOOR OFF	
206		8	~		0		0			↓							17g
207		0	-8		21		∞	70		4							
208		4.2	~		24		1.5			30							19e
209		5			21		1.1										
110		8			24		.8										
211		8			10		.4										
212		14	↓		8		.2										↓
213		14	14		~		~										
214		25	14		~		~										
215		8	~		0		0	↓									19e
216		4.2			24		1.5	30									16c
217		5			21		1.1										
218		8	↓		24		.8	↓		↓							↓
219		0	-8		21		∞	40		4						TETITARY SLOT SEALED	
220		4.2	~		24		1.5			30							17h
221		5			21		1.1										
222		8			24		.8										
223		8			0		0	↓								↓	↓
224		4.2			24		1.5	70								4 NACELLES ON	19f
225		5			21		1.1										
226		8	↓	↓	24	↓	.8	↓		↓	↓	↓	↓			↓	↓

TABLE VI. - SWEPT AUGMENTOR WING RUN INDEX

RUN		TUNNEL			POWER			WING					TAIL				
RUN NO		q, psf	α, deg	β, deg	AUGP, "Hg	FUS BLC, psig	C_J	δ_f, deg	δ_{ID}, deg	δ_a deg	δ_s deg	SLAT GAP, %	POS.	i_t, deg	$\delta_{e_1}/\delta_{e_2}$	REMARKS	FIG NO
227		4.2	~	0	24	0	1.5	40		30	60	1.0	OFF	—	—	SHROUD & INTAKE DOOR OFF - 4 NACELLES ON	17i
228		5	↓	↓	21	↓	1.1	↓		↓	↓	↓	↓			↓	↓
229		8	↓	↓	24	↓	.8	↓		↓	↓	↓	↓			↓	↓
230		0	0	↓	21	↓	∞	30		4	↓	↓	↓			↓	

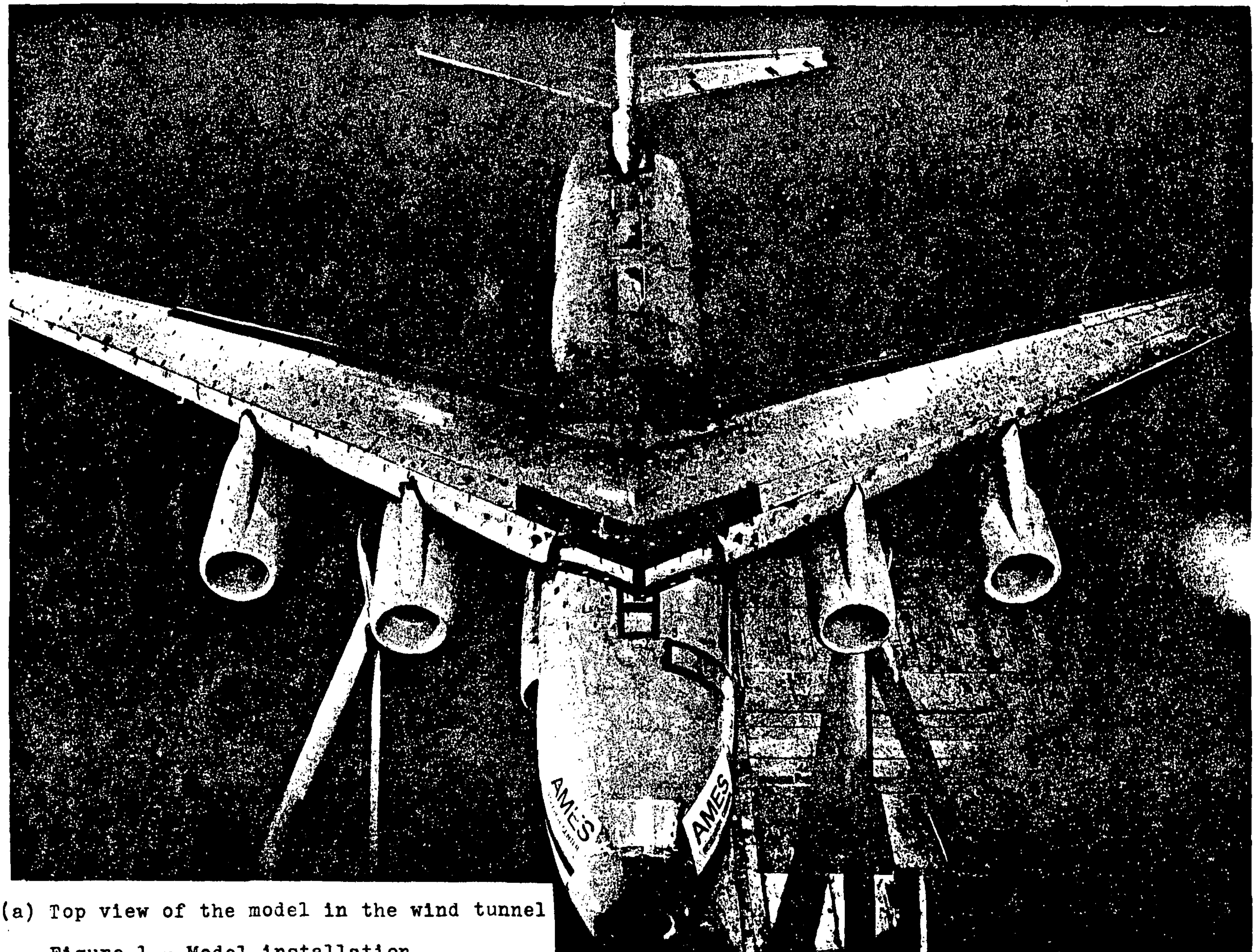

(a) Top view of the model in the wind tunnel

Figure 1.- Model installation.

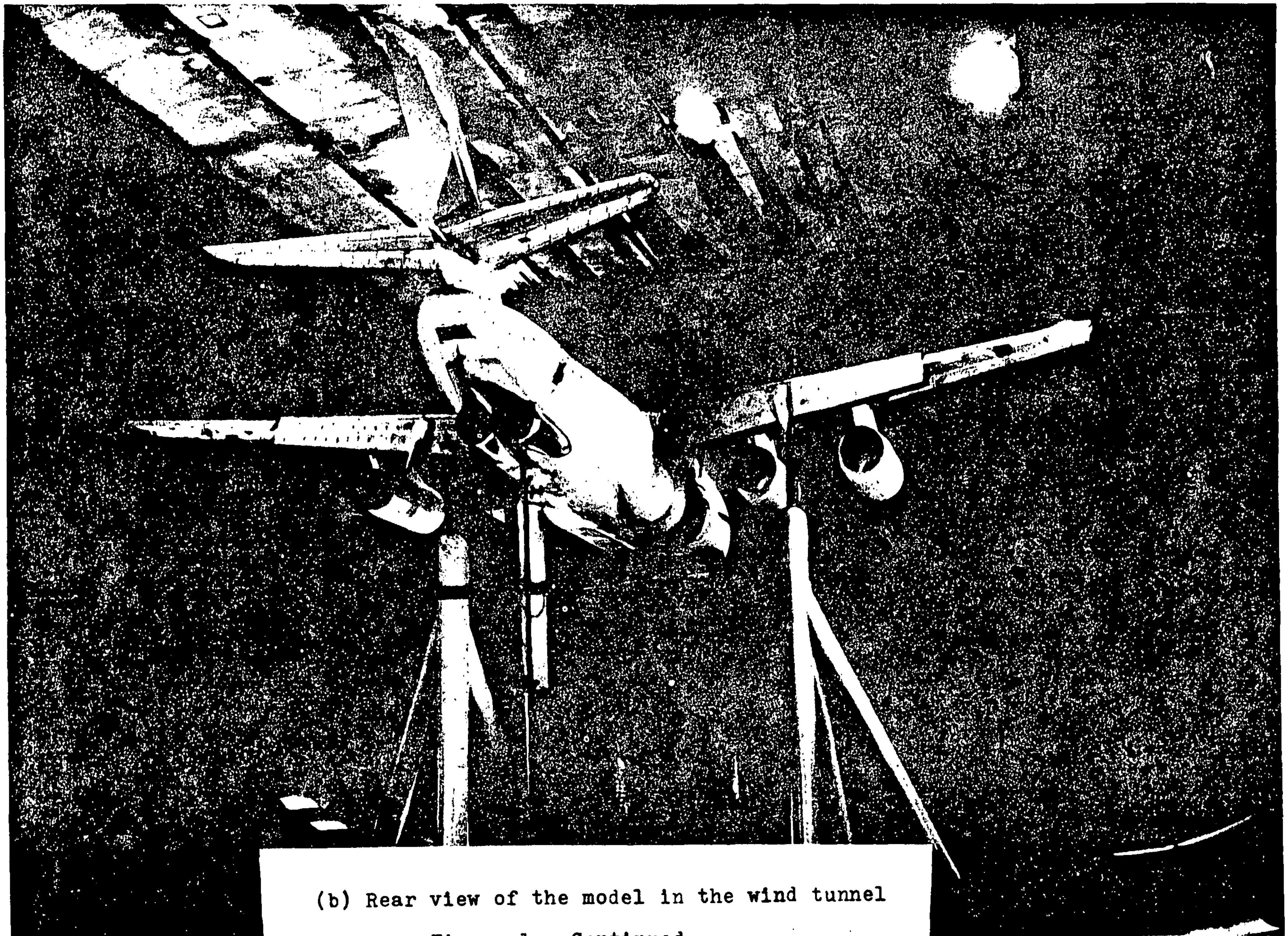

(b) Rear view of the model in the wind tunnel

Figure 1.- Continued.

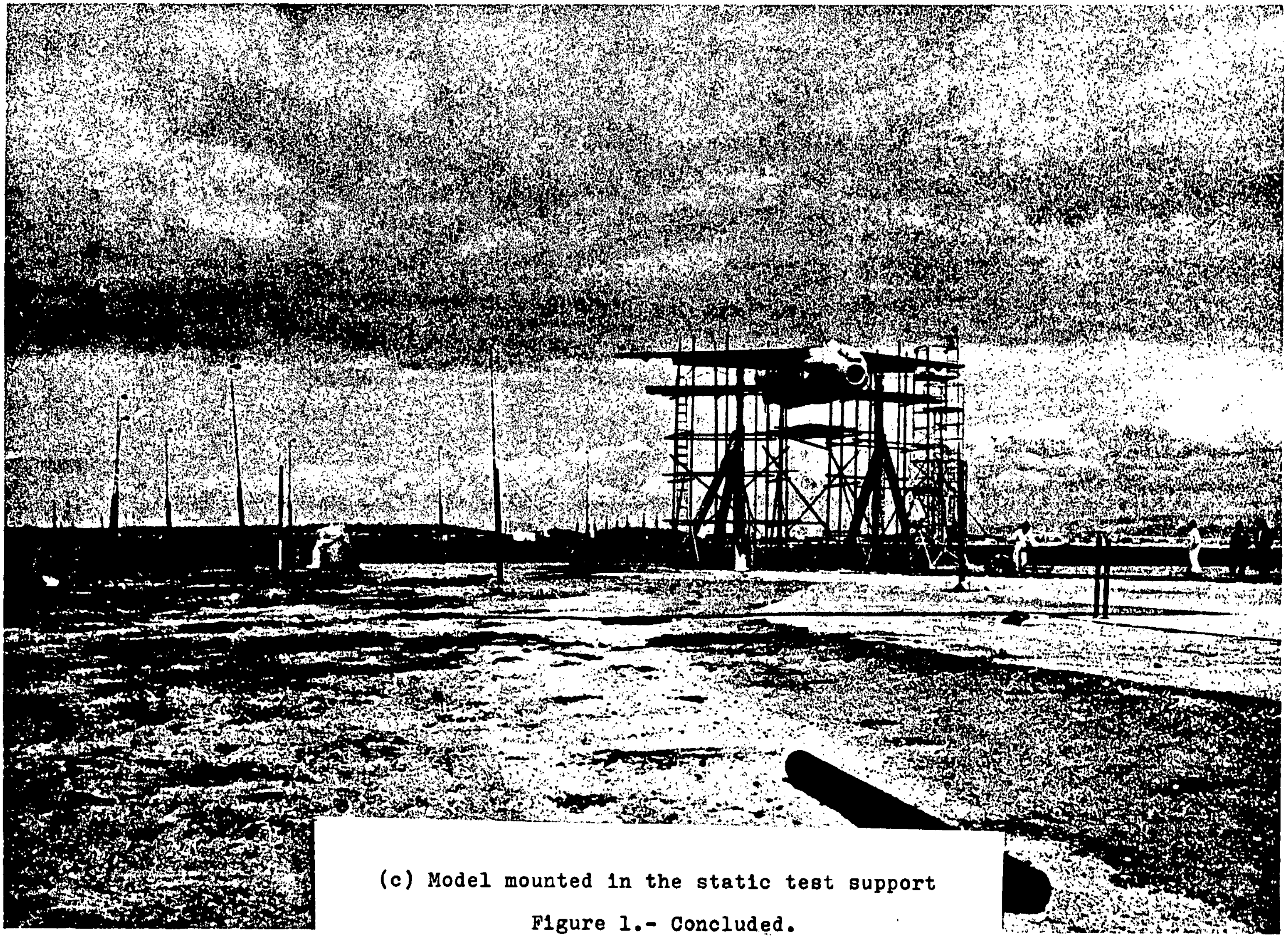

(c) Model mounted in the static test support

Figure 1.- Concluded.

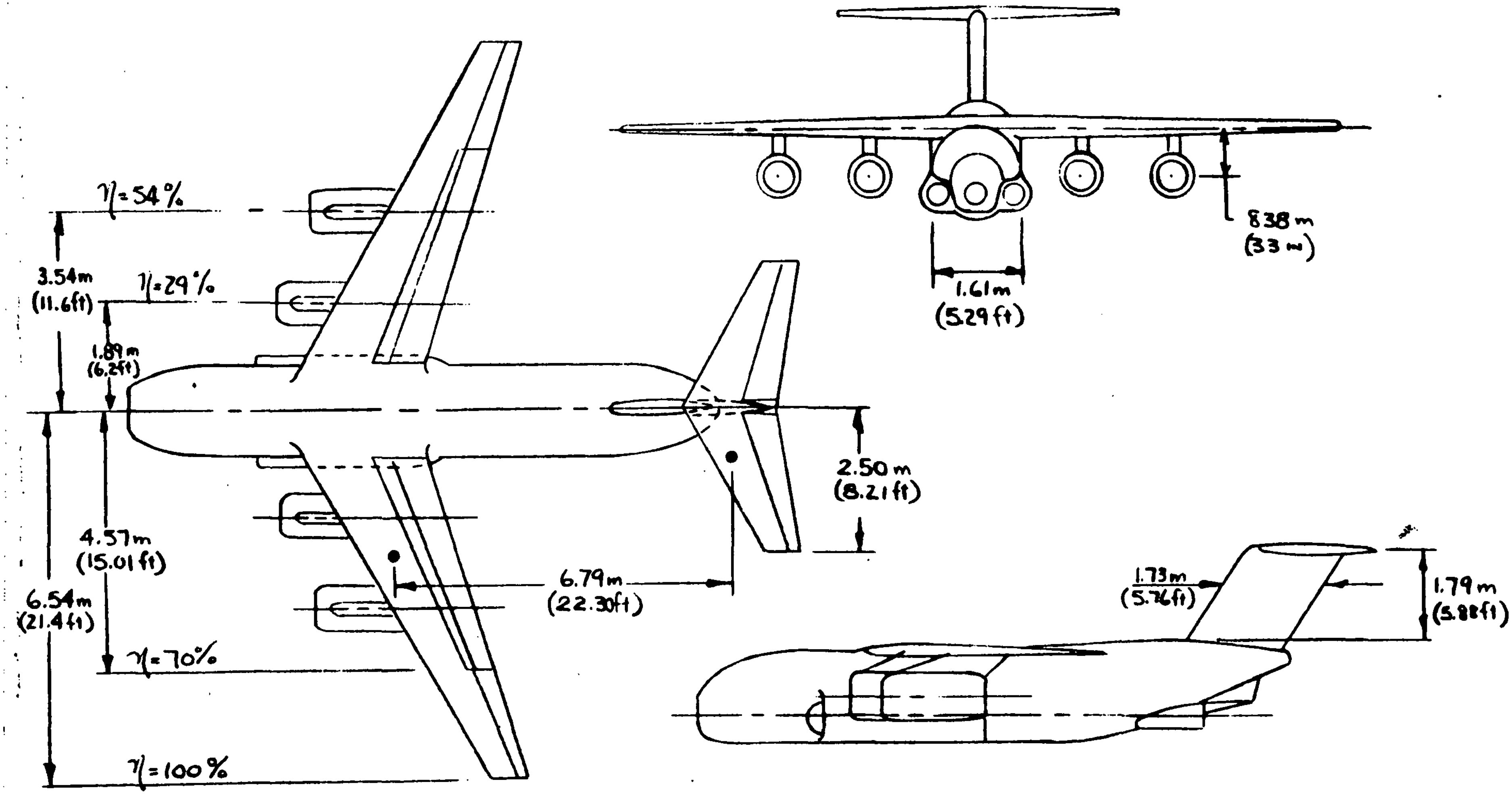

Figure 2.- Basic model geometry.

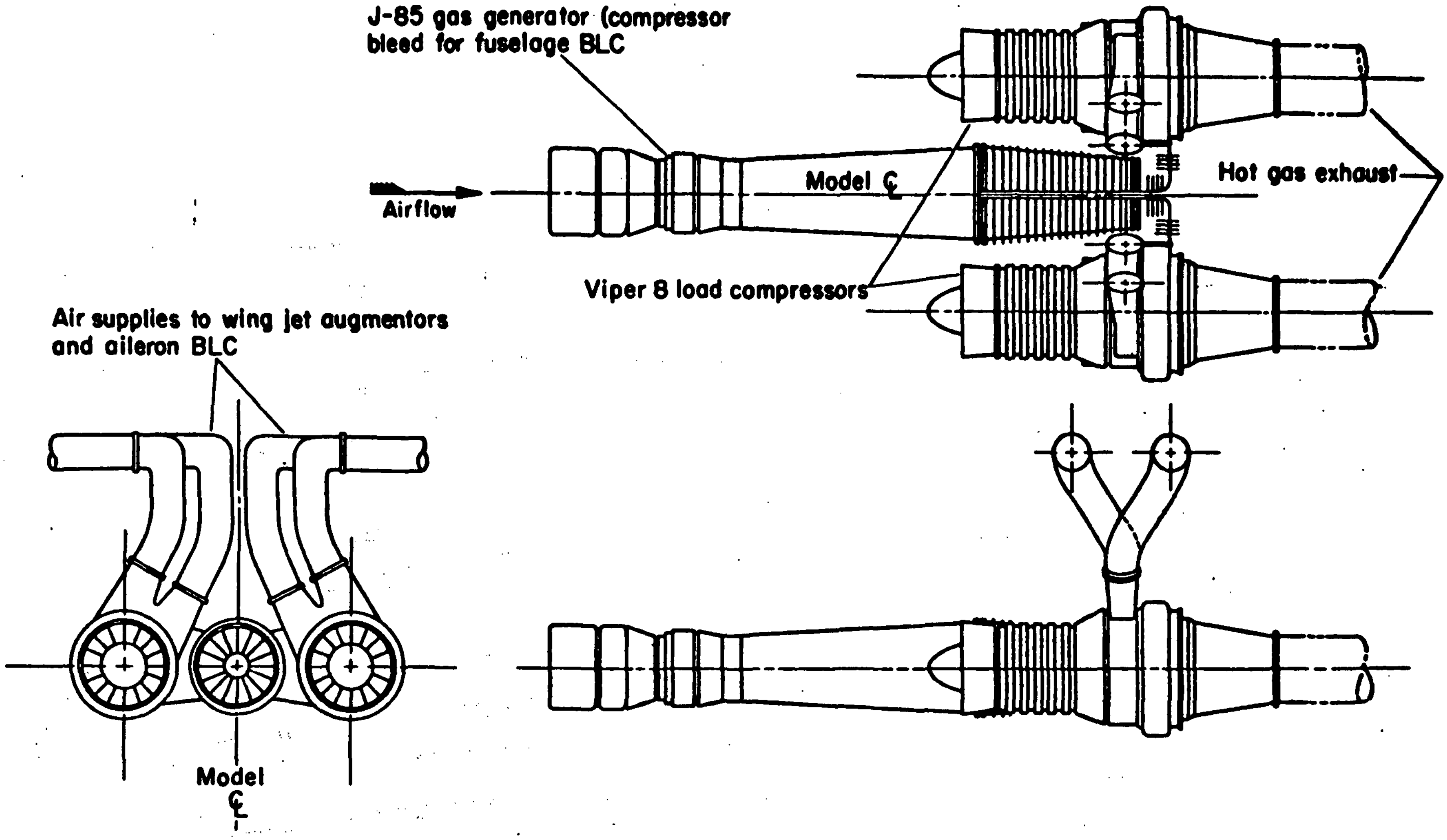

Figure 3.- Augmentor air compressor system.

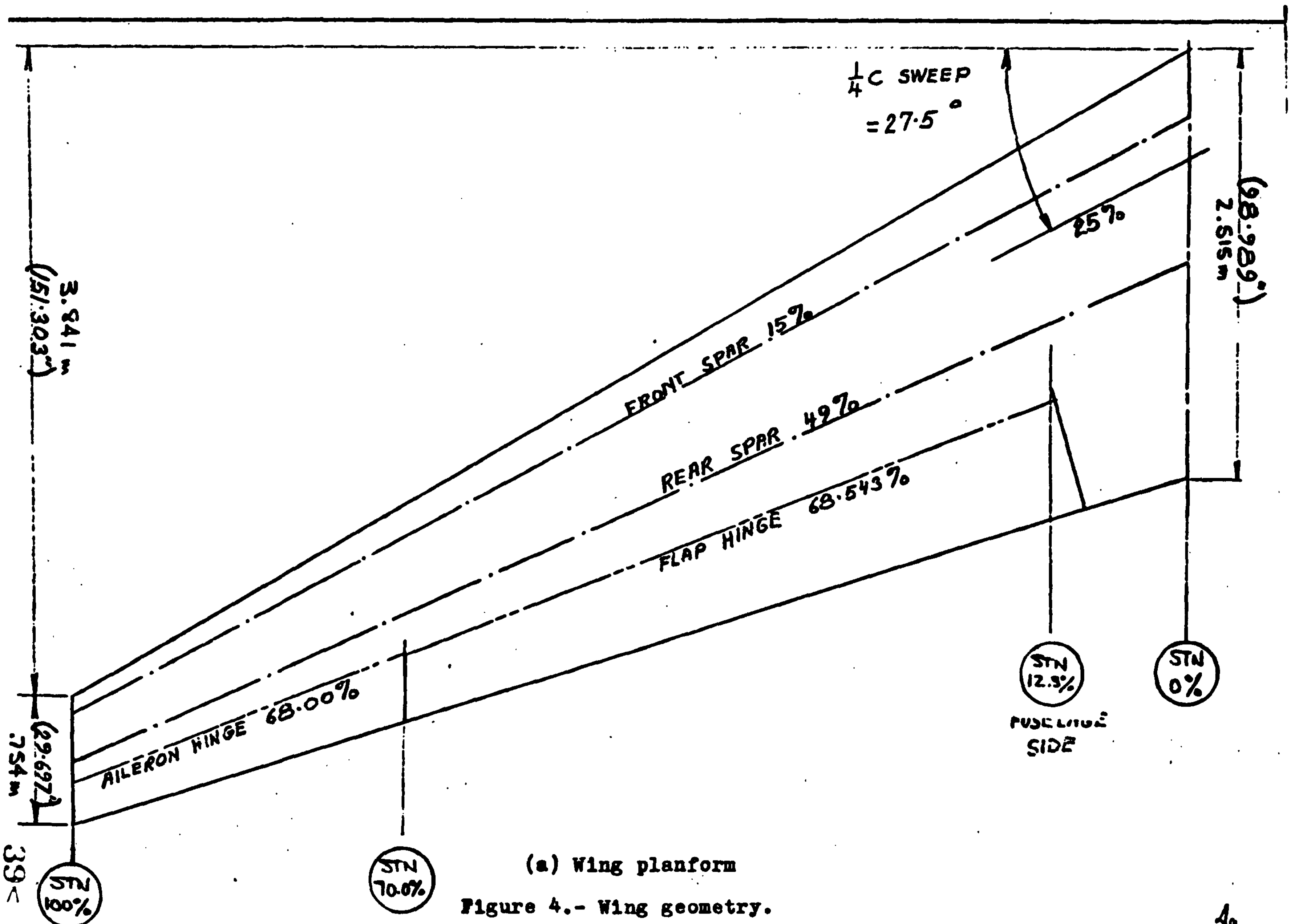

(a) Wing planform

Figure 4.- Wing geometry.

4a

SLAT CO-ORDINATES	
x/c_s	y/c_s Upper
0.025	0.0667
0.05	0.1000
0.10	0.1520
0.15	0.1843
0.20	0.2088
0.25	0.2255
0.30	0.2375
0.40	0.2500
0.50	0.2476
0.60	0.2265
0.70	0.1941
0.80	0.1431
0.90	0.0794
1.00	0.0000
L/E RADIUS = 9.314 % c_s	

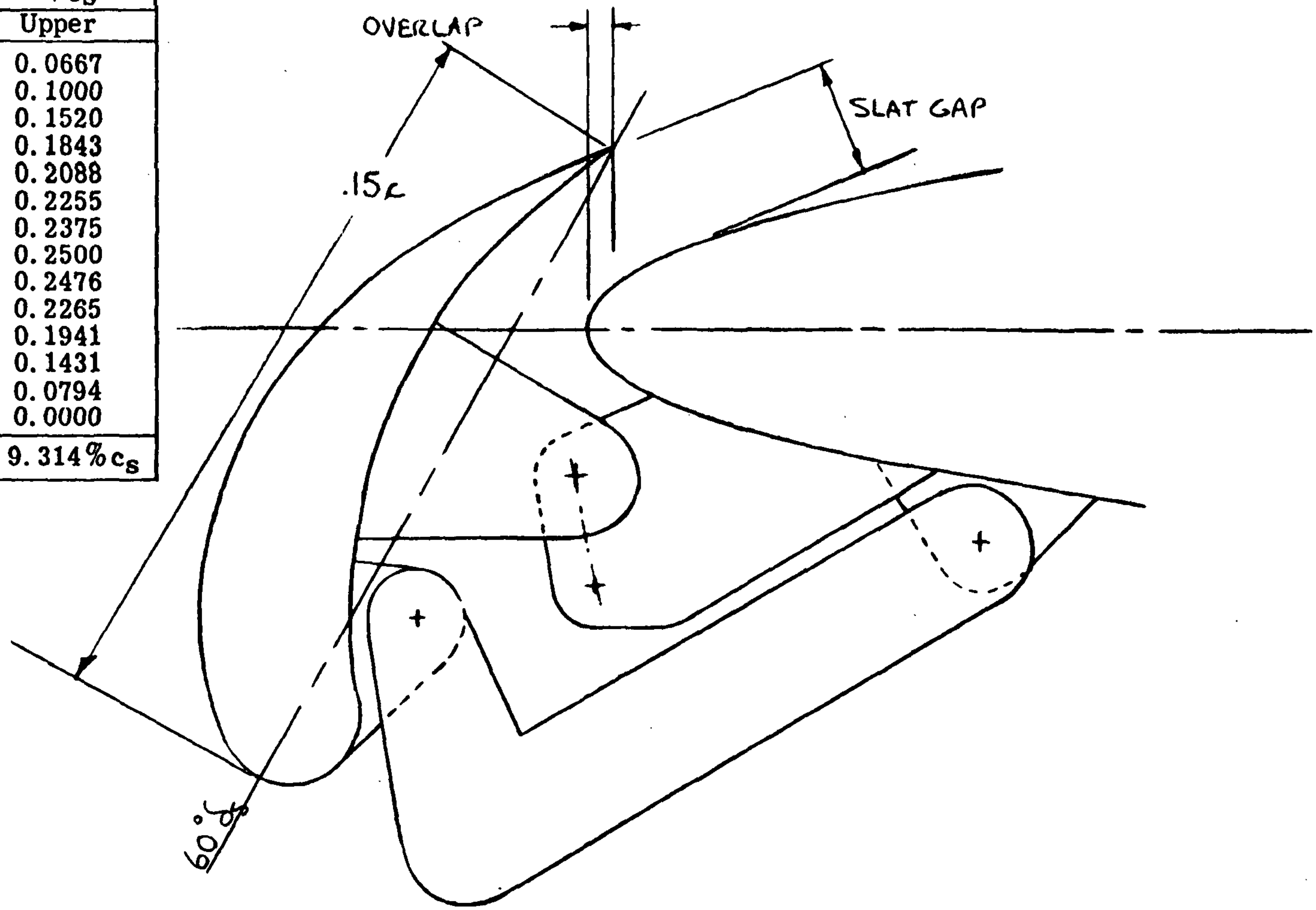

(b) Wing leading edge slat

Figure 4.- Concluded.

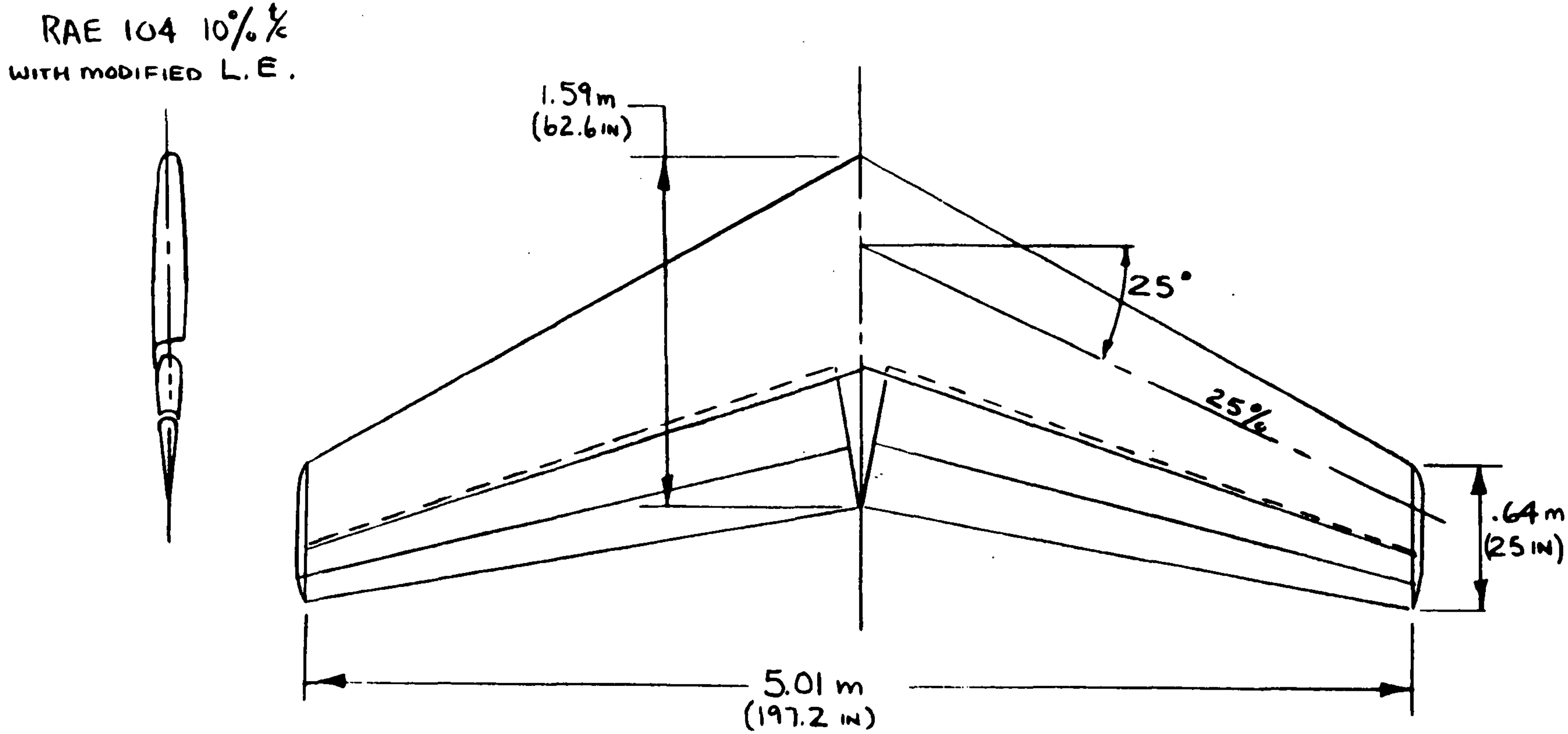

(a) Basic geometry

Figure 5.- Horizontal tail geometry.

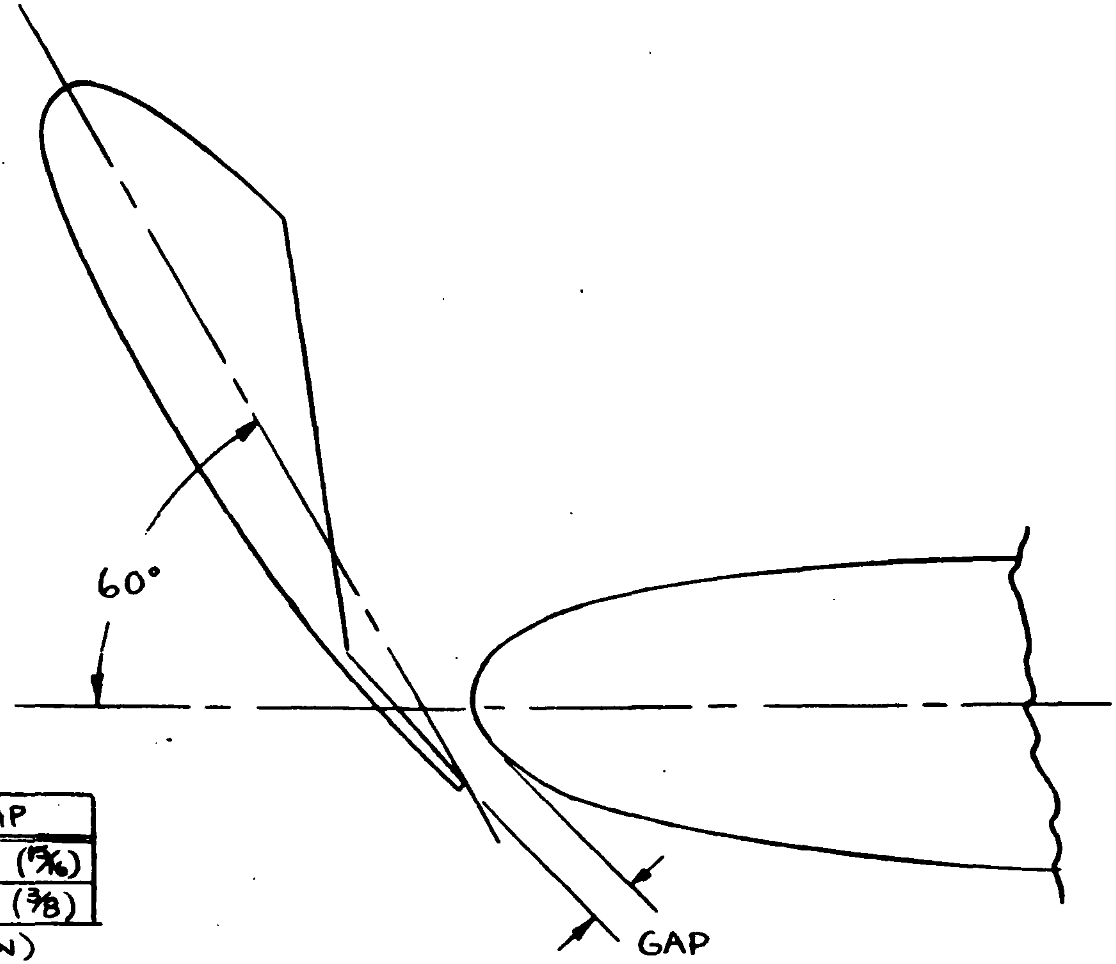

	CHORD	GAP
ROOT	20.3 (8)	2.4 (15/16)
TIP	10.2 (4)	1.0 (3/8)

DIMENSIONS IN CM (IN)

(b) Leading edge slat

Figure 5.- Continued.

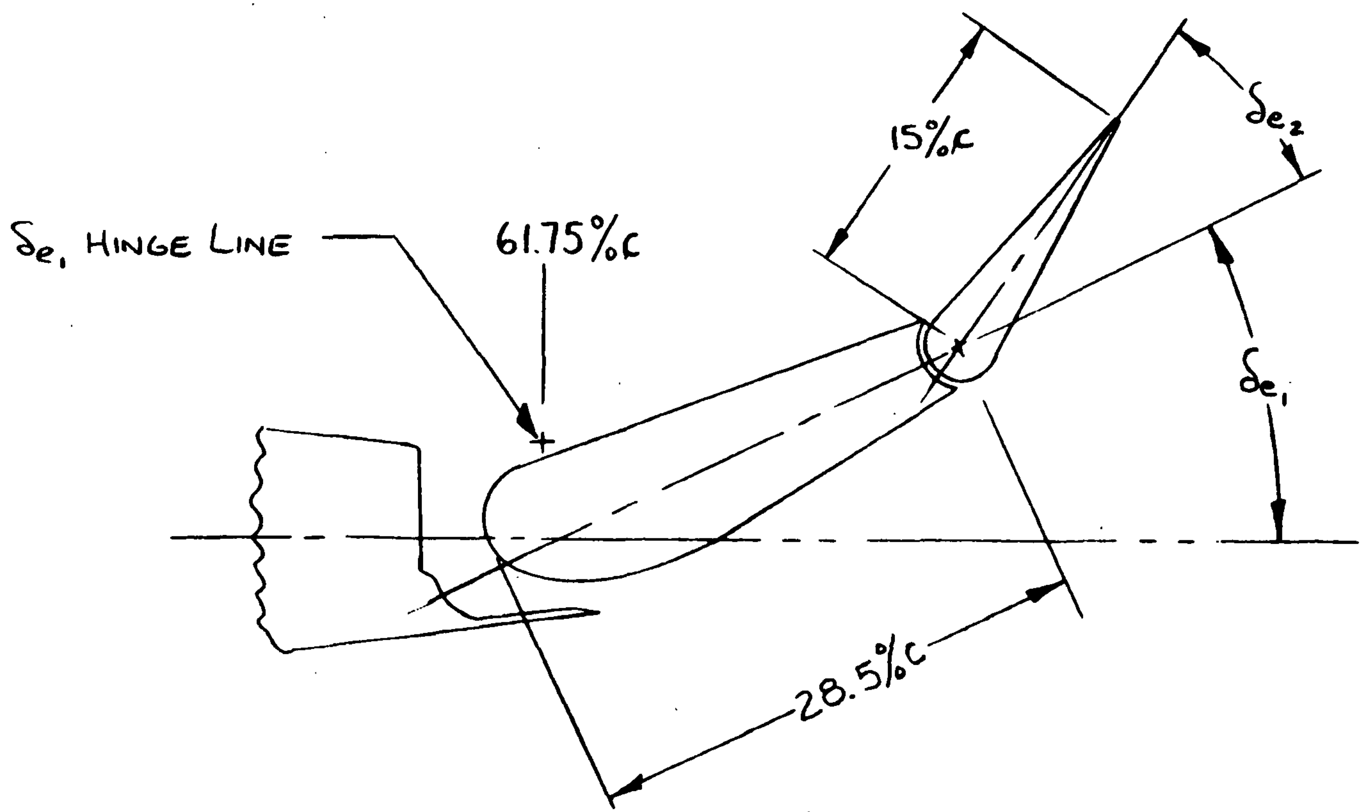

(c) Slotted,double-hinged elevator

Figure 5.- Continued.

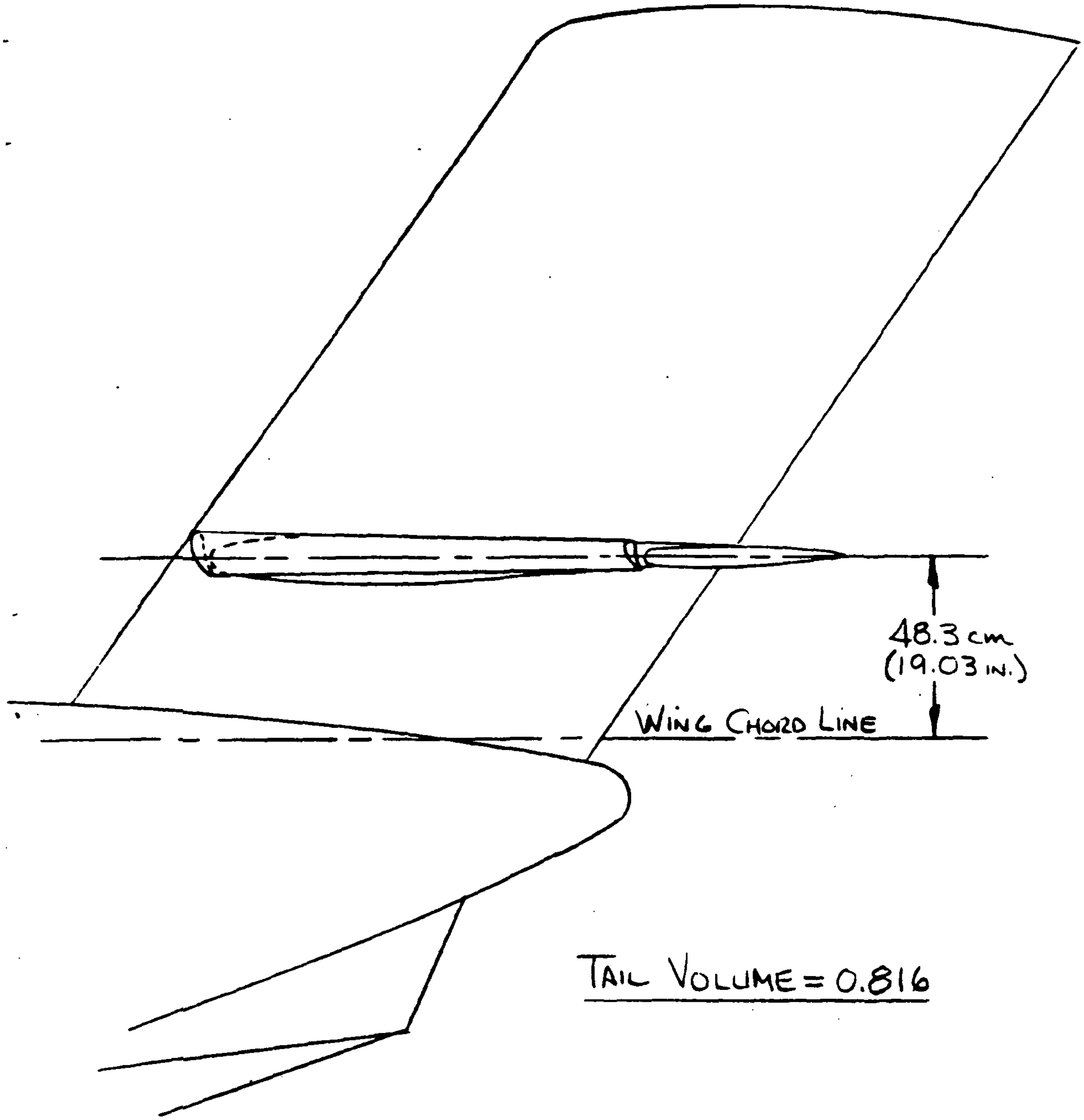

(d) Low tail position

Figure 5.- Concluded.

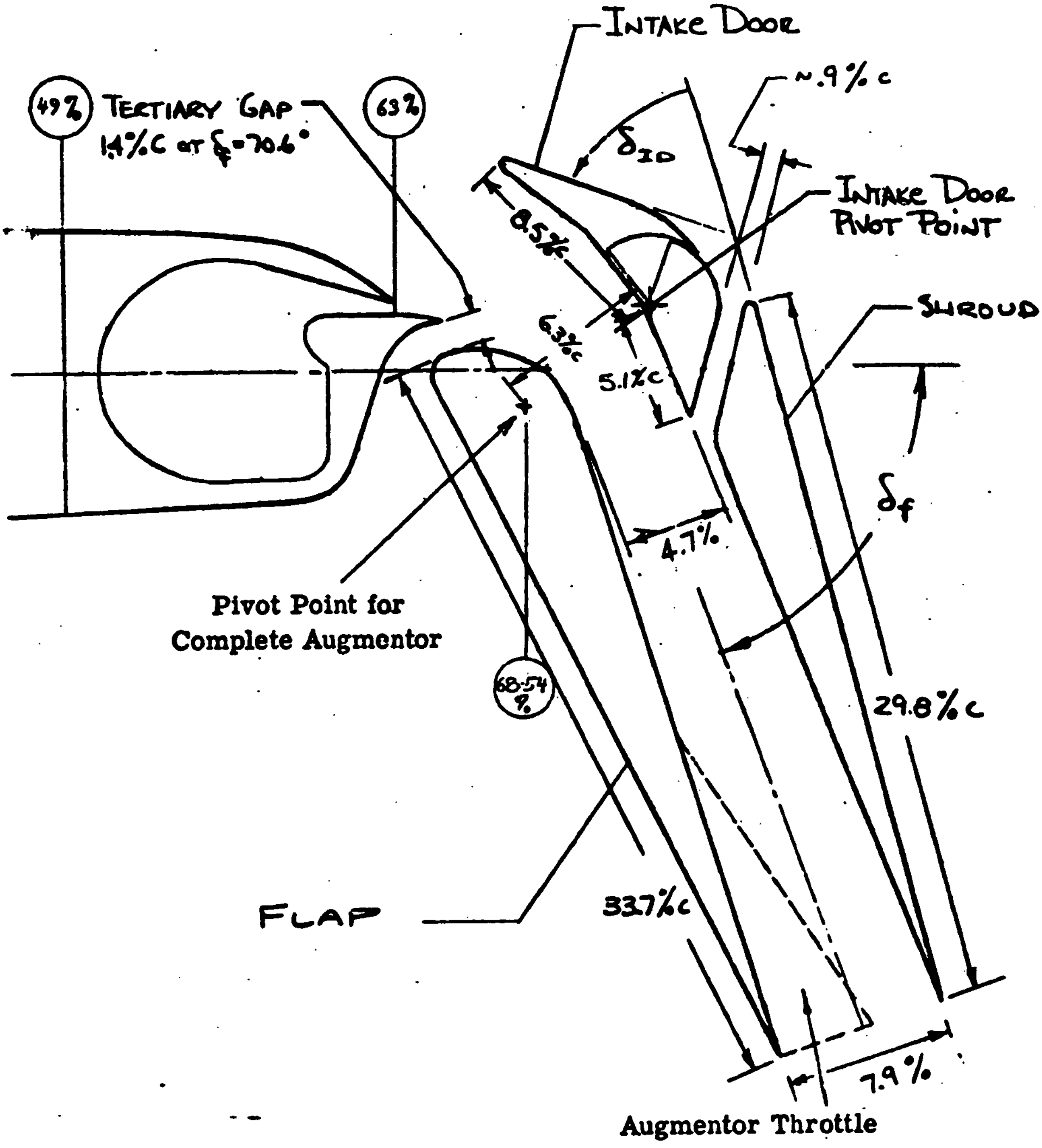

(a) Basic geometry

Figure 6.- Augmentor geometry.

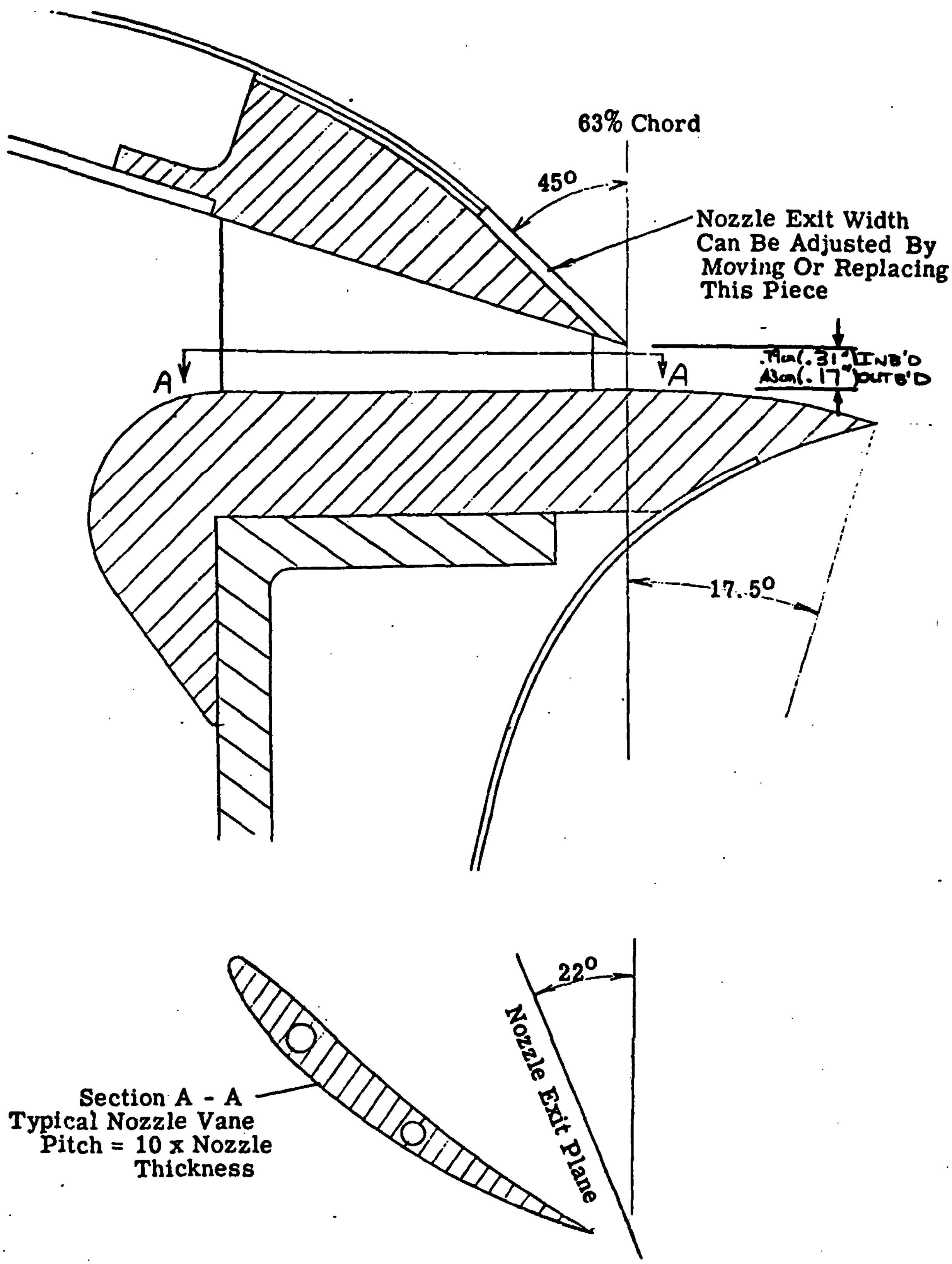

(b) Primary nozzle geometry

Figure 6.- Continued.

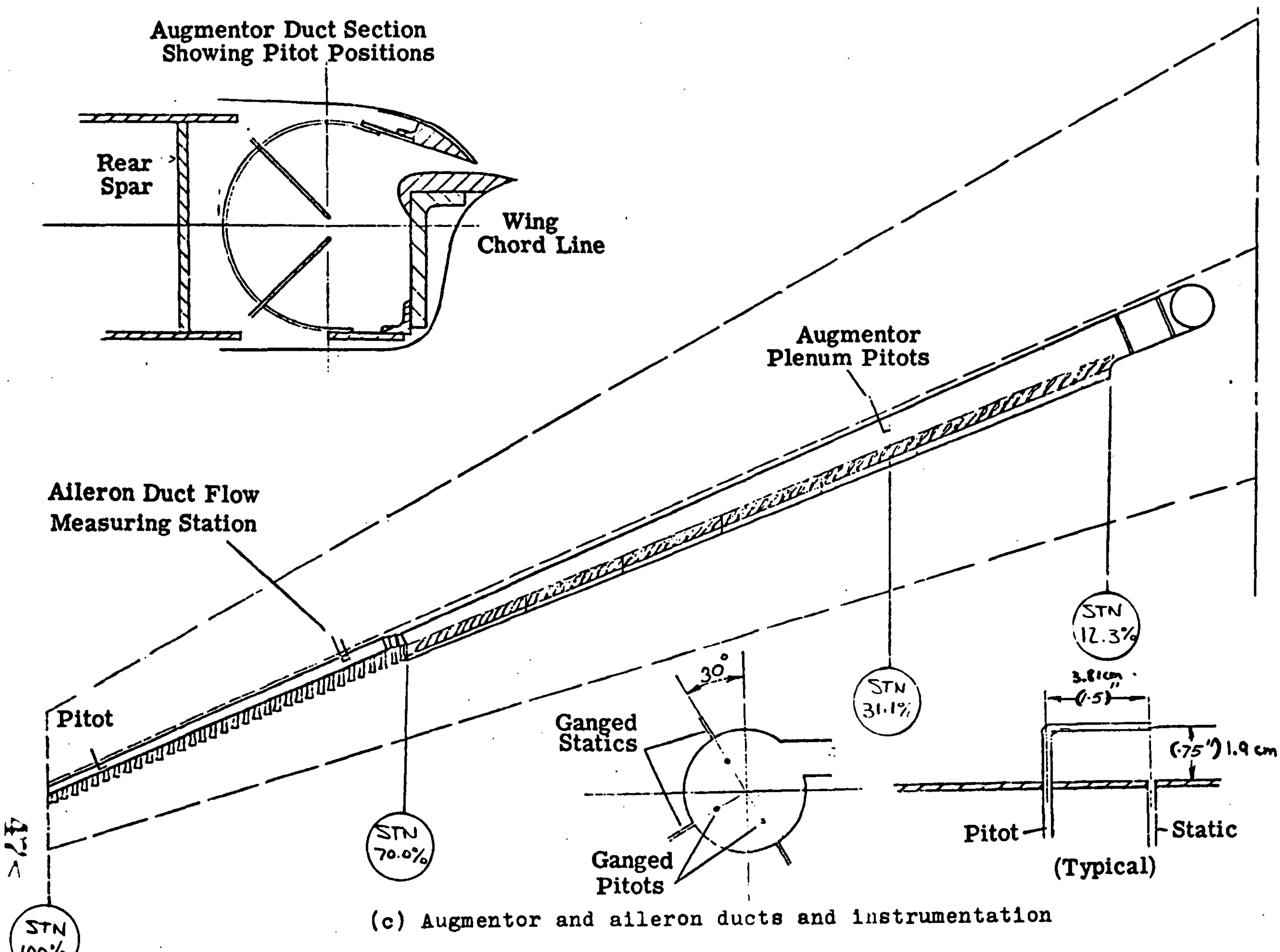

(c) Augmentor and aileron ducts and instrumentation

Figure 6.- Continued.

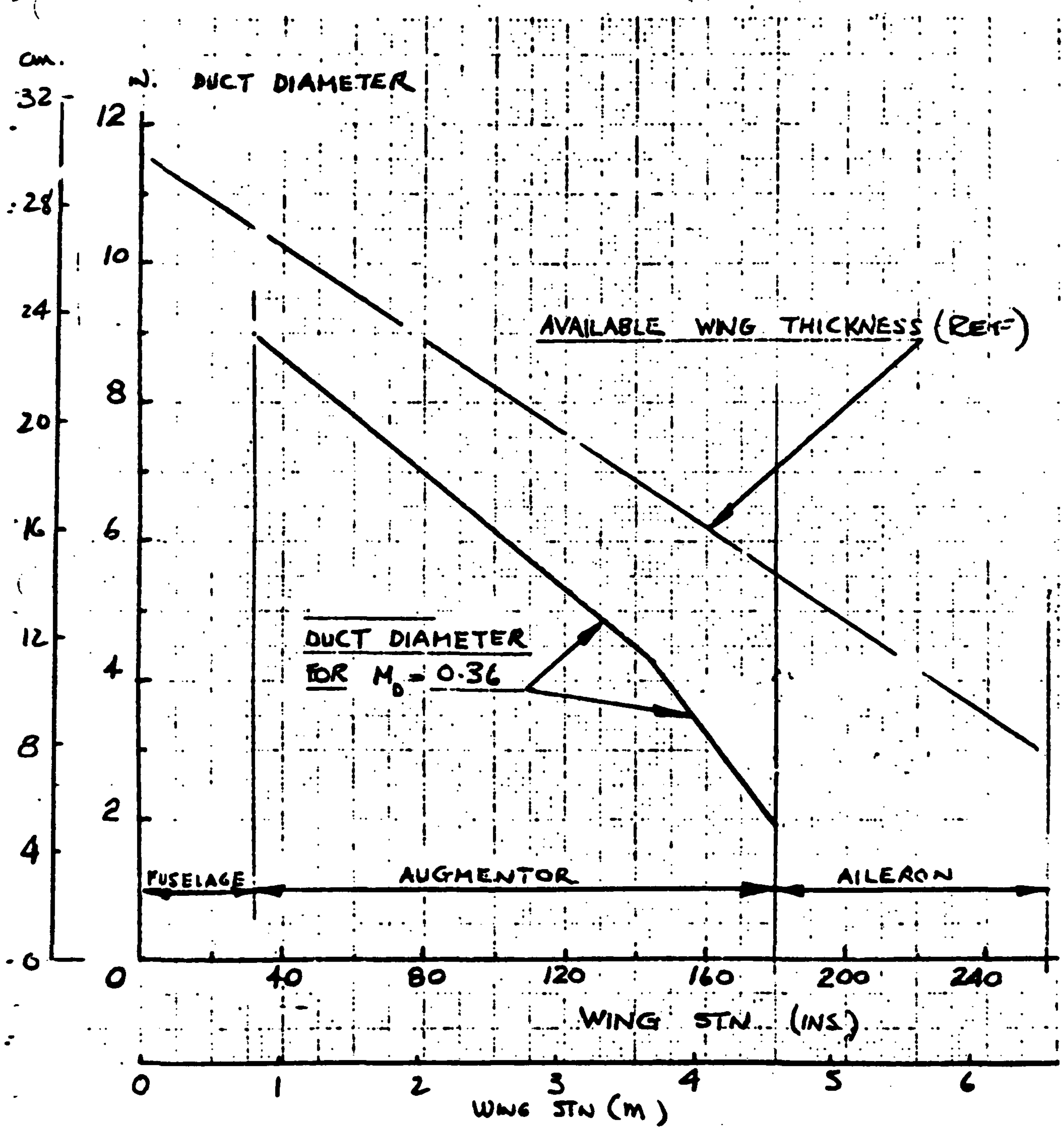

(d) Augmentor duct diameter as a function of wing span

Figure 6.- Concluded.

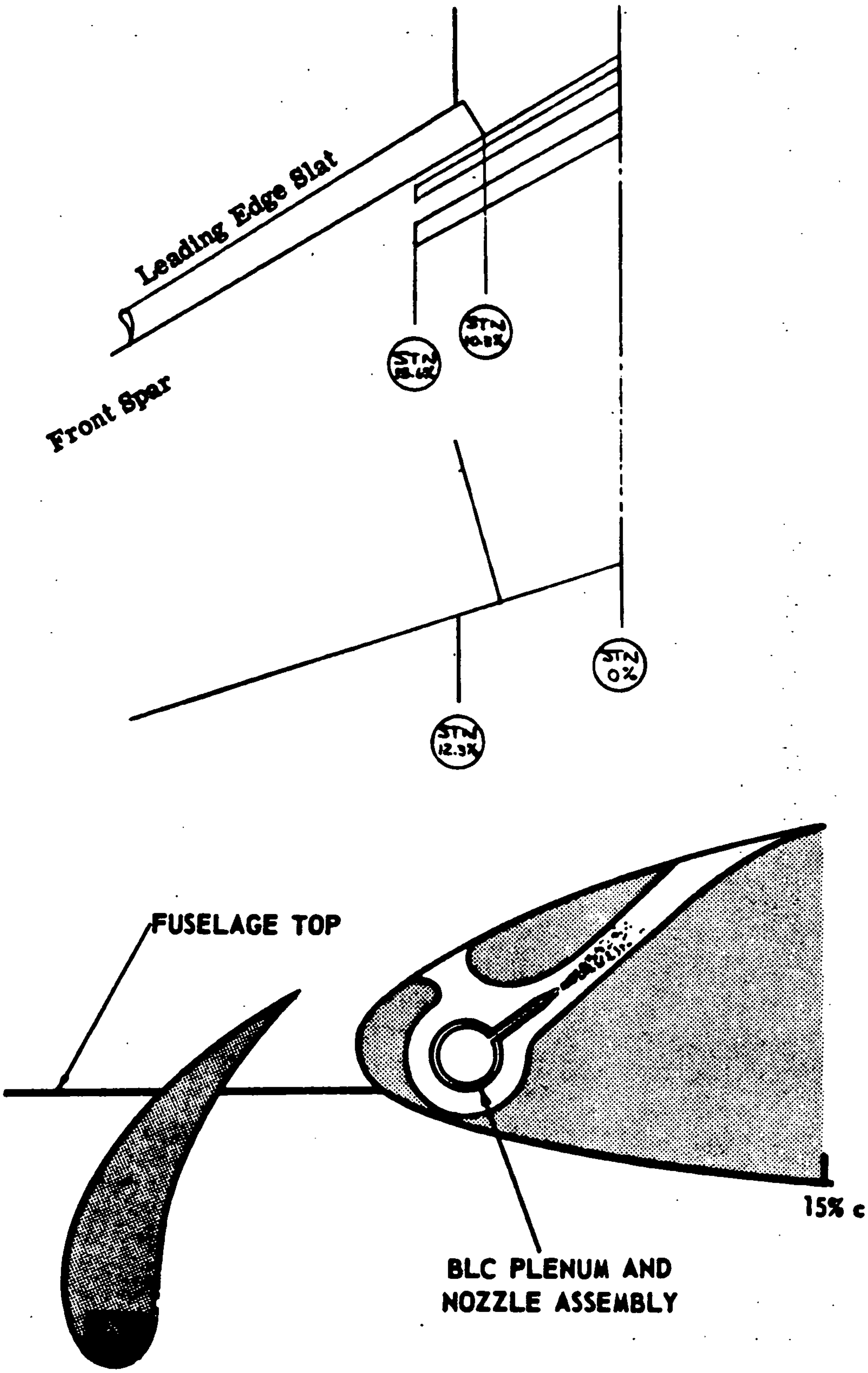

Figure 7.- Fuselage BLC geometry.

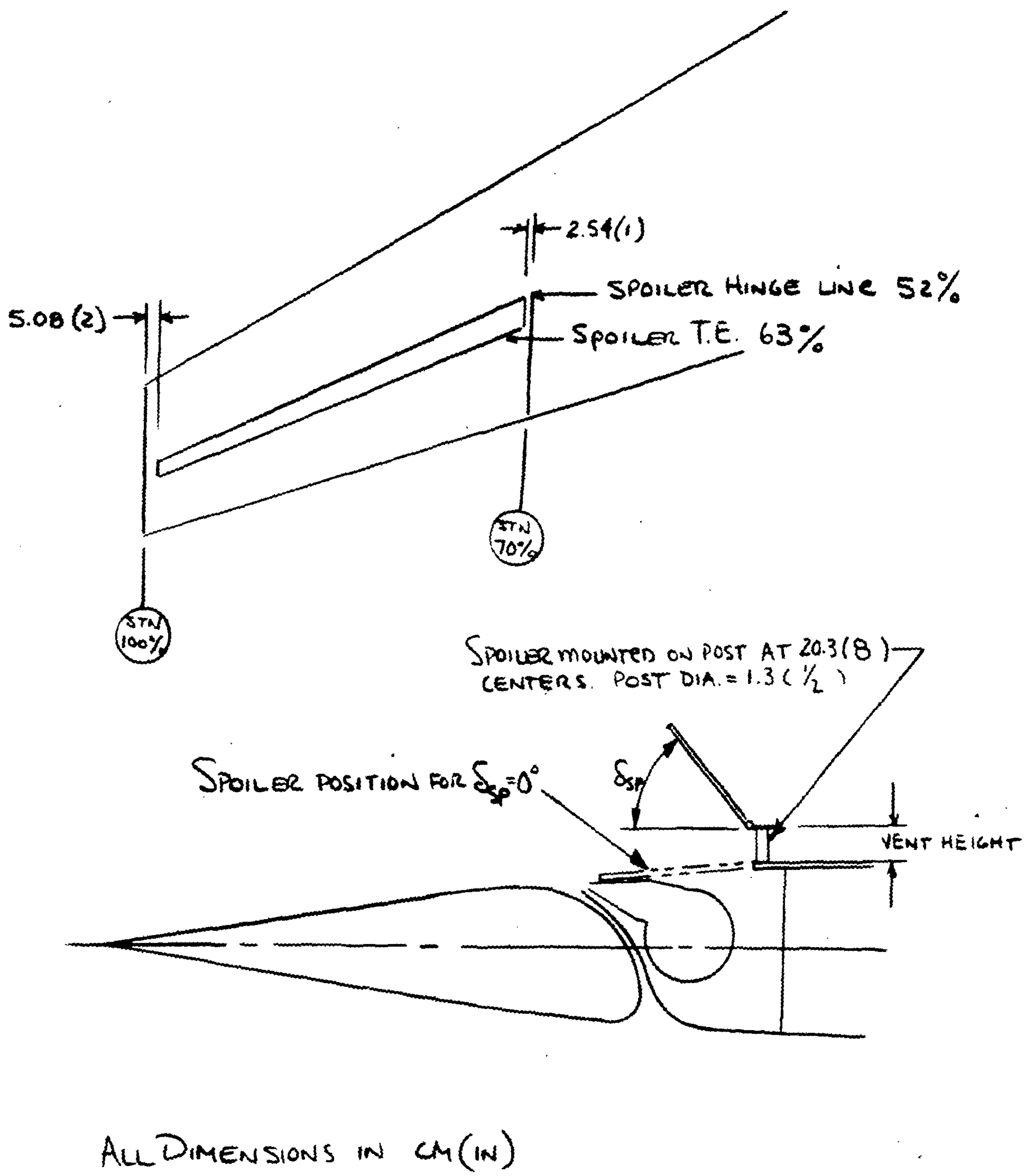

Figure 8.- Geometry of aileron BLC and vented spoiler.

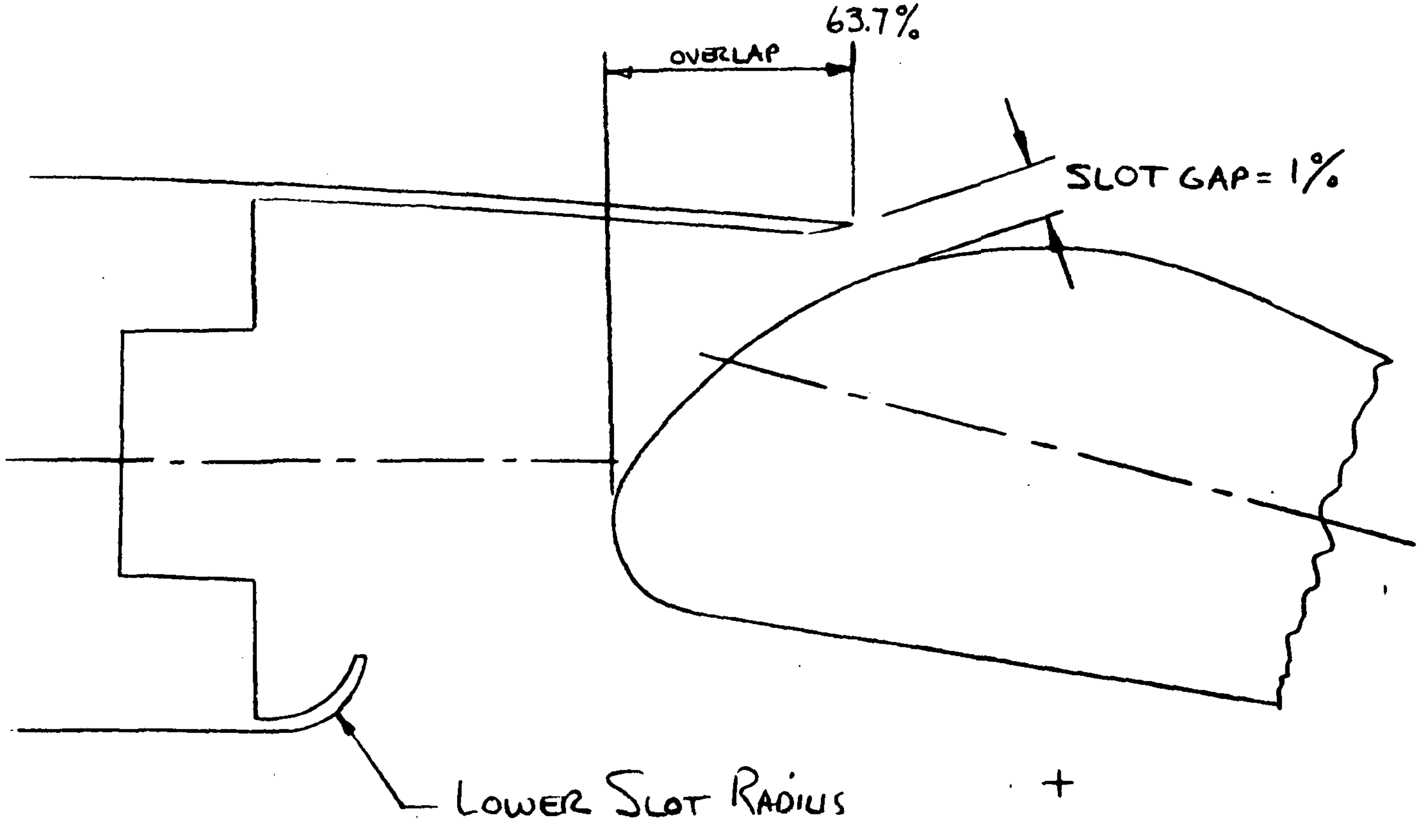

Figure 9.- Slotted aileron geometry.

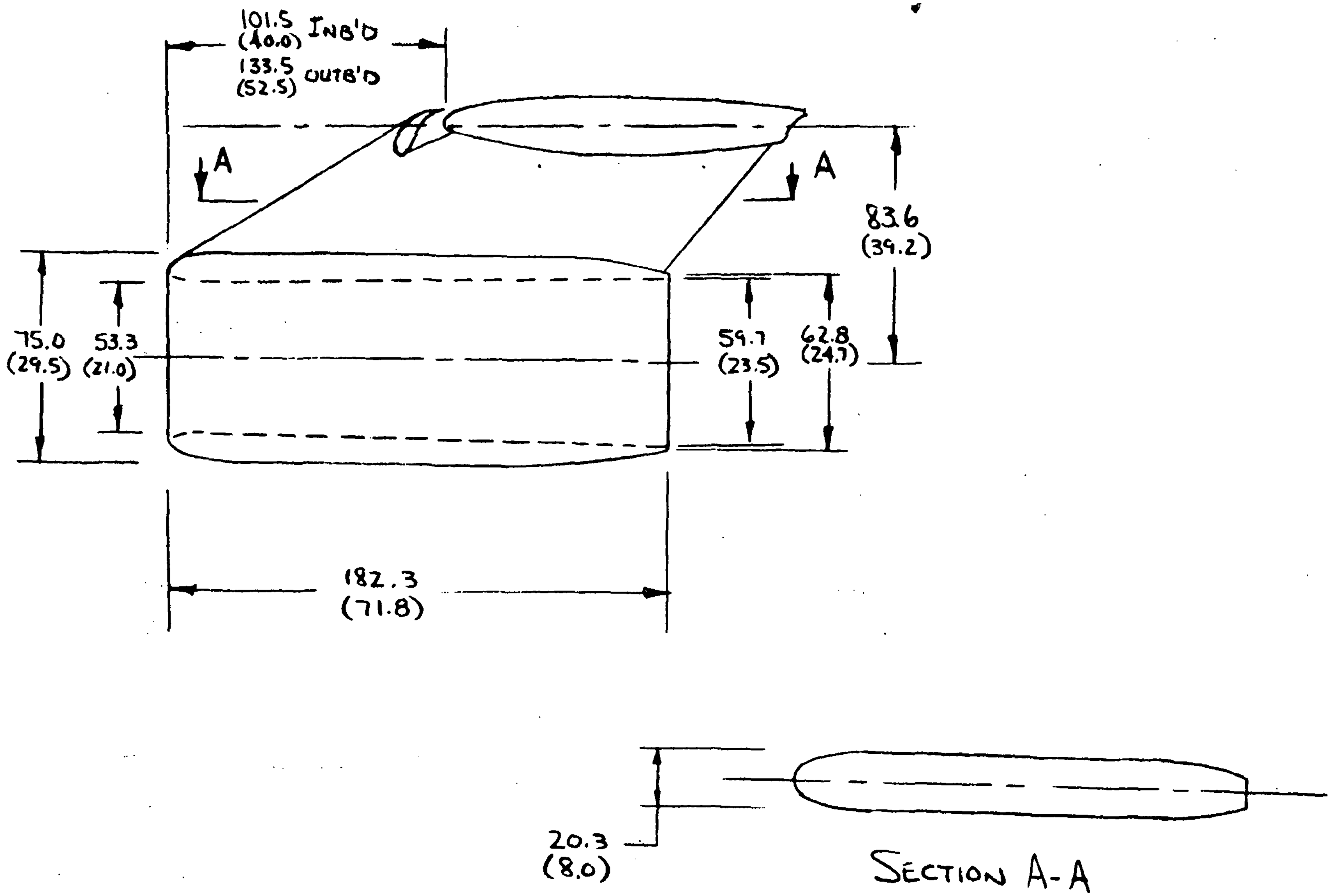

(a) Basic geometry

Figure 10.- Flow-thru nacelle geometry and flow characteristic.

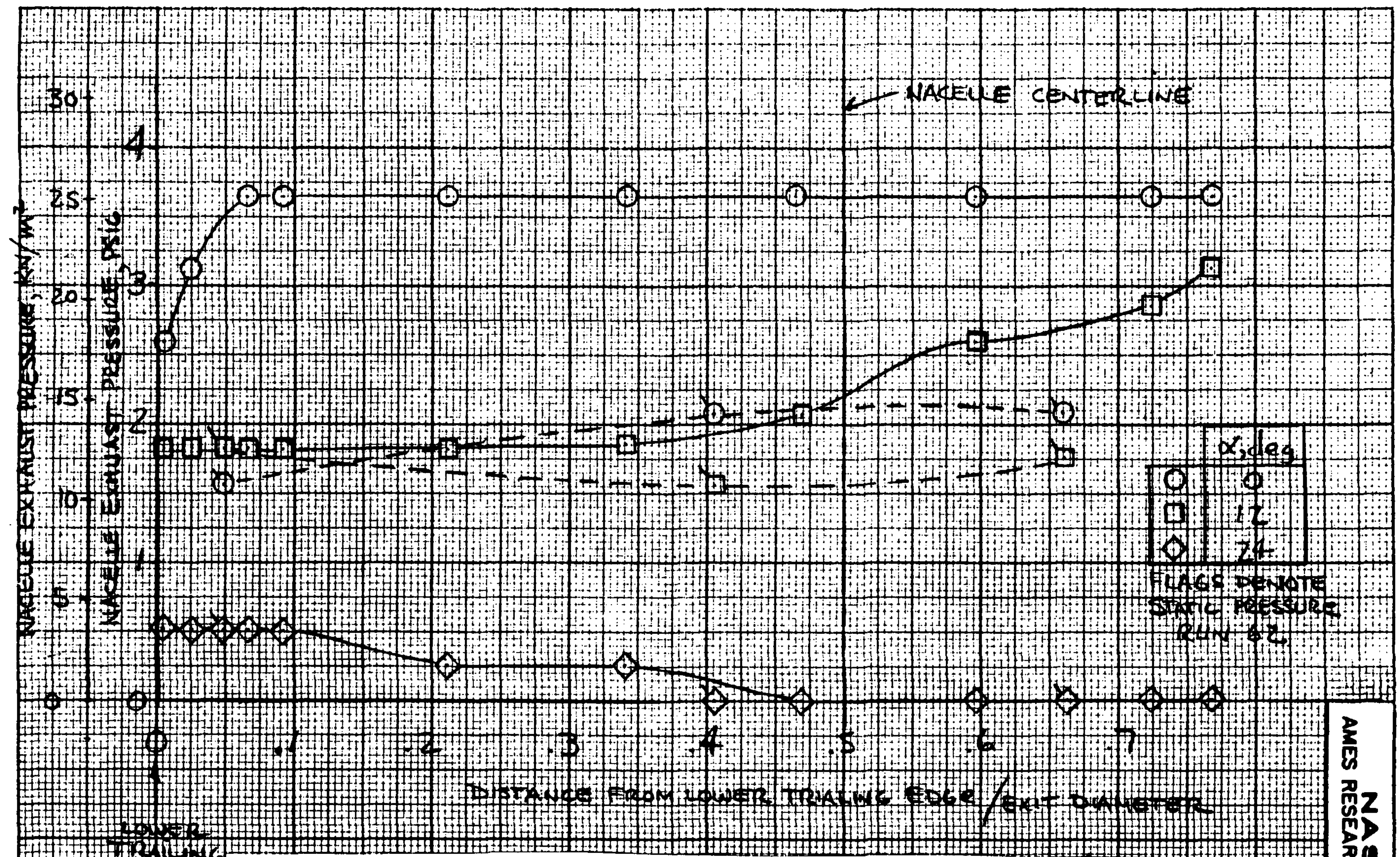

(b) Nacelle exit pressure distribution; $\delta_f = 70°$, $C_{J_I} = 1.1$

Figure 10.- Concluded.

NASA
AMES RESEARCH CENTER

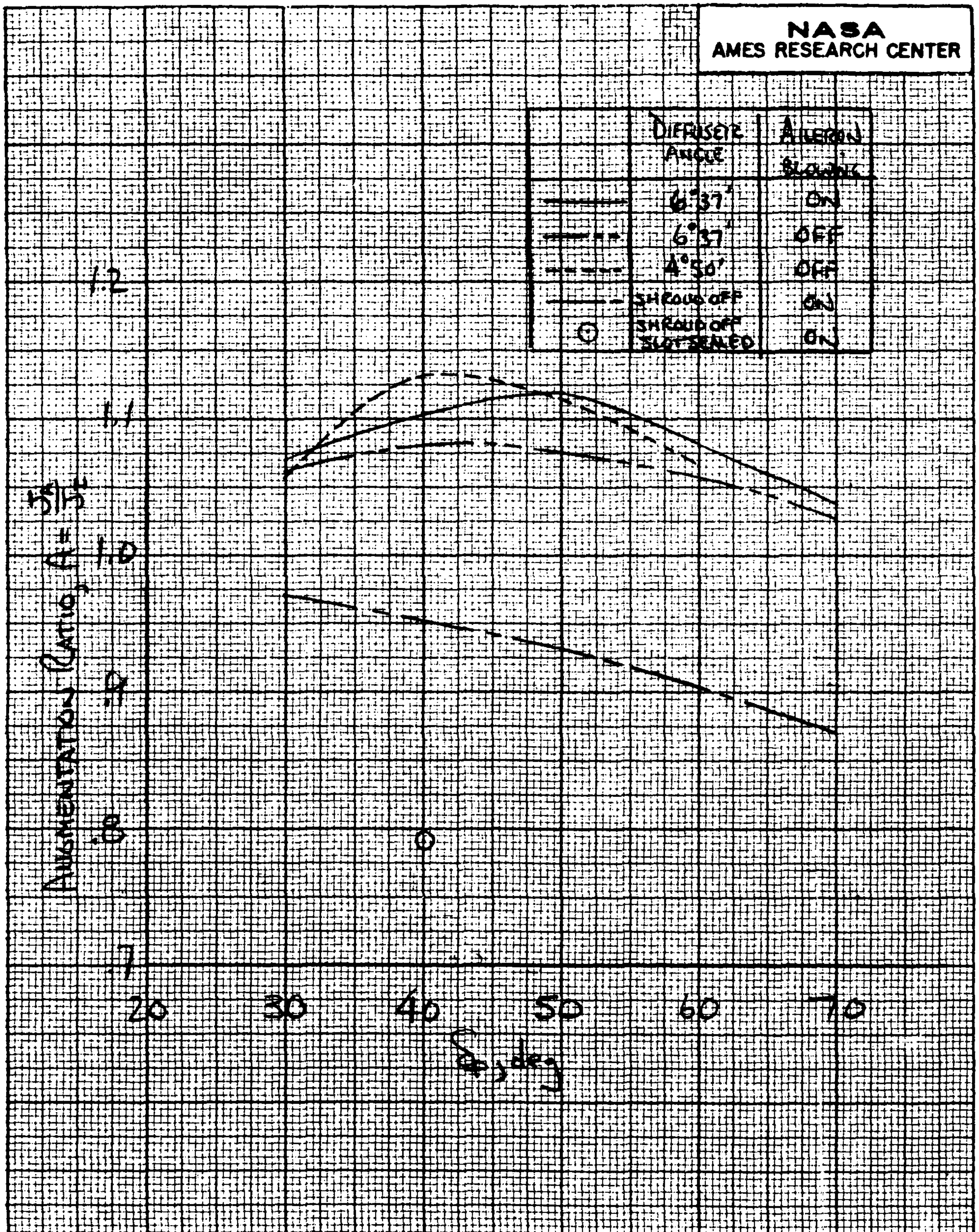

(a) Net augmentation ratio

Figure 11.- Static augmentor wing performance.

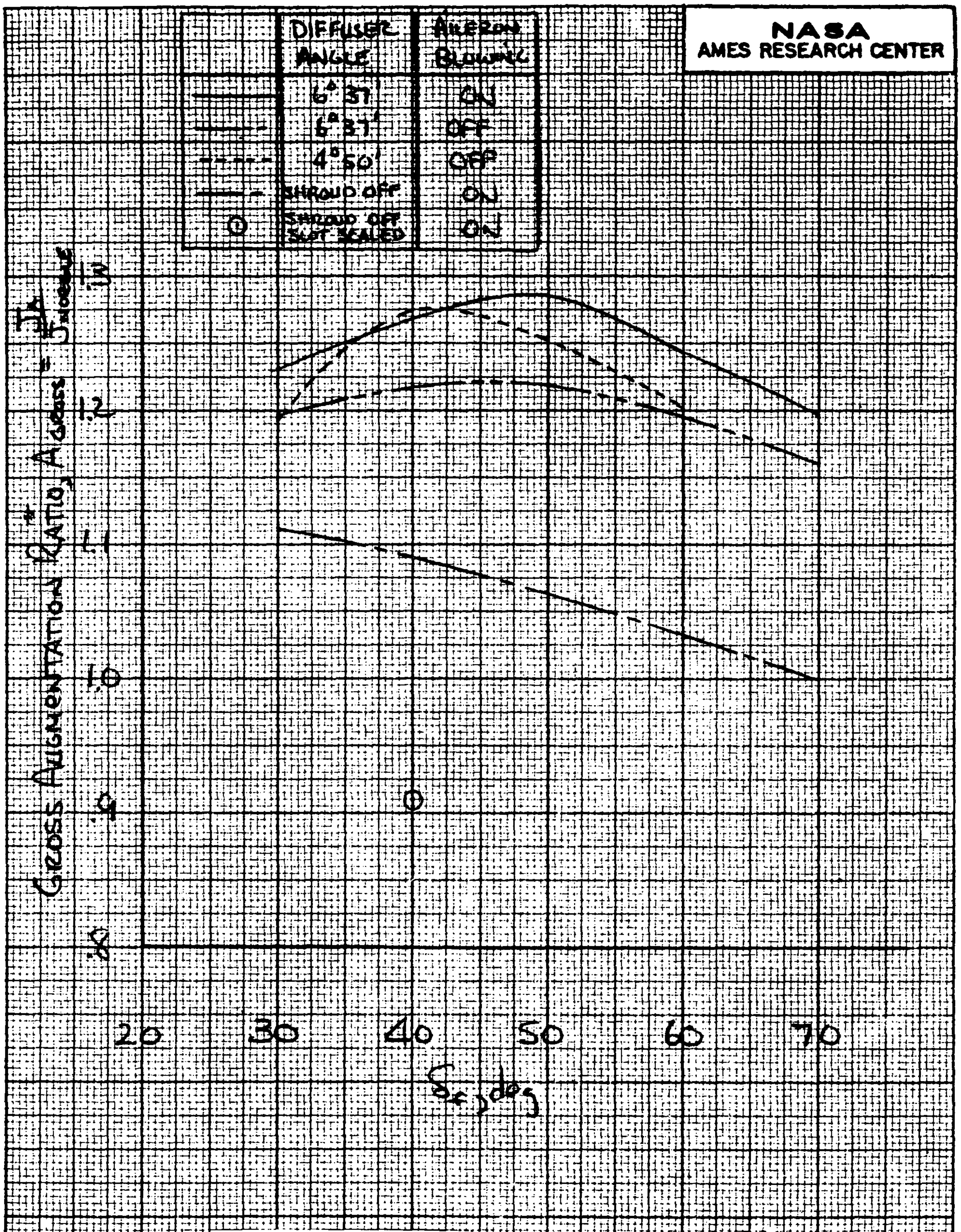

(b) Gross augmentation ratio

Figure 11.- Continued.

11b

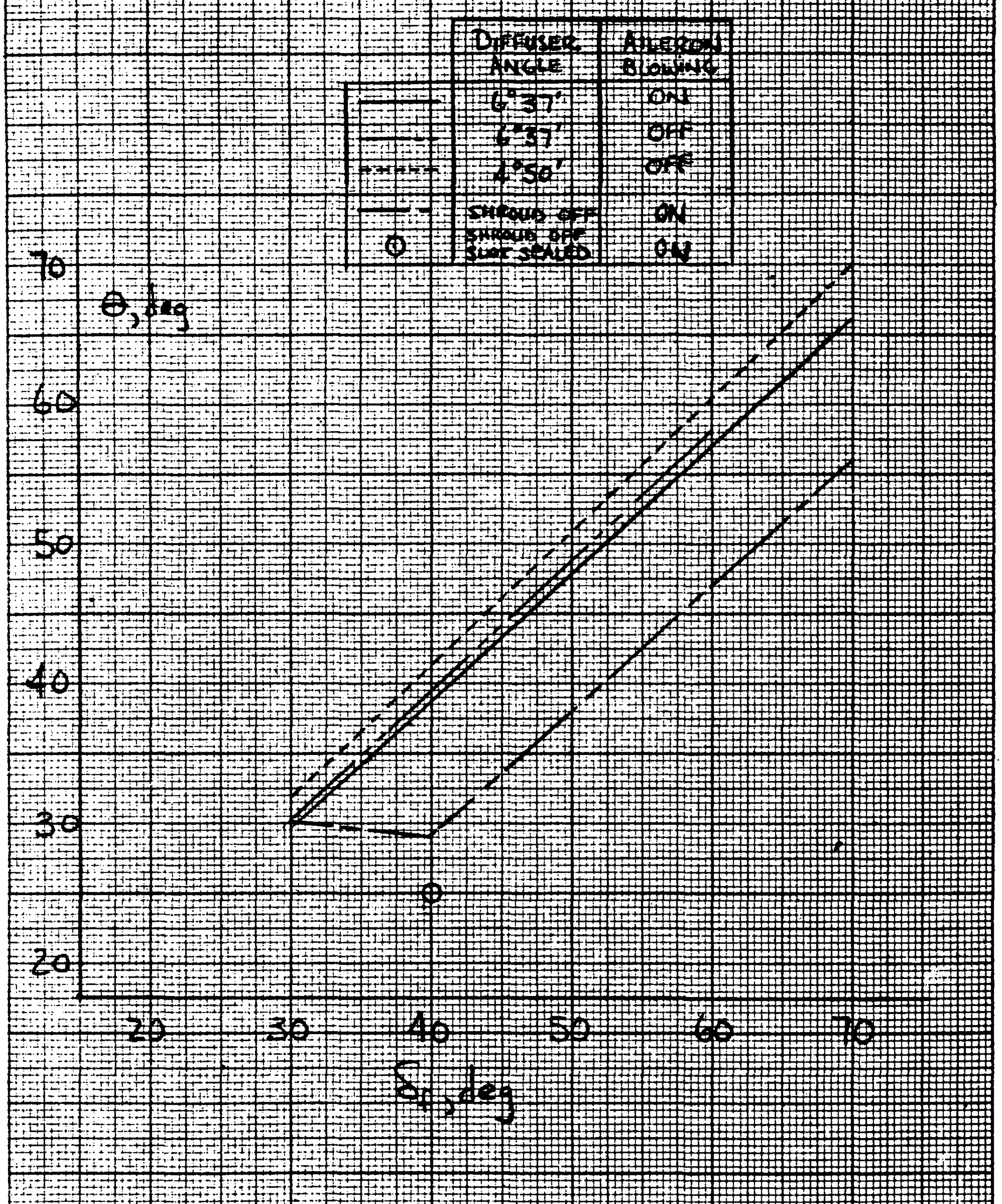

(c) Jet turning

Figure 11.- Concluded.

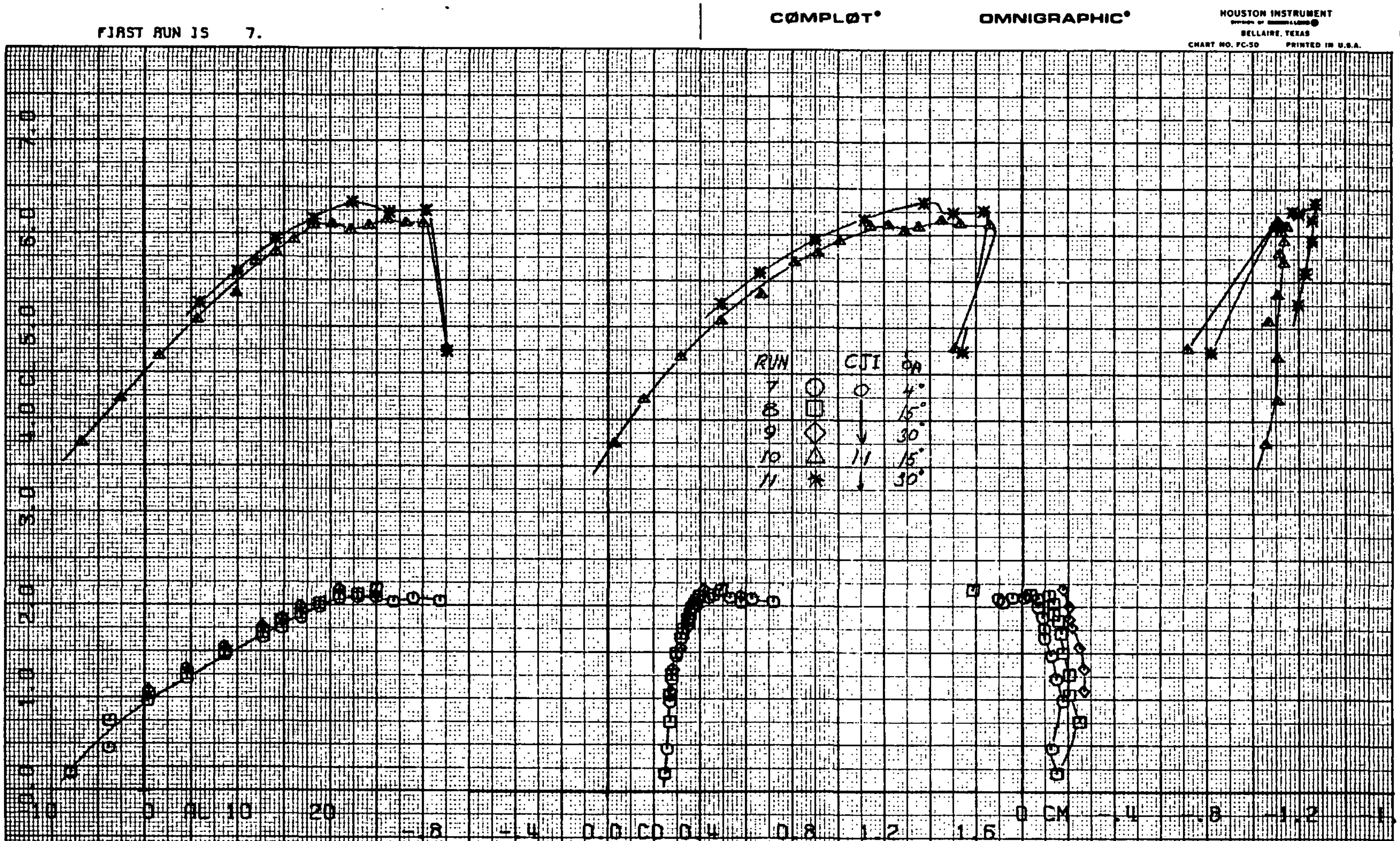

(a) Effect of δ_a and C_{J_z}; $\delta_f = 70°$

Figure 12.- Longitudinal characteristic with a slotted aileron; no tail, vert. fin off.

12a

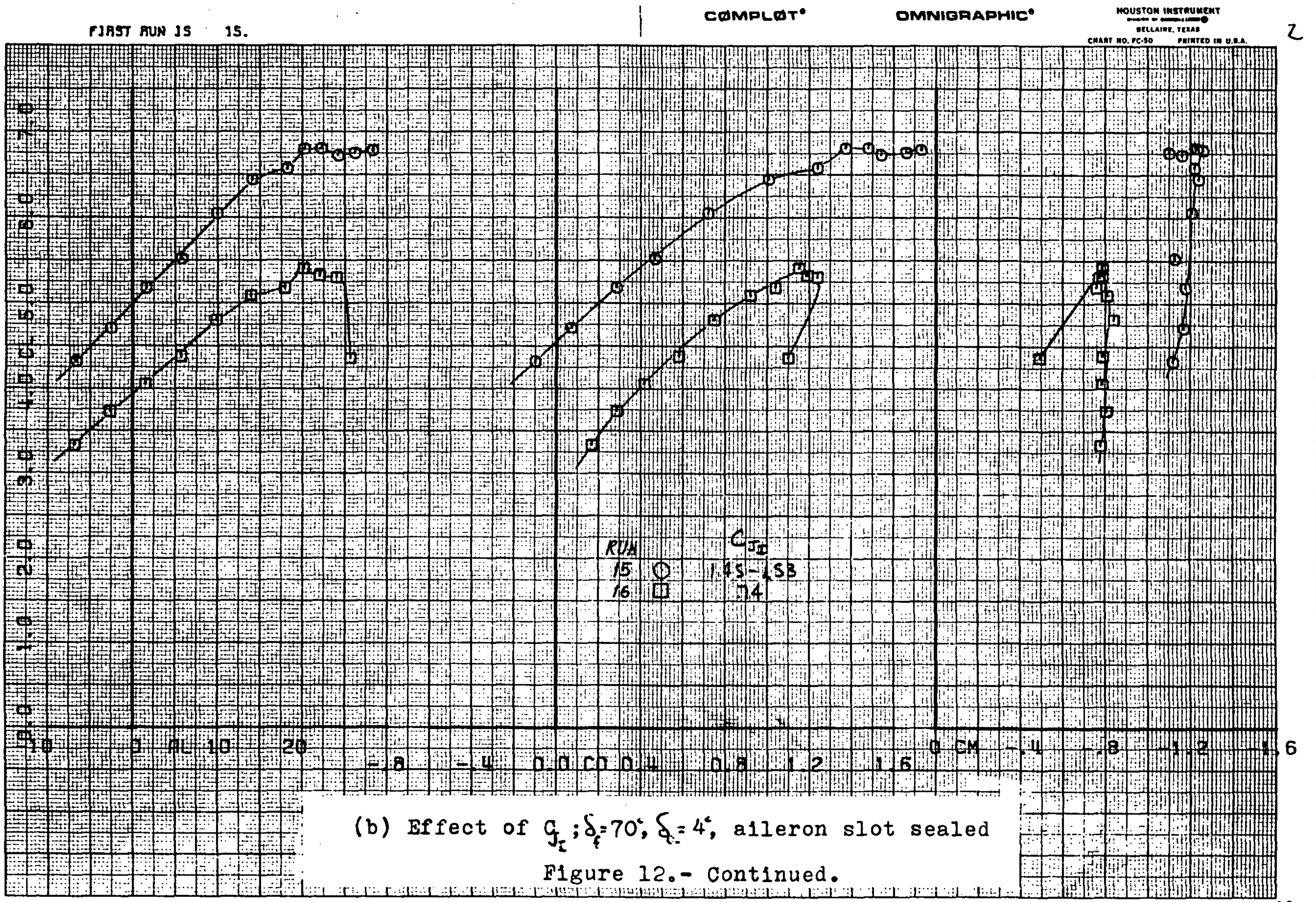

(b) Effect of C_{J_I}; $\delta_f = 70°$, $\delta_a = 4°$, aileron slot sealed

Figure 12.- Continued.

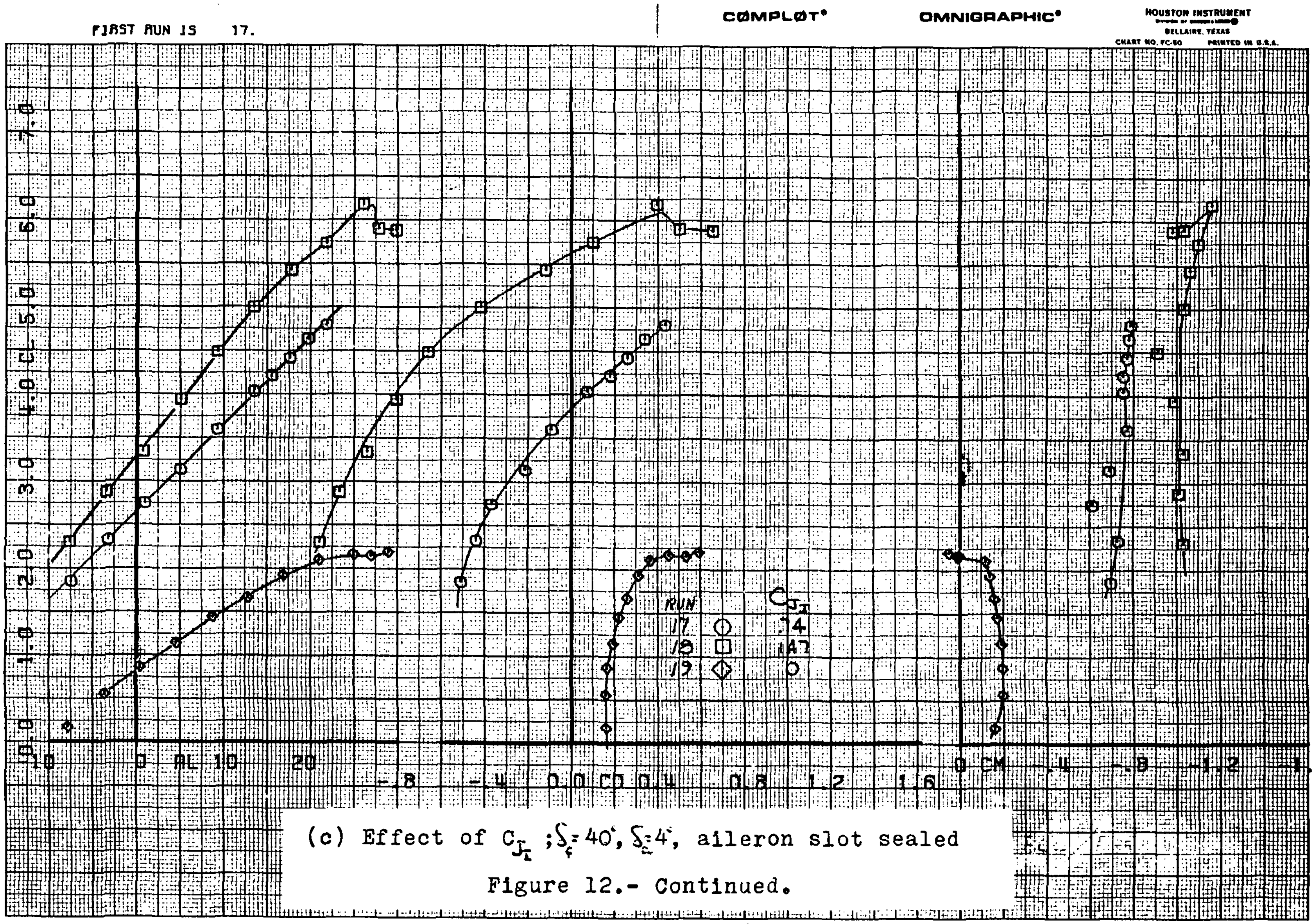

(c) Effect of C_{J_I} ; $\delta_f = 40°$, $\delta_a = 4°$, aileron slot sealed

Figure 12.- Continued.

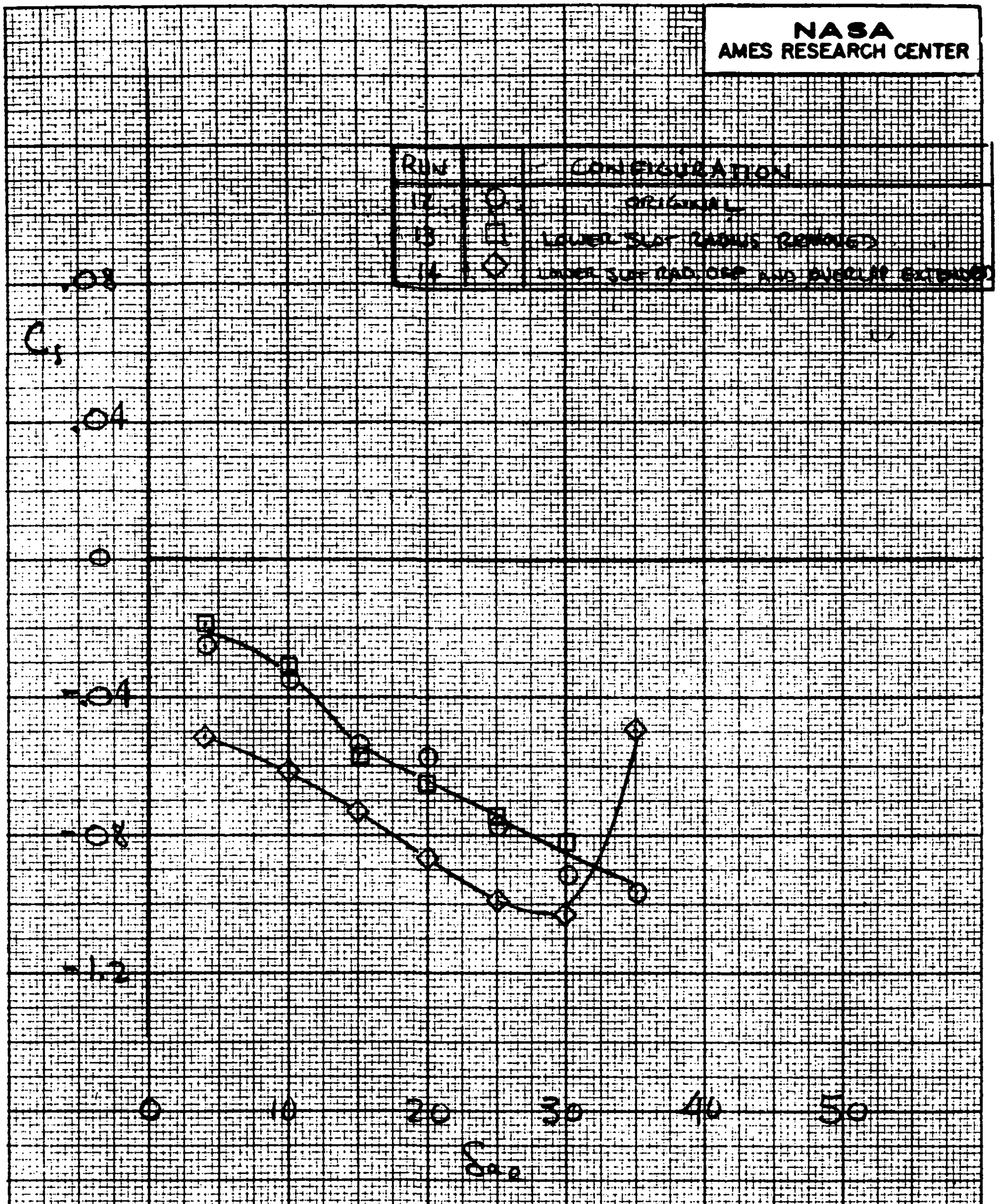

(d) Aileron control effectiveness; δ_f = 70°, C_J = 1.1, α = 0°

Figure 12.- Continued.

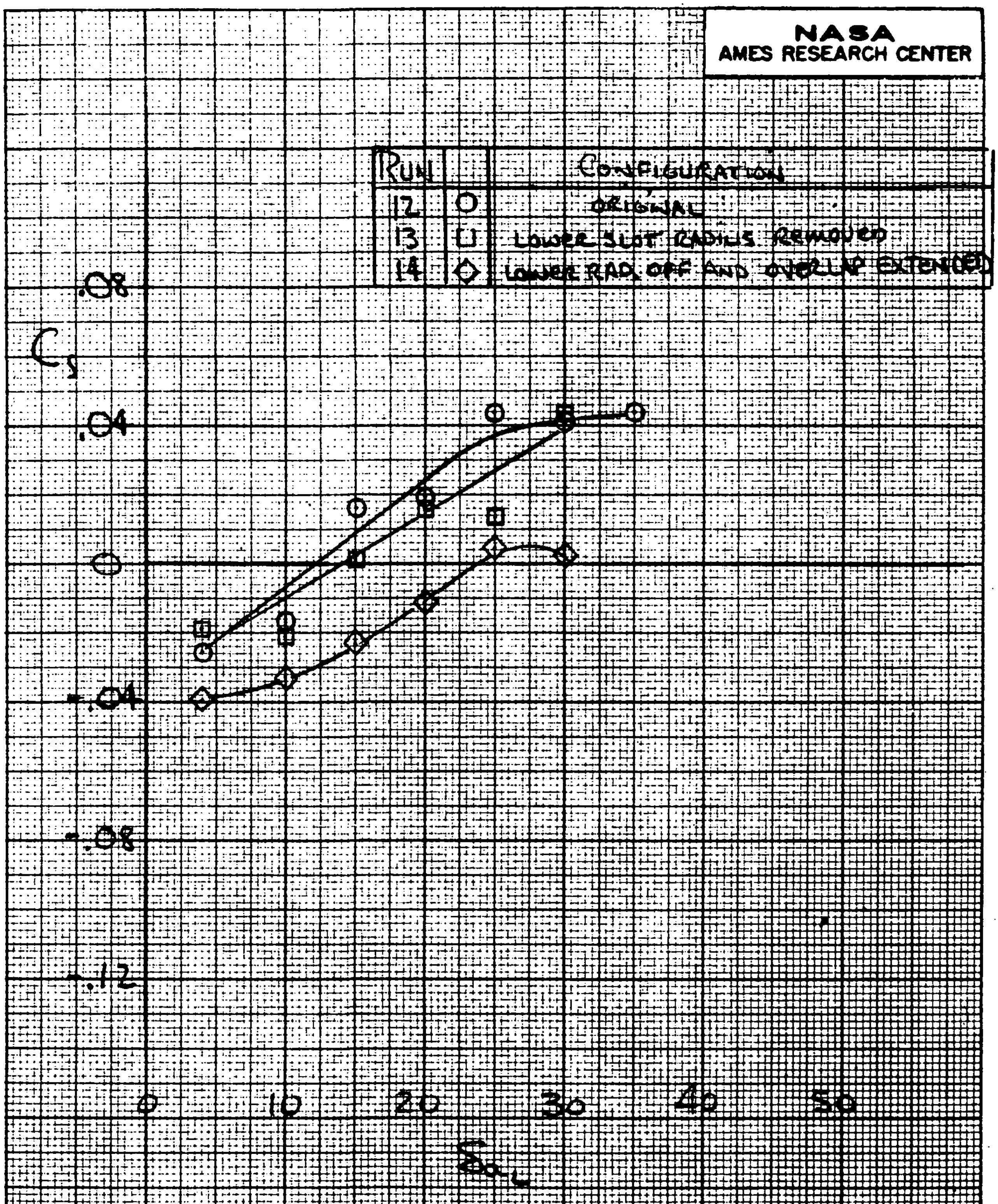

(e) Aileron control effectiveness; $\delta_f = 70°$, $C_{J_T} = 1.1$, $\alpha = 0°$

Figure 12.- Continued.

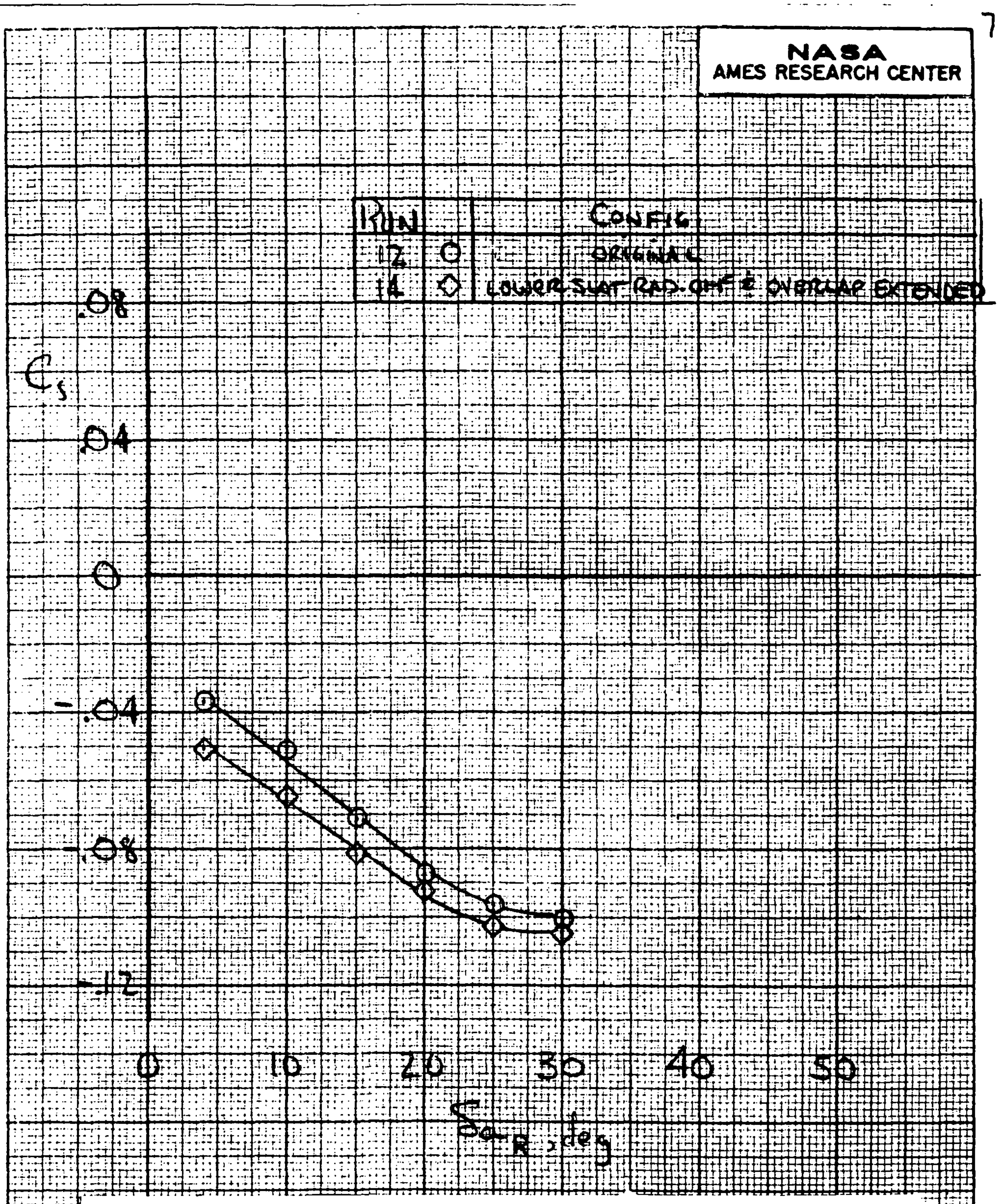

(f) Aileron control effectiveness; $\delta_f = 70°$, $C_{J_T} = 1.1$, $\alpha = 12°$

Figure 12.- Concluded.

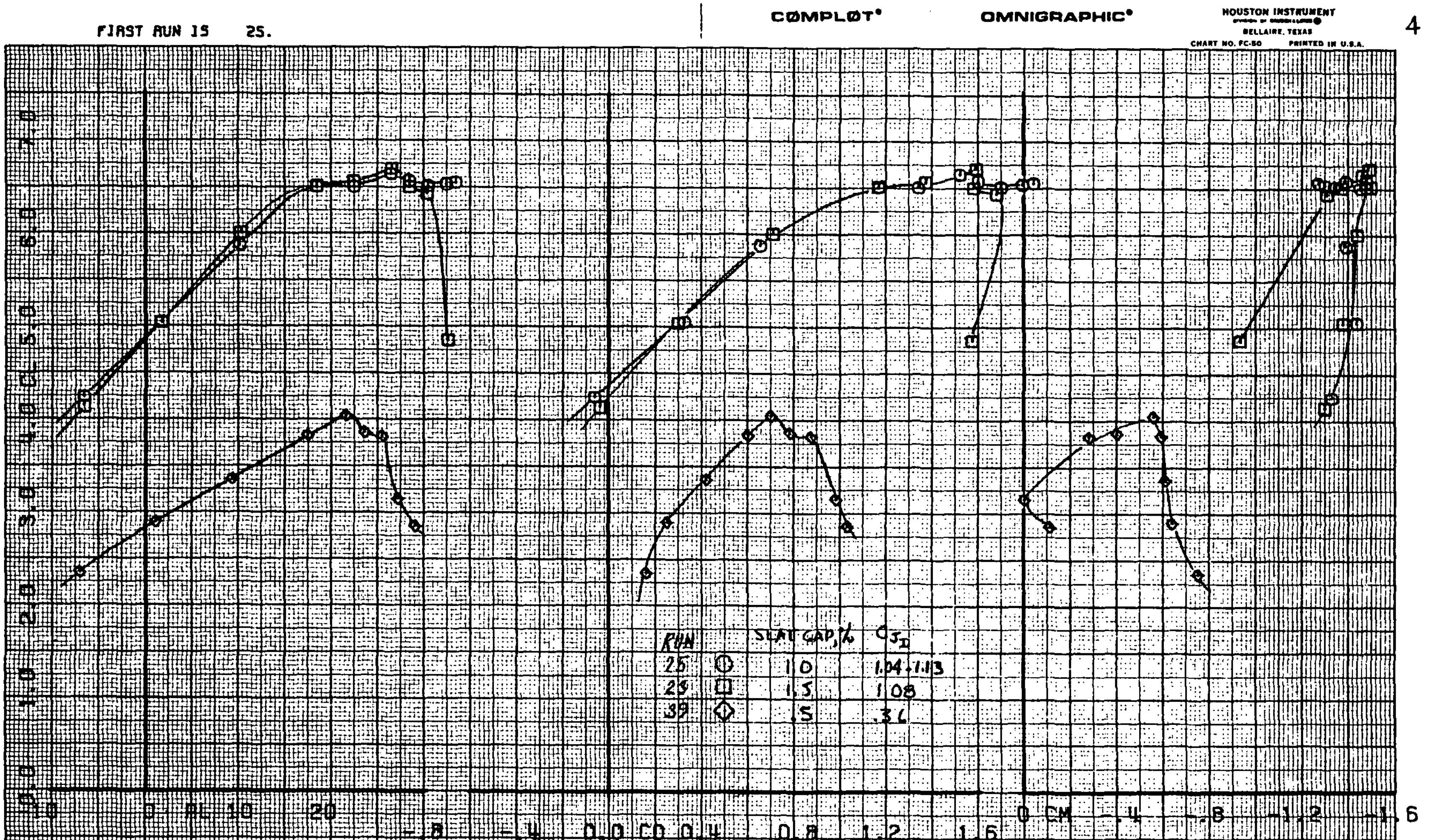

(a) Effect of slat gap

Figure 13.- Longitudinal characteristic for various wing leading edge slat gaps; $\delta_f = 70°$, no tail, vert. fin off.

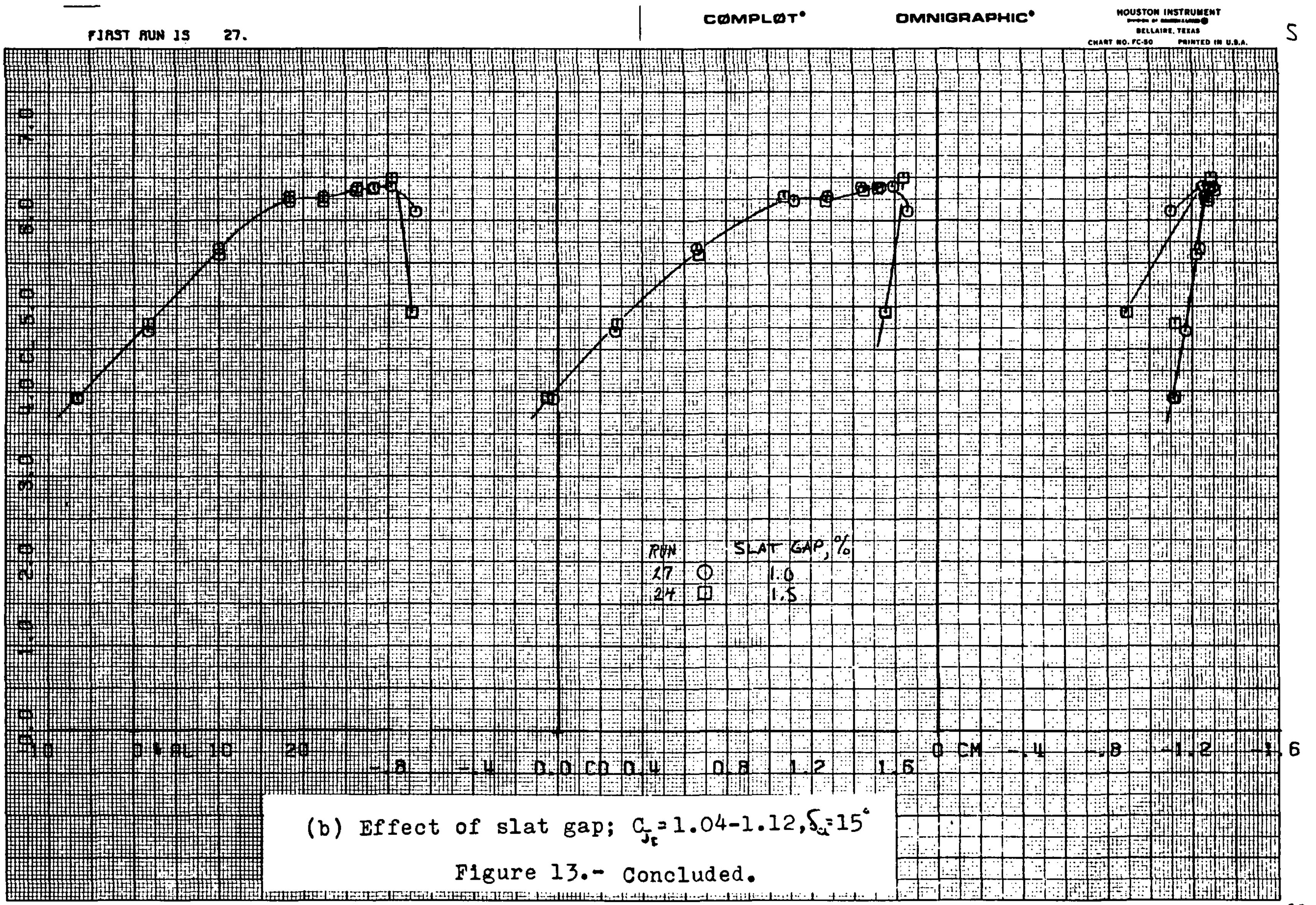

(b) Effect of slat gap; C_{J_E}=1.04-1.12, δ_a=15°

Figure 13.- Concluded.

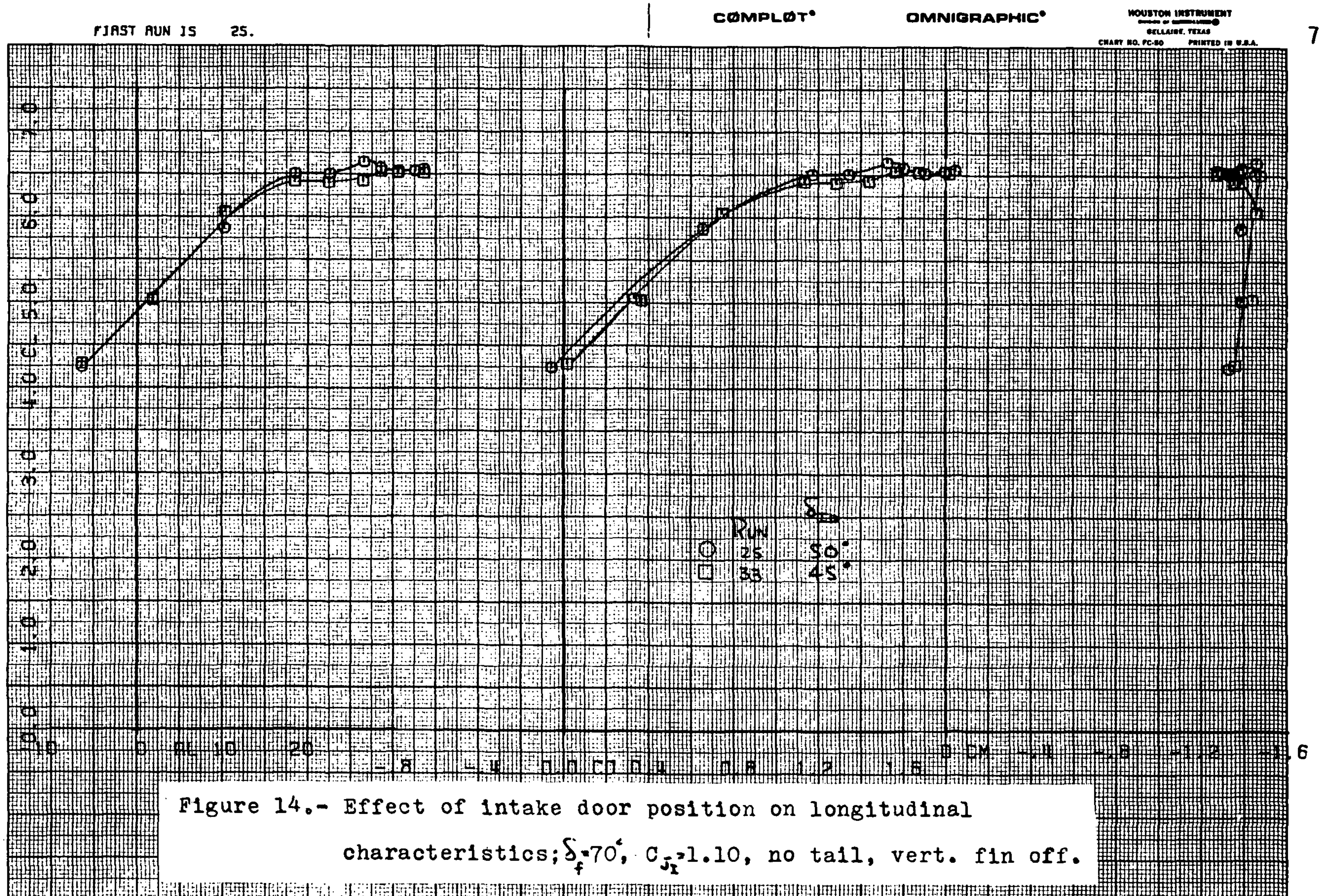

Figure 14.- Effect of intake door position on longitudinal characteristics; $\delta_f = 70°$, $C_{J_T} = 1.10$, no tail, vert. fin off.

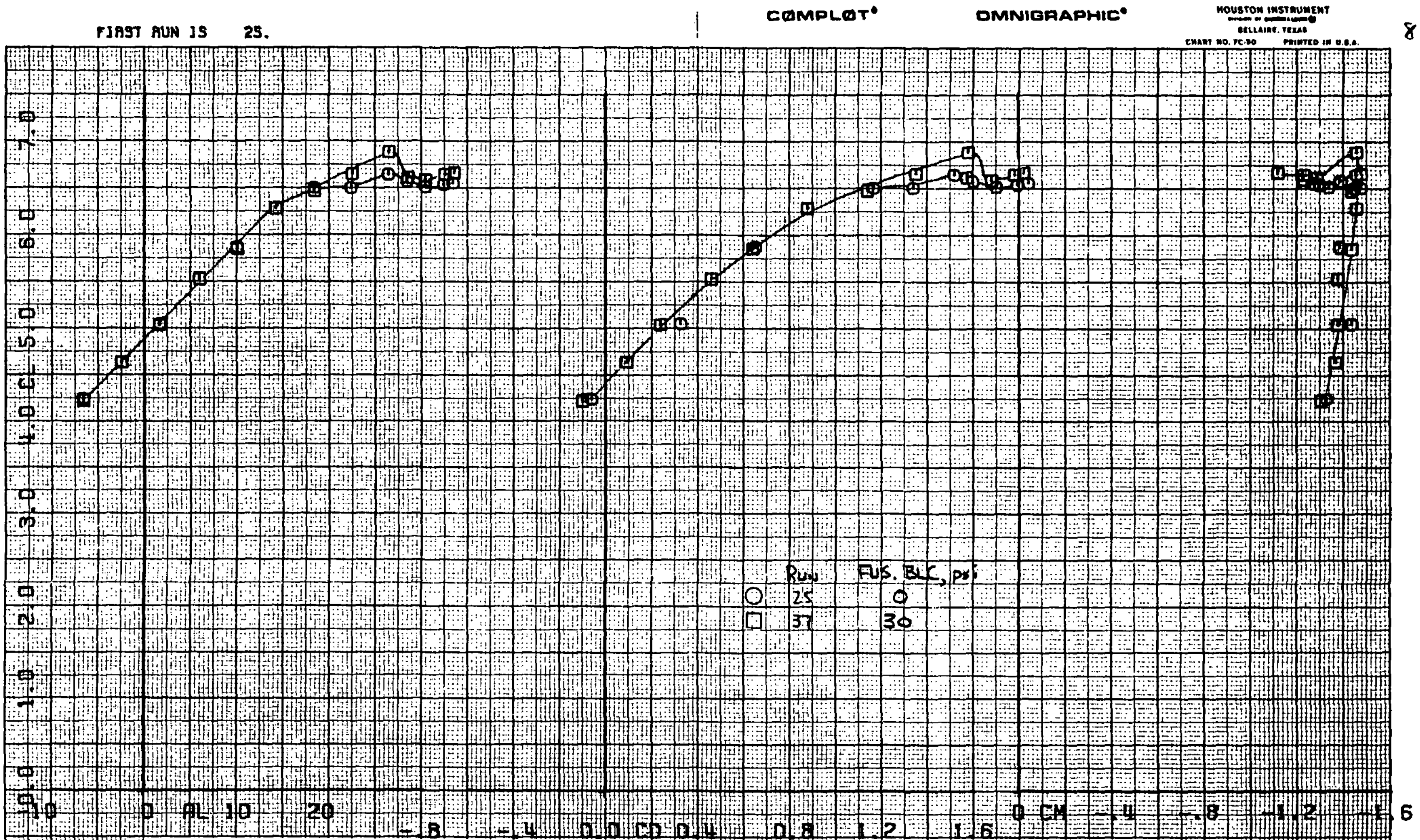

(a) C_{J_I}=1.04-1.13

Figure 15.- Effect of fuselage BLC on longitudinal characteristic;

δ_f=70°, no tail, vert. fin off.

15a

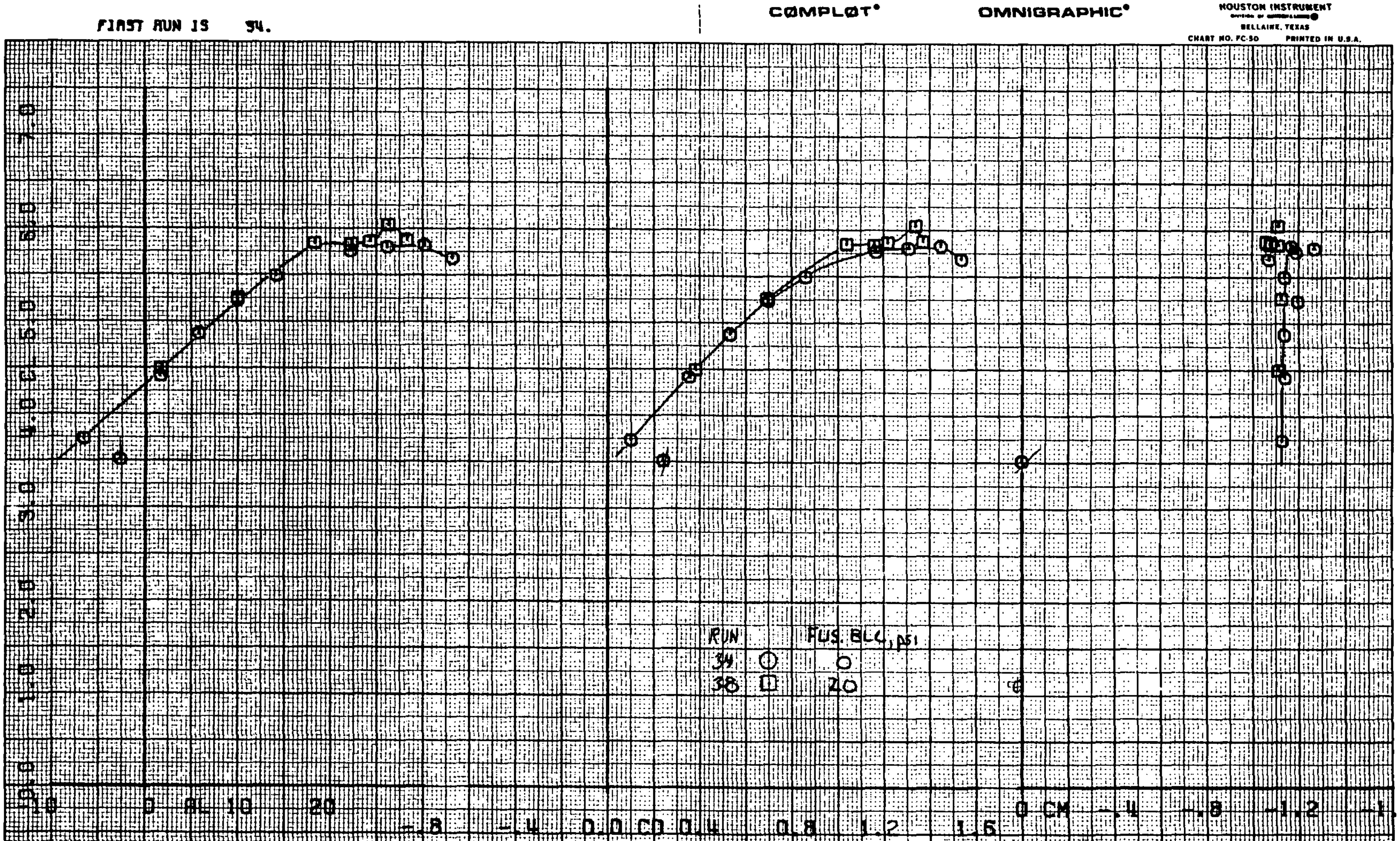

(b) $C_{J_I} = .76$

Figure 15.- Concluded.

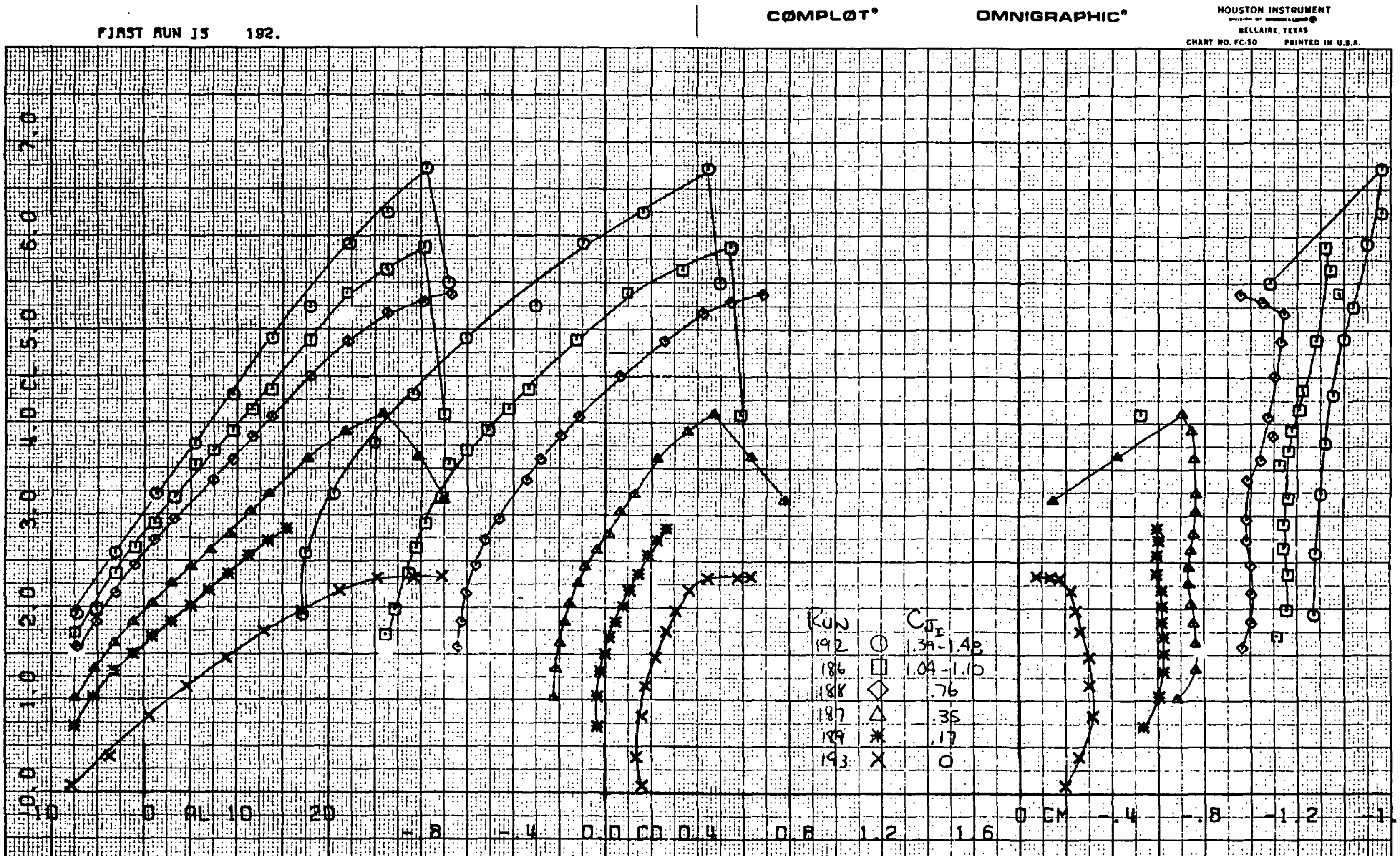

(a) Effect of C_{J_I}

Figure 16.- Longitudinal characteristic; δ_f=30°, no tail.

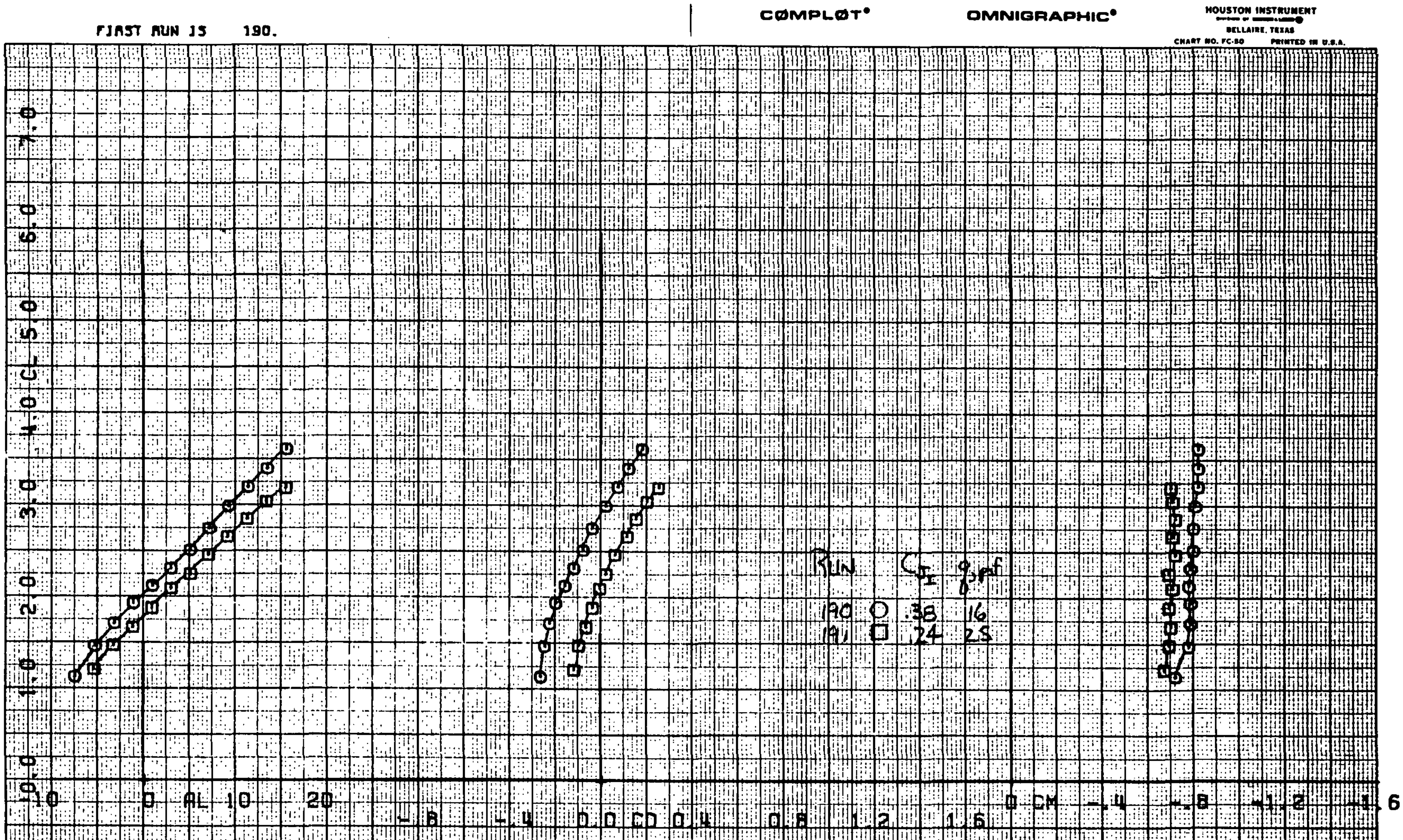

(b) q=16 and 25psf

Figure 16.- Continued.

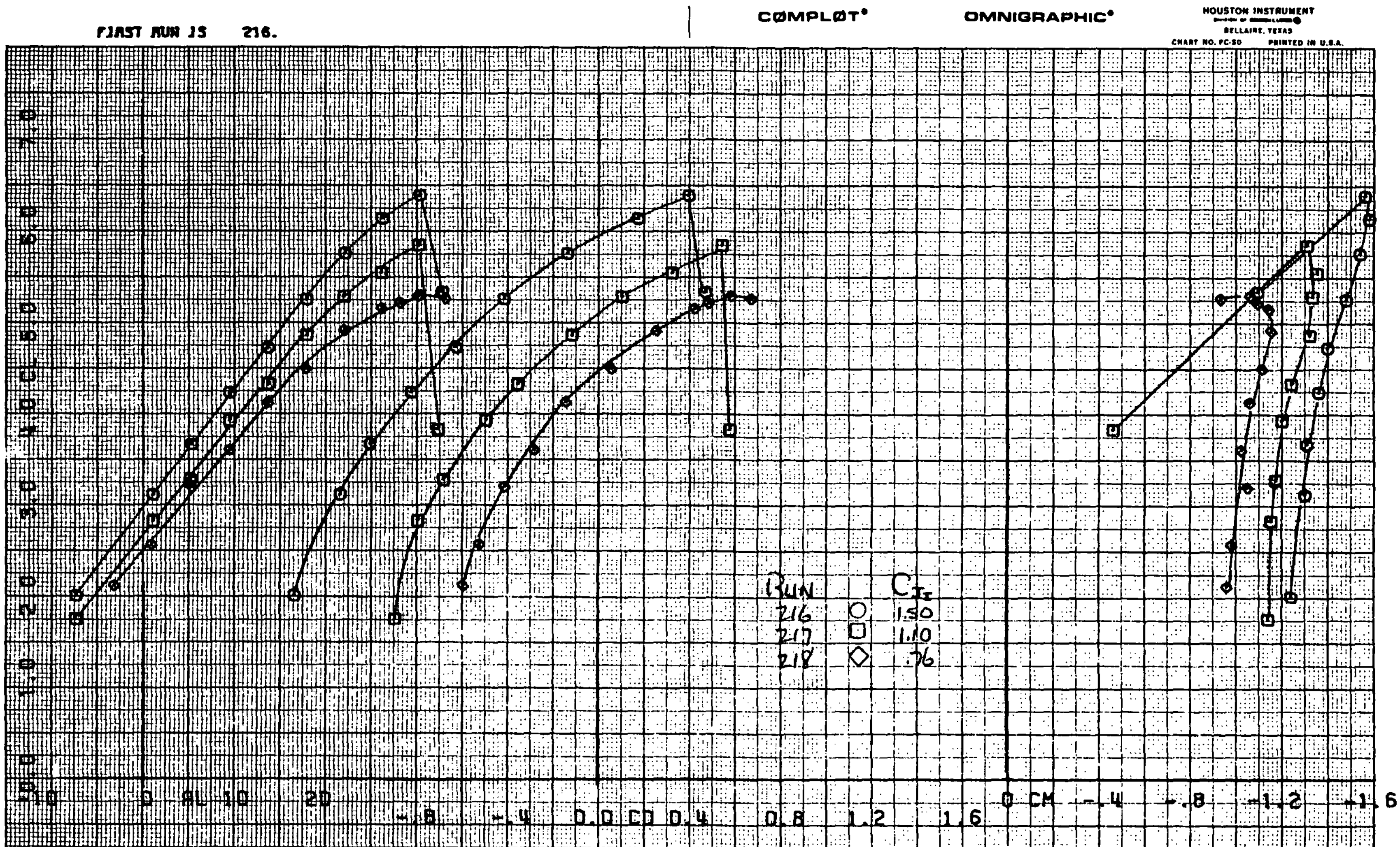

(c) Shroud and intake door off

Figure 16.- Concluded.

33

16c

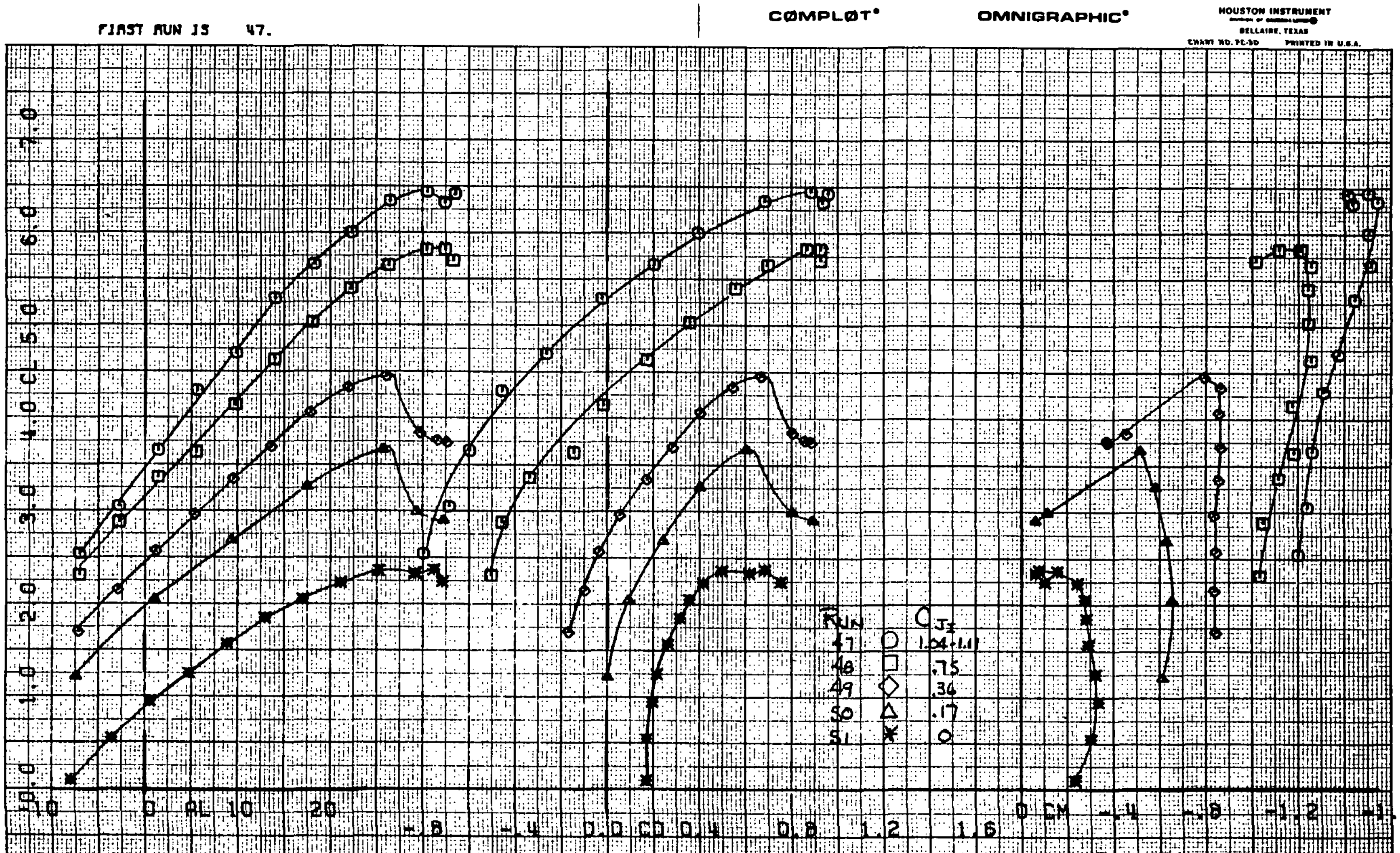

(a) No tail and vert. fin off

Figure 17.- Longitudinal characteristic; $\delta_f = 40°$.

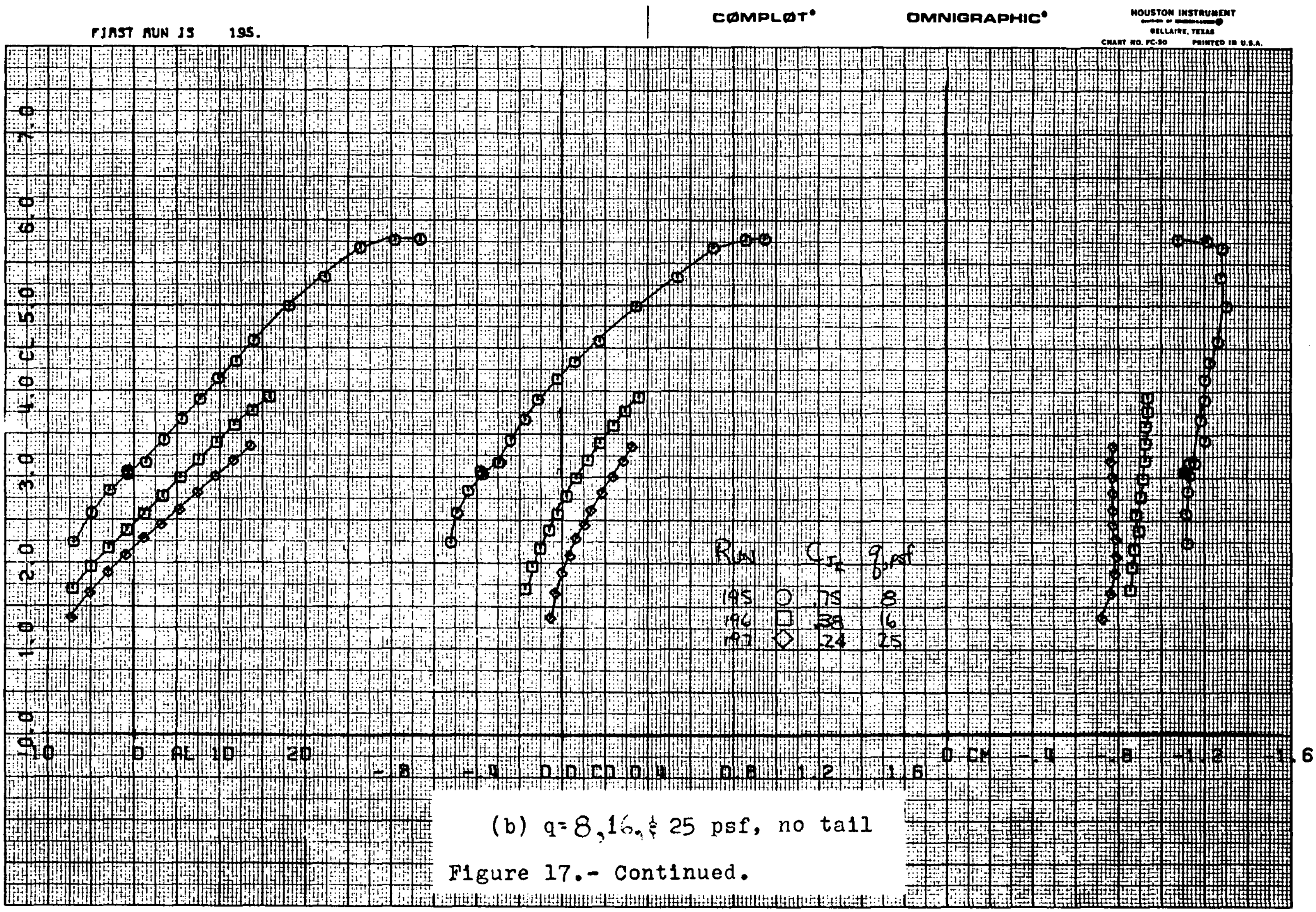

(b) q=8,16,& 25 psf, no tail

Figure 17.- Continued.

15

176

90

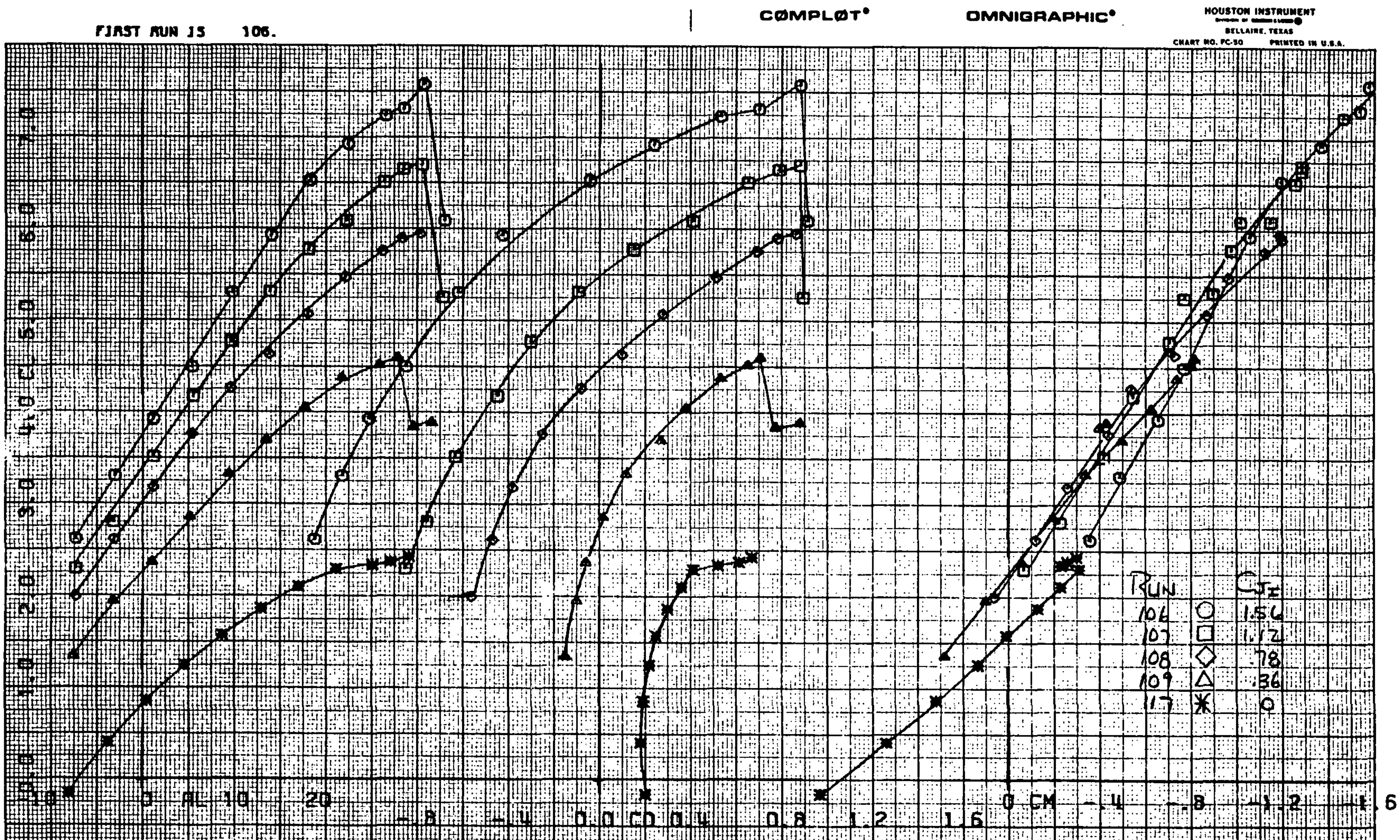

(c) High tail

Figure 17.- Continued.

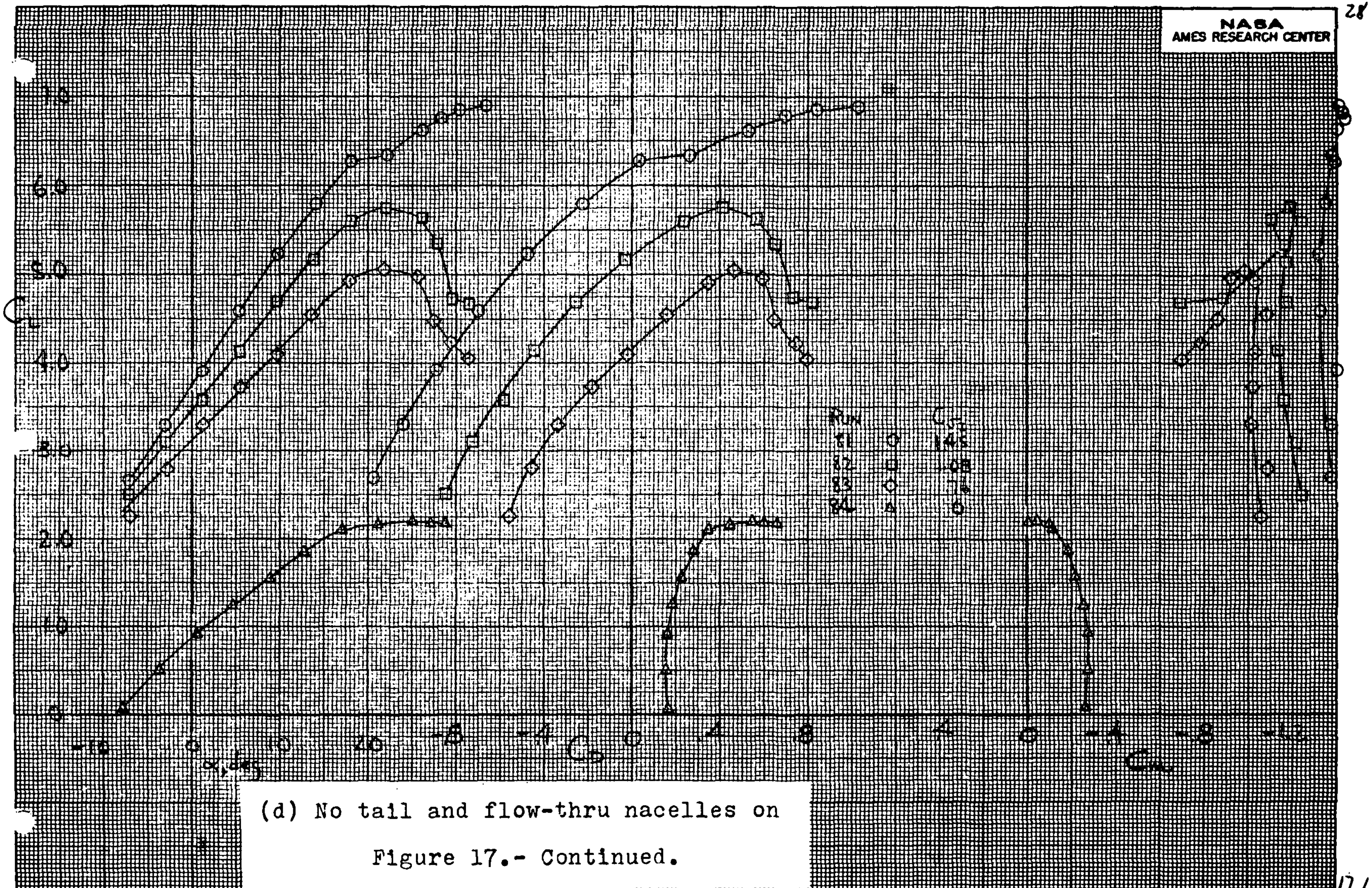

(d) No tail and flow-thru nacelles on

Figure 17.- Continued.

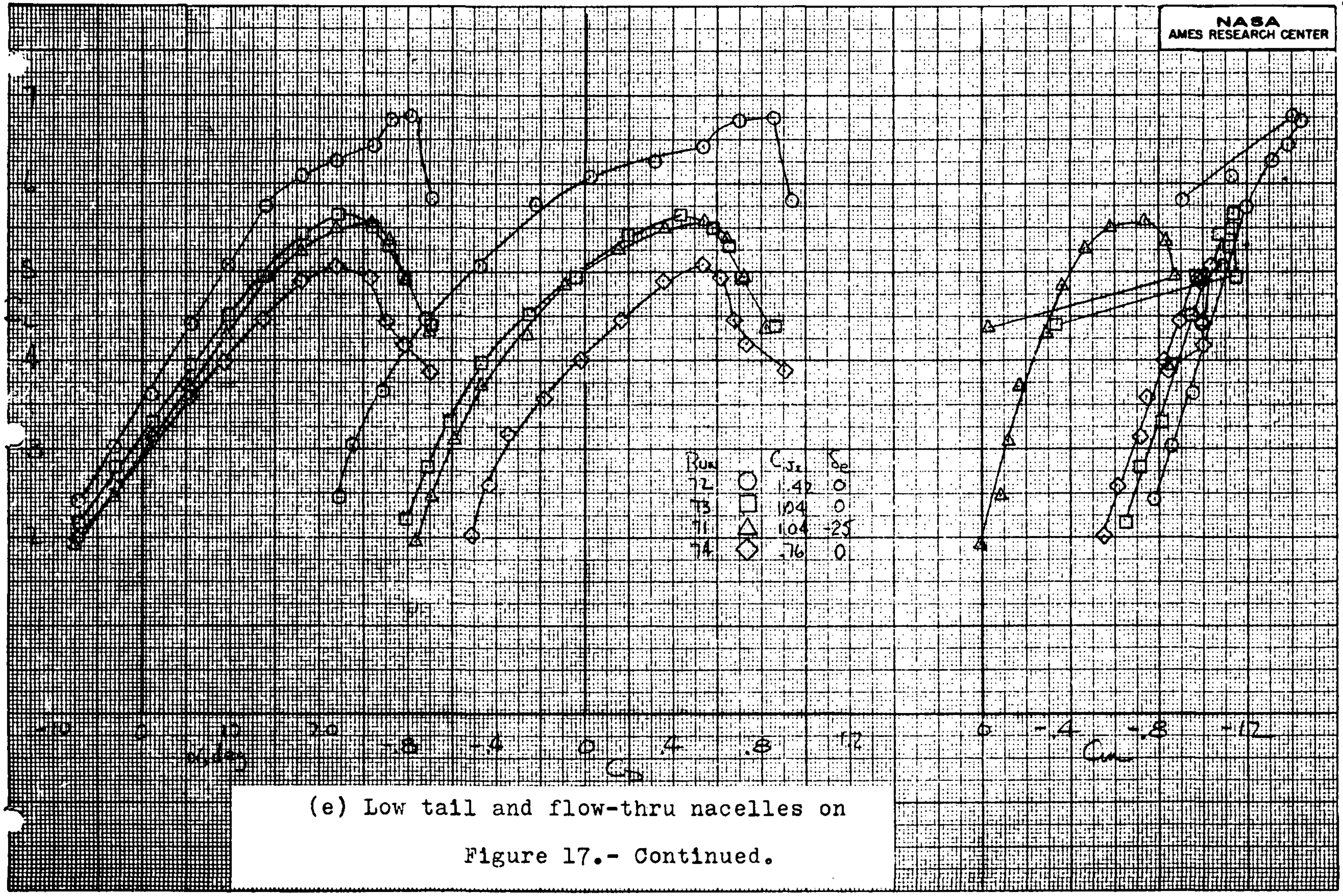

(e) Low tail and flow-thru nacelles on

Figure 17.- Continued.

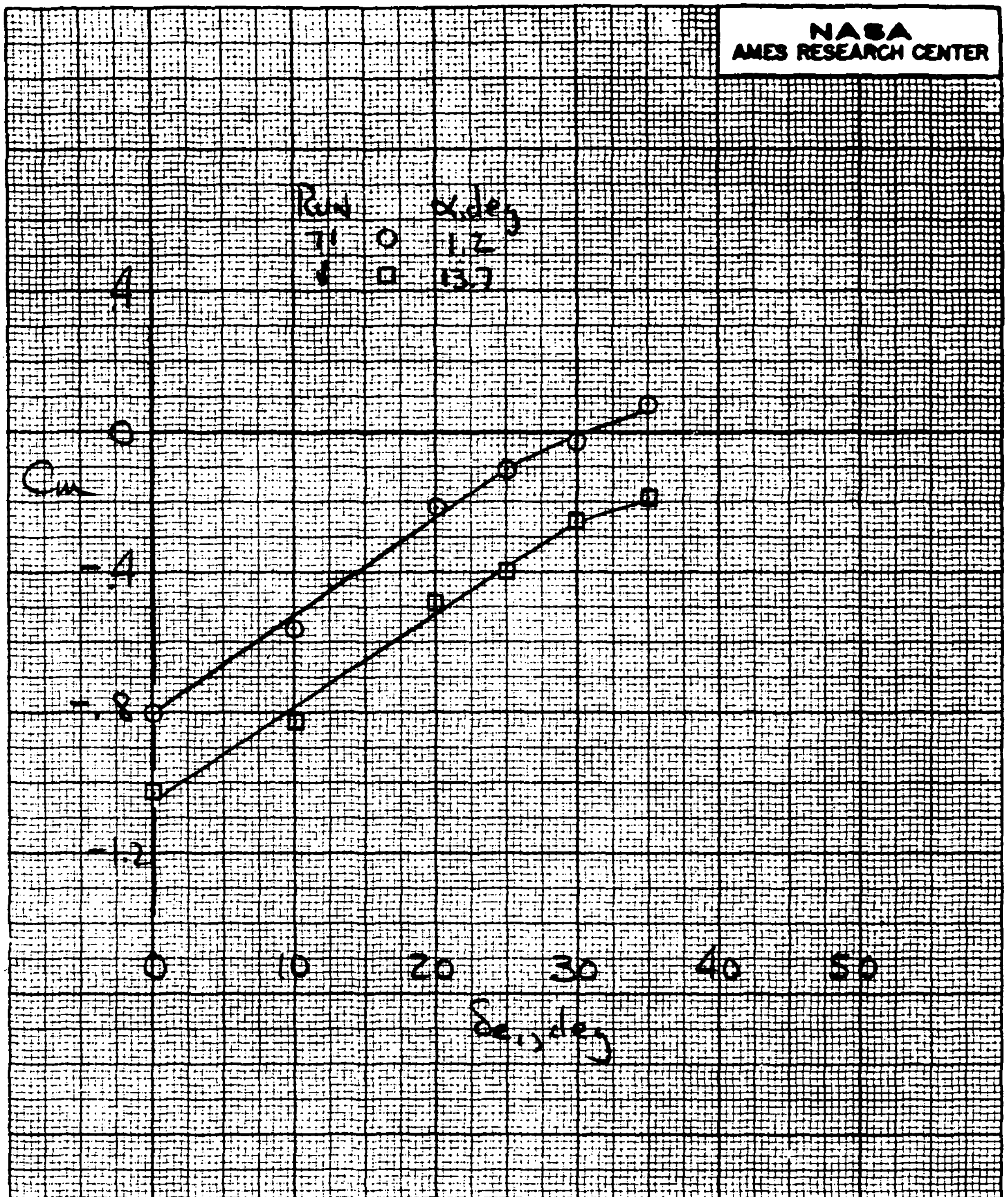

(f) Elevator control effectiveness; low tail and flow-thru nacelles on, $C_{J_2} = 1.1$, $\delta_{e_2} = 0°$

Figure 17.- Continued.

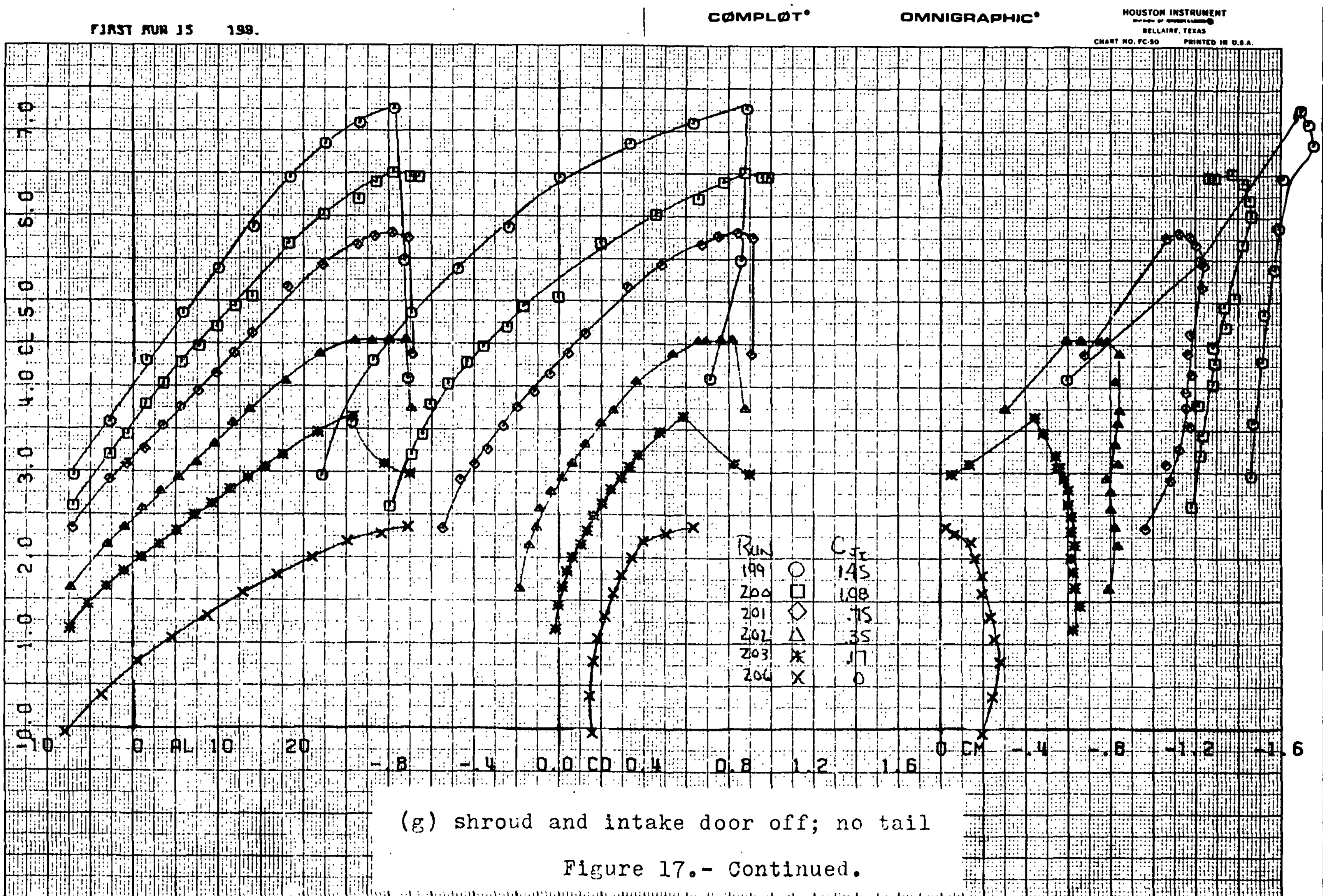

(g) shroud and intake door off; no tail

Figure 17.- Continued.

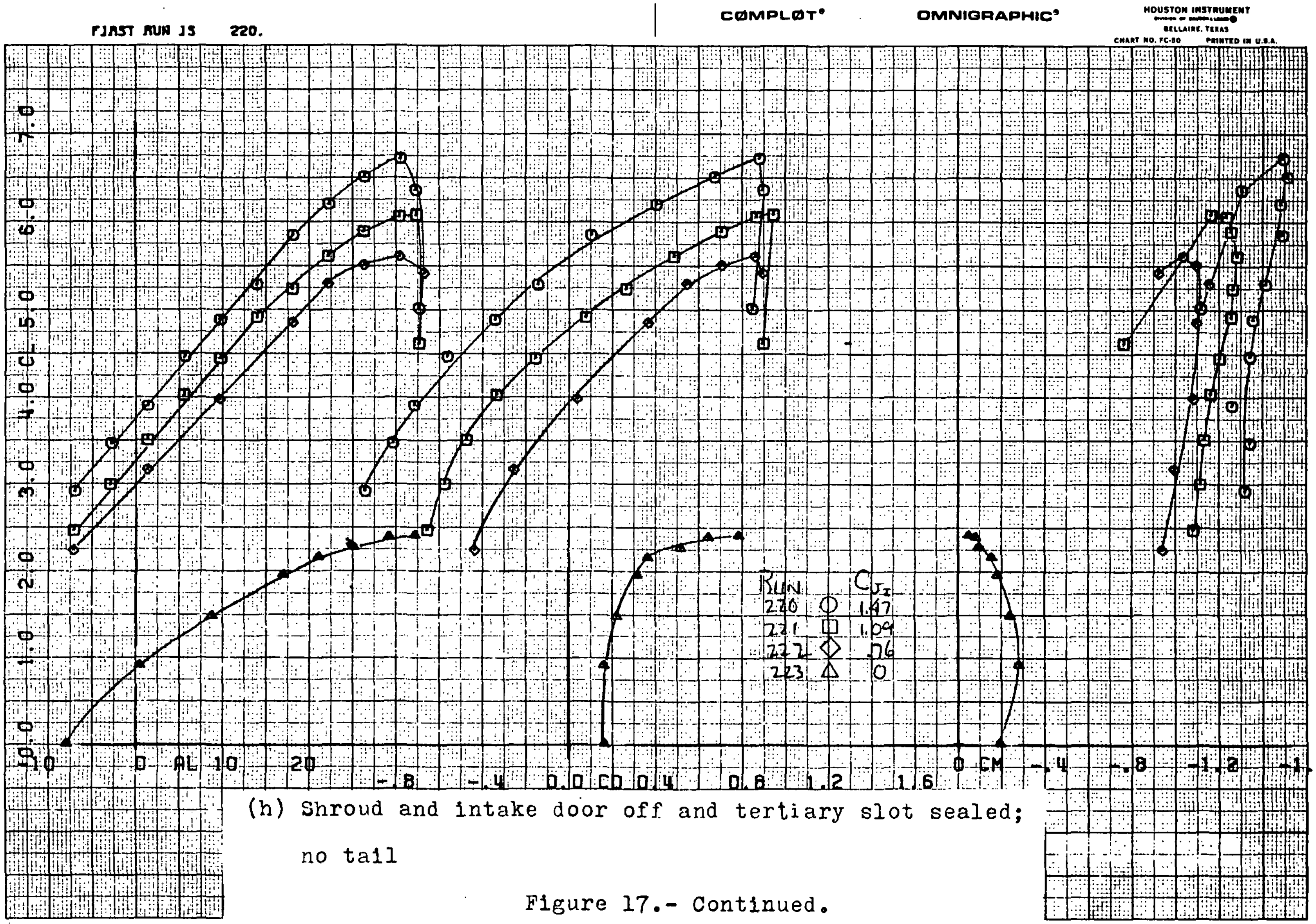

(h) Shroud and intake door off and tertiary slot sealed; no tail

Figure 17.- Continued.

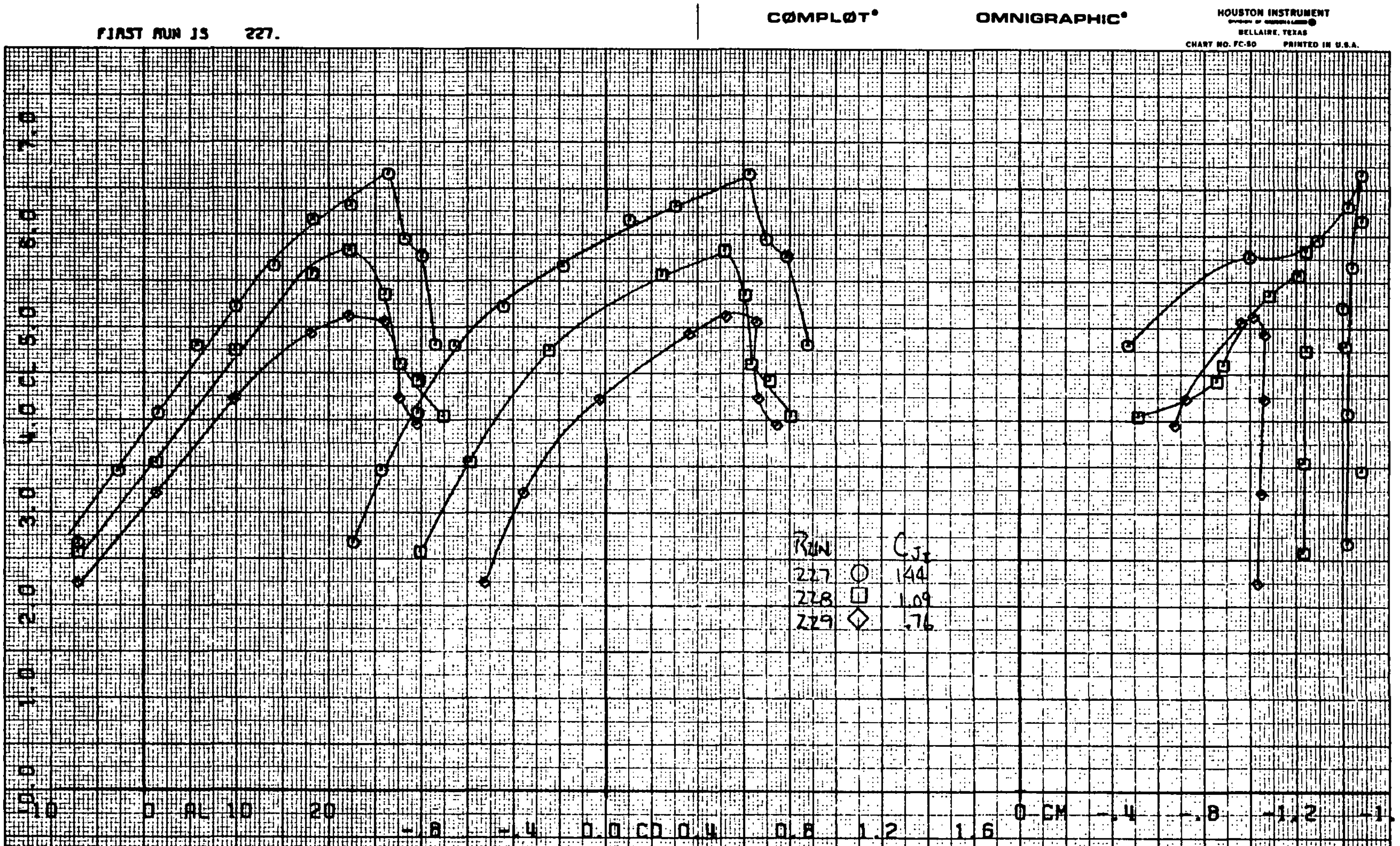

(i) Shroud and intake door off and flow-thru nacelles on;no tail

Figure 17.- Concluded.

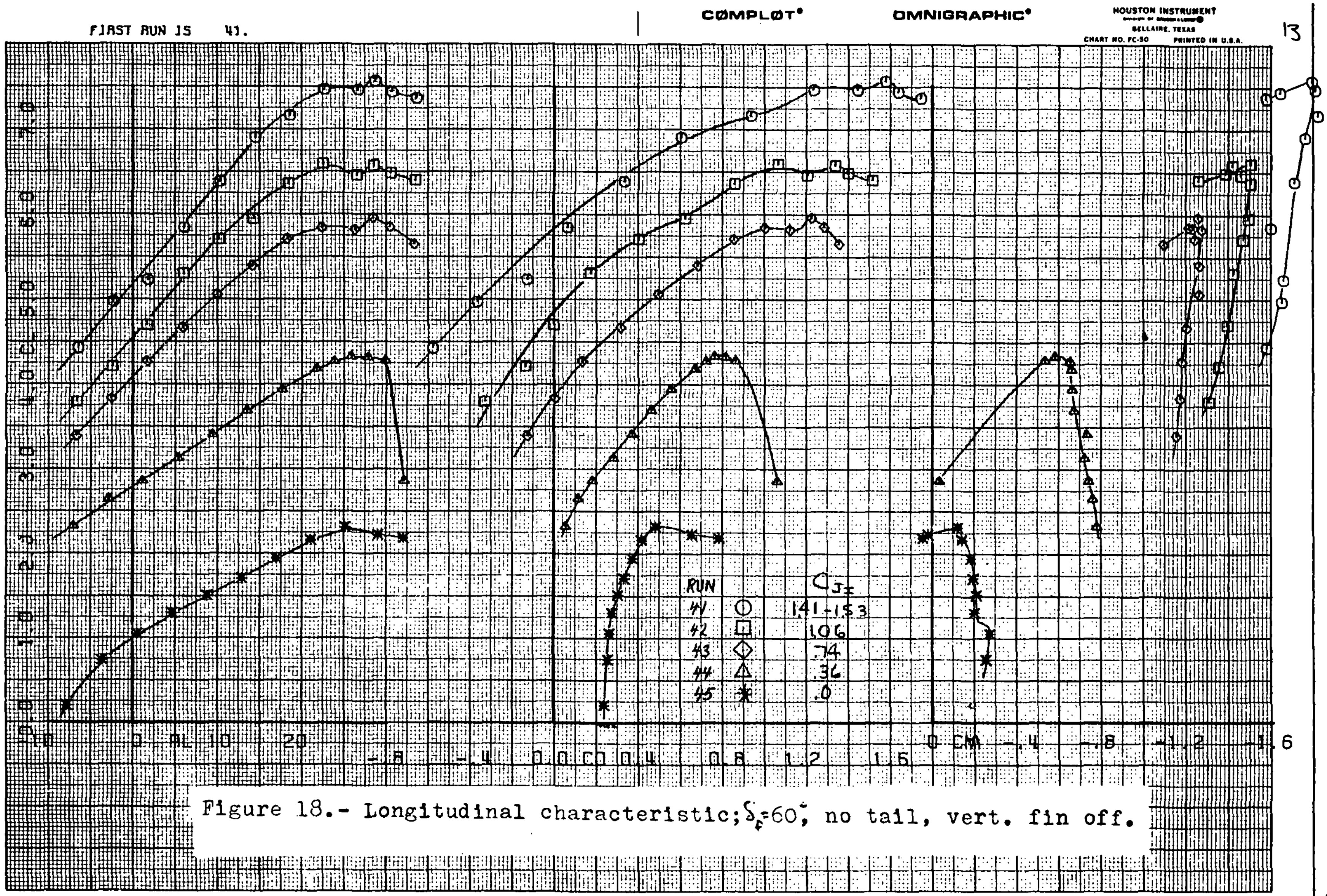

Figure 18.- Longitudinal characteristic; δ_f=60°, no tail, vert. fin off.

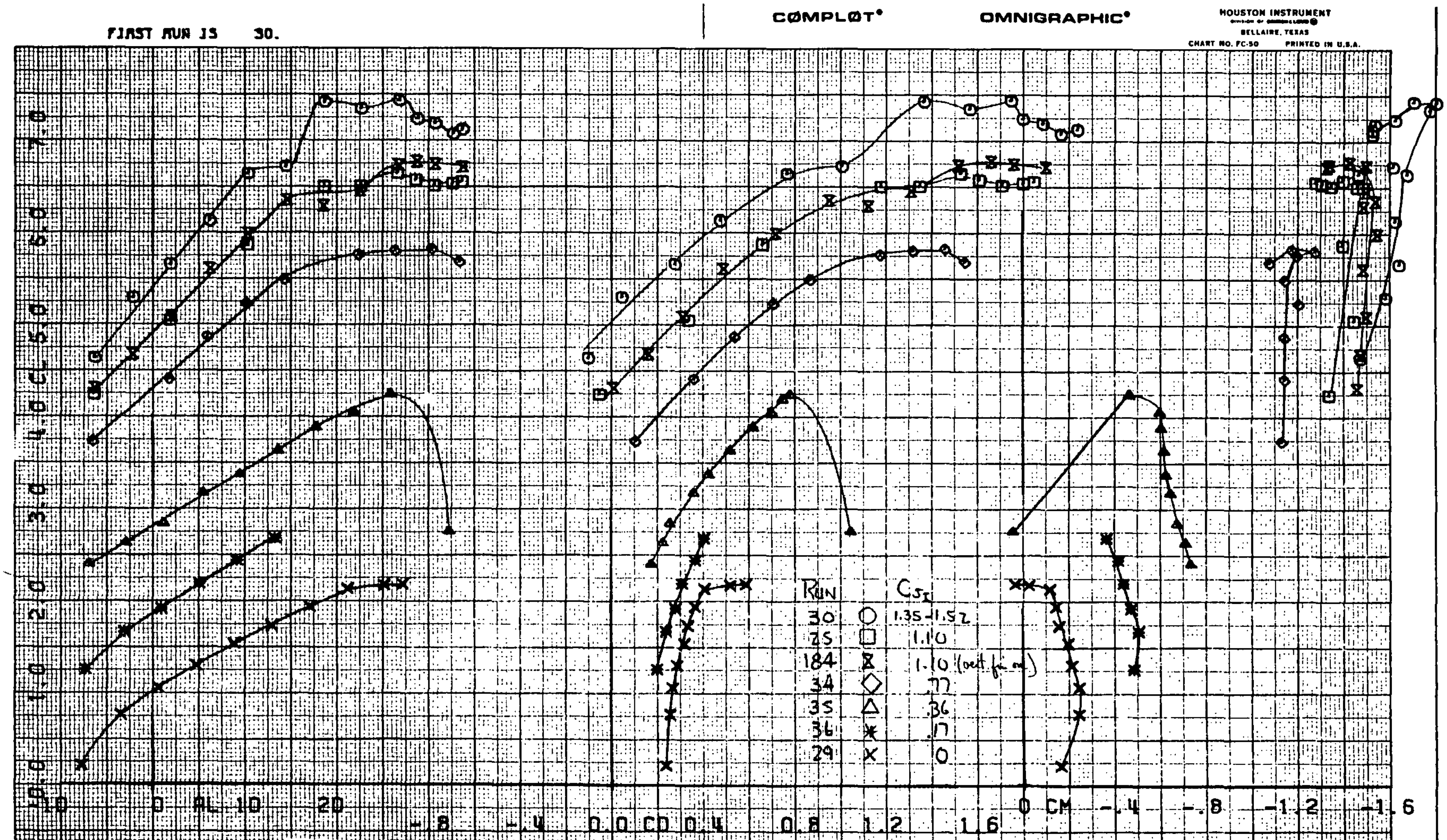

(a) Effect of C_{J_I} ; vert fin off

Figure 19.- Longitudinal characteristic; δ_f = 70°, no tail.

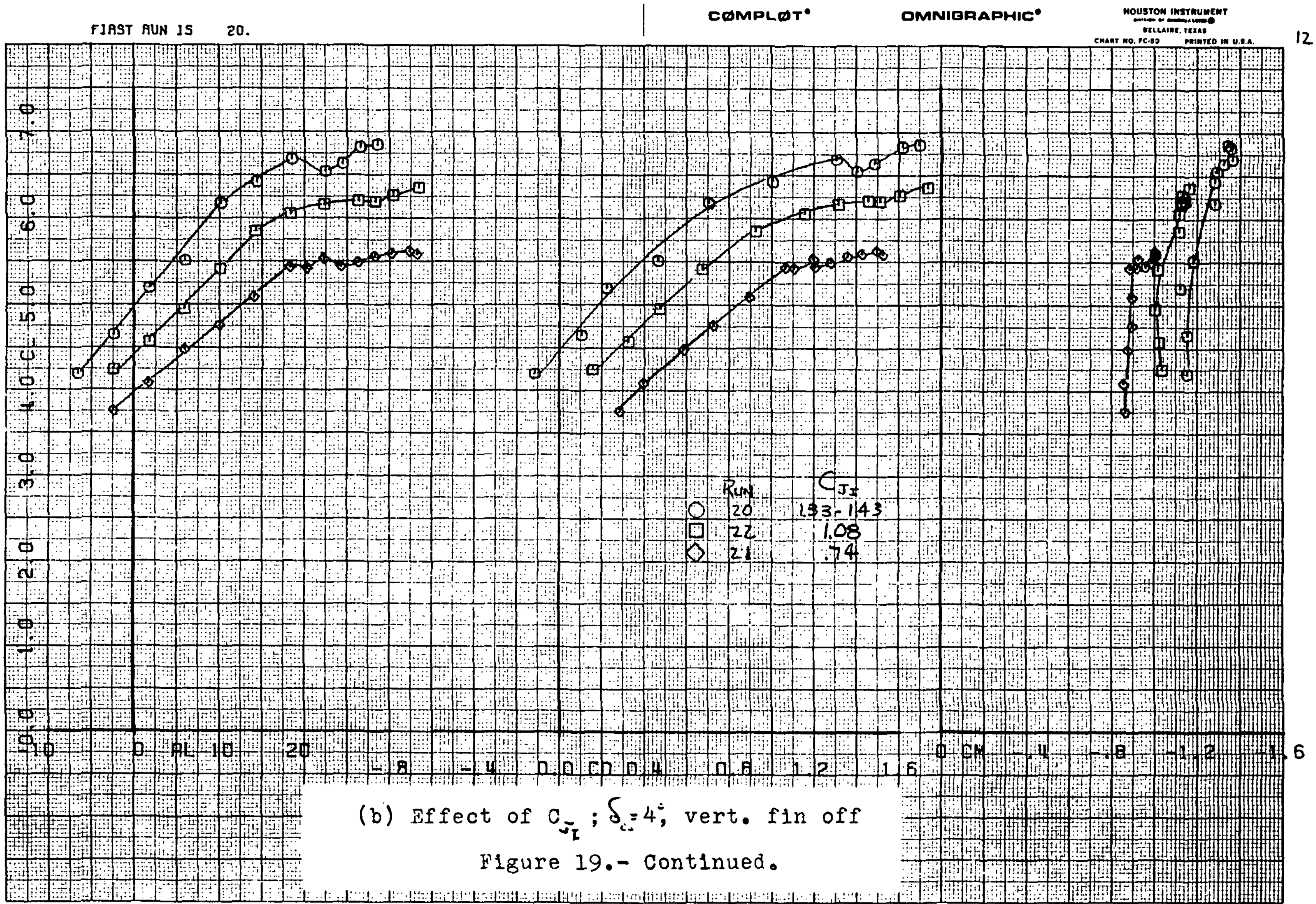

(b) Effect of C_{J_I} ; $\delta_c = 4°$, vert. fin off

Figure 19.- Continued.

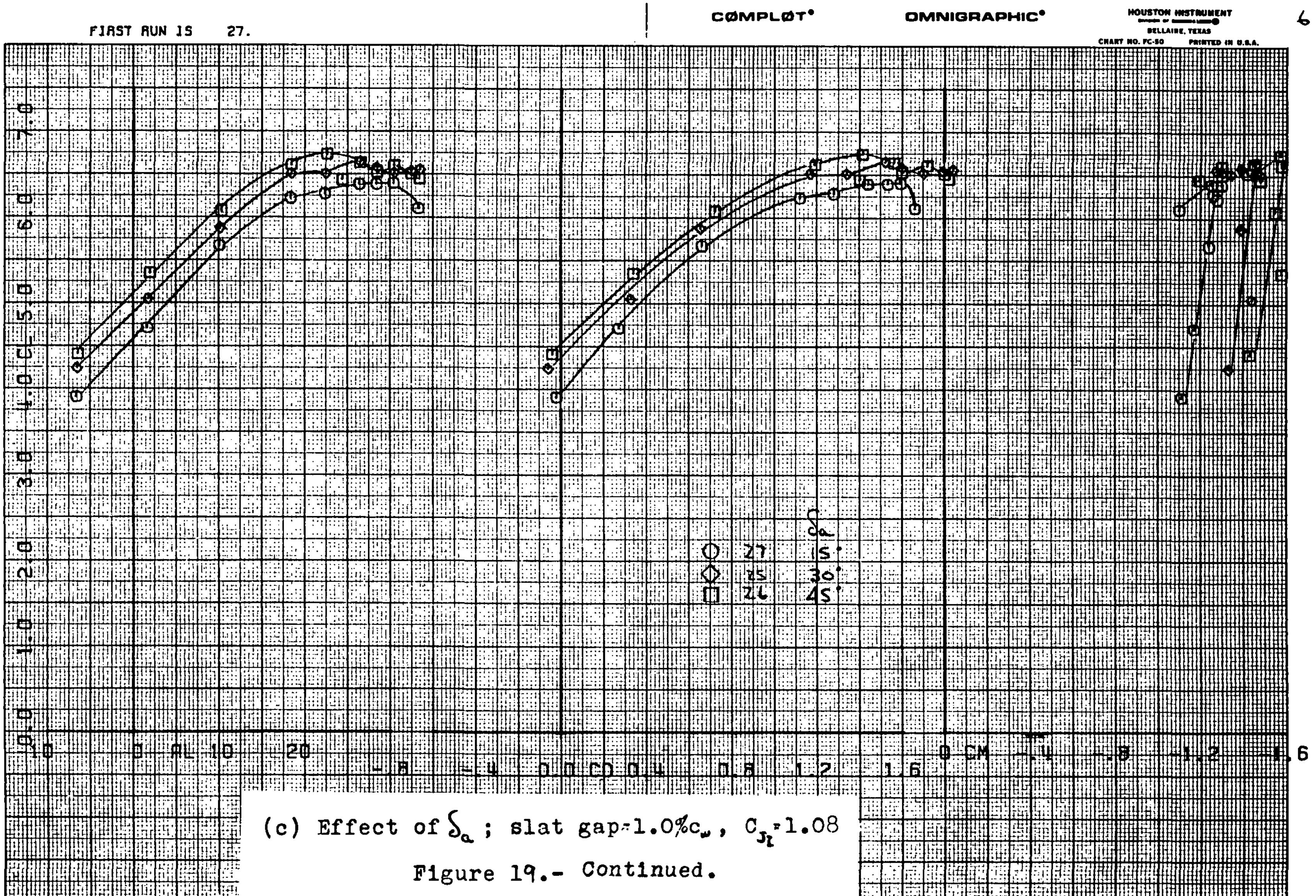

(c) Effect of δ_a; slat gap=1.0%c_w, C_{J_l}=1.08

Figure 19.- Continued.

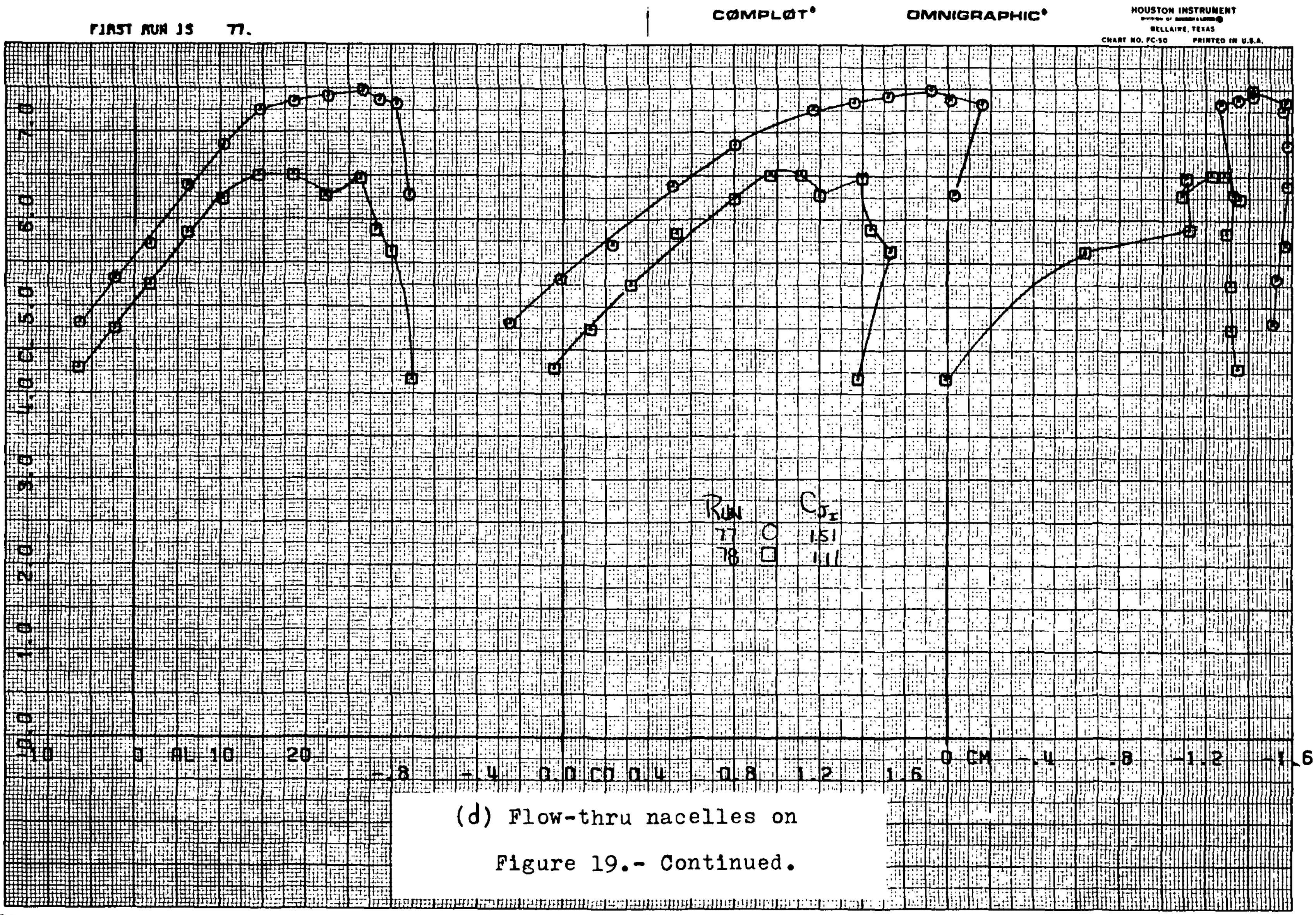

(d) Flow-thru nacelles on

Figure 19.- Continued.

27

19d

14

84

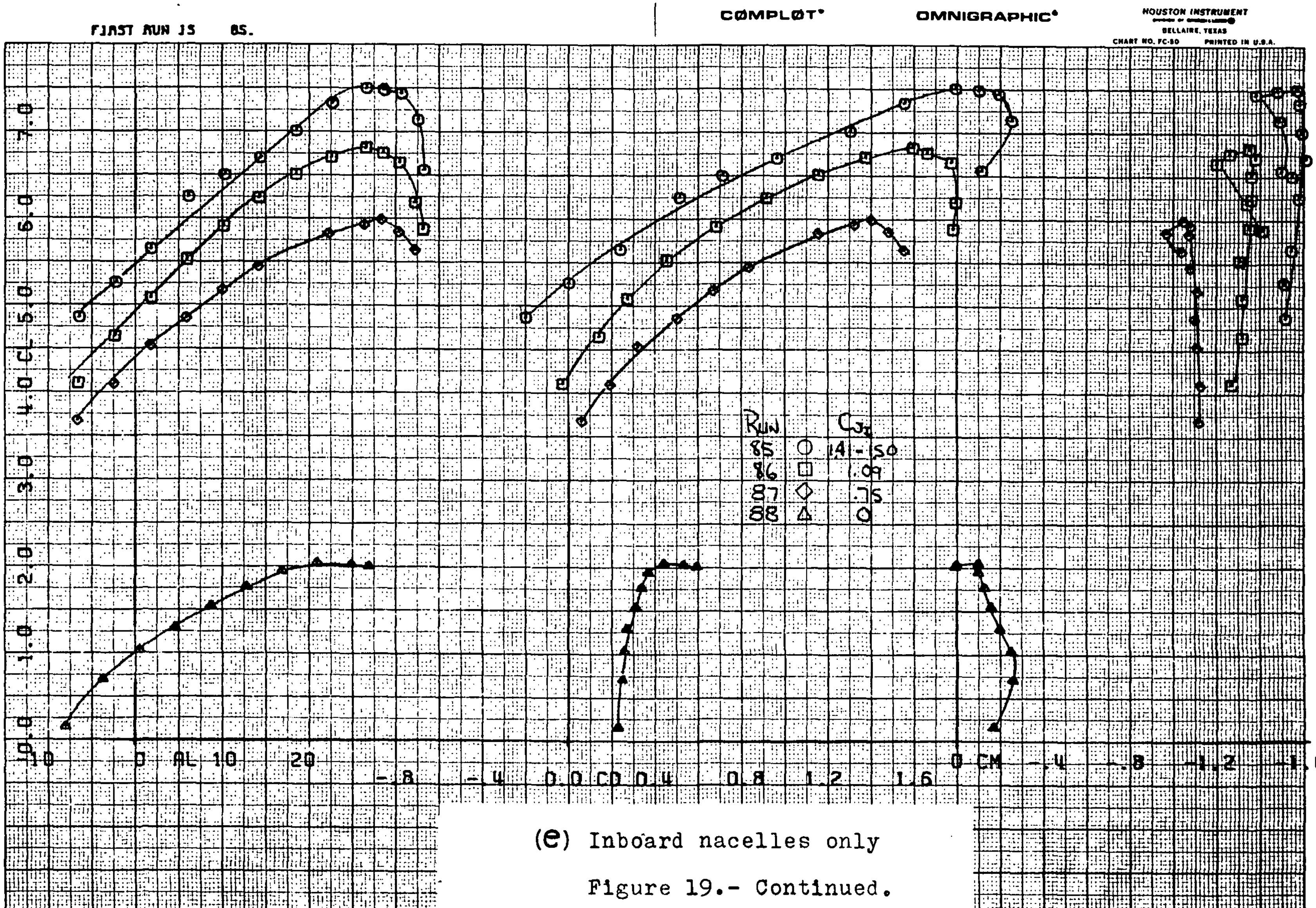

(e) Inboard nacelles only

Figure 19.- Continued.

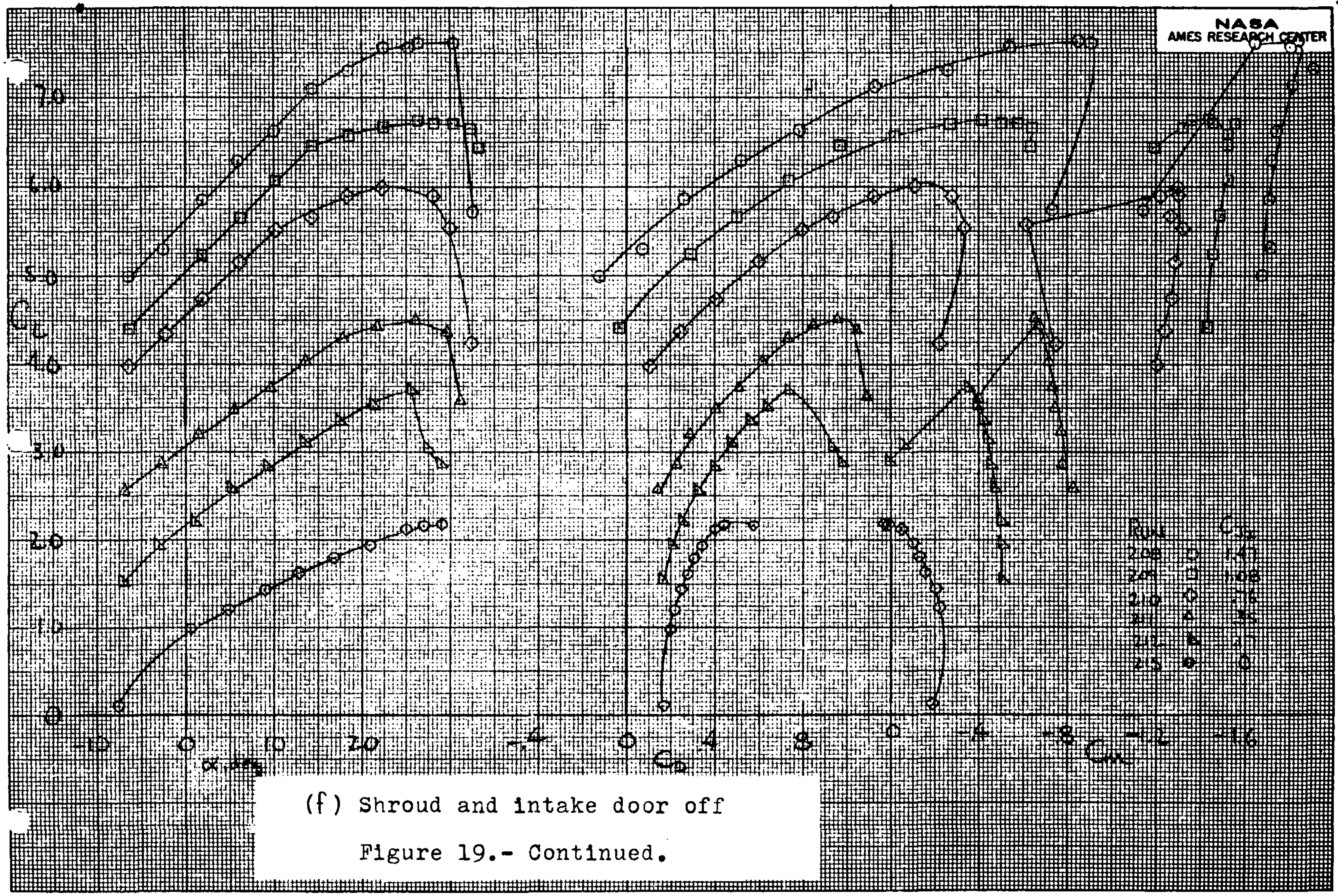

(f) Shroud and intake door off

Figure 19.- Continued.

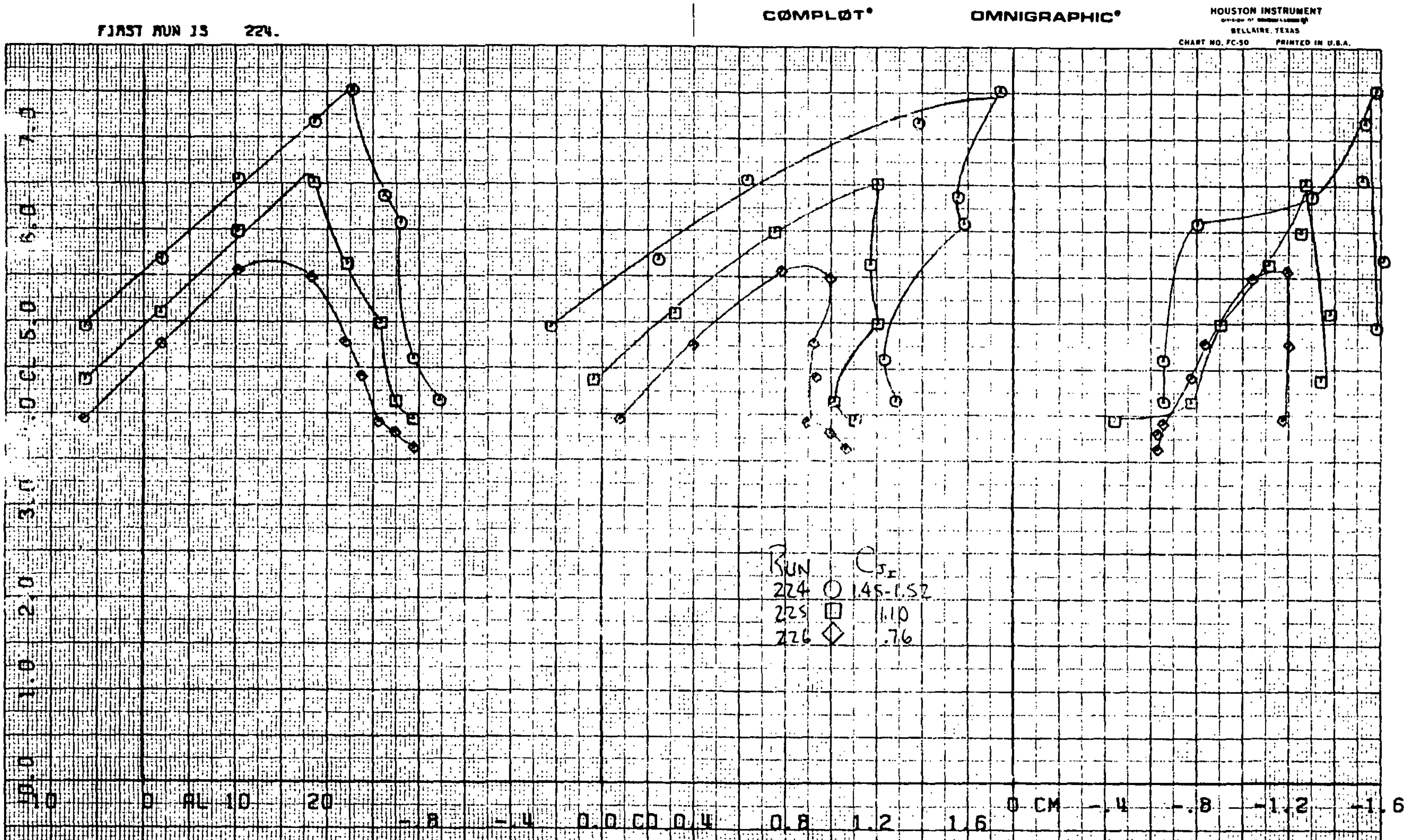

(g) Shroud and intake door off and flow-thru nacelles on

Figure 19.- Concluded.

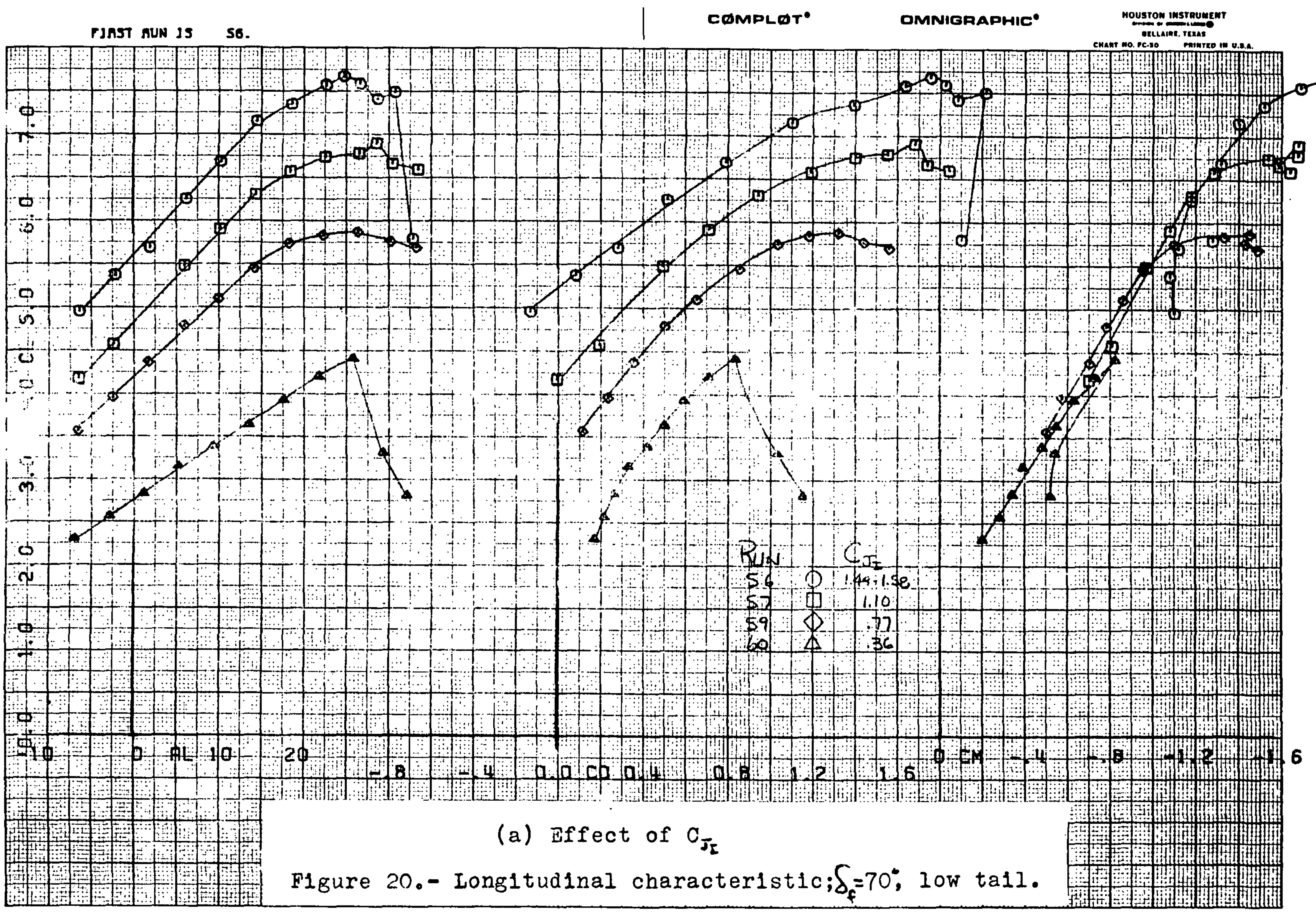

(a) Effect of $C_{J_{I}}$

Figure 20.- Longitudinal characteristic; δ_f=70°, low tail.

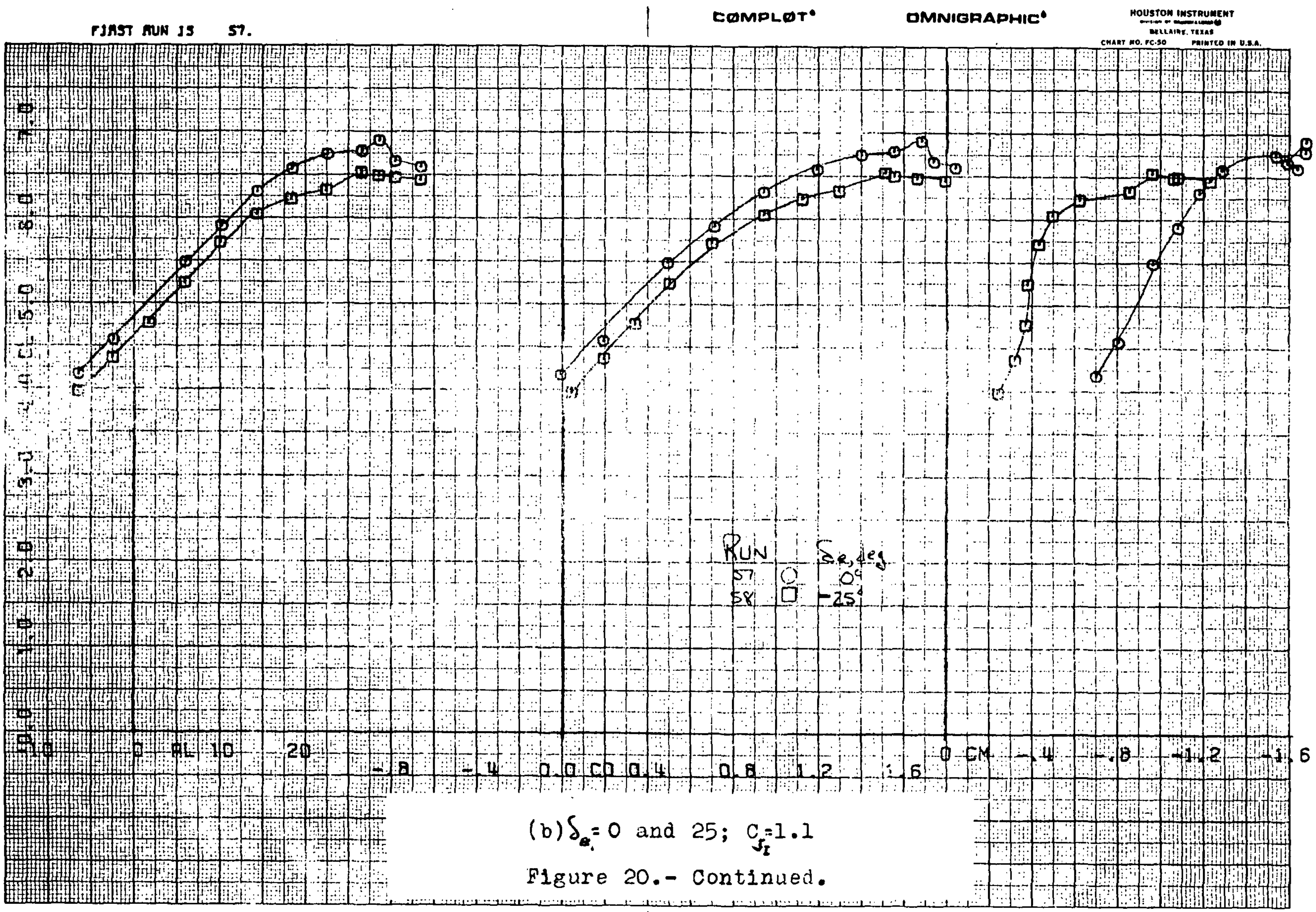

(b) δ_e = 0 and 25; C_{J_I}=1.1

Figure 20.- Continued.

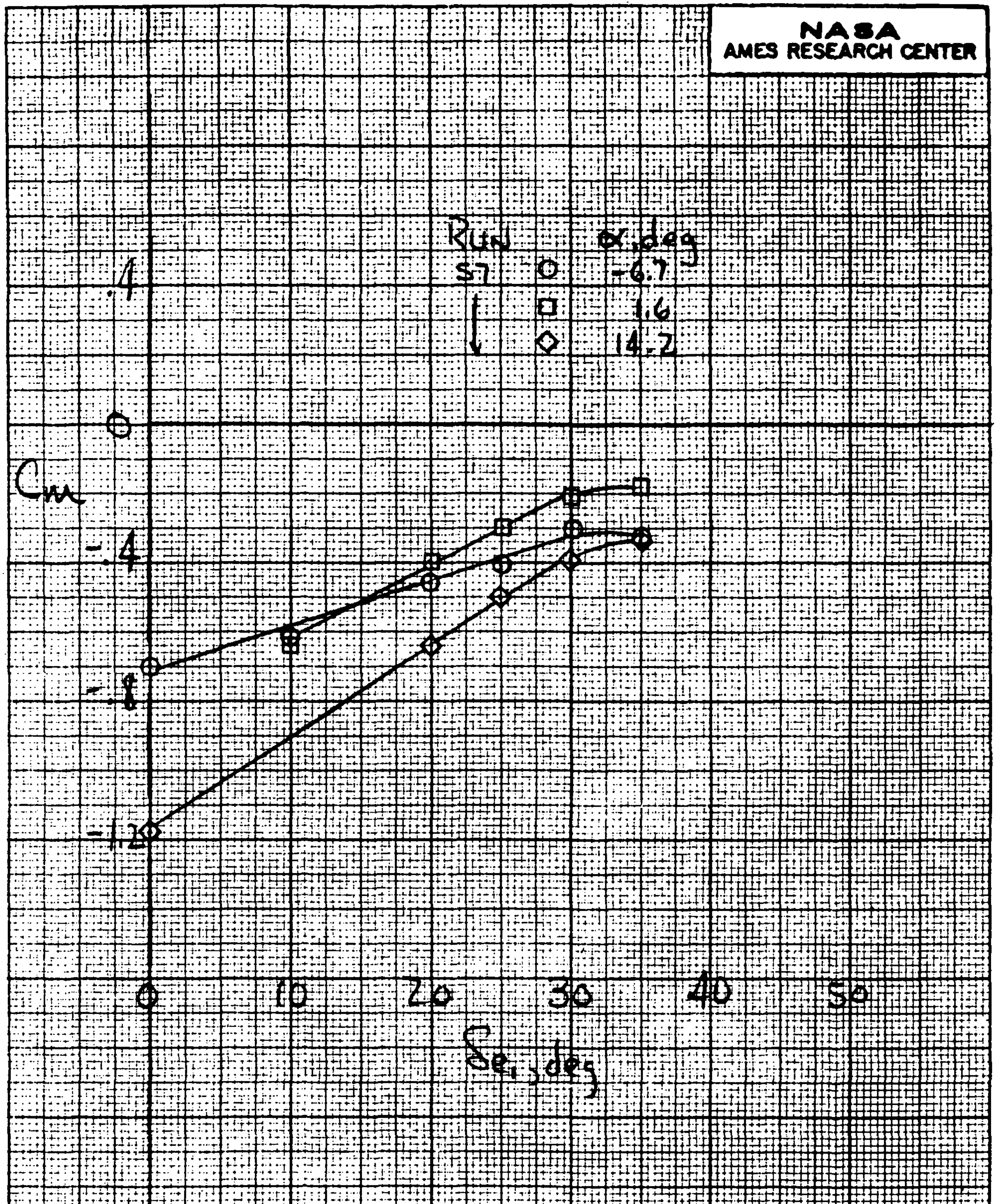

(c) Elevator effectiveness; δ_{e_2} = 0°, C_{J_T} = 1.1

Figure 20.- Continued.

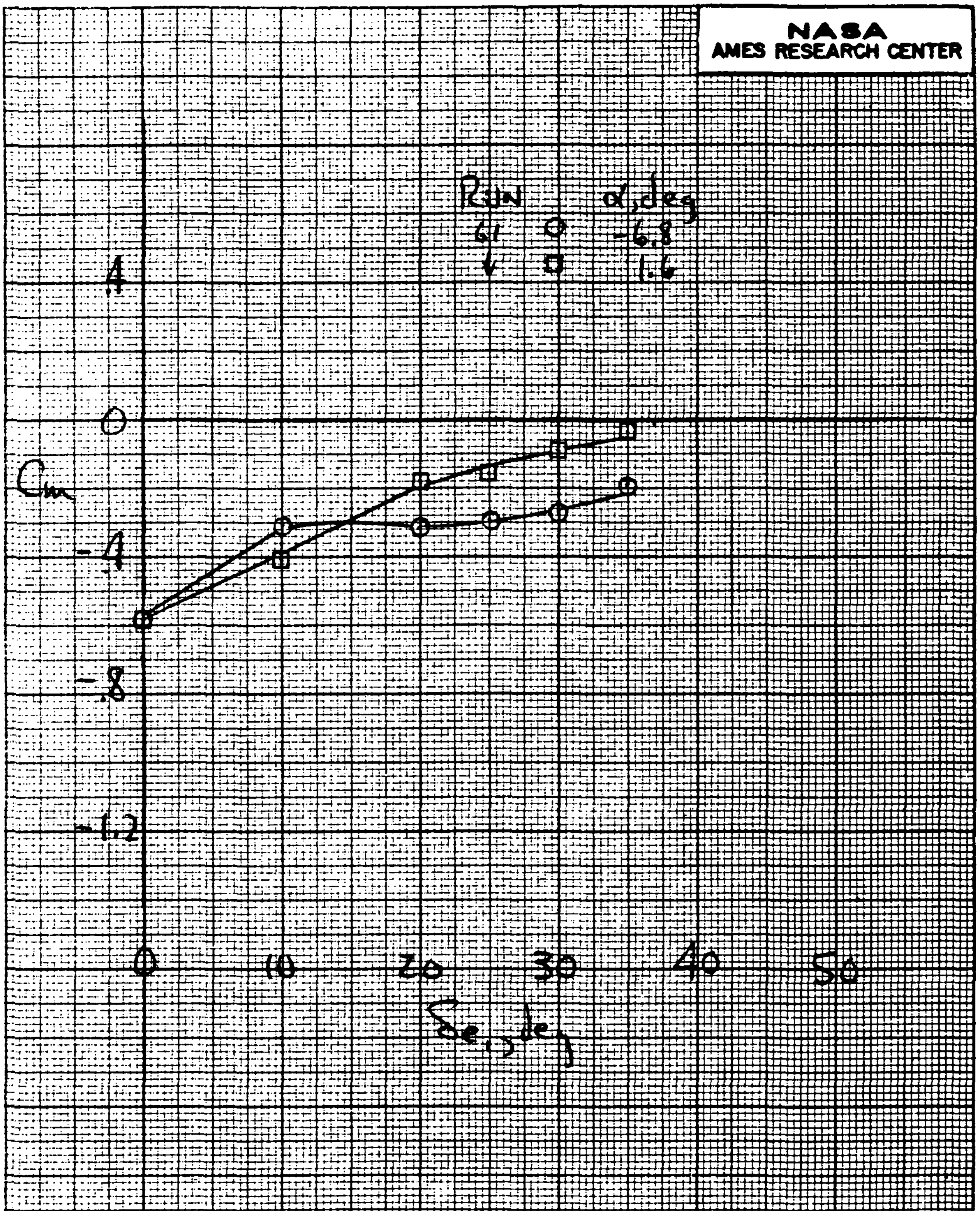

(d) Elevator effectiveness; $\delta_{e_i} = -15^\circ$, $C_{J_I} = 1.1$

Figure 20.- Concluded.

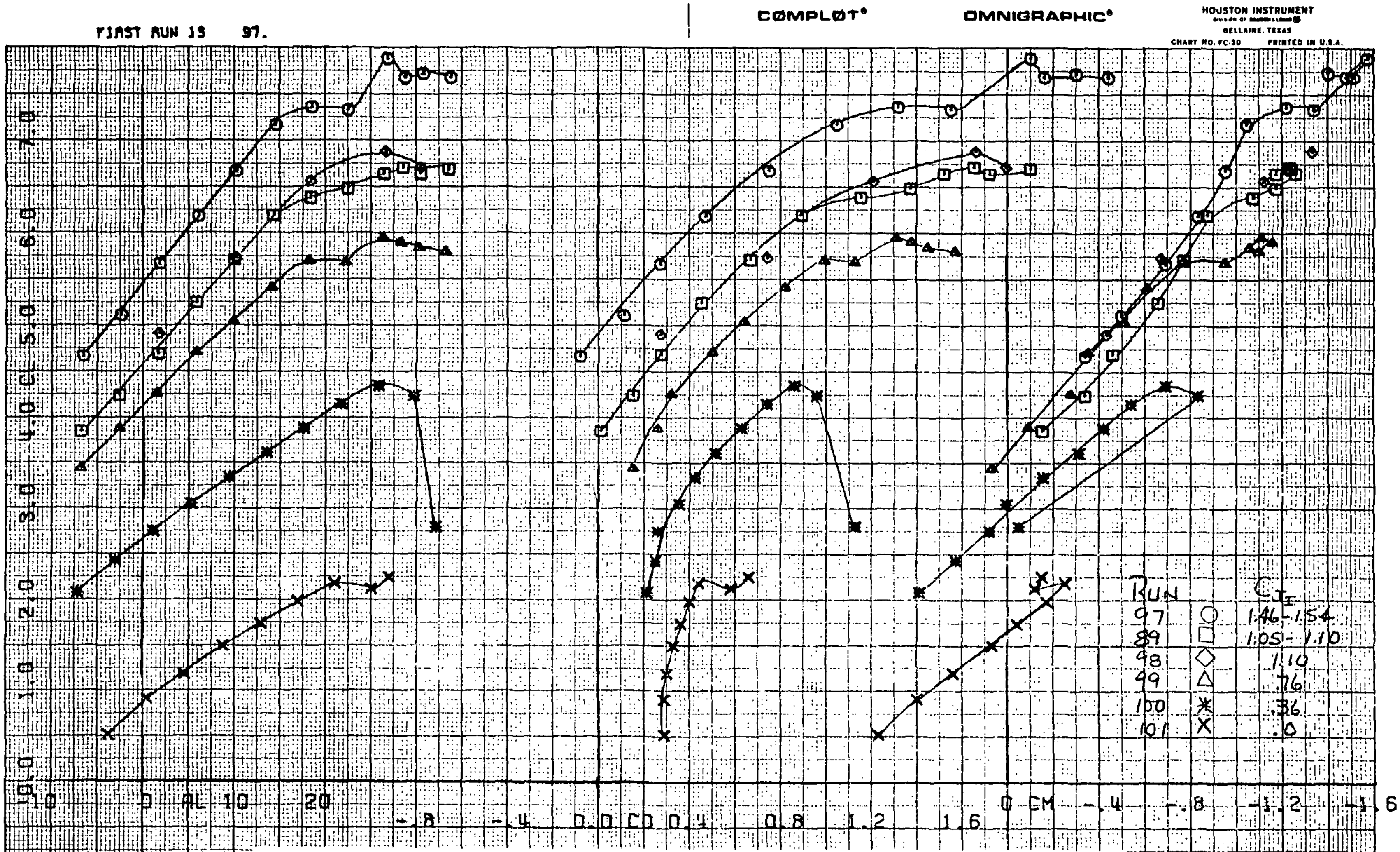

(a) Effect of C_{J_I}

Figure 21.- Longitudinal characteristic; δ_f=70°, high tail.

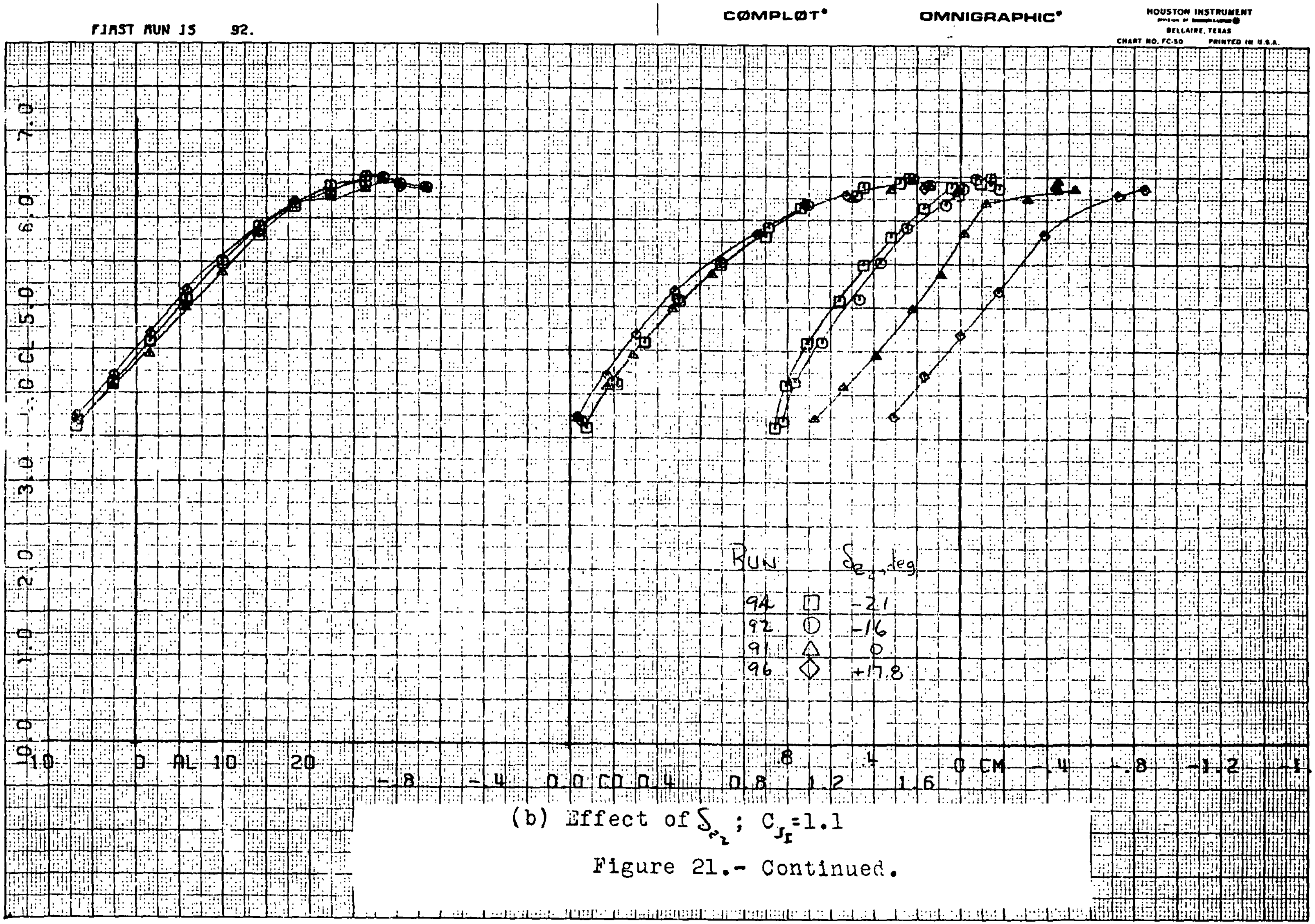

(b) Effect of δ_{e_2}; C_{J_I}=1.1

Figure 21.- Continued.

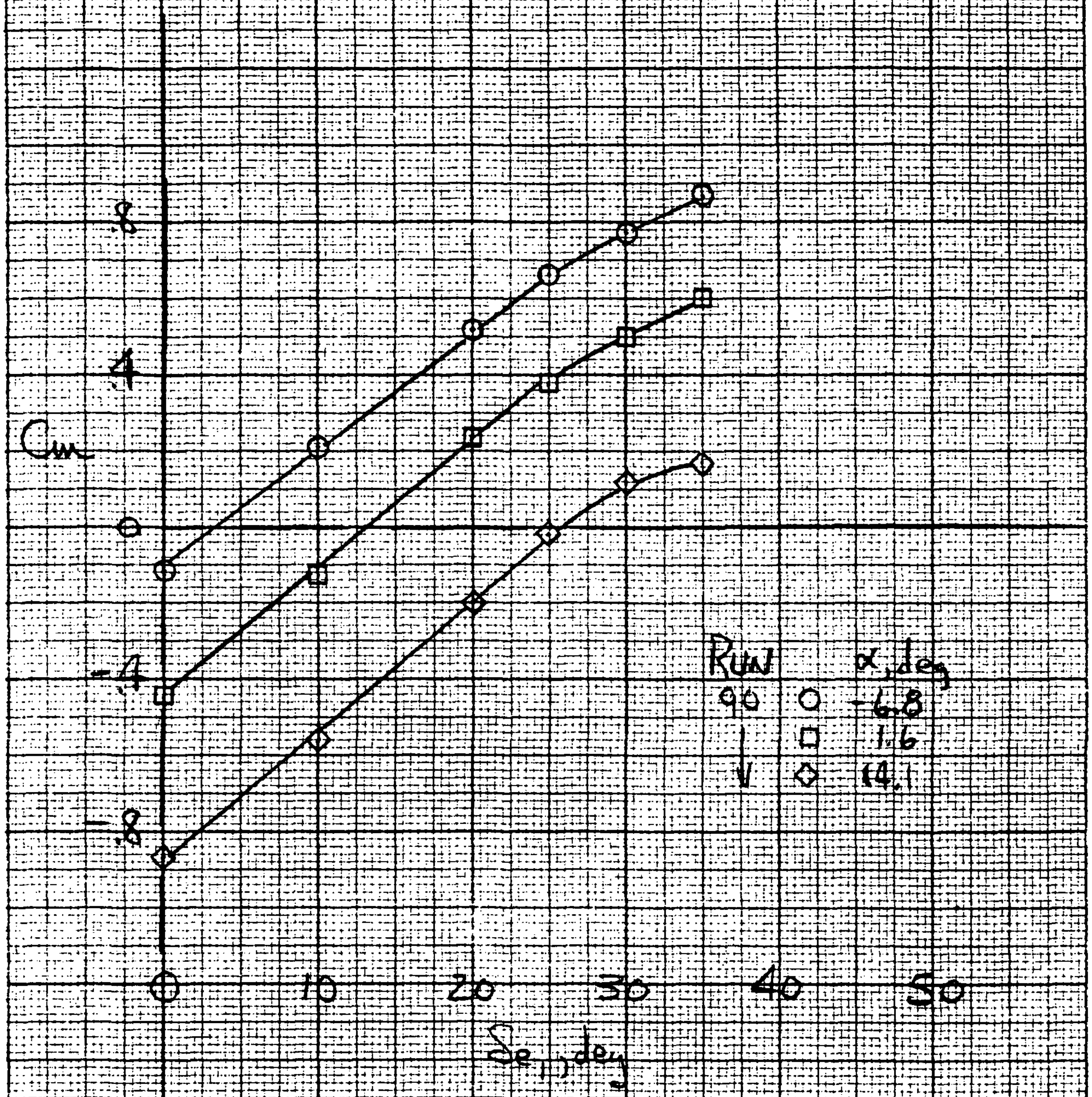

(c) Elevator effectiveness; $\delta_{e_2} = 0^\circ$, $C_{J_1} = 1.1$

Figure 21.- Continued.

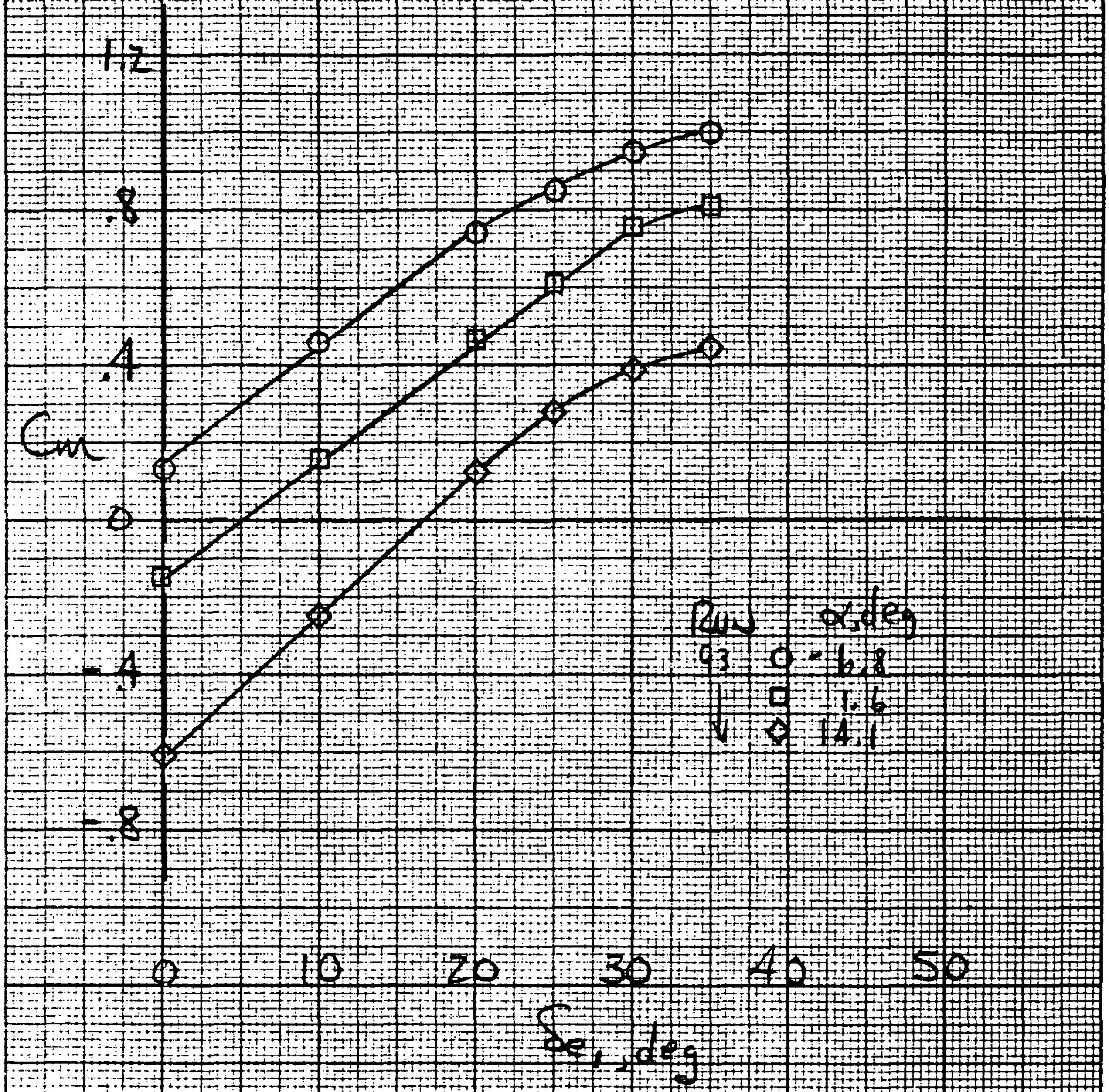

(d) Elevator effectiveness; $\delta_{e_t} = -16°$, $C_{J} = 1.1$

Figure 21.- Continued.

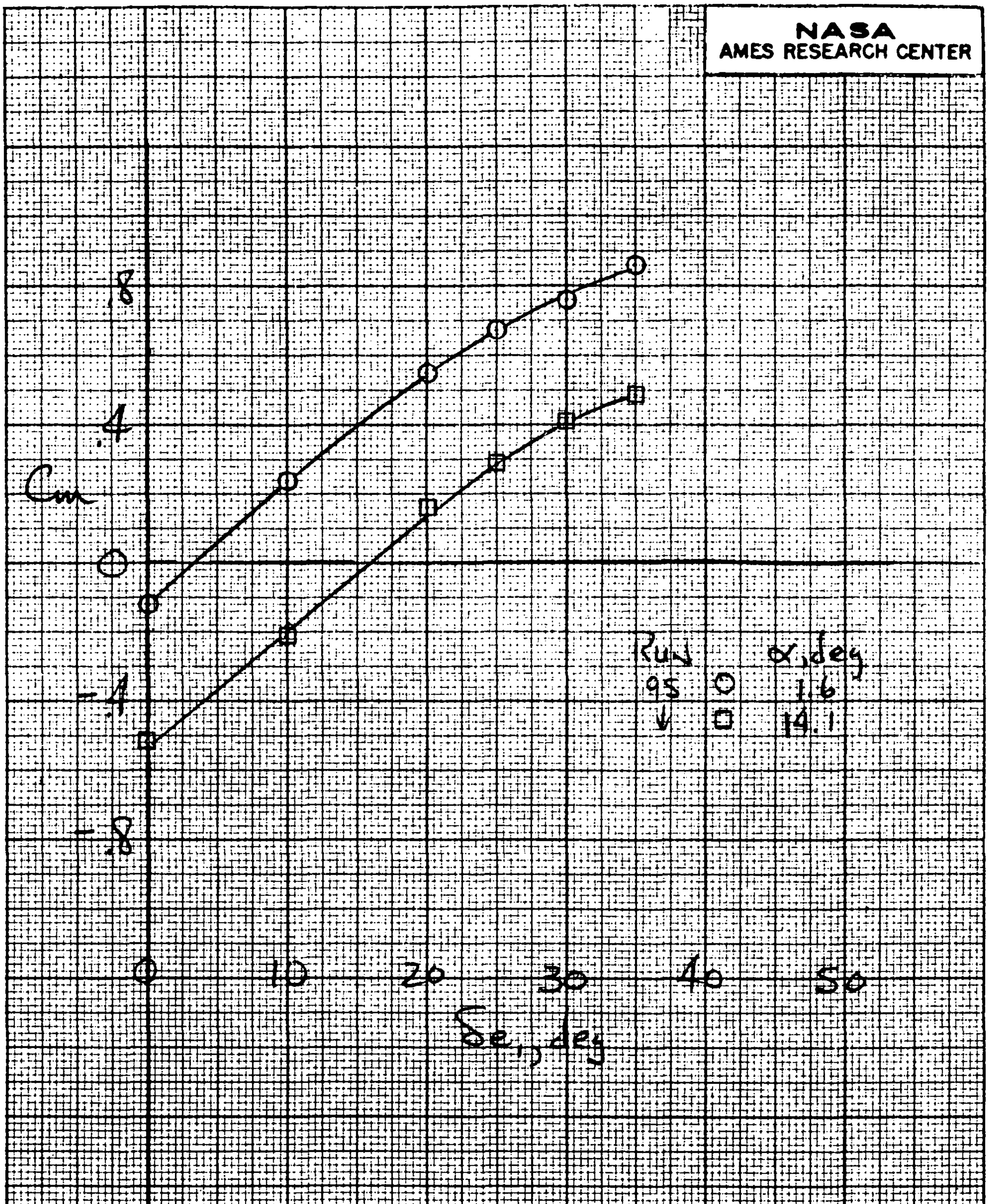

(e) Elevator effectiveness; $\delta_{e_2} = -21°$, $C_{J_2} = 1.1$

Figure 21.- Continued.

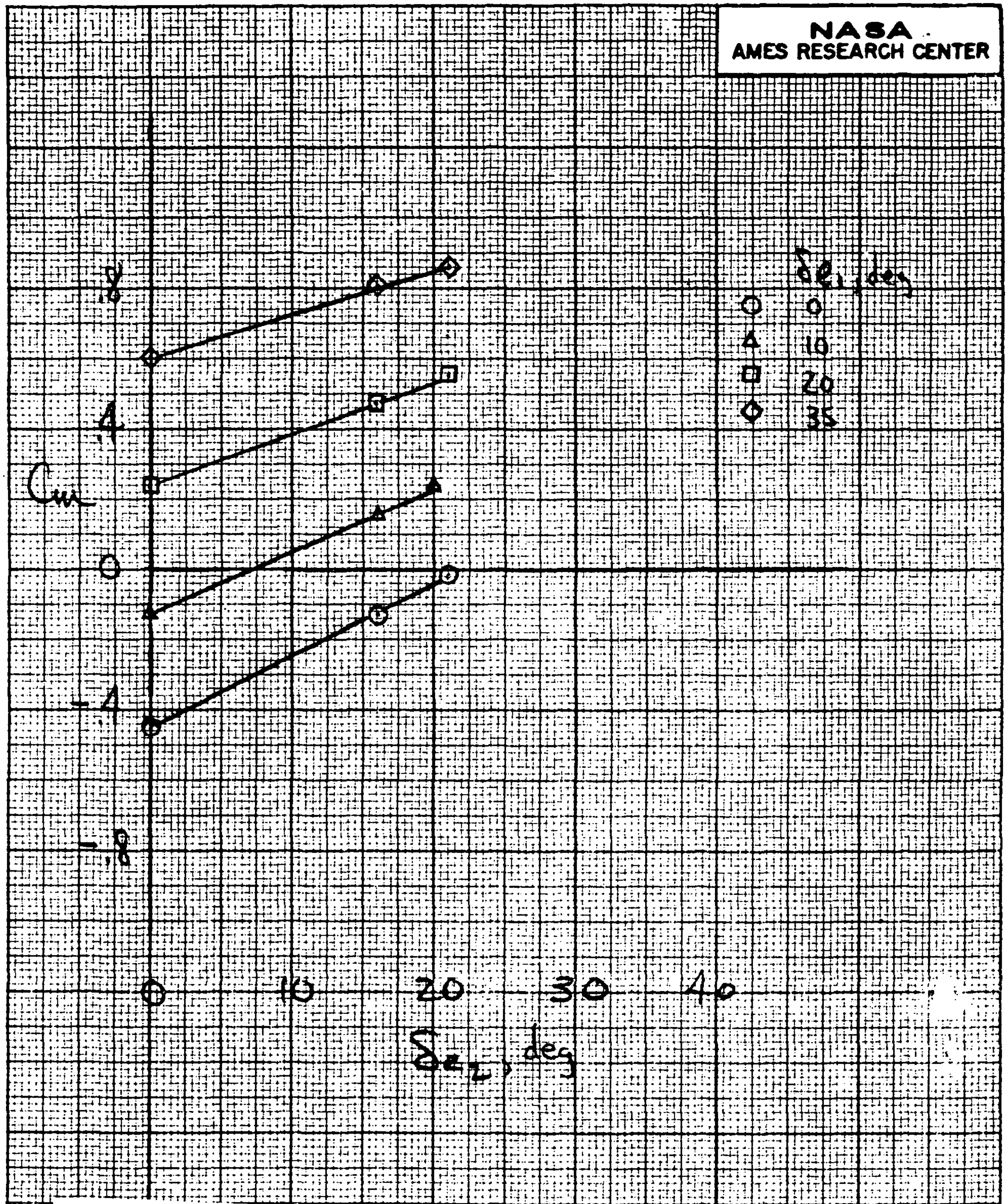

(f) Aft elevator element effectiveness; $\alpha = 0°$, $C_J = 1.1$

Figure 21.- Concluded.

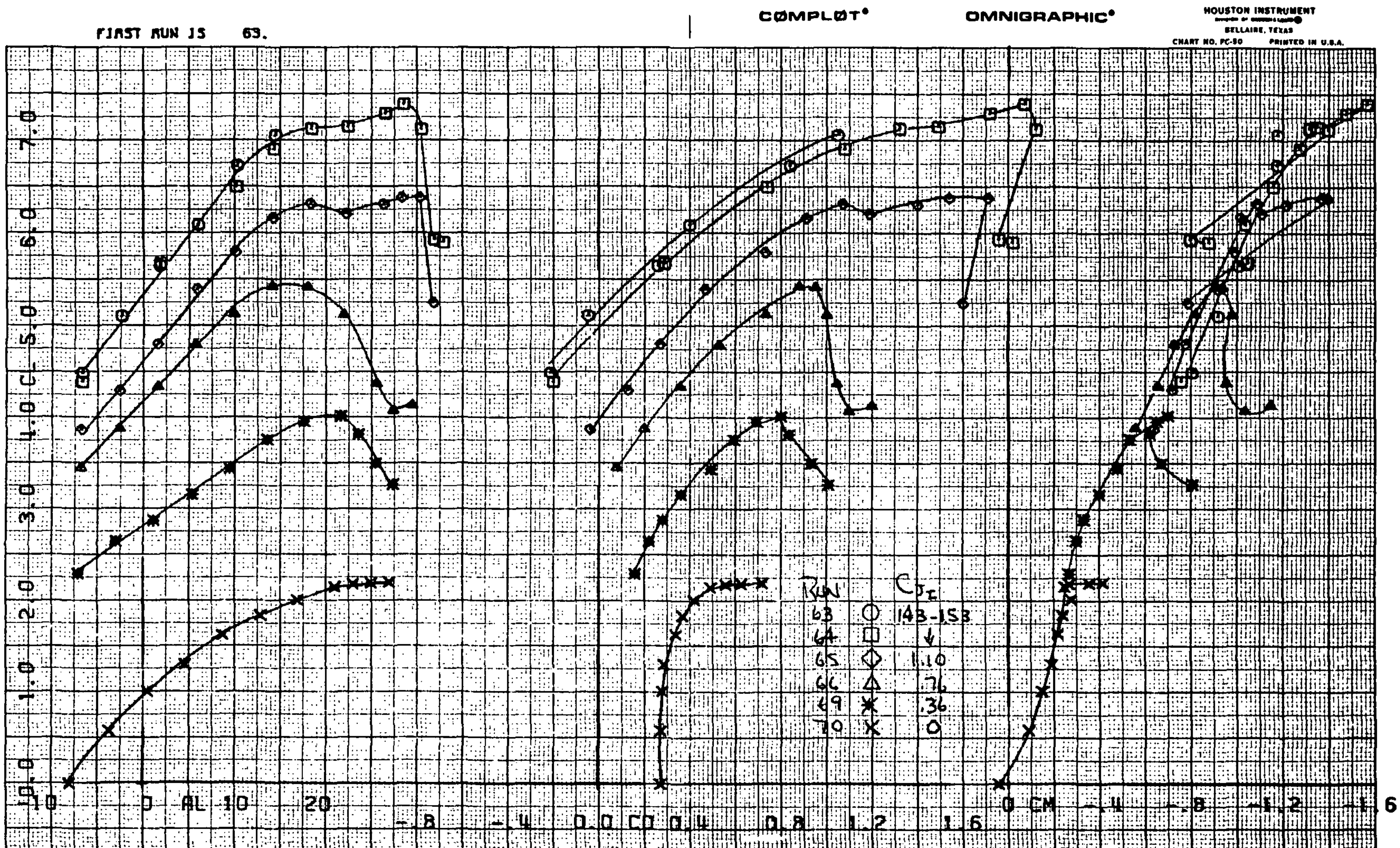

(a) Effect of C_{J_I}

Figure 22.- Longitudinal characteristic; δ_f=70°, low tail, flow-thru nacelles on.

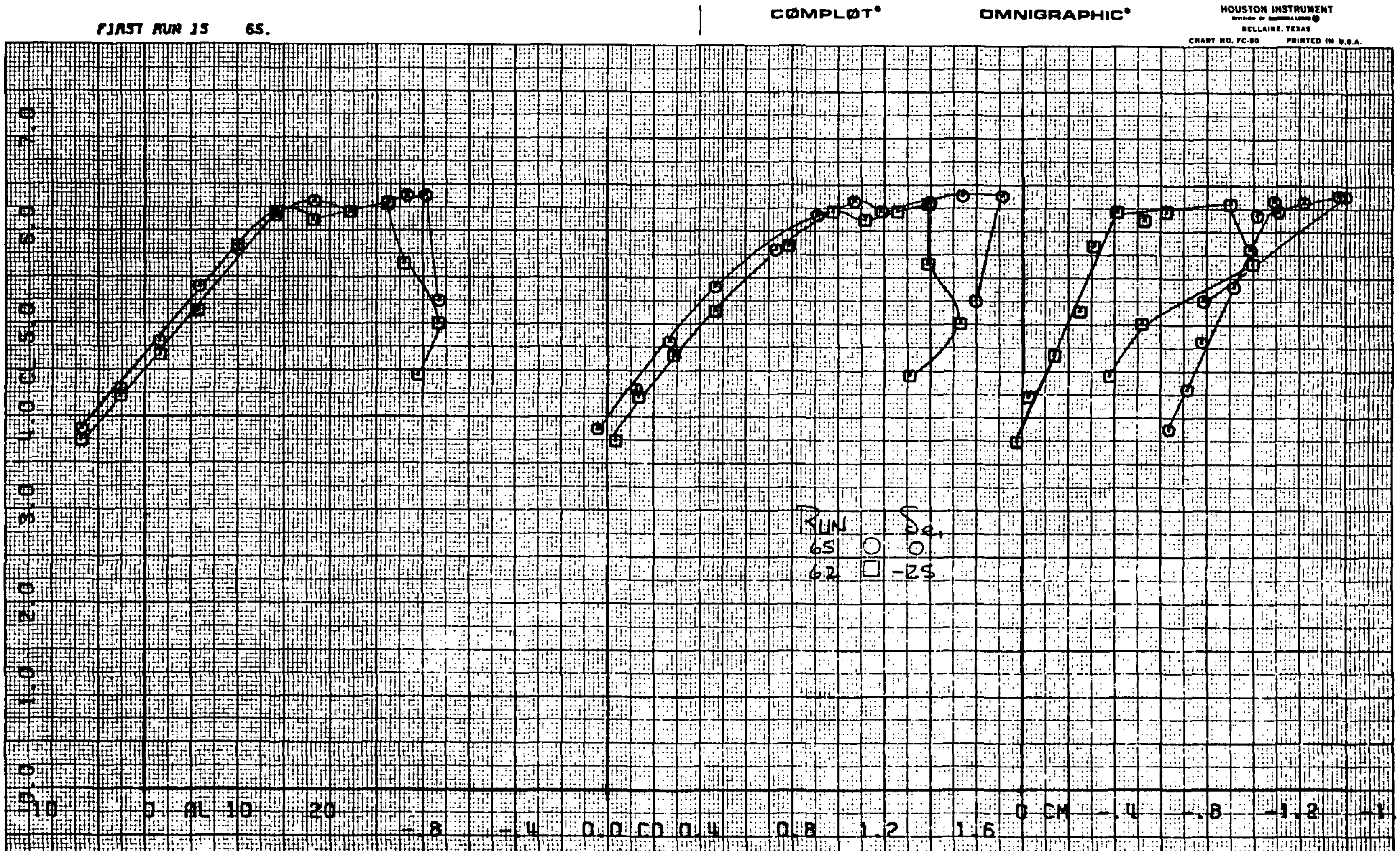

(b) Effect of δ_e ; C_{J_T}=1.09

Figure 22.- Continued.

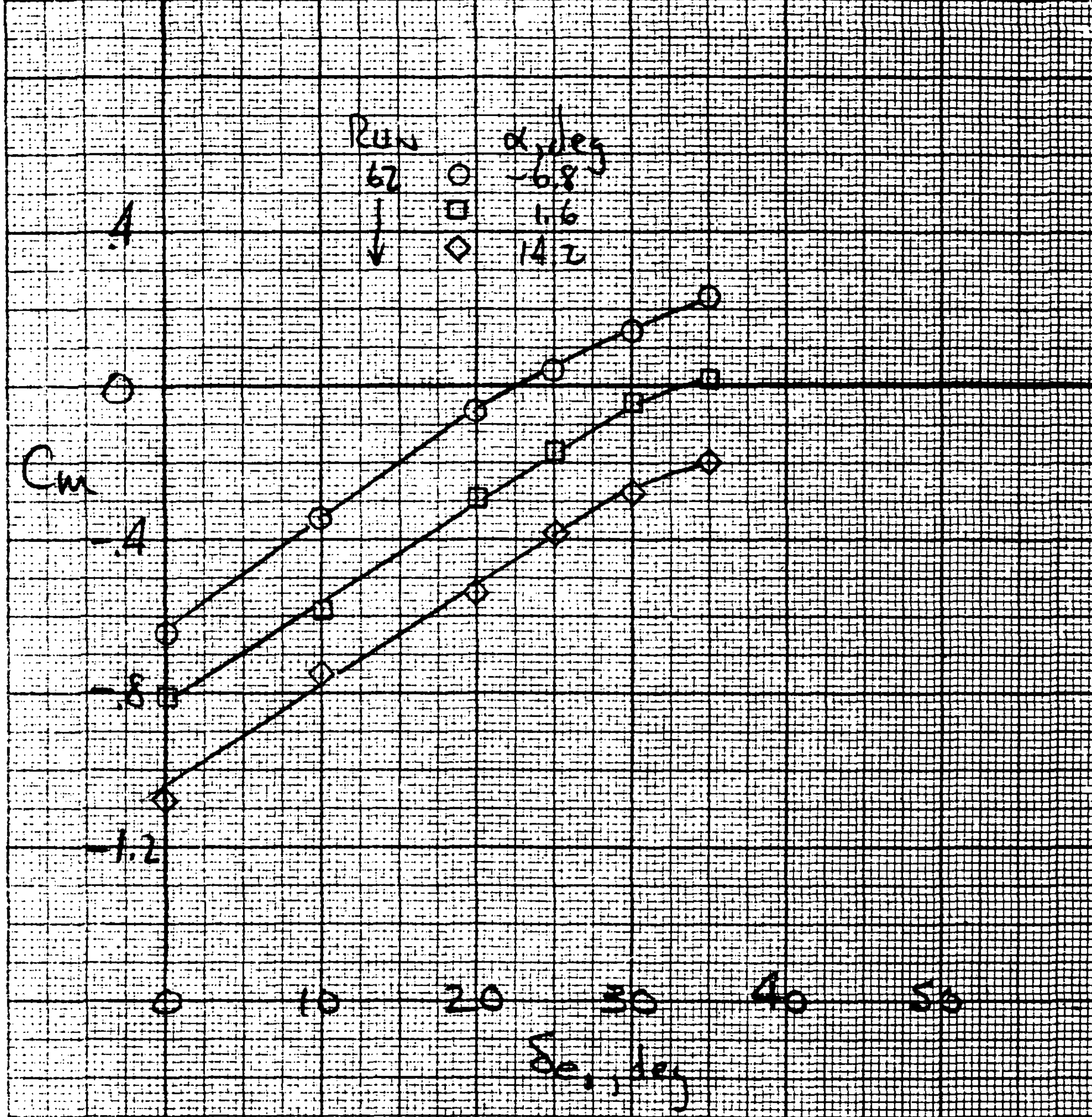

(c) Elevator effectiveness; $\delta_{e_2} = 0°$, $C_{J_1} = 1.1$

Figure 22.- Concluded.

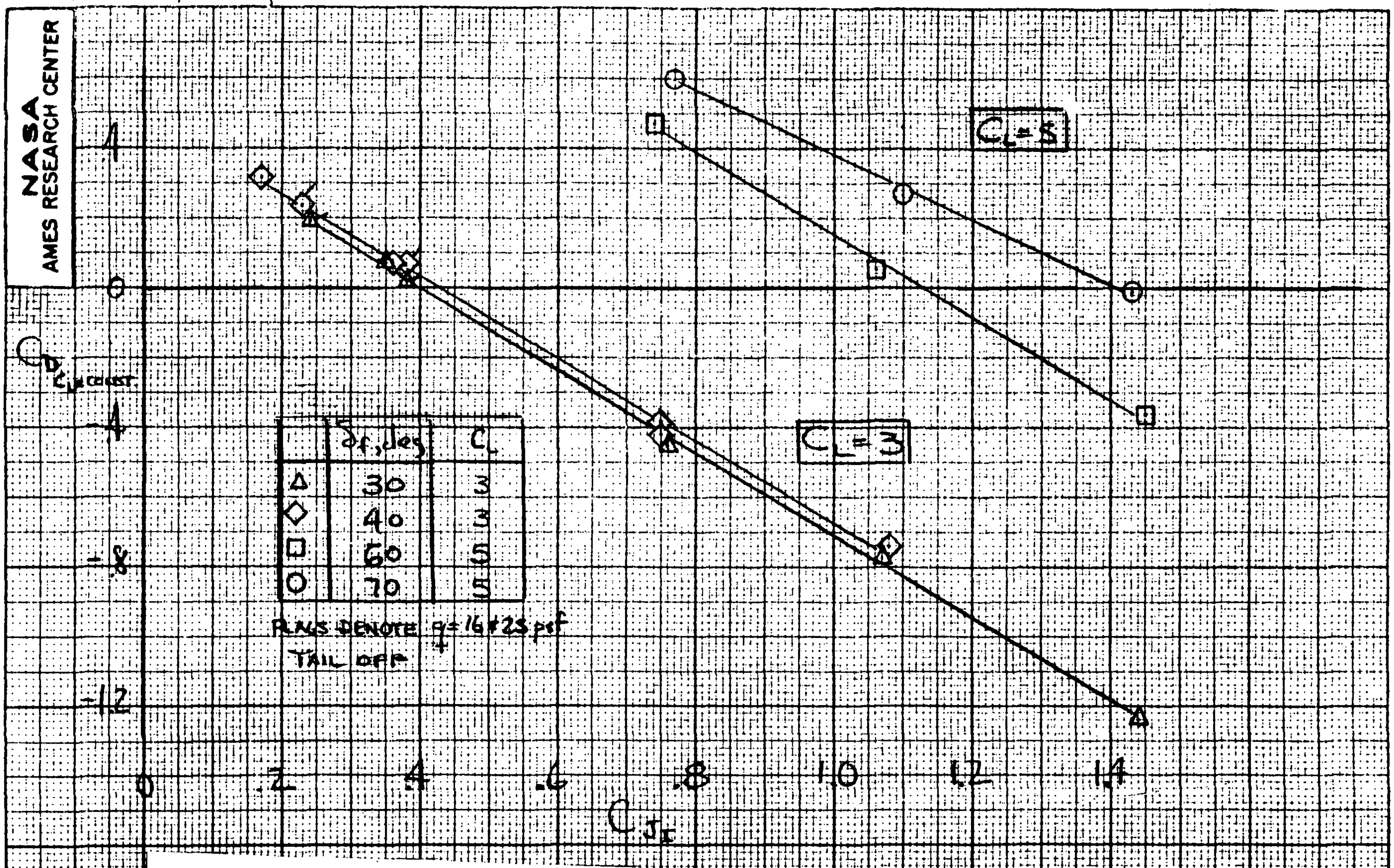

(a) C_D at constant lift as a function of C_{J_T}

Figure 23.- Summary of the longitudinal characteristic;no tail.

101<

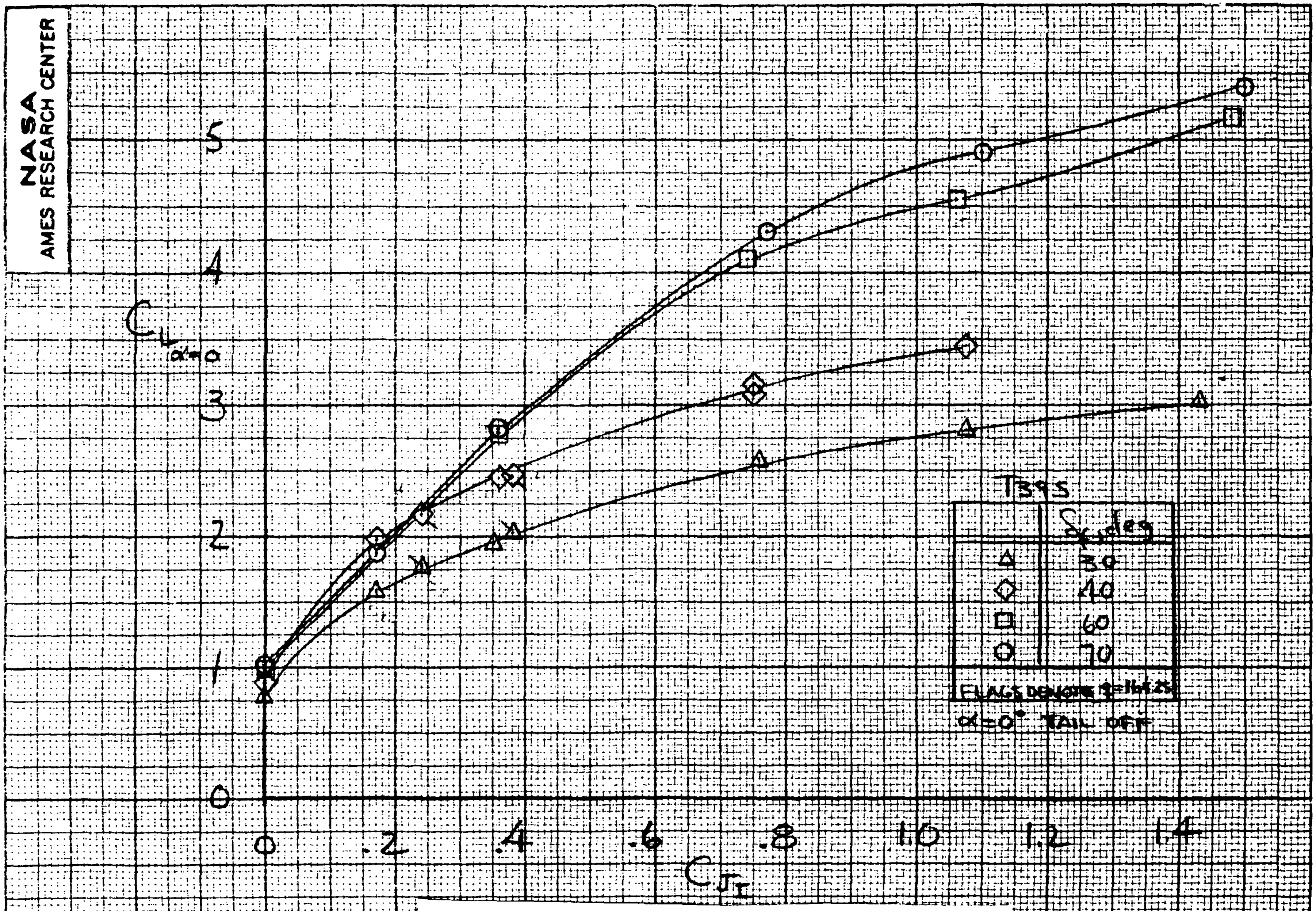

(b) Lift at α= 0° as a function of C_{J_I}

Figure 23.- Continued.

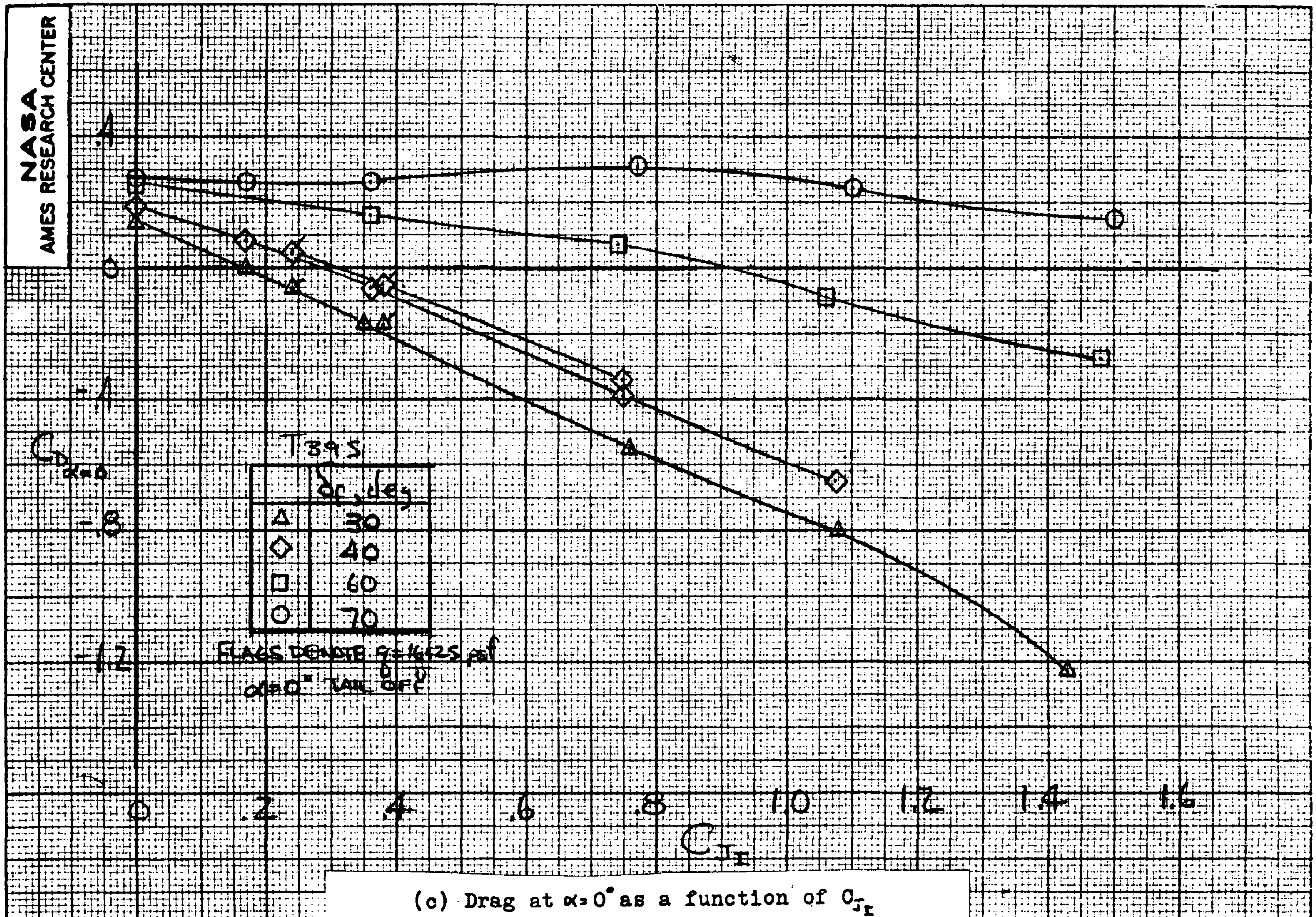

(c) Drag at $\alpha = 0°$ as a function of C_{J_E}

Figure 23.- Continued.

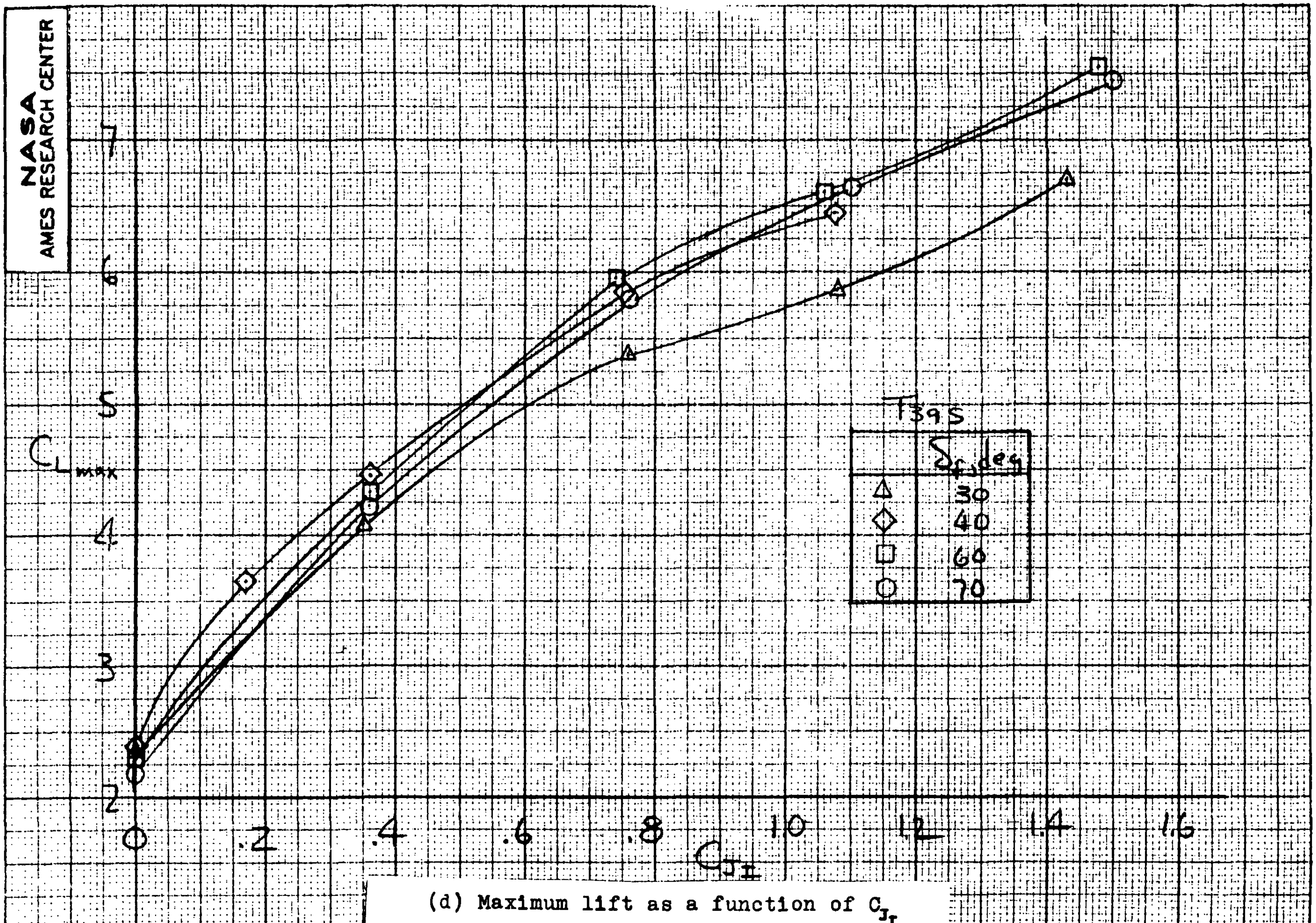

(d) Maximum lift as a function of C_{J_I}

Figure 23.- Concluded.

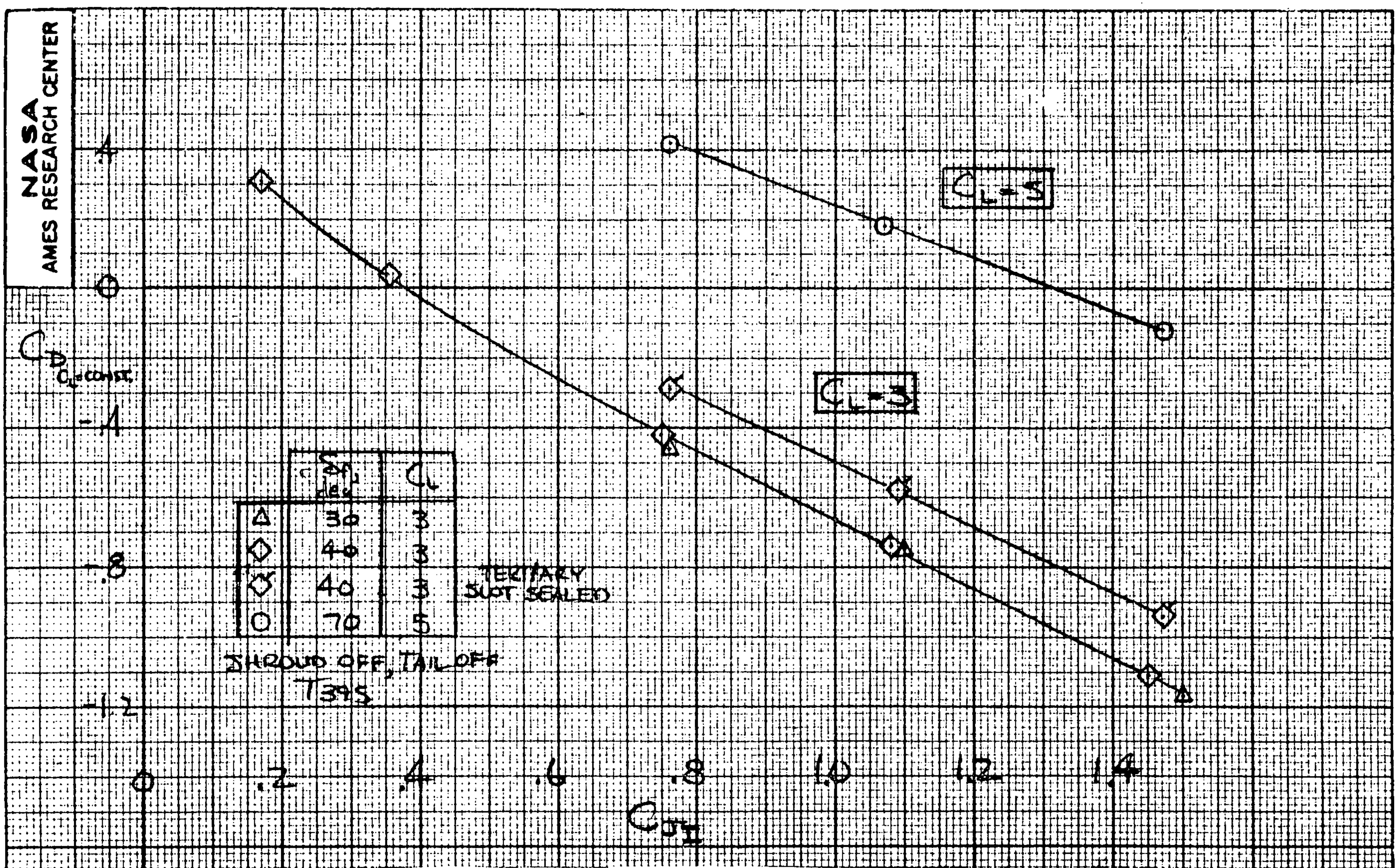

(a) Drag at constant lift as a function of C_{J_I}

Figure 24.- Summary of the longitudinal characteristic; shroud and intake door off.

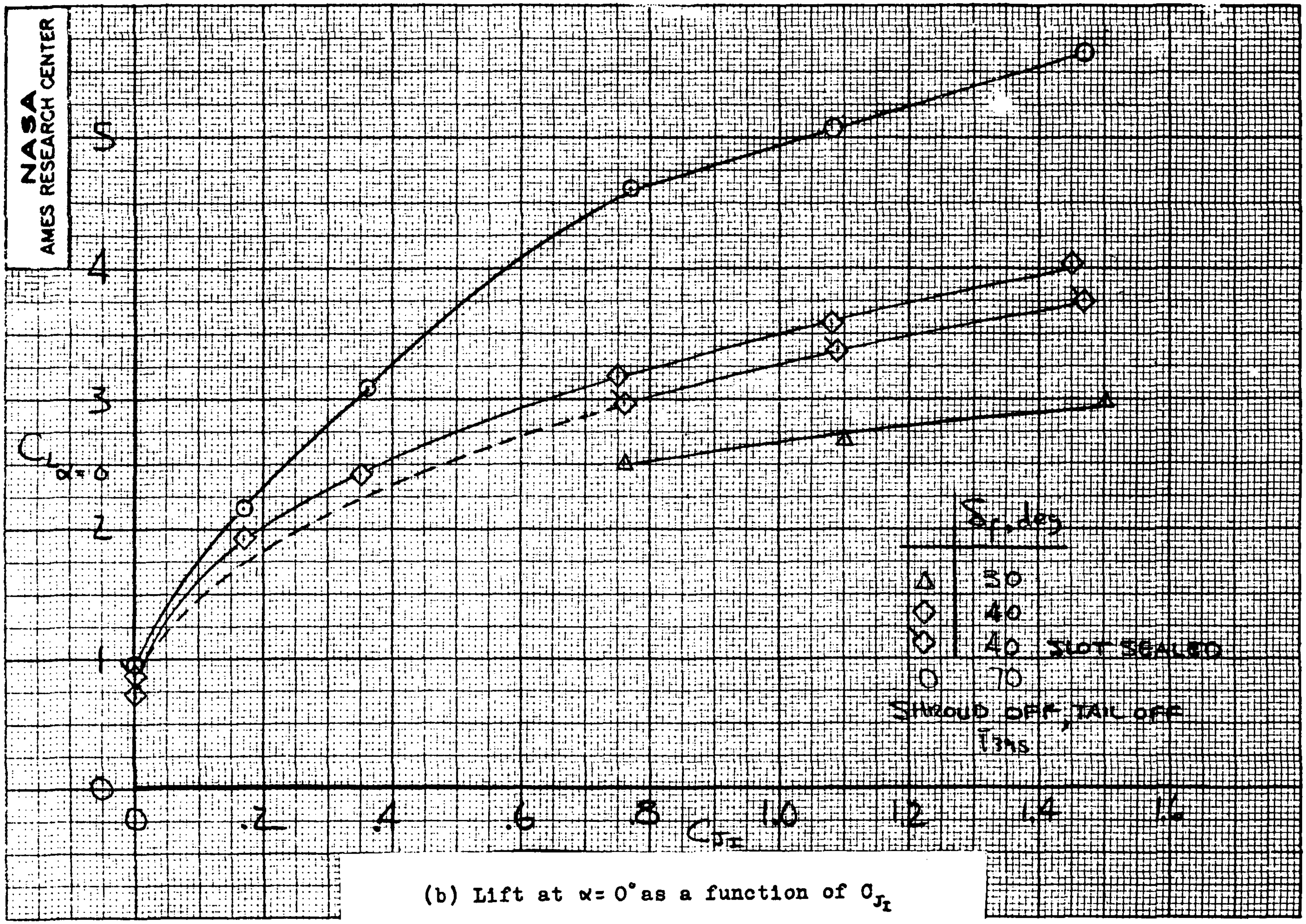

(b) Lift at $\alpha = 0°$ as a function of C_{J_I}

Figure 24.- Continued.

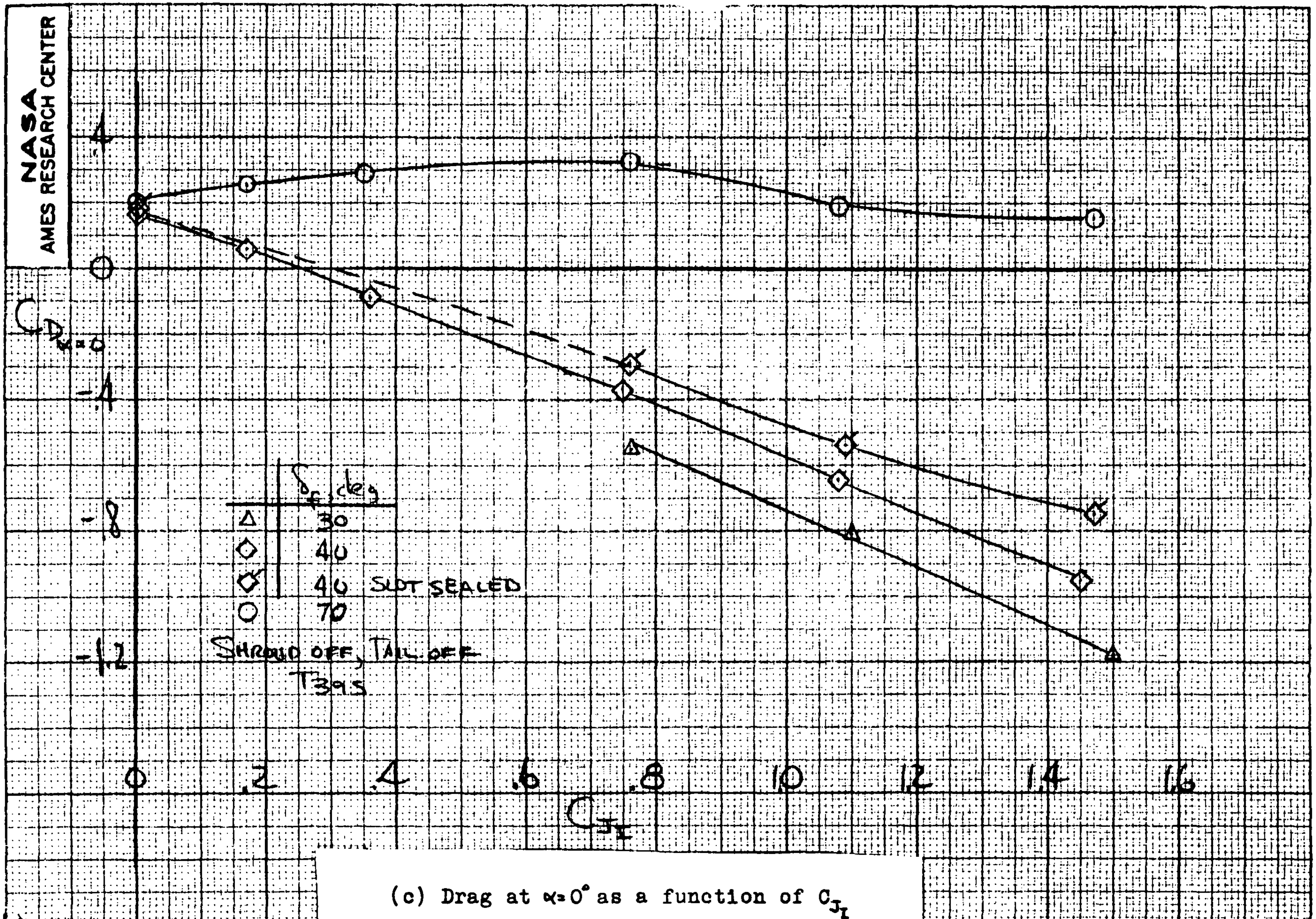

(c) Drag at $\alpha = 0^\circ$ as a function of C_{J_I}

Figure 24.- Continued.

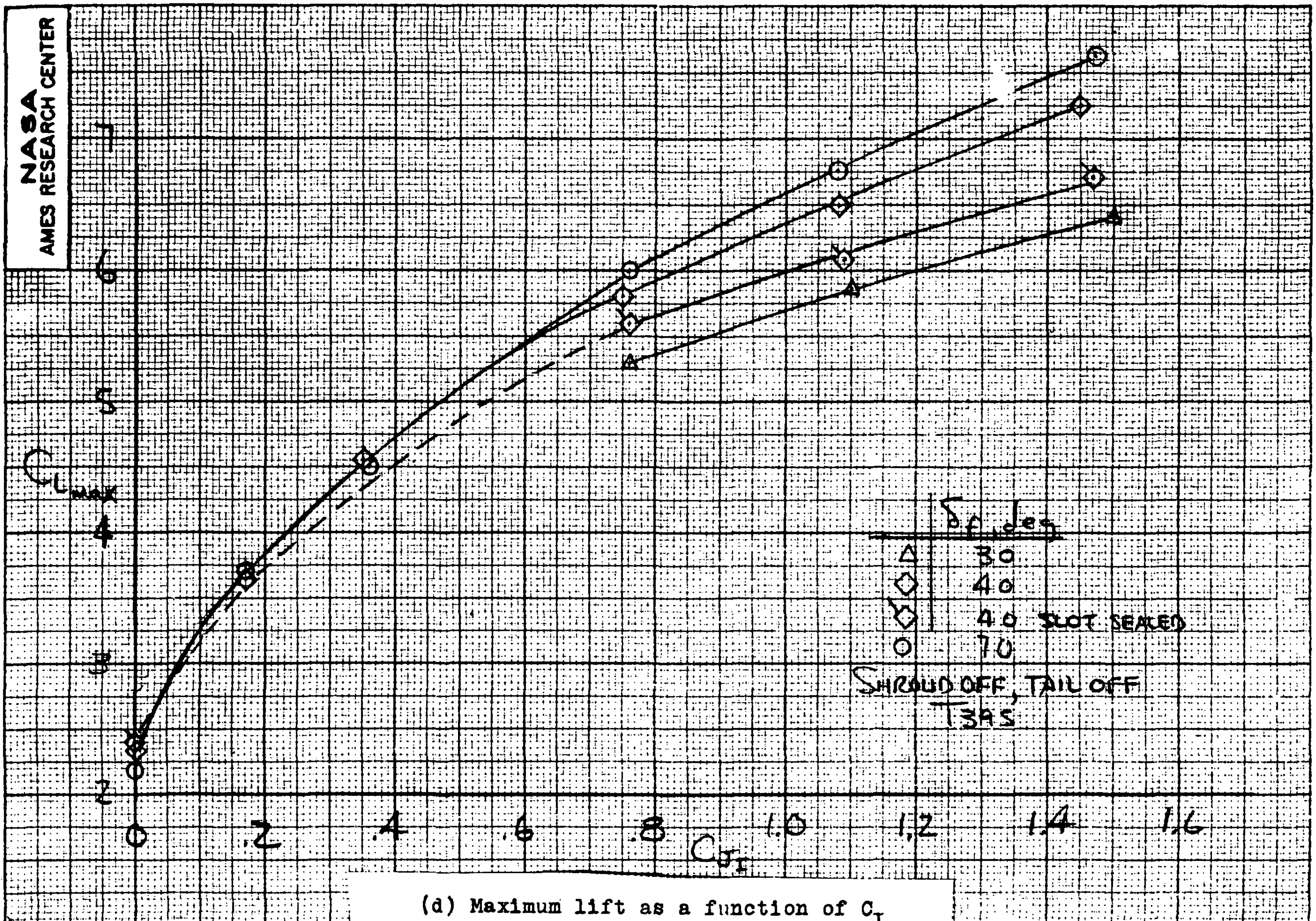

(d) Maximum lift as a function of C_{J_I}

Figure 24.- Concluded.

24d

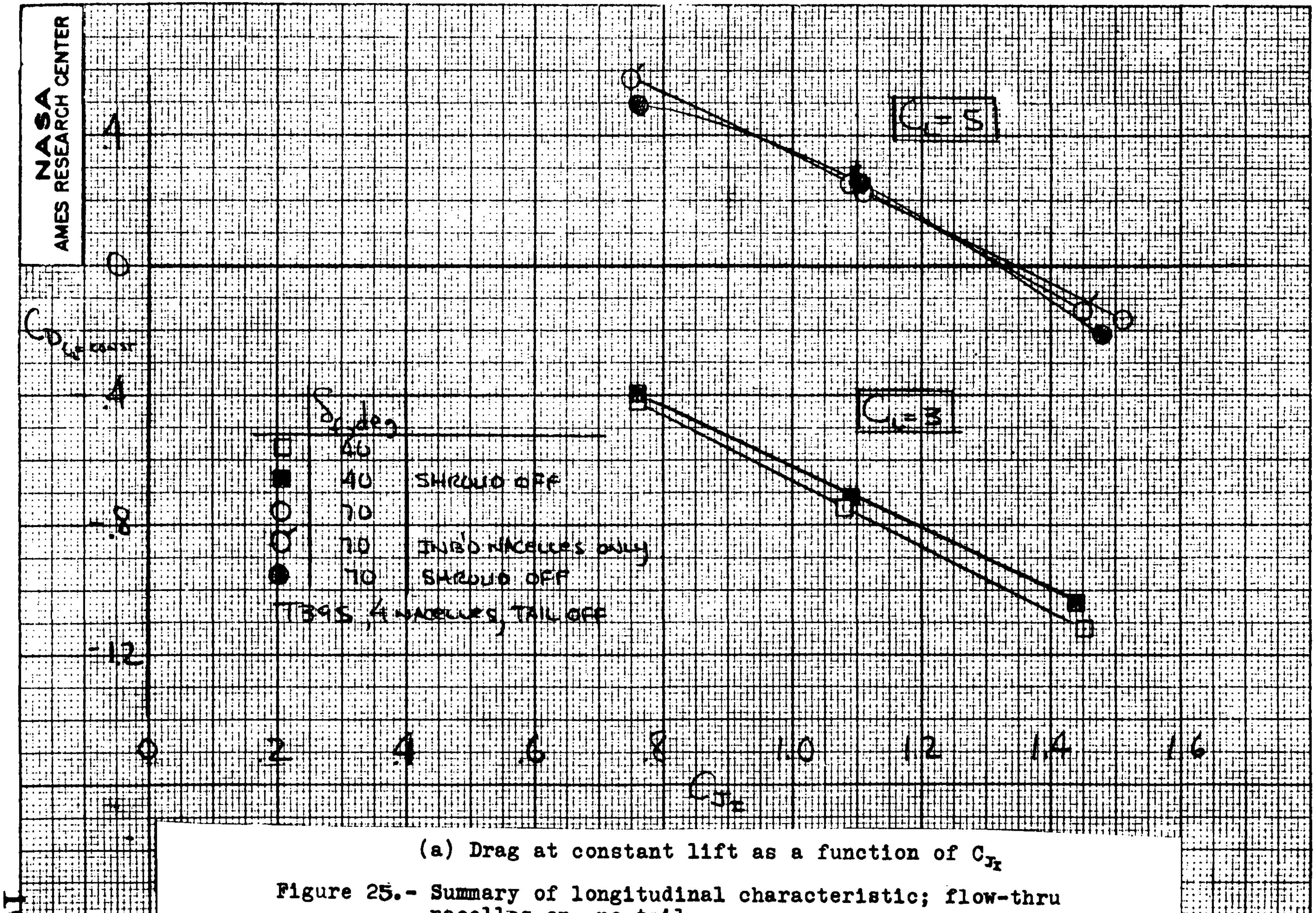

(a) Drag at constant lift as a function of C_{J_T}

Figure 25.- Summary of longitudinal characteristic; flow-thru nacelles on, no tail.

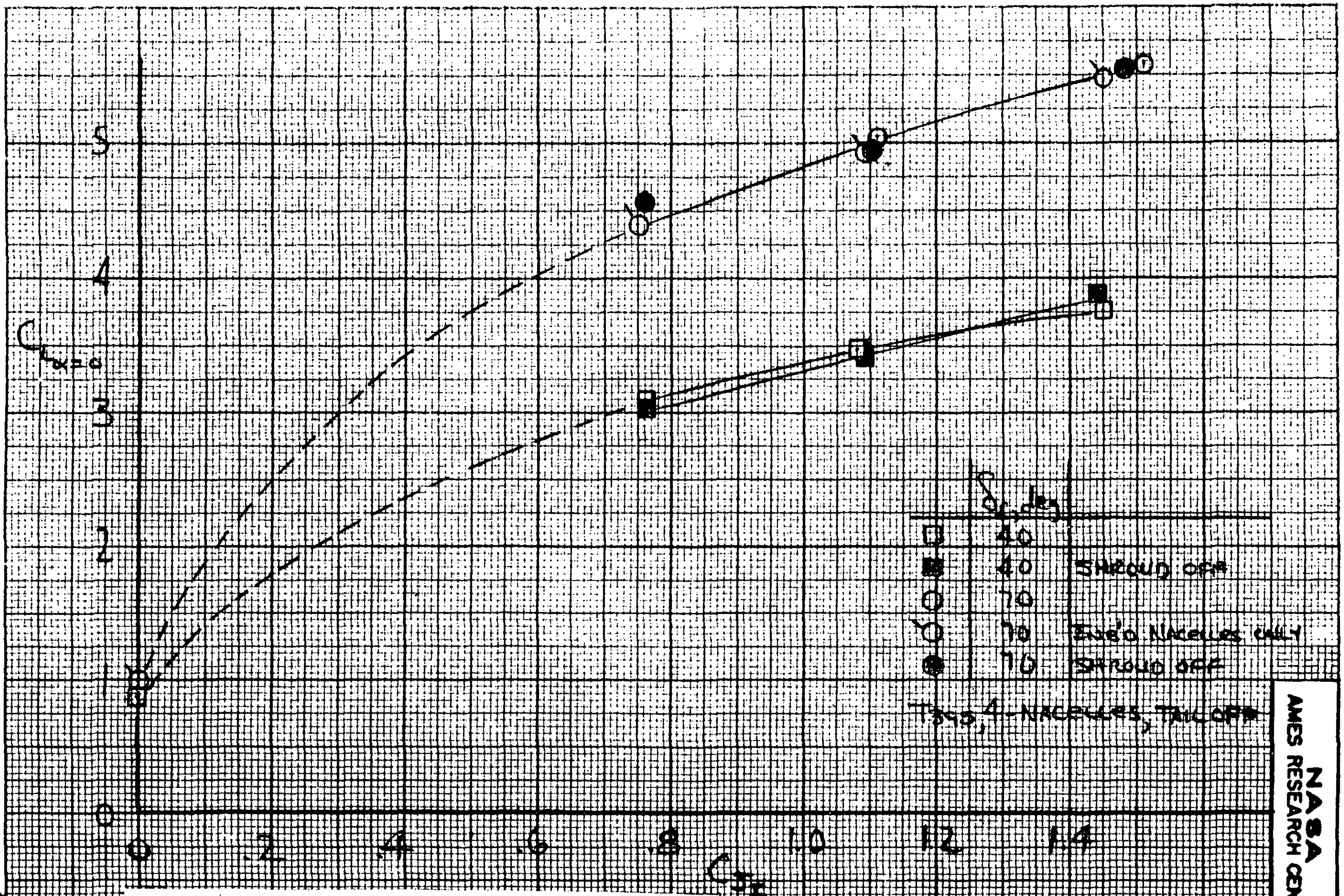

NASA
AMES RESEARCH CENTER

(b) Lift at $\alpha = 0°$ as a function of C_{J_I}

Figure 25.- Continued.

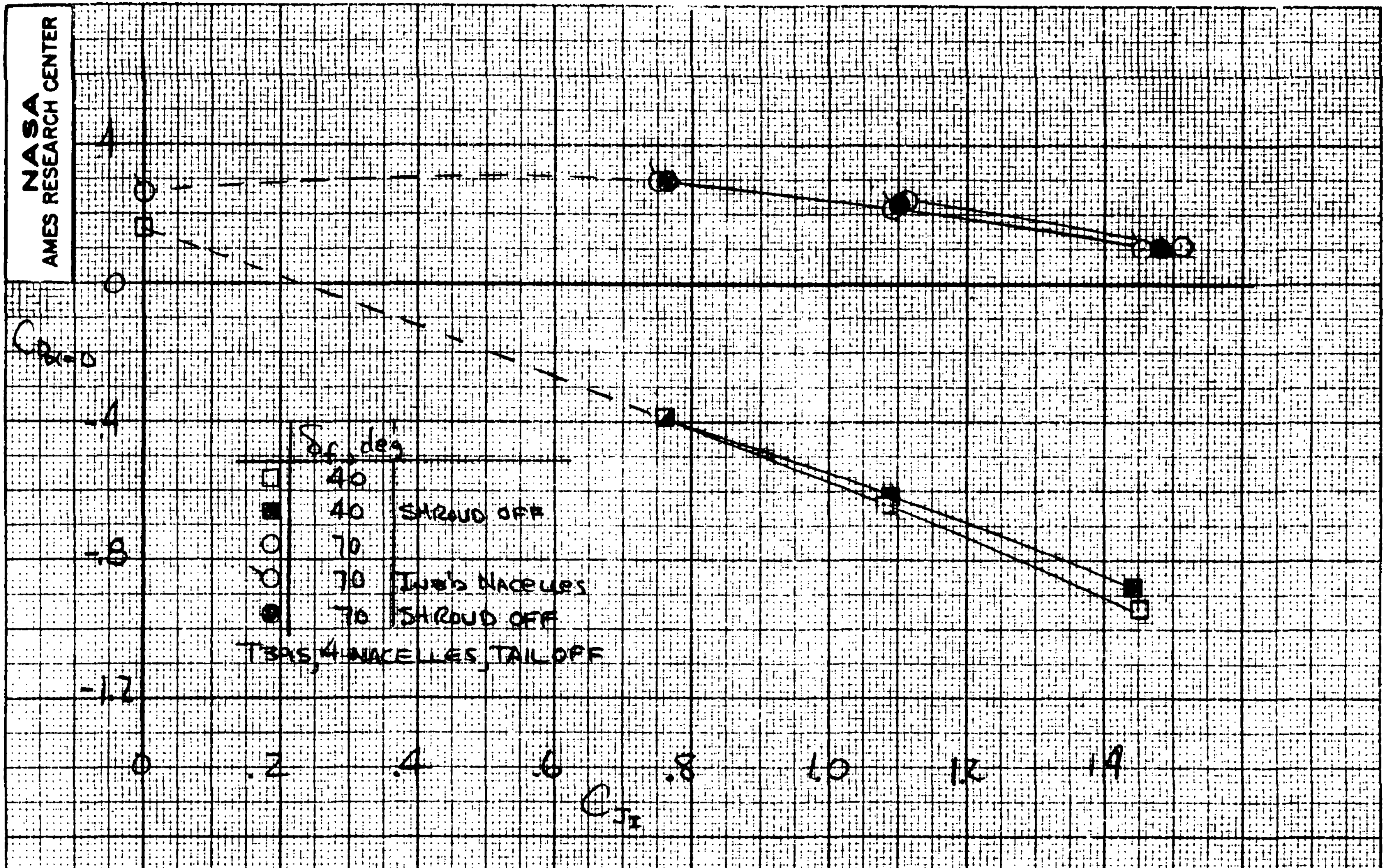

(c) Drag at $\alpha=0°$ as a function of C_{J_I}

Figure 25.- Continued.

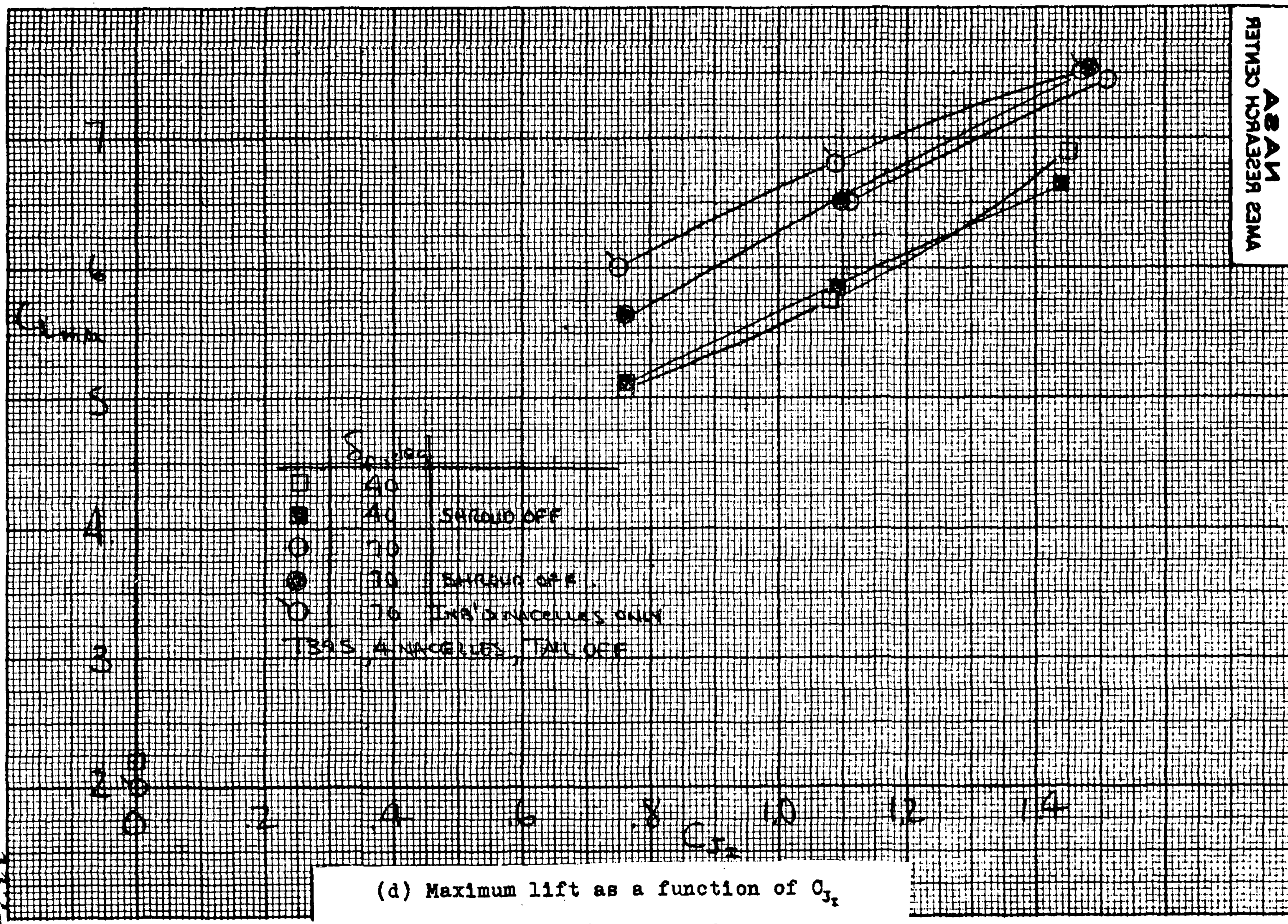

(d) Maximum lift as a function of C_{J_T}

Figure 25.- Concluded.

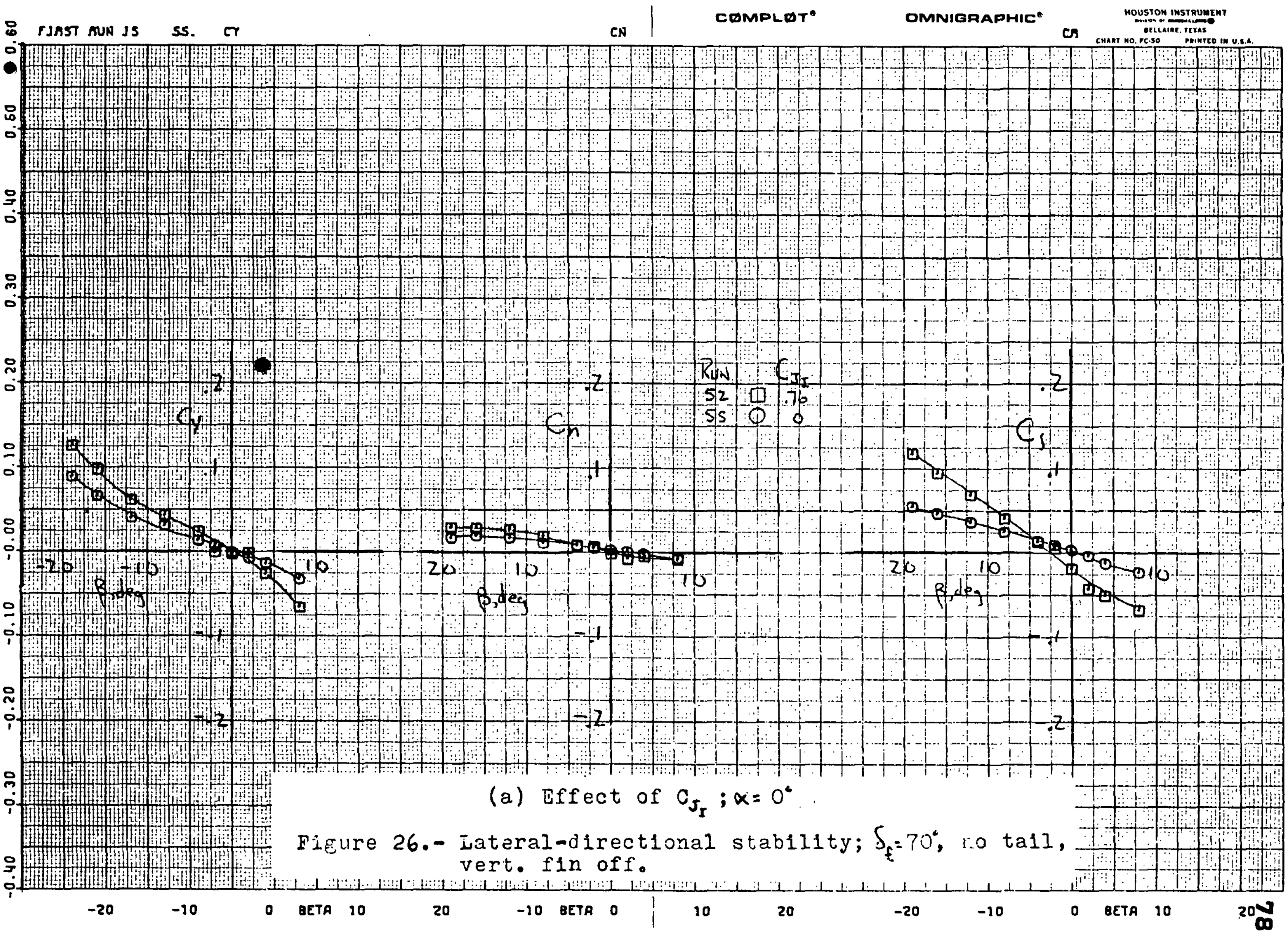

(a) Effect of C_{J_T} ; $\alpha = 0°$

Figure 26.- Lateral-directional stability; $\delta_f = 70°$, no tail, vert. fin off.

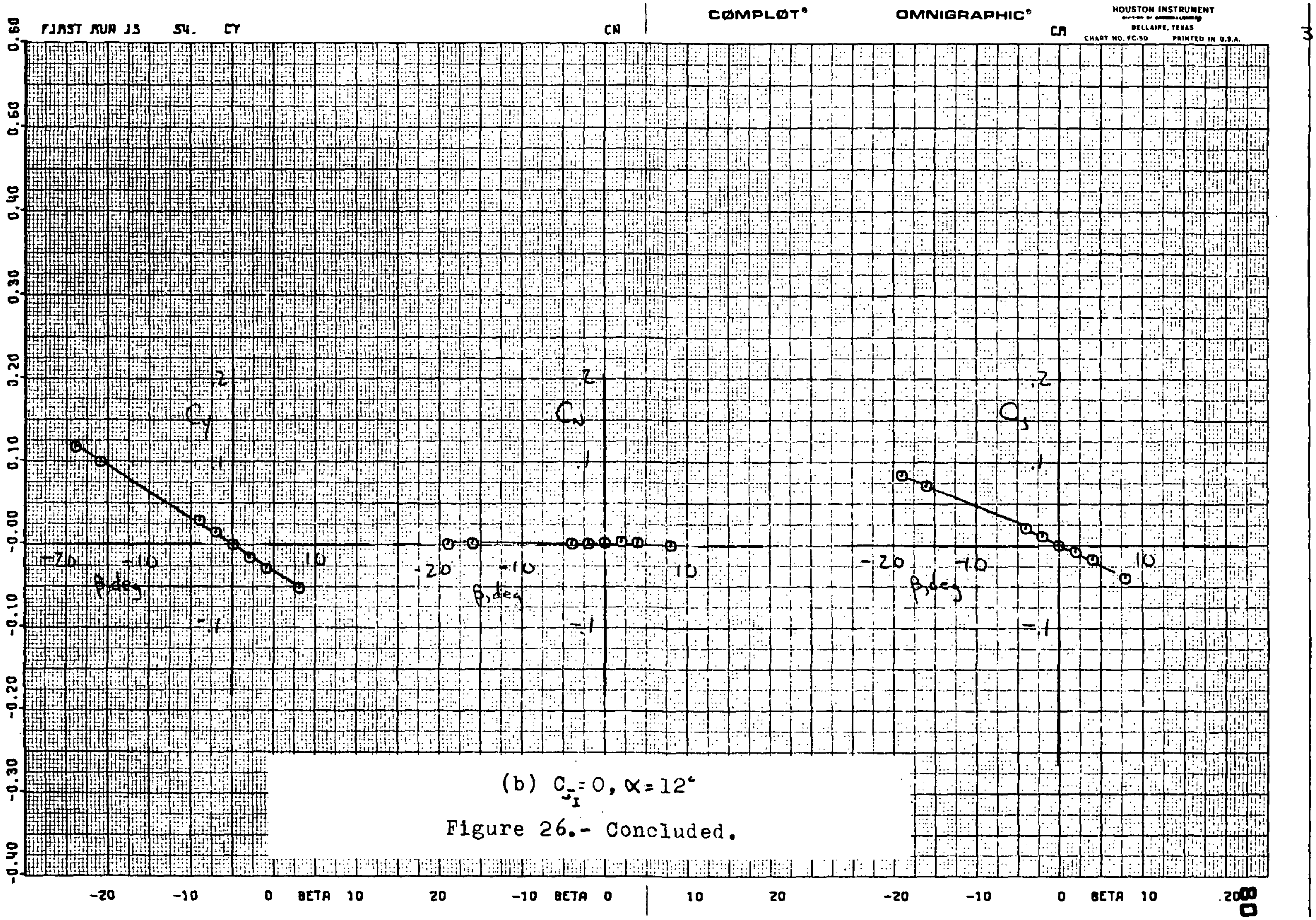

(b) $C_{J_I} = 0$, $\alpha = 12°$

Figure 26.- Concluded.

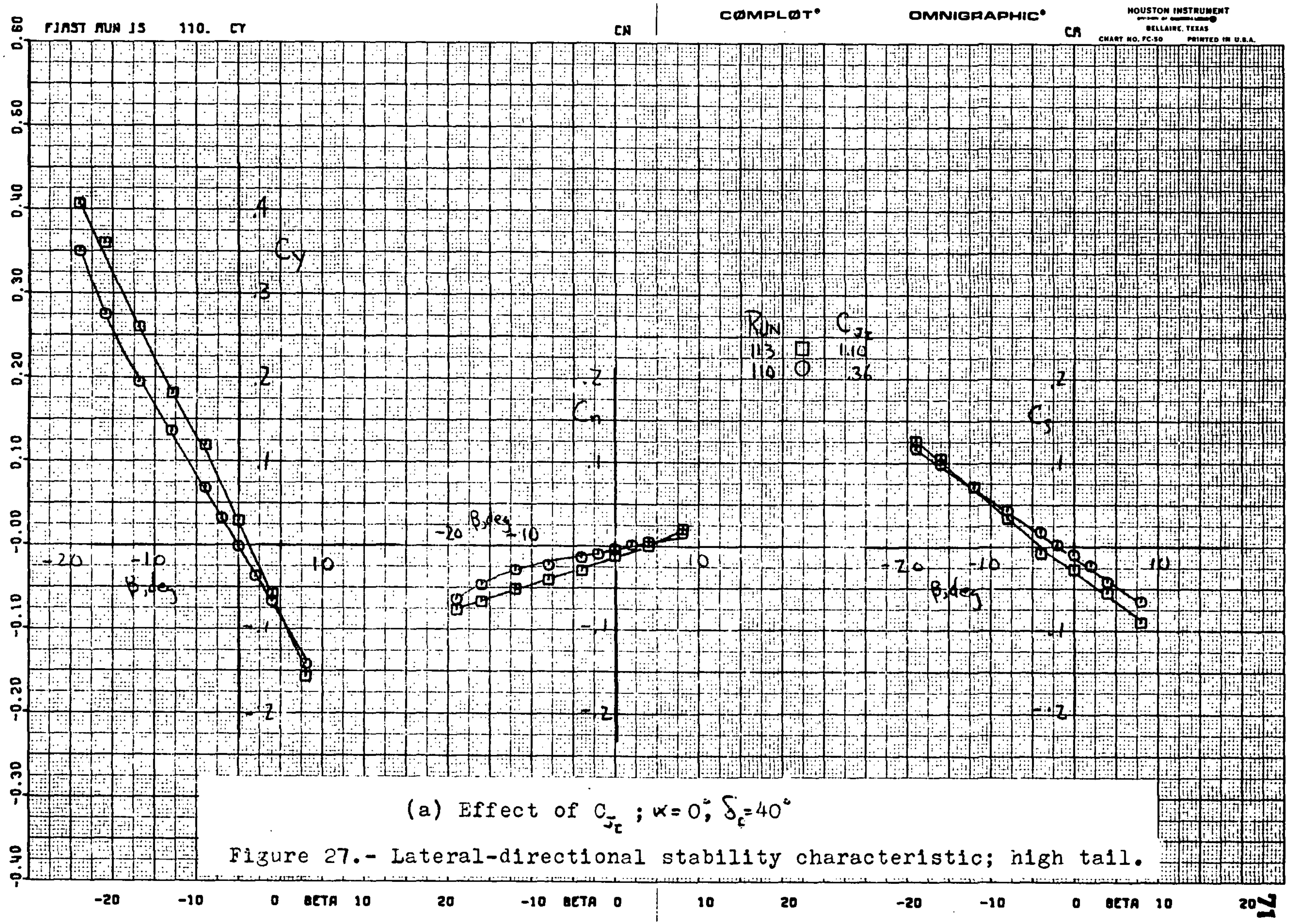

(a) Effect of C_{J_c} ; $\alpha = 0°$, $\delta_c = 40°$

Figure 27.- Lateral-directional stability characteristic; high tail.

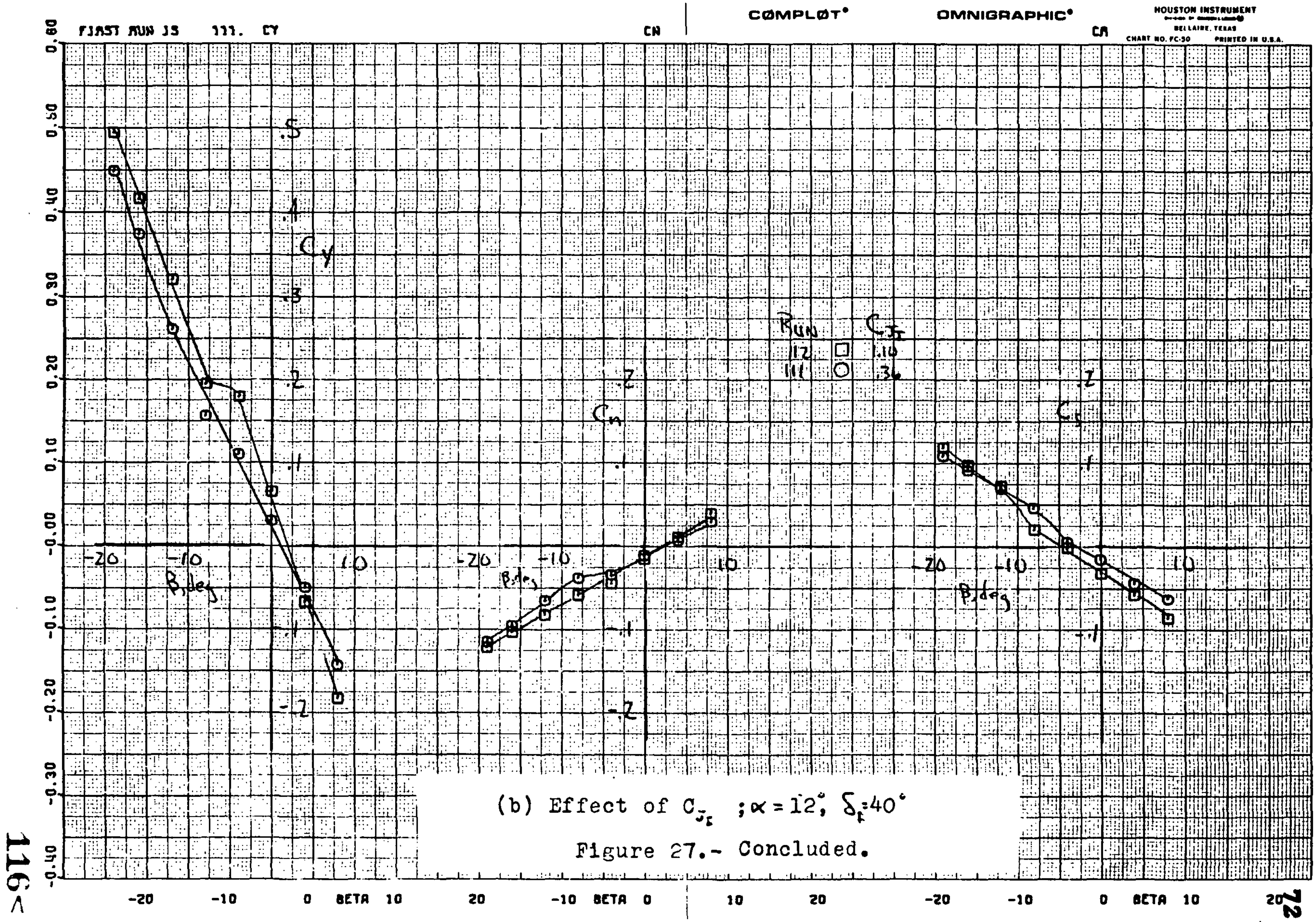

(b) Effect of C_{J_Σ} ; $\alpha = 12°$, $\delta_f = 40°$

Figure 27.- Concluded.

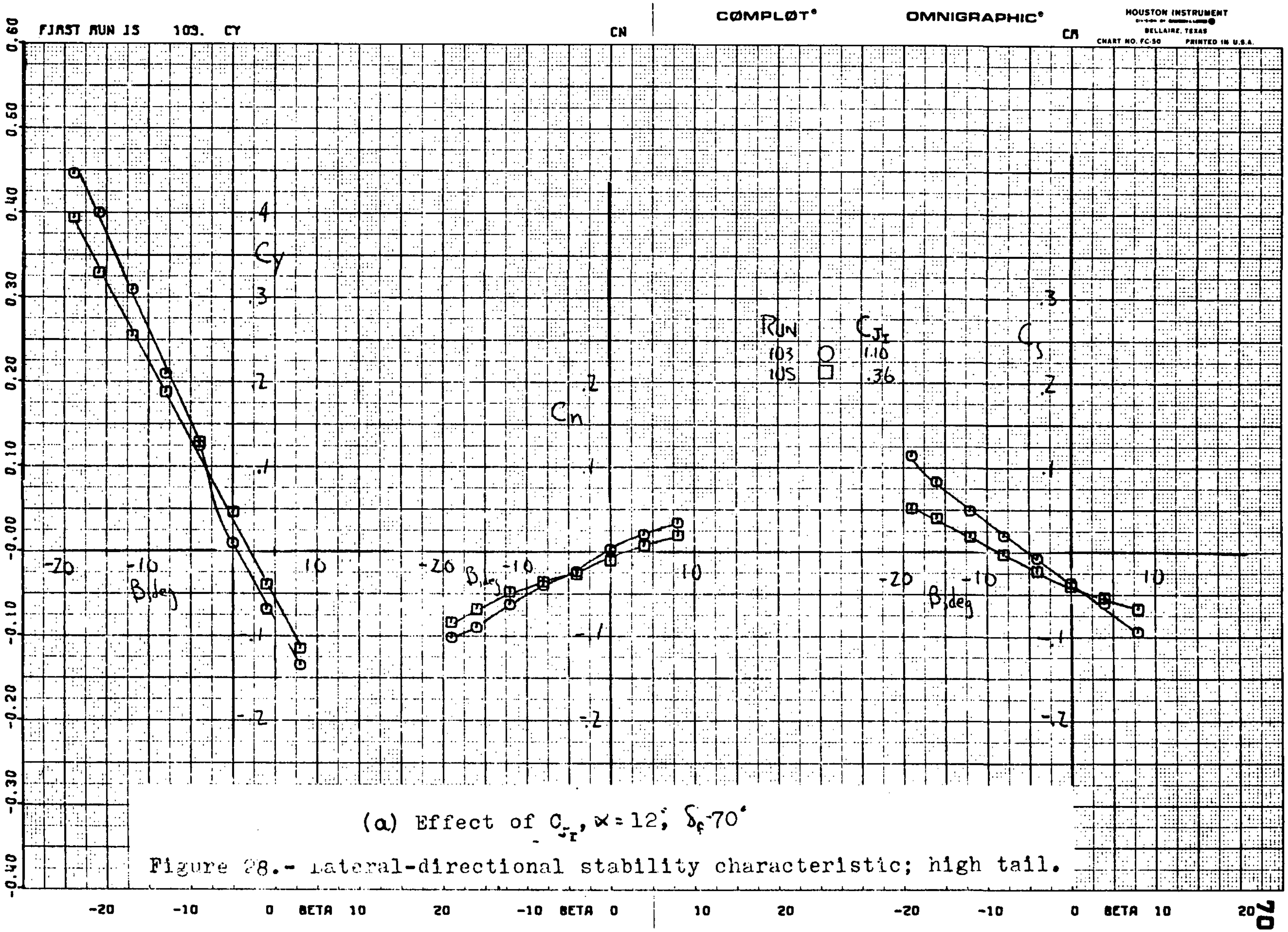

(a) Effect of C_{J_T}, $\alpha = 12°$, δ_f 70°

Figure 28.- Lateral-directional stability characteristic; high tail.

38

28a

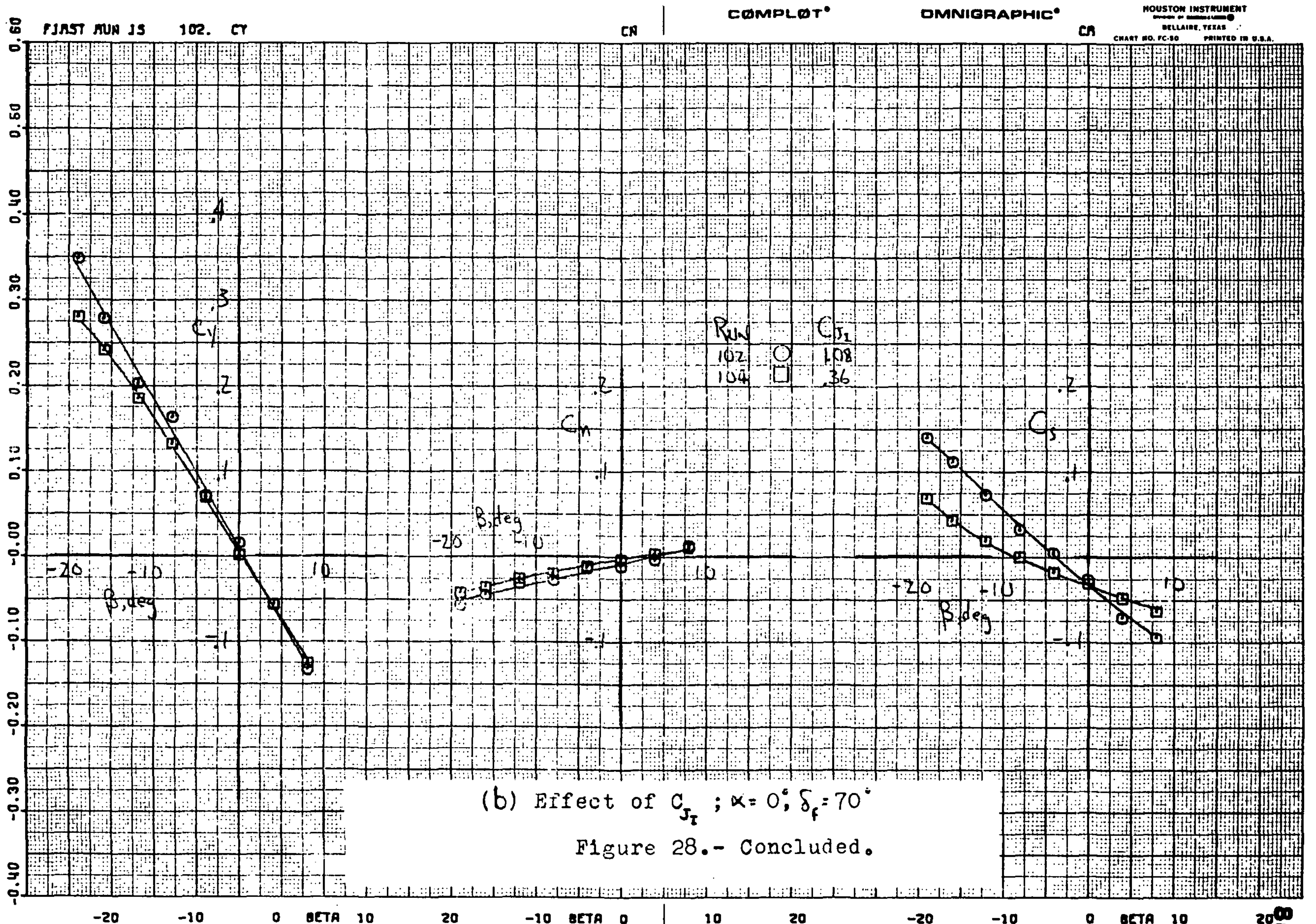

(b) Effect of C_{J_I} ; $\alpha = 0°$, $\delta_f = 70°$

Figure 28.- Concluded.

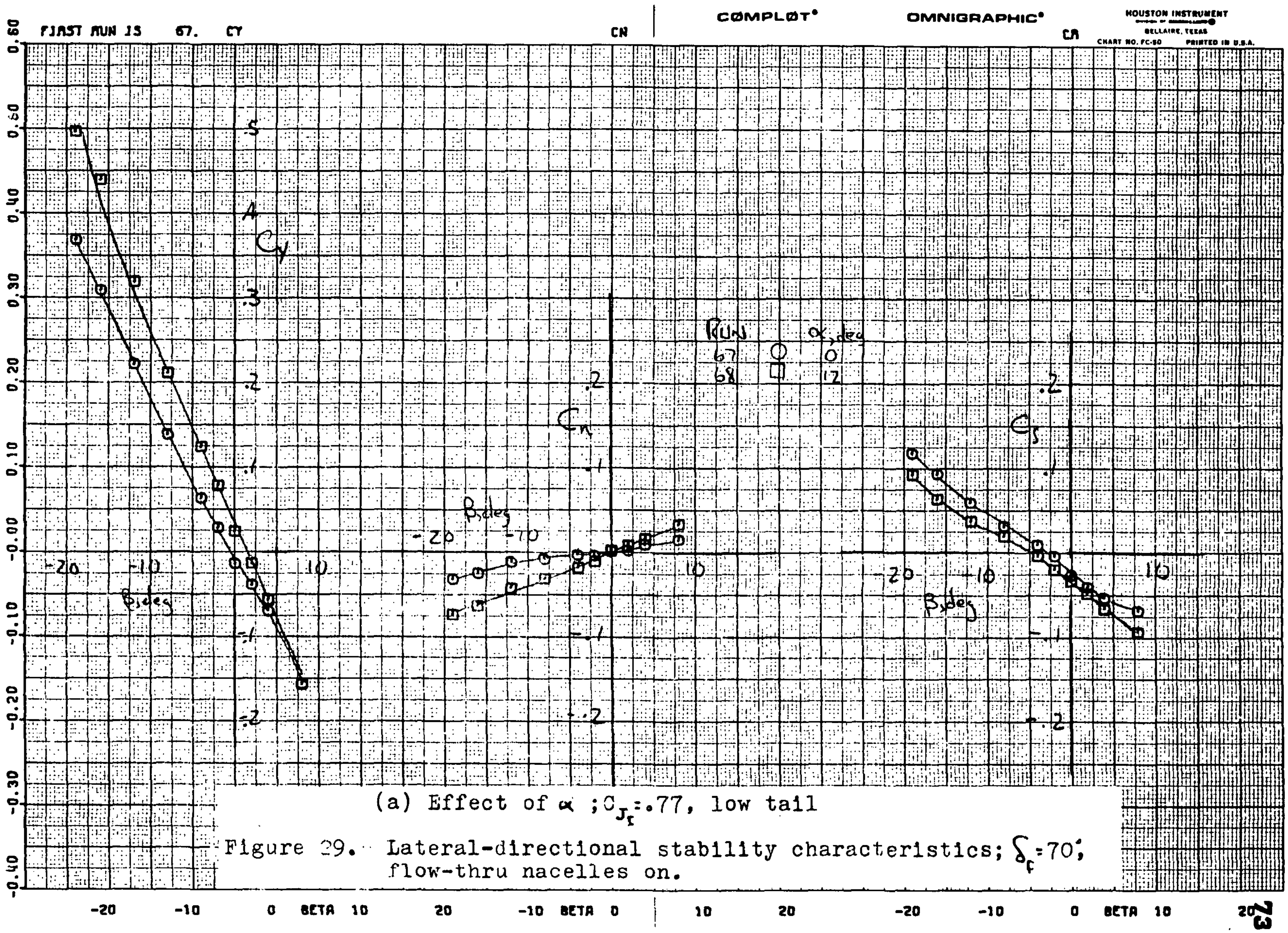

(a) Effect of α ; C_{J_r} = .77, low tail

Figure 29. Lateral-directional stability characteristics; δ_f = 70°, flow-thru nacelles on.

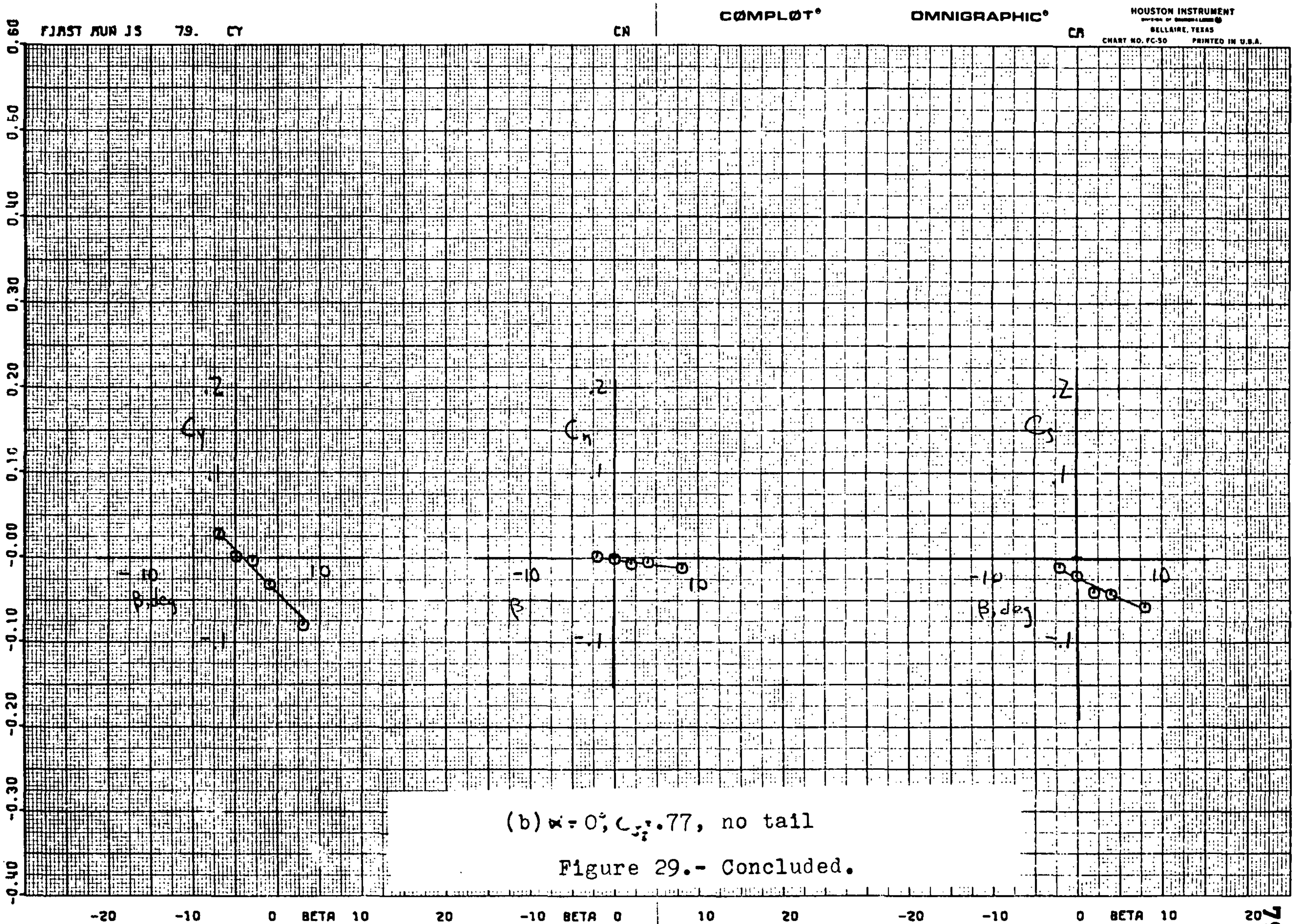

(b) $\alpha = 0°$, $C_{J_i} = .77$, no tail

Figure 29.- Concluded.

44

296

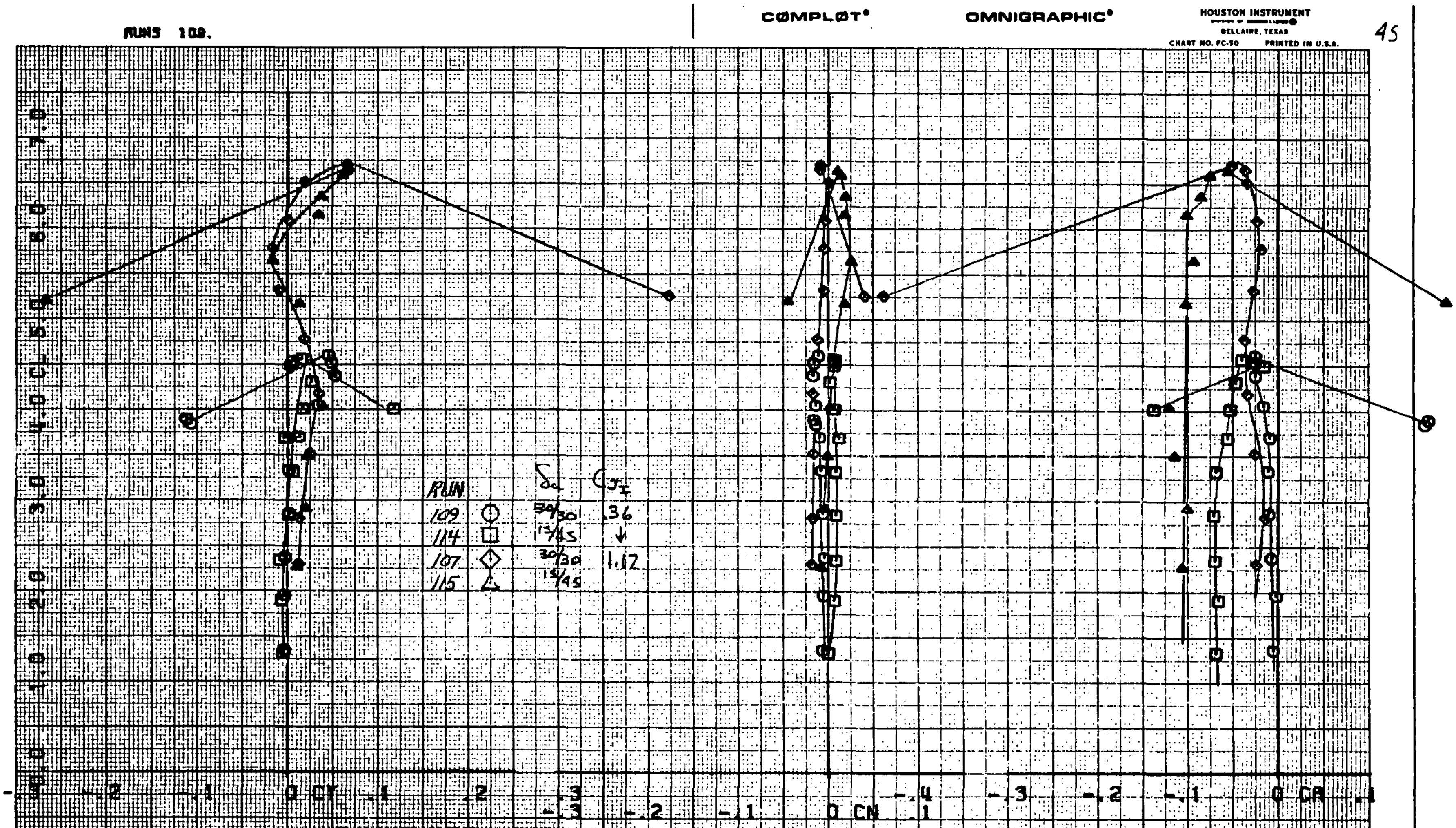

(a) $\beta = 0°$, $C_{J_I} = .36$ and 1.12

Figure 30.- Lateral stability and control with blown aileron; $\delta_f = 40°$, high tail.

30a

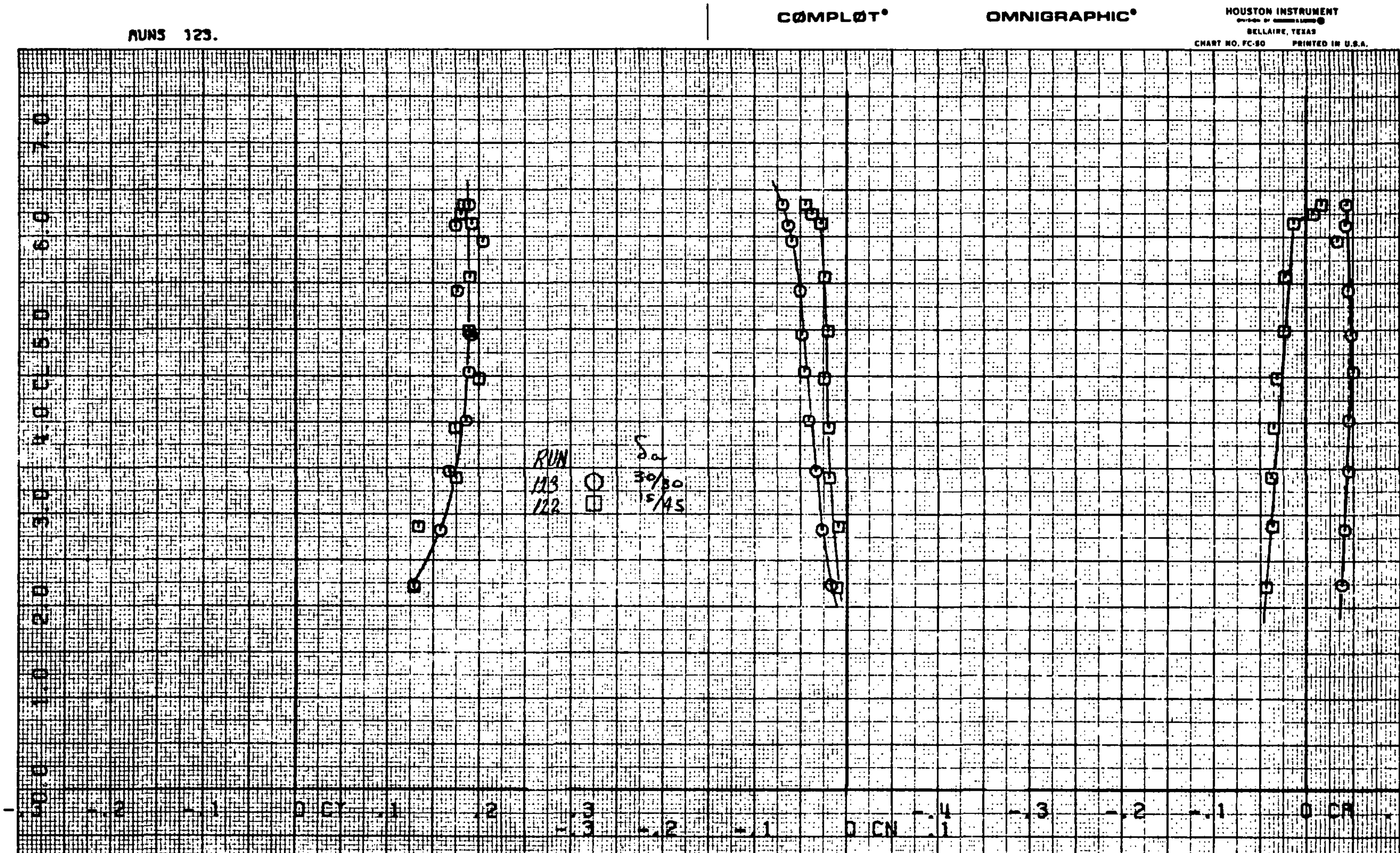

(b) $\beta = 8^\circ$; $C_{J_I} = 1.1$

Figure 30.- Continued.

47

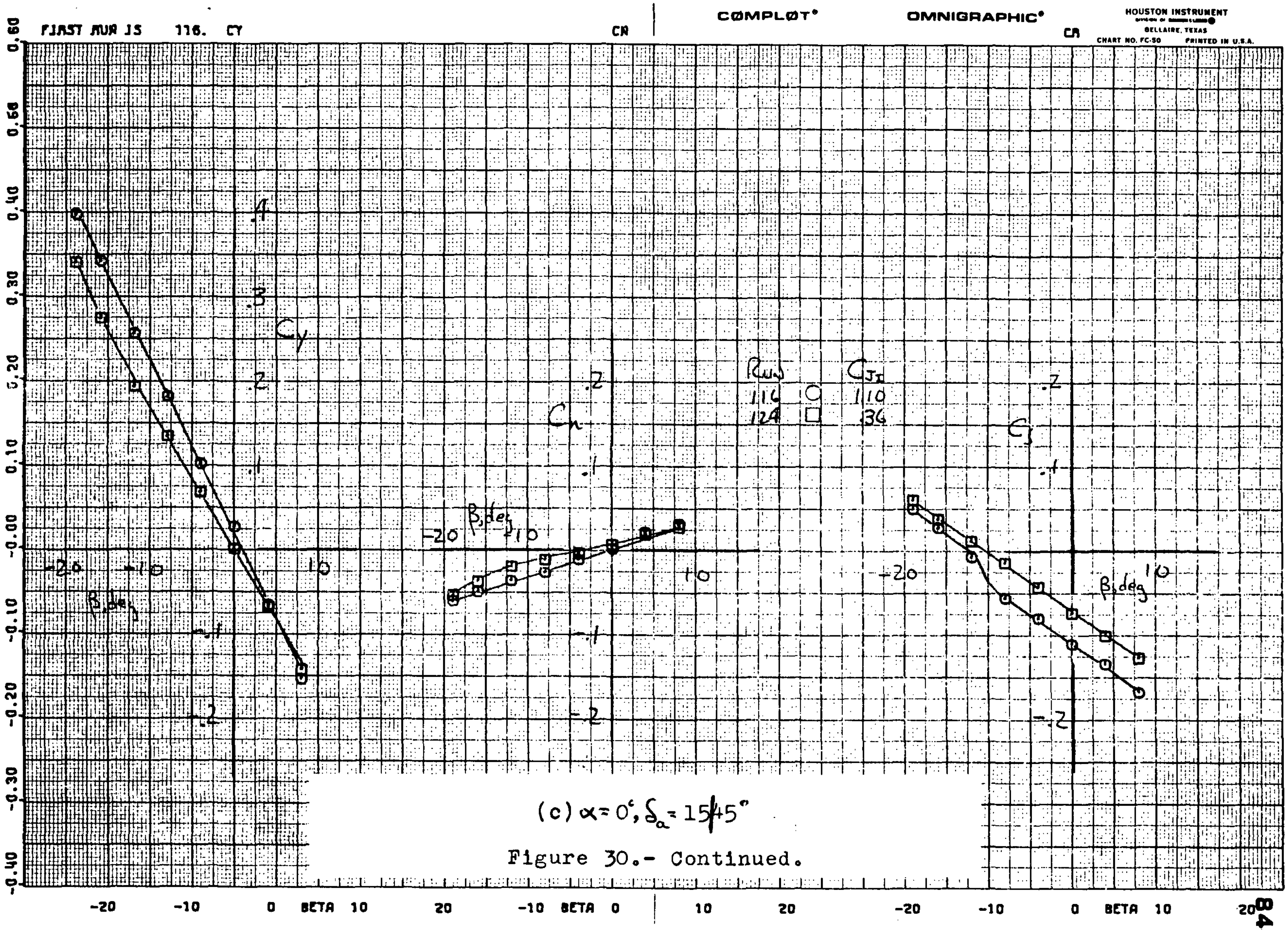

(c) $\alpha = 0°, \delta_a = 15°$

Figure 30.- Continued.

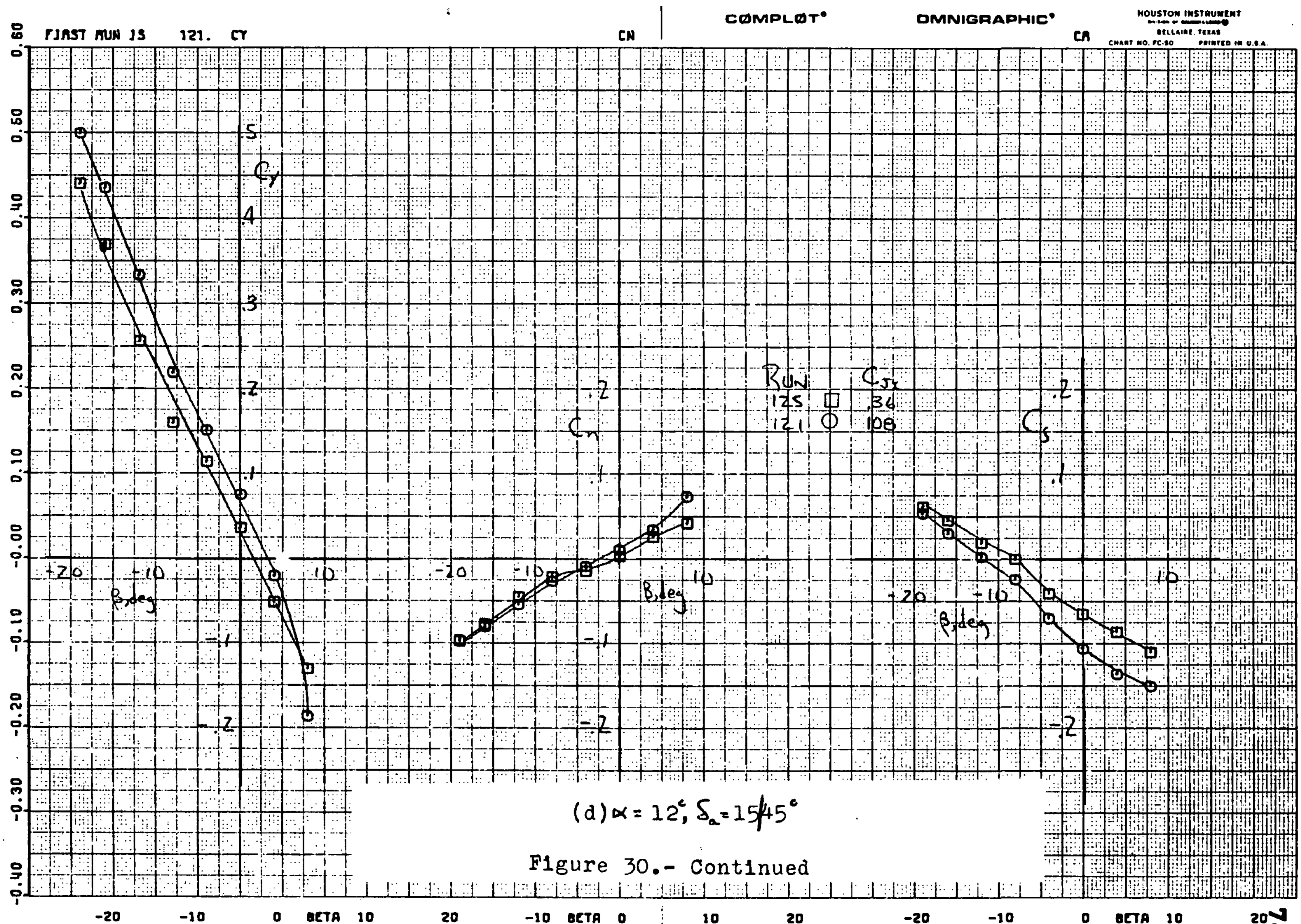

(d) $\alpha = 12°$, $\delta_a = 15/45°$

Figure 30.- Continued

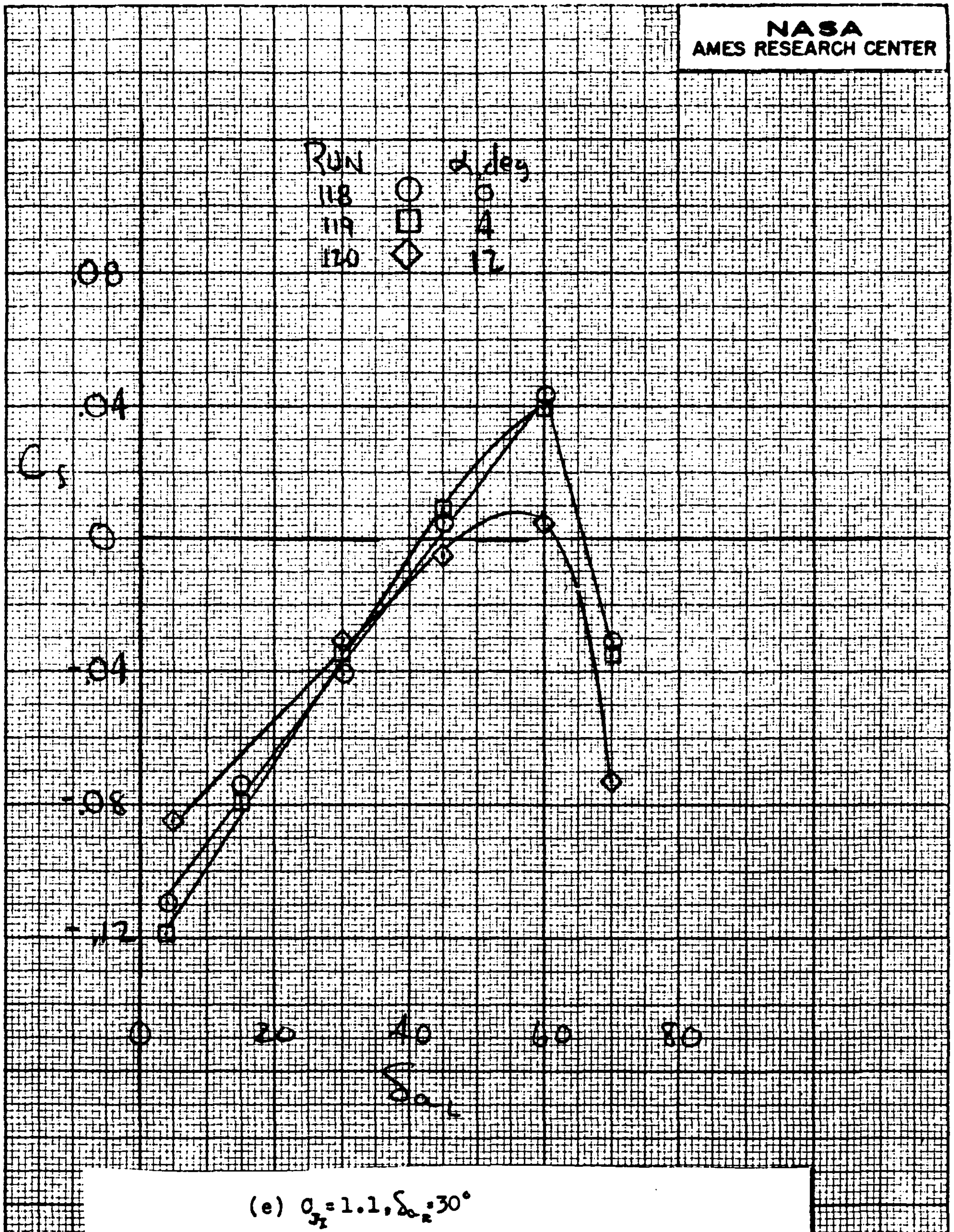

(e) $C_{J_T} = 1.1, \delta_{a_R} = 30°$

Figure 30.- Continued.

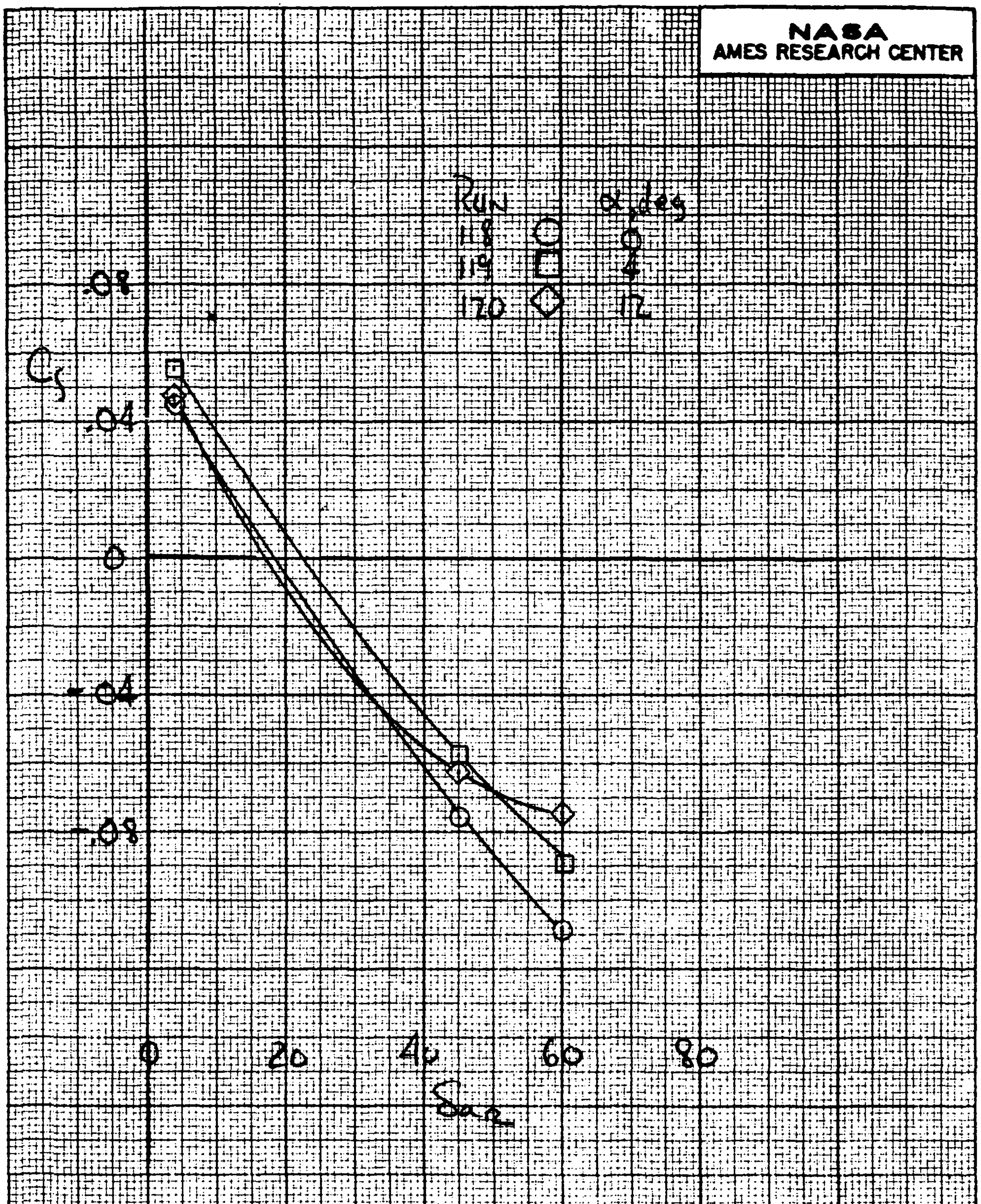

(f) C_{J_I}=1.1, δ_{a_L}=30°

Figure 30.- Concluded.

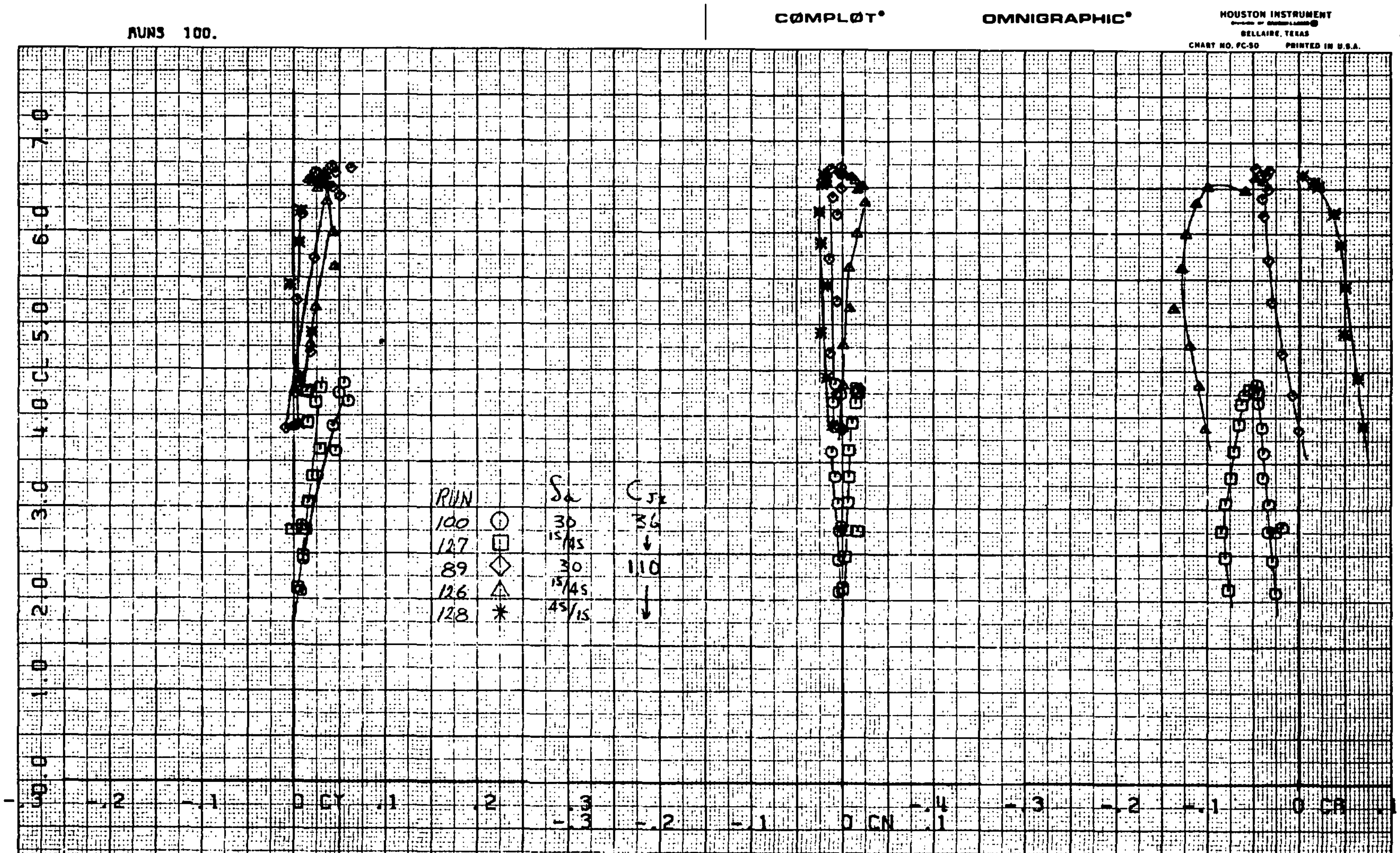

(a) C_{J_Z} = .36 and 1.10

Figure 31.- Lateral stability and control with a blown aileron; δ_f = 70°, high tail.

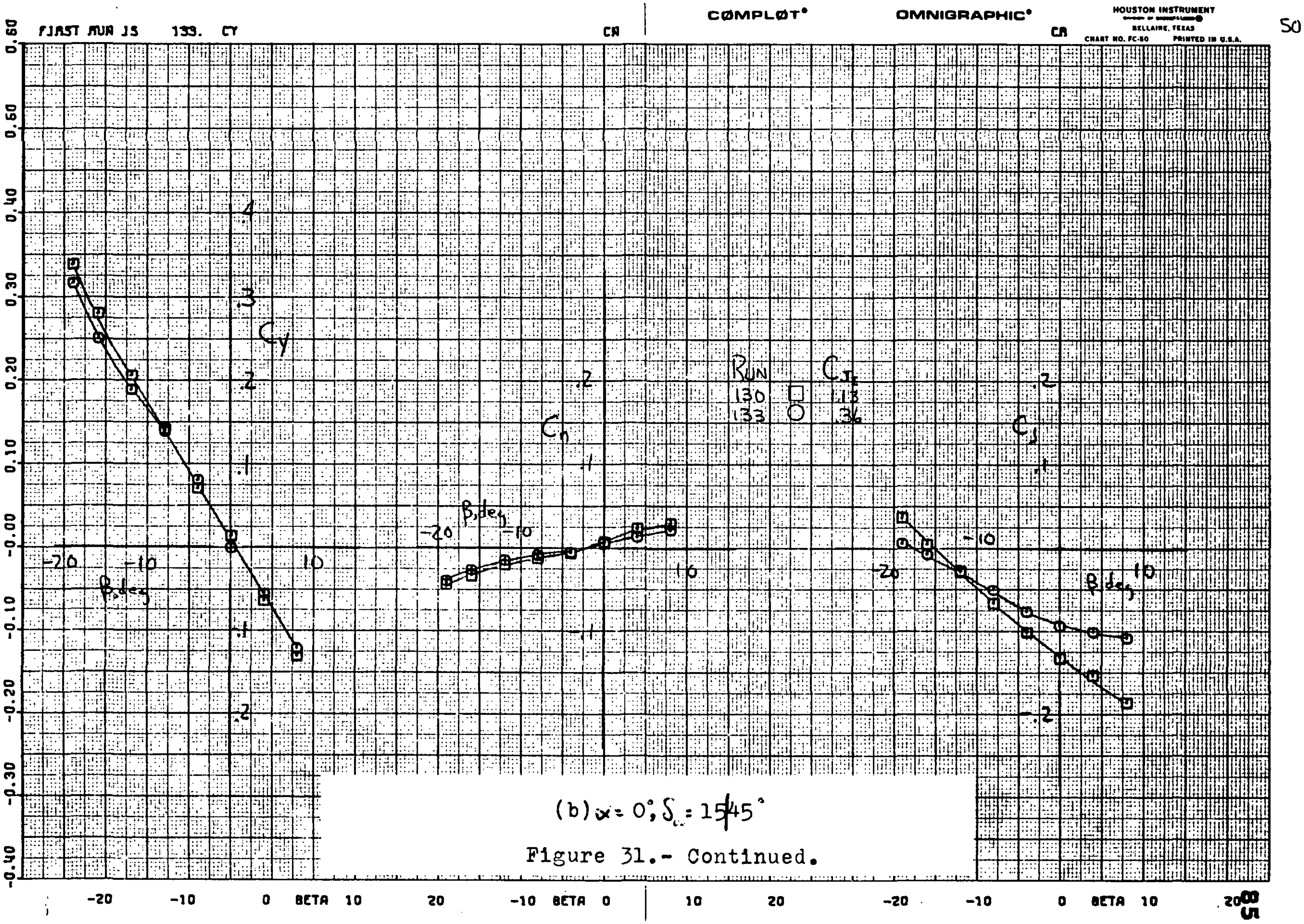

(b) $\alpha = 0^\circ, \delta = 15/45^\circ$

Figure 31.- Continued.

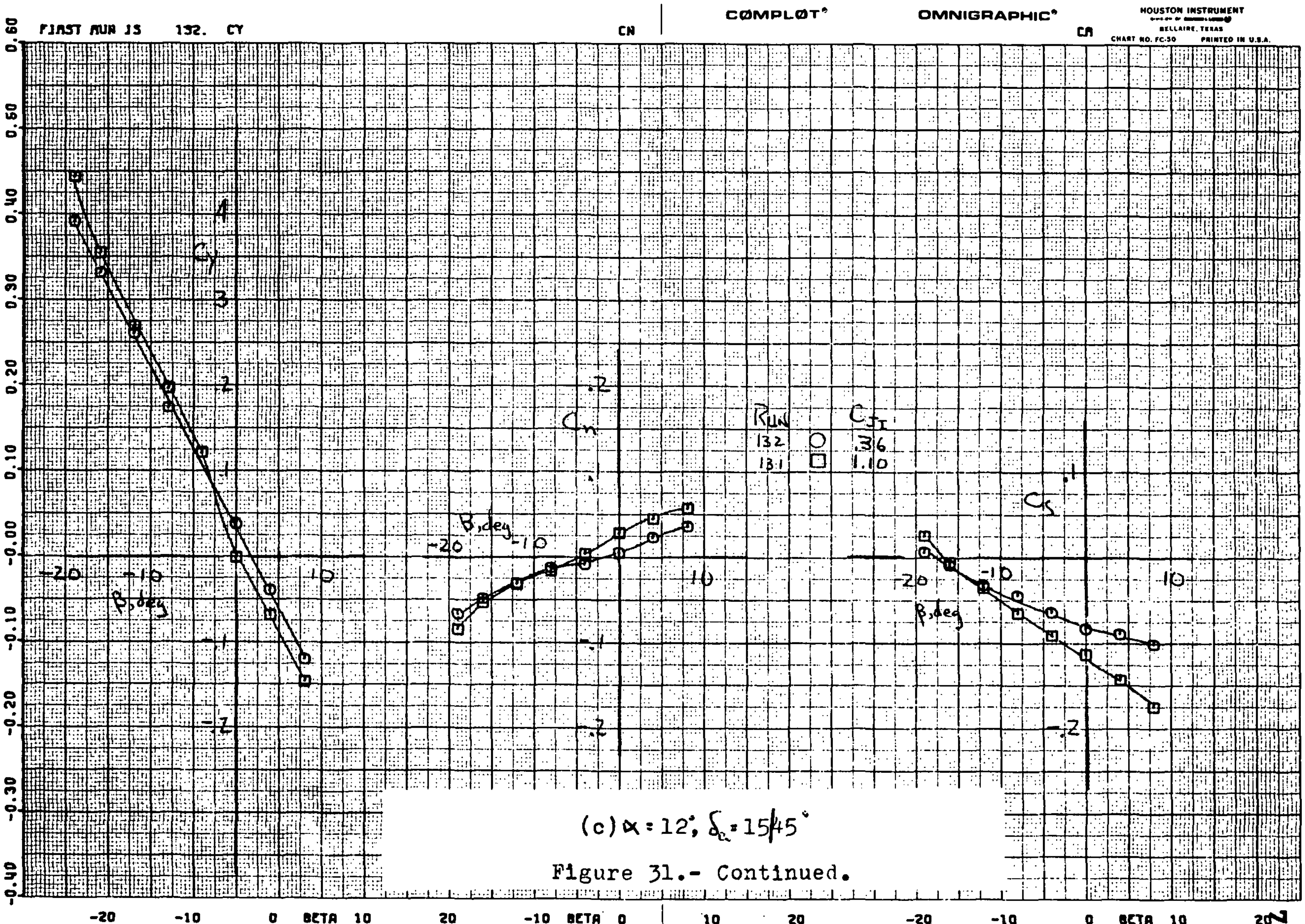

(c) $\alpha = 12°$, $\delta_c = 15/45°$

Figure 31.- Continued.

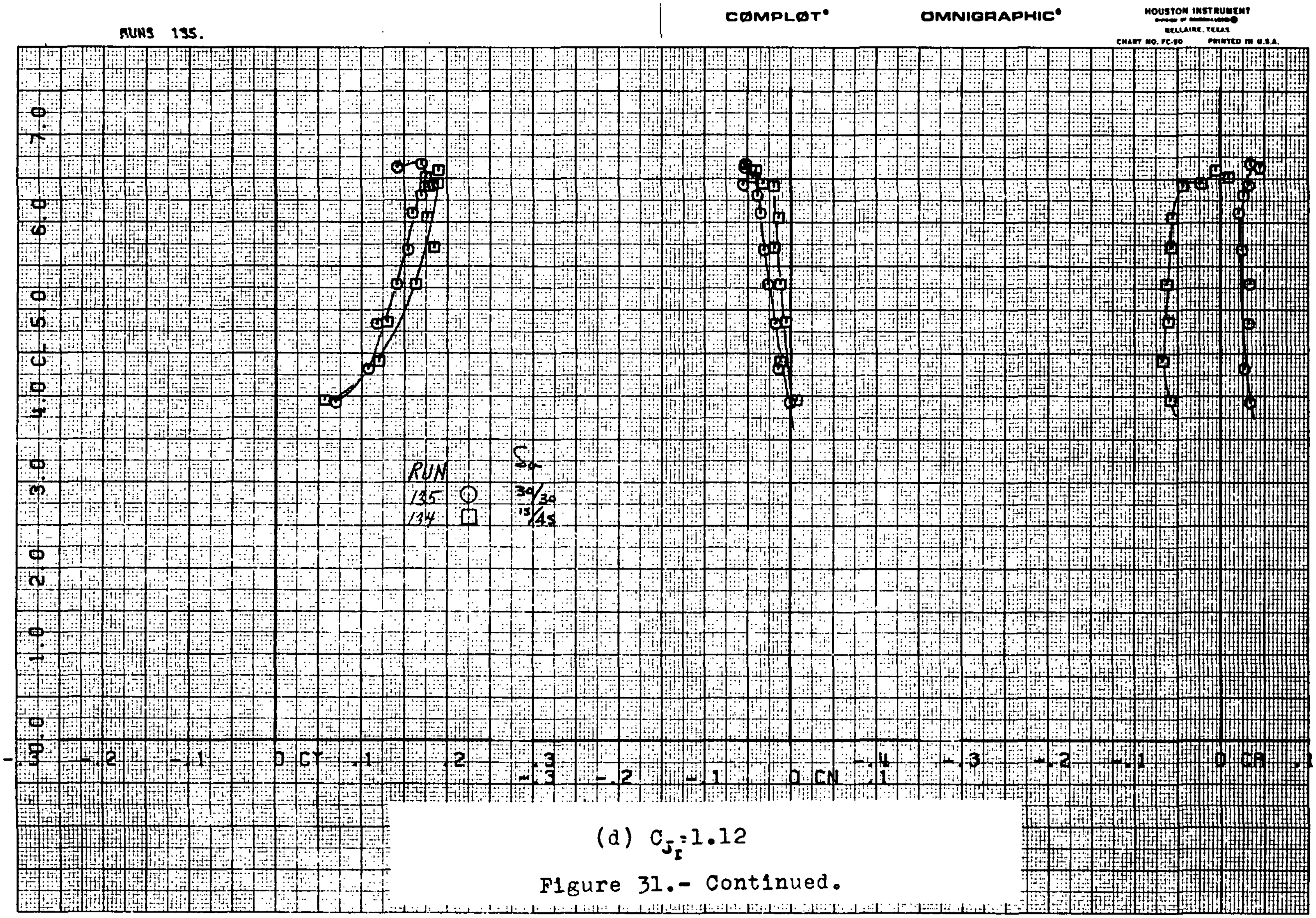

(d) C_{J_r}=1.12

Figure 31.- Continued.

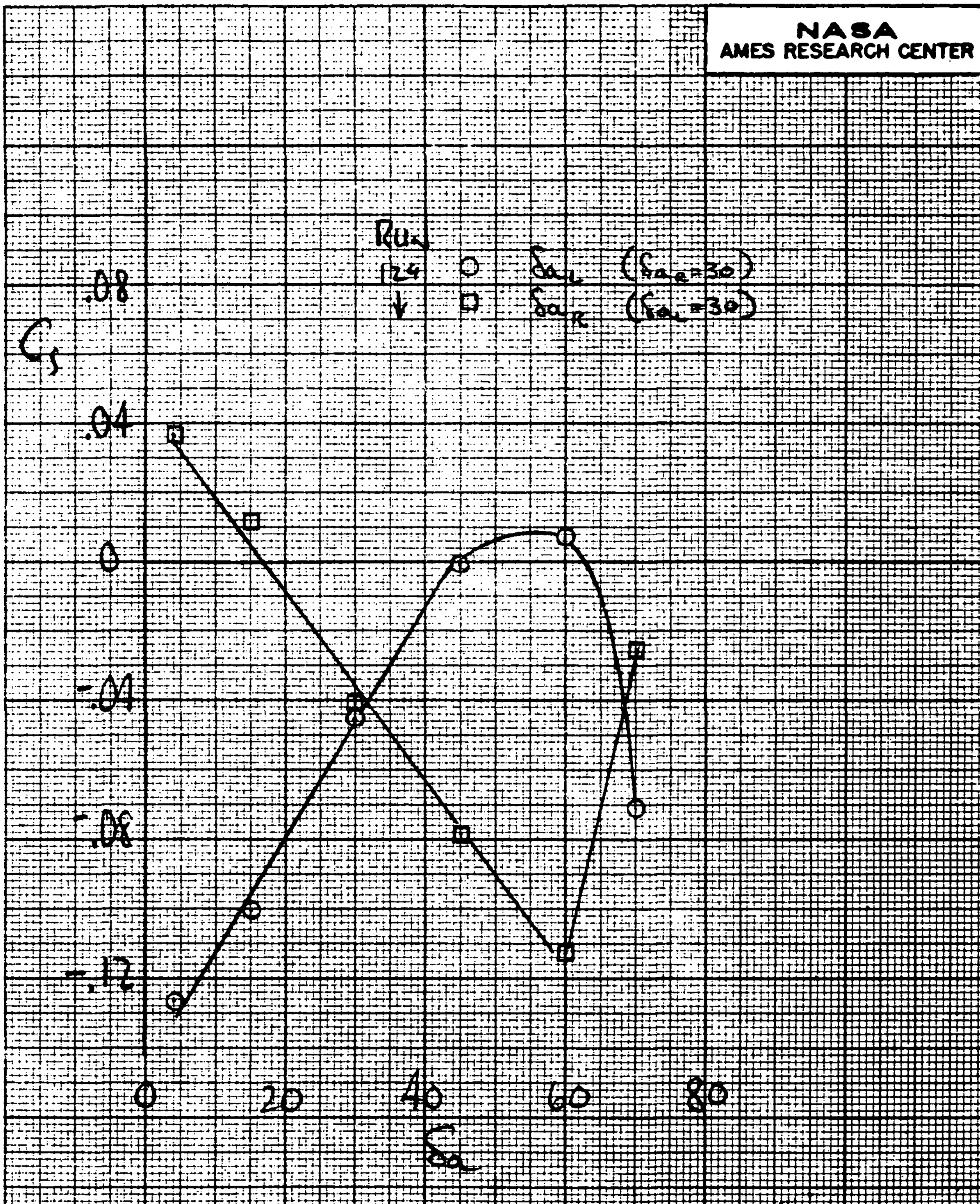

(e) $\alpha = 4°$, $C_{J_T} = 1.1$

Figure 31.- Continued.

31e

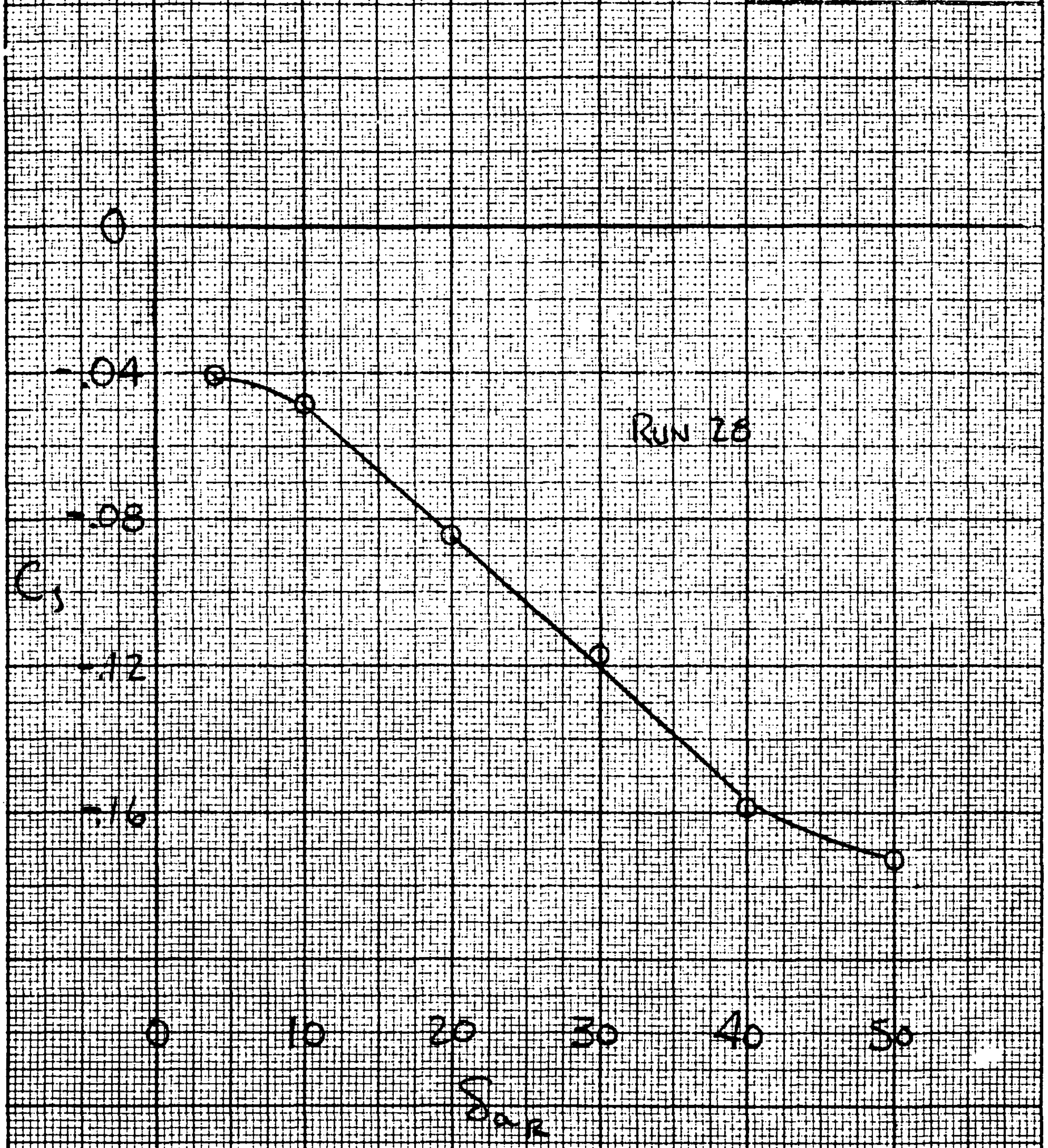

(f) $\alpha = 0^\circ$, $C_{J_T} = 1.1$, $\delta_{a_L} = 4$

Figure 31.- Concluded.

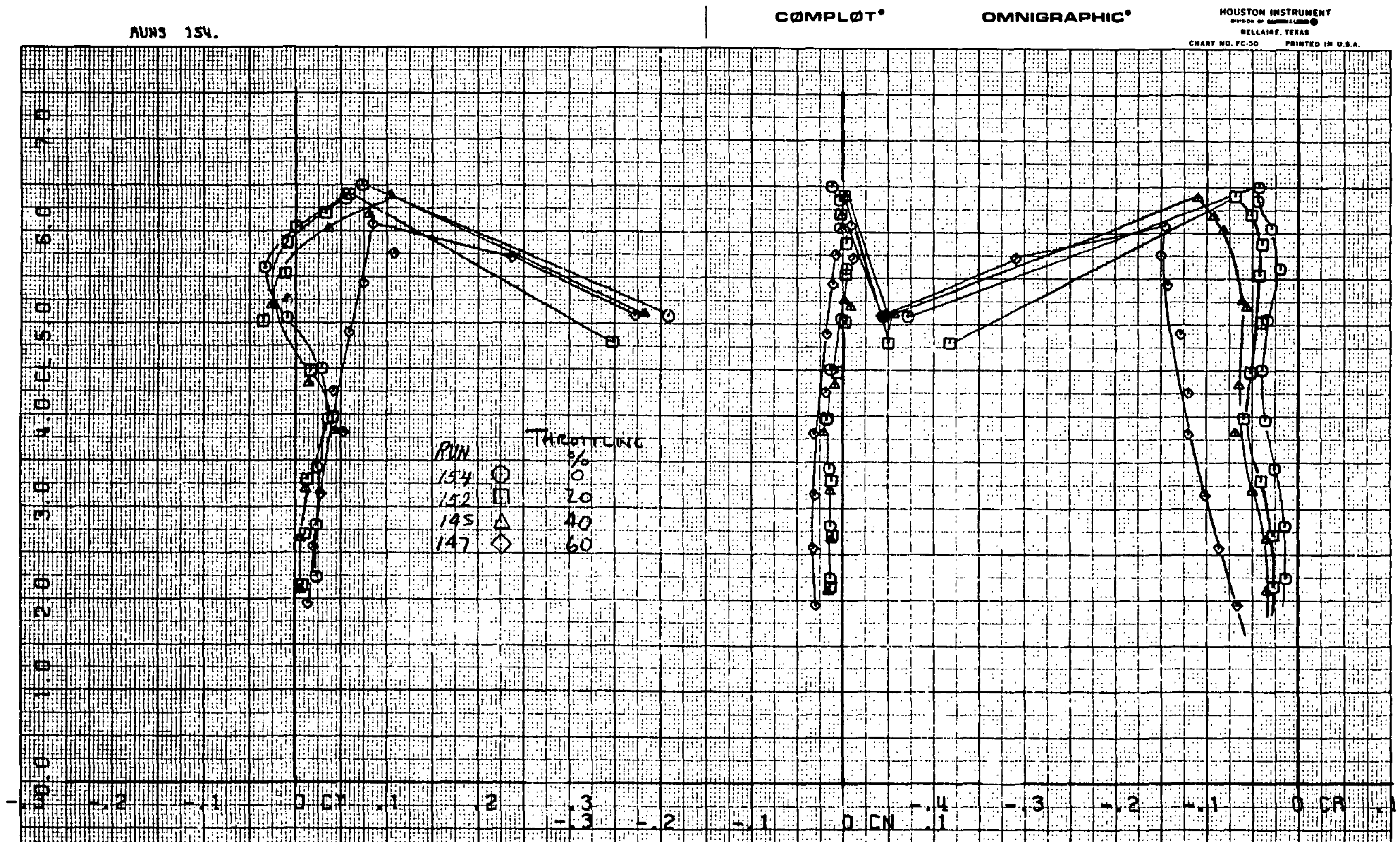

(a) $C_{J_T} = 1.1$

Figure 32.- Lateral stability and control with augmentor throttling; $\delta_f = 40^\circ$, high tail.

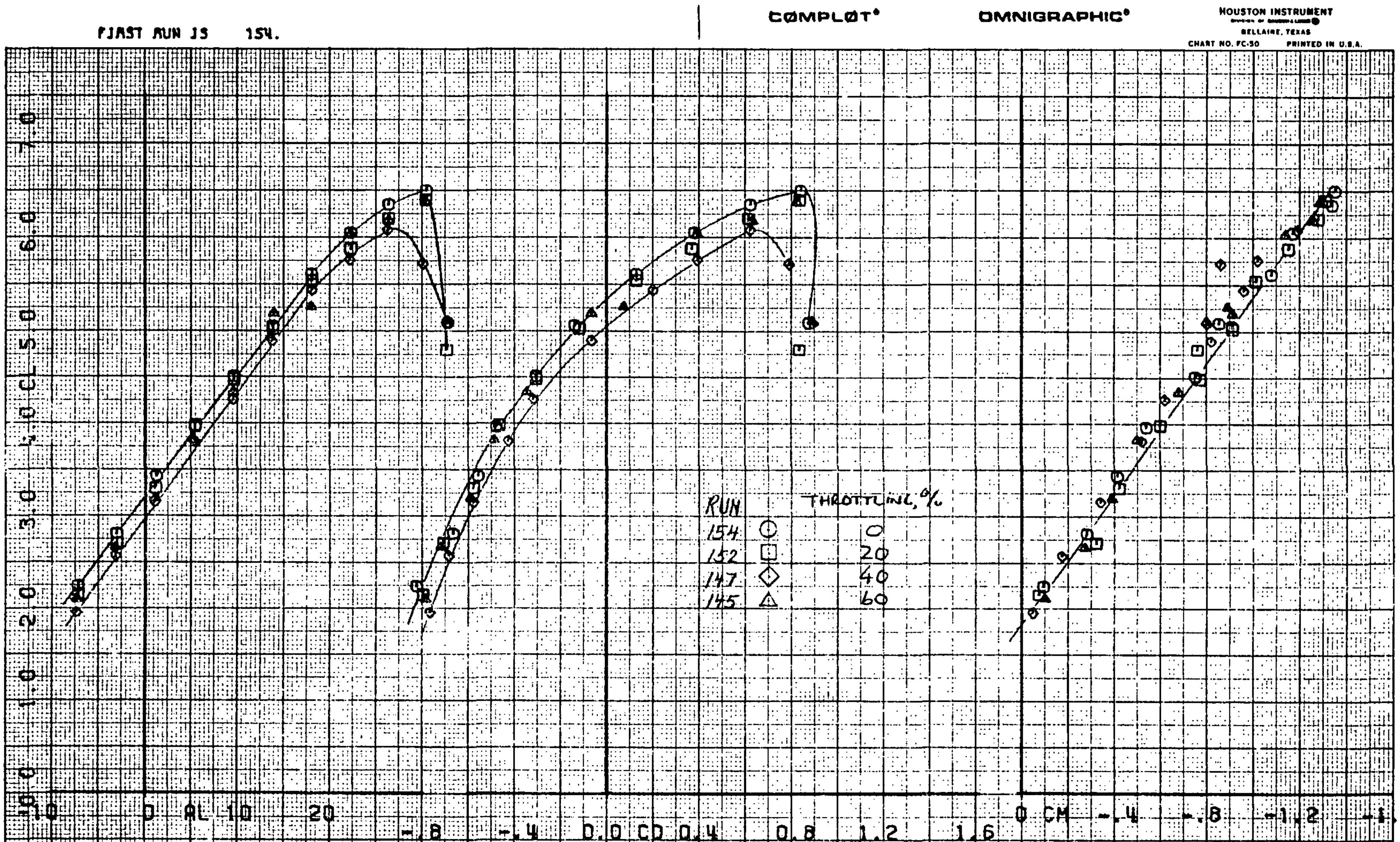

(b) Longitudinal characteristics, $C_{J_I} = 1.1$

Figure 32.- Continued.

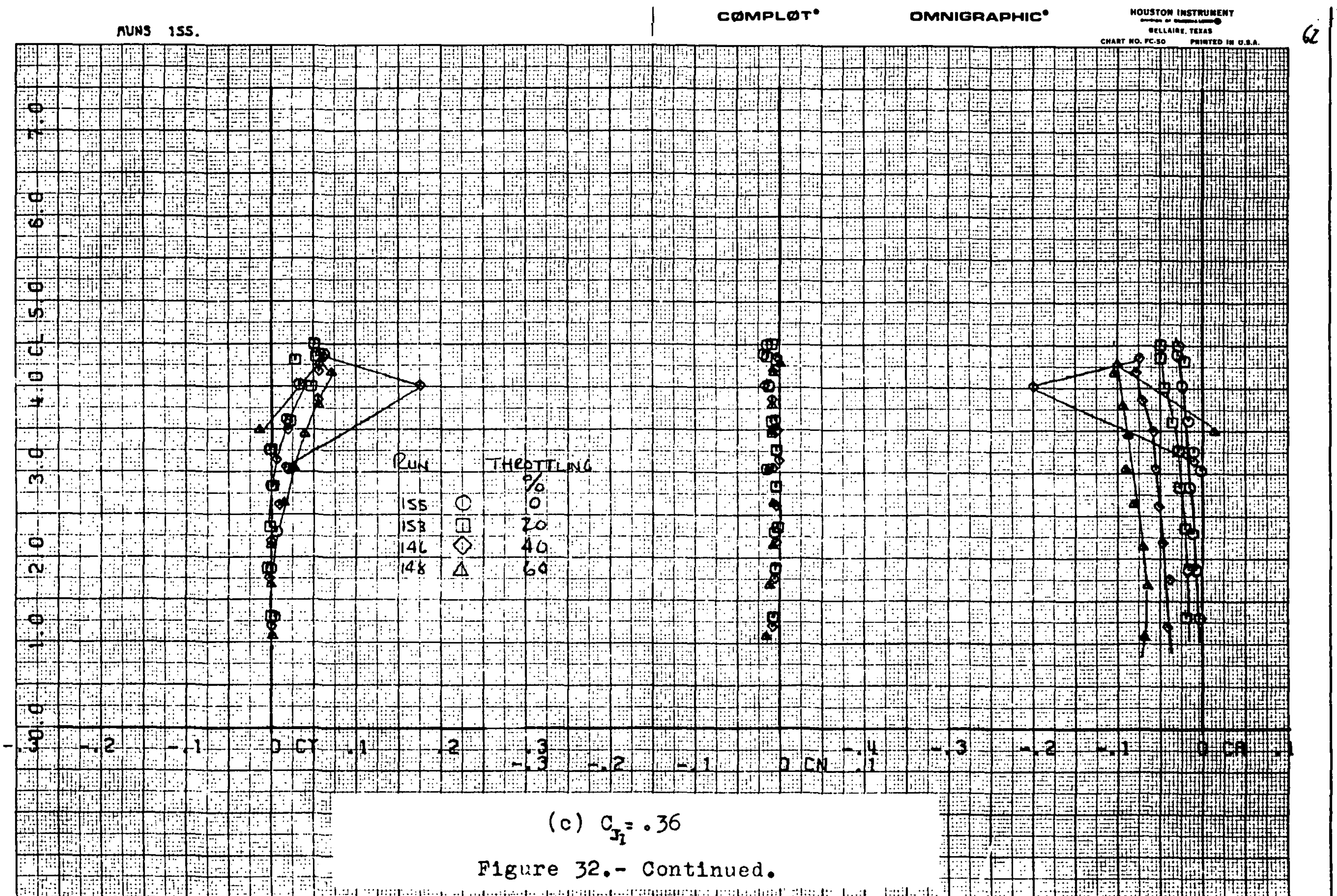

(c) $C_{J_1} = .36$

Figure 32.- Continued.

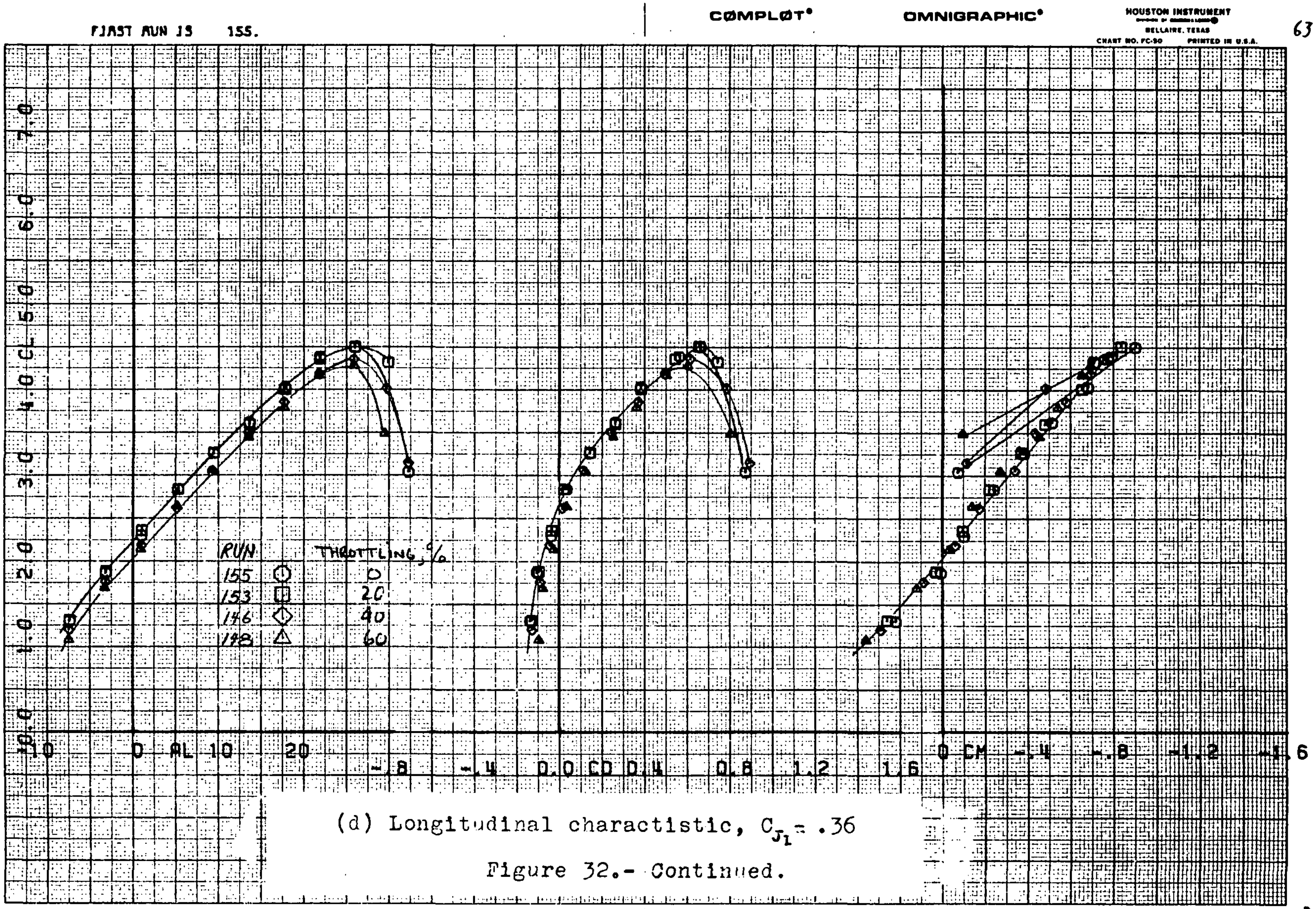

(d) Longitudinal charactistic, C_{J_1} = .36

Figure 32.- Continued.

32d

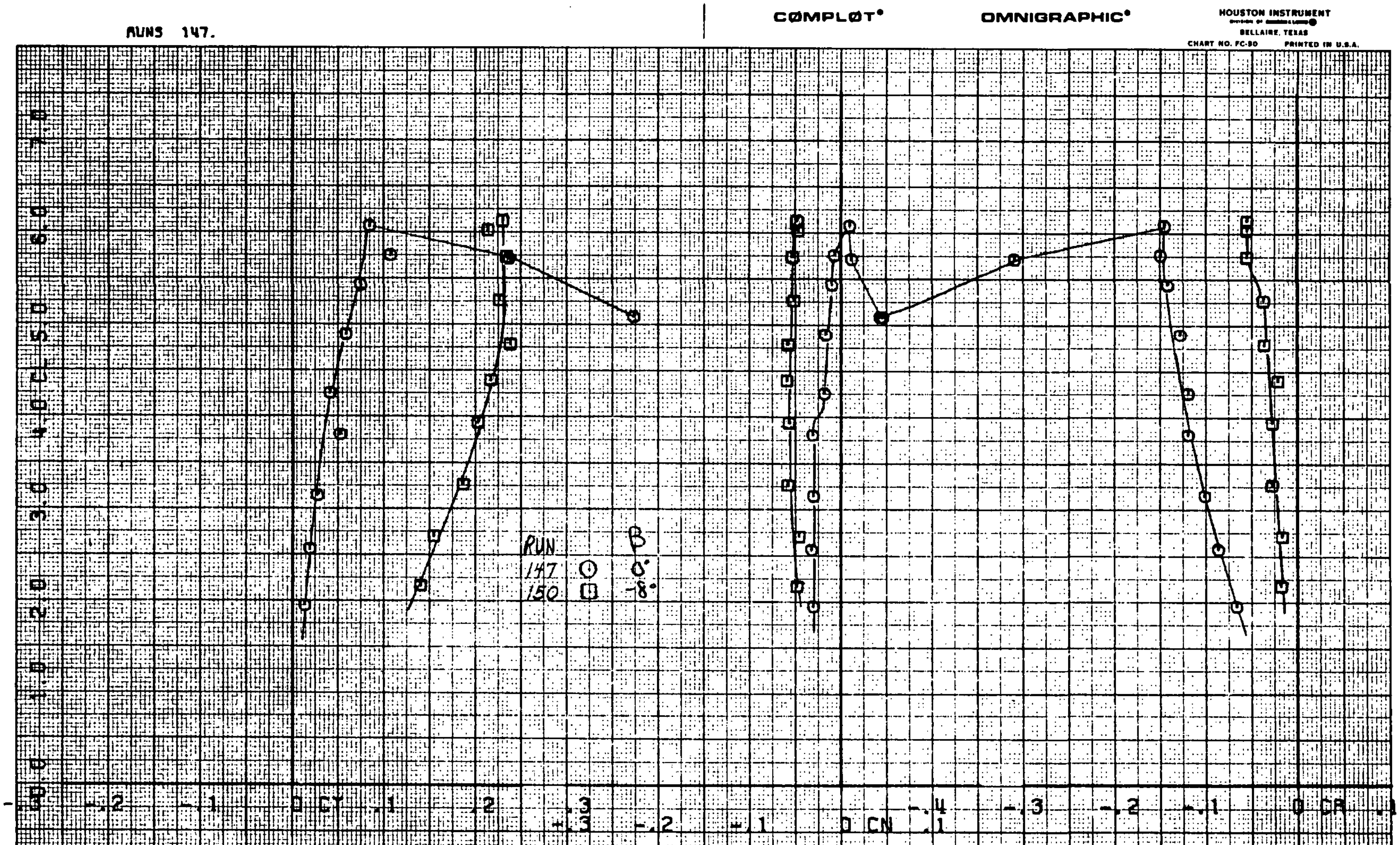

(e) Δ_a=60%, C_{J_I}= 1.06-1.15

Figure 32.- Concluded.

64

31

32e

137

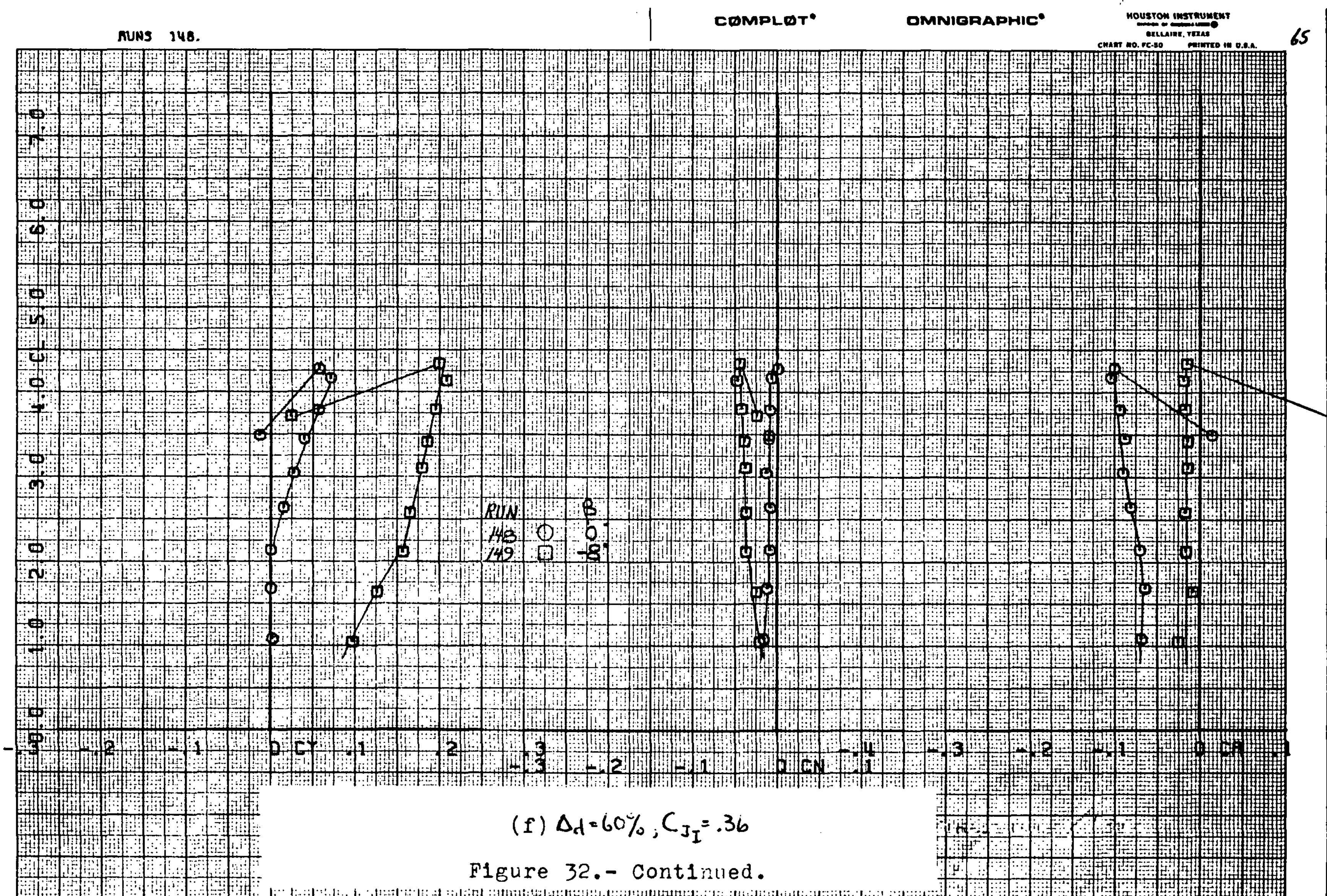

(f) $\Delta_d = 60\%$; $C_{J_I} = .36$

Figure 32.- Continued.

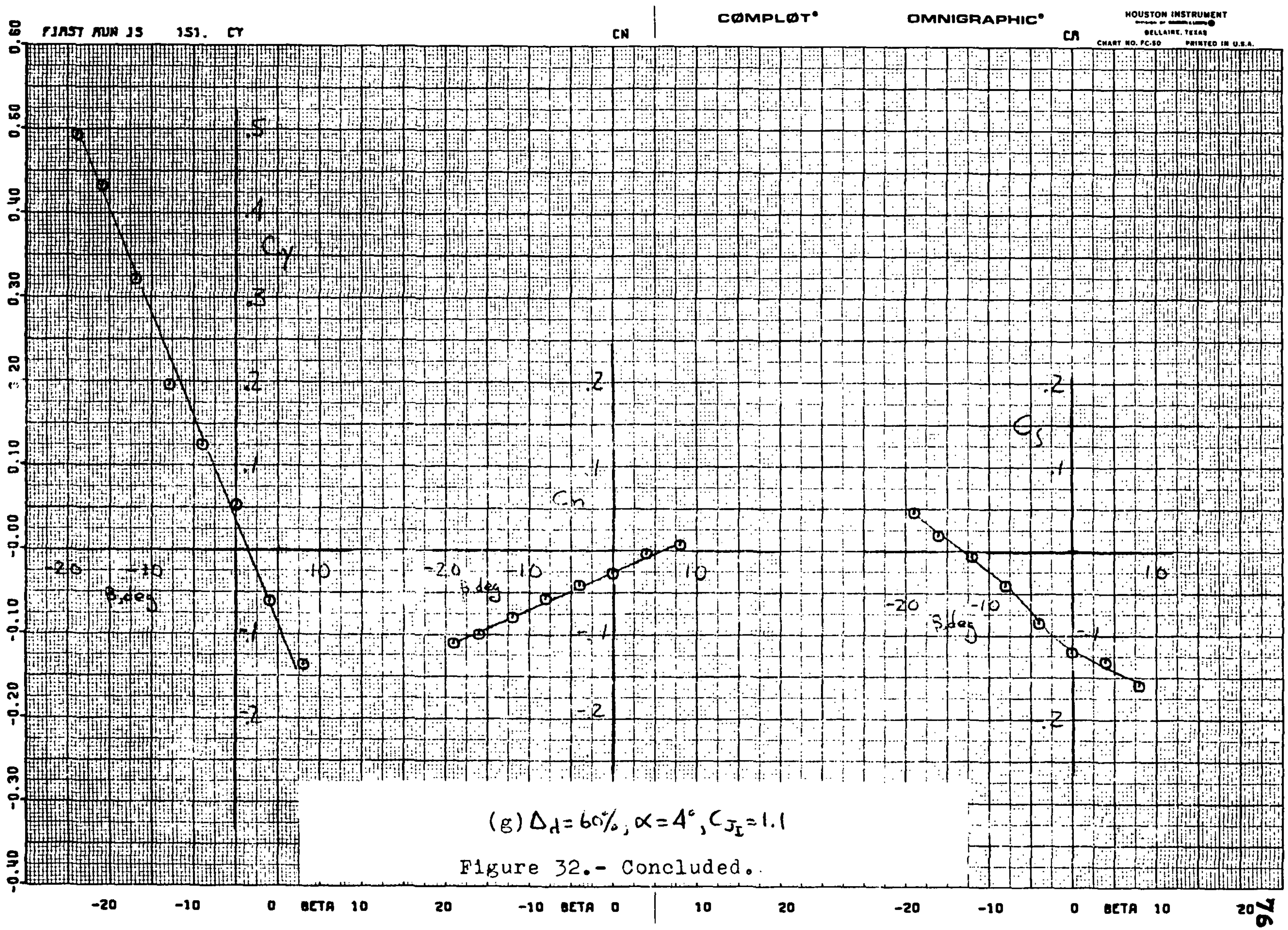

(g) $\Delta_d = 60\%$, $\alpha = 4°$, $C_{J_I} = 1.1$

Figure 32.- Concluded.

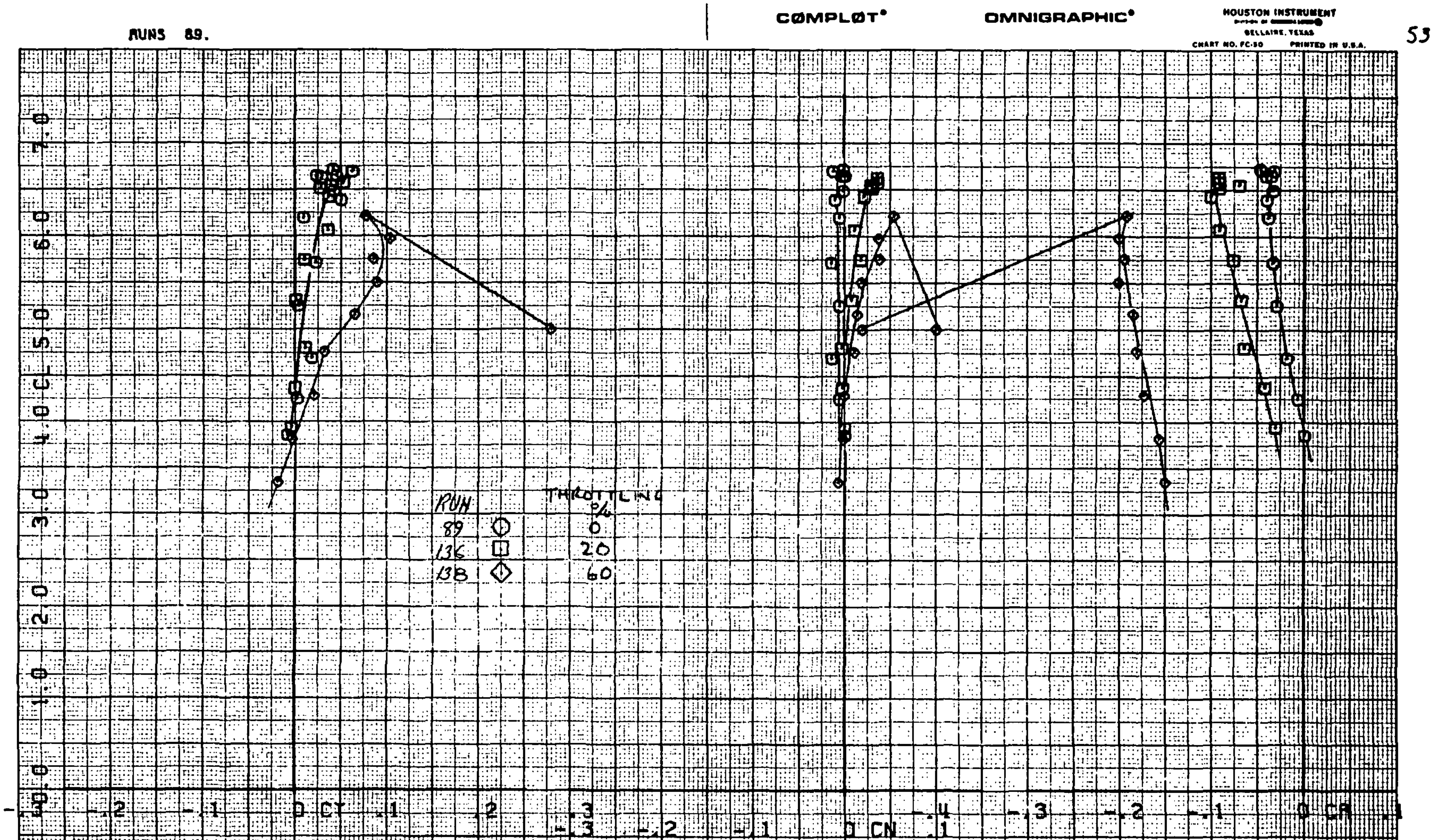

(a) C_{J_I}=1.09

Figure 33.- Lateral stability and control with augmentor throttling; δ_f=70°, high tail.

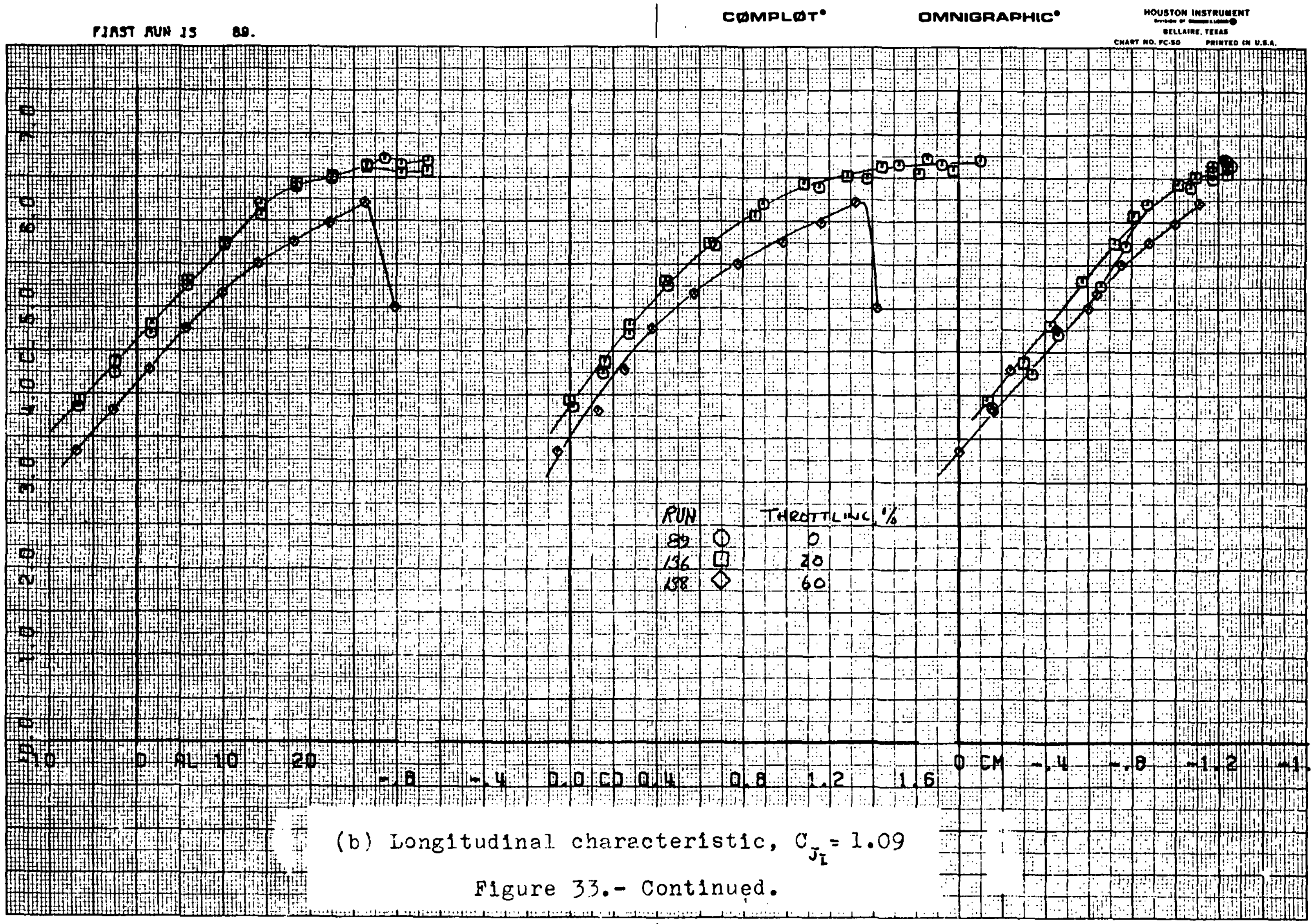

(b) Longitudinal characteristic, $C_{J_I} = 1.09$

Figure 33.- Continued.

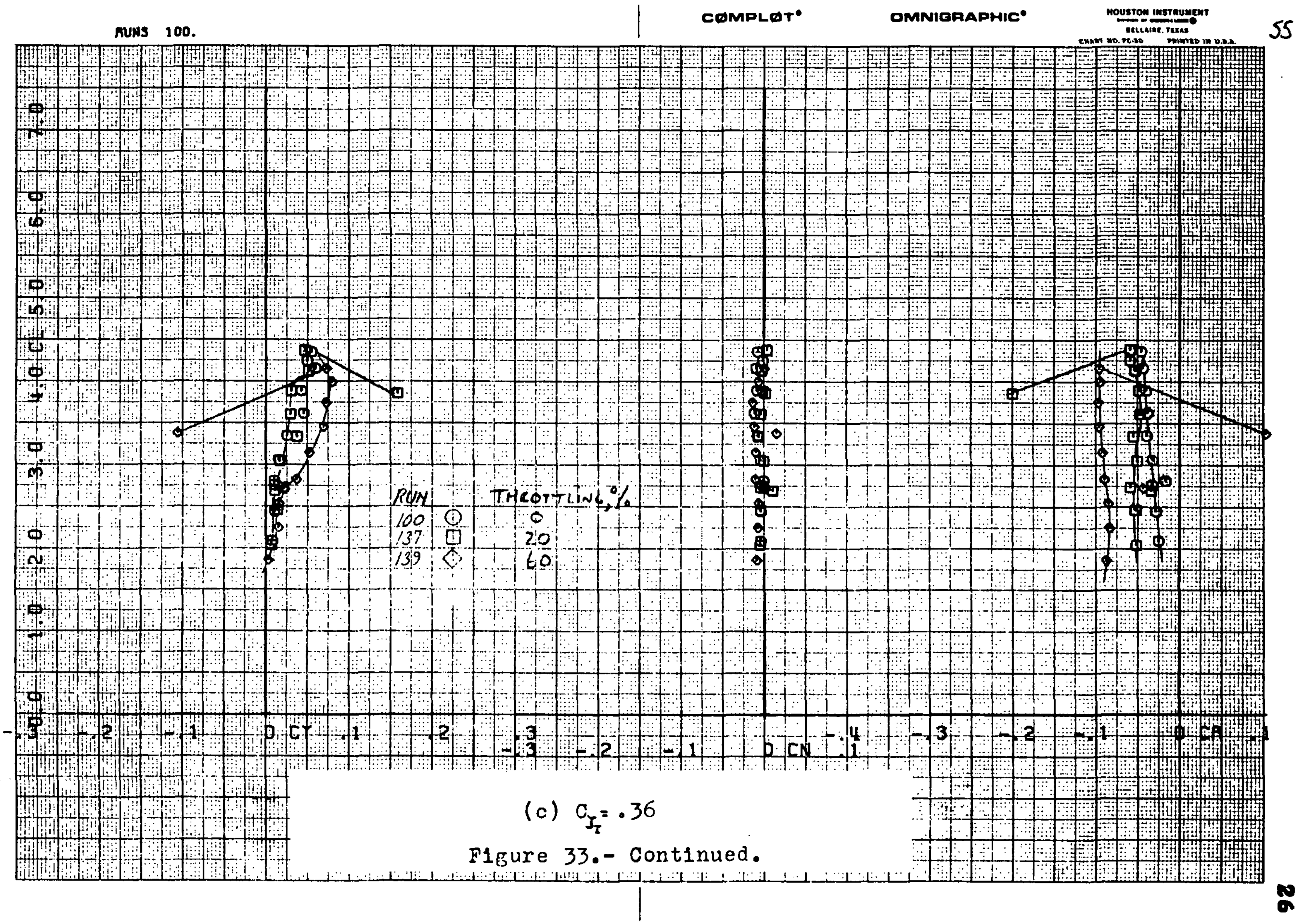

(c) $C_{J_T} = .36$

Figure 33.- Continued.

56

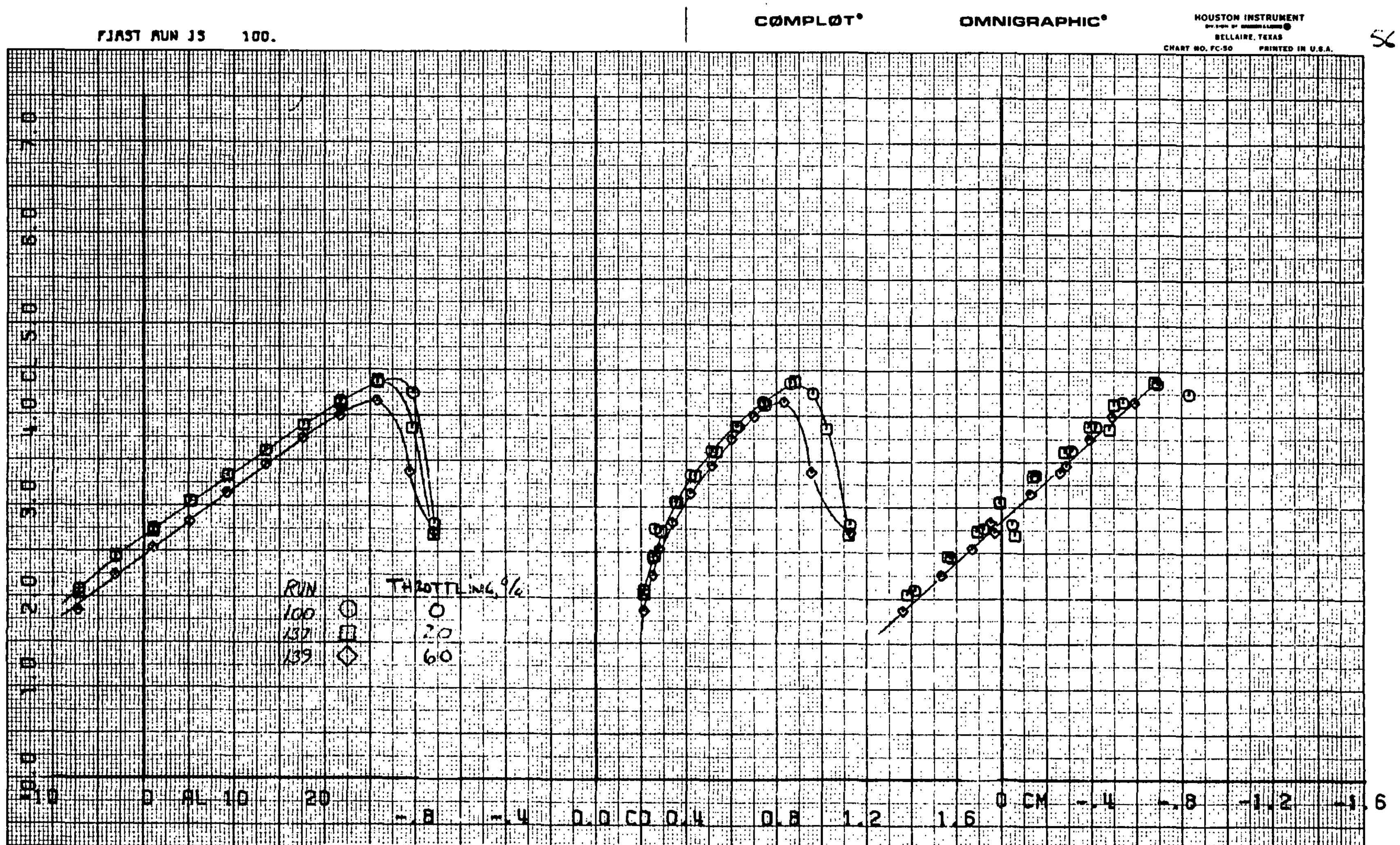

(d) Longitudinal characteristics, $C_{J_I} = .36$

Figure 33.- Continued.

33d

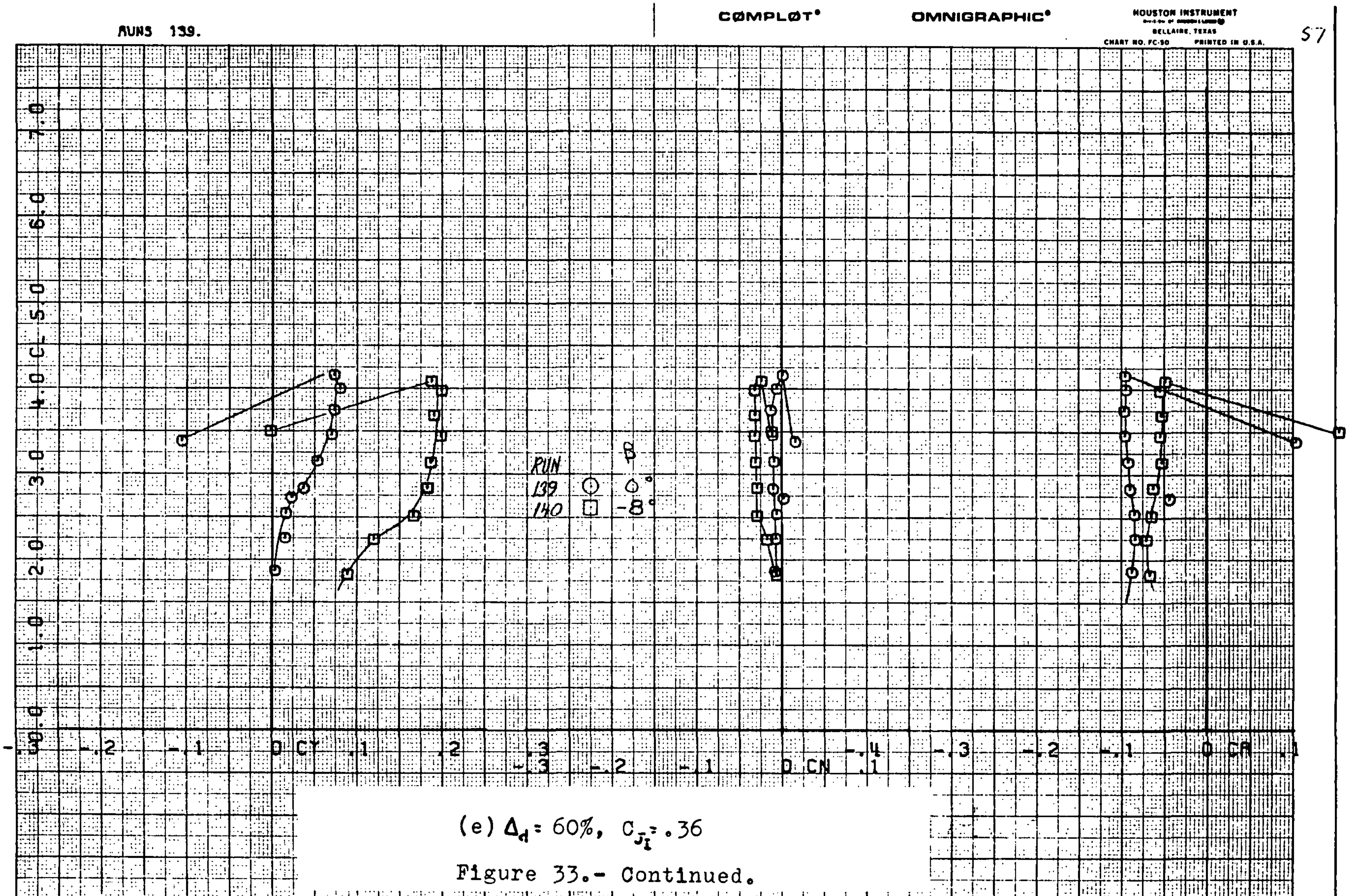

(e) Δ_d = 60%, C_{J_I} = .36

Figure 33.- Continued.

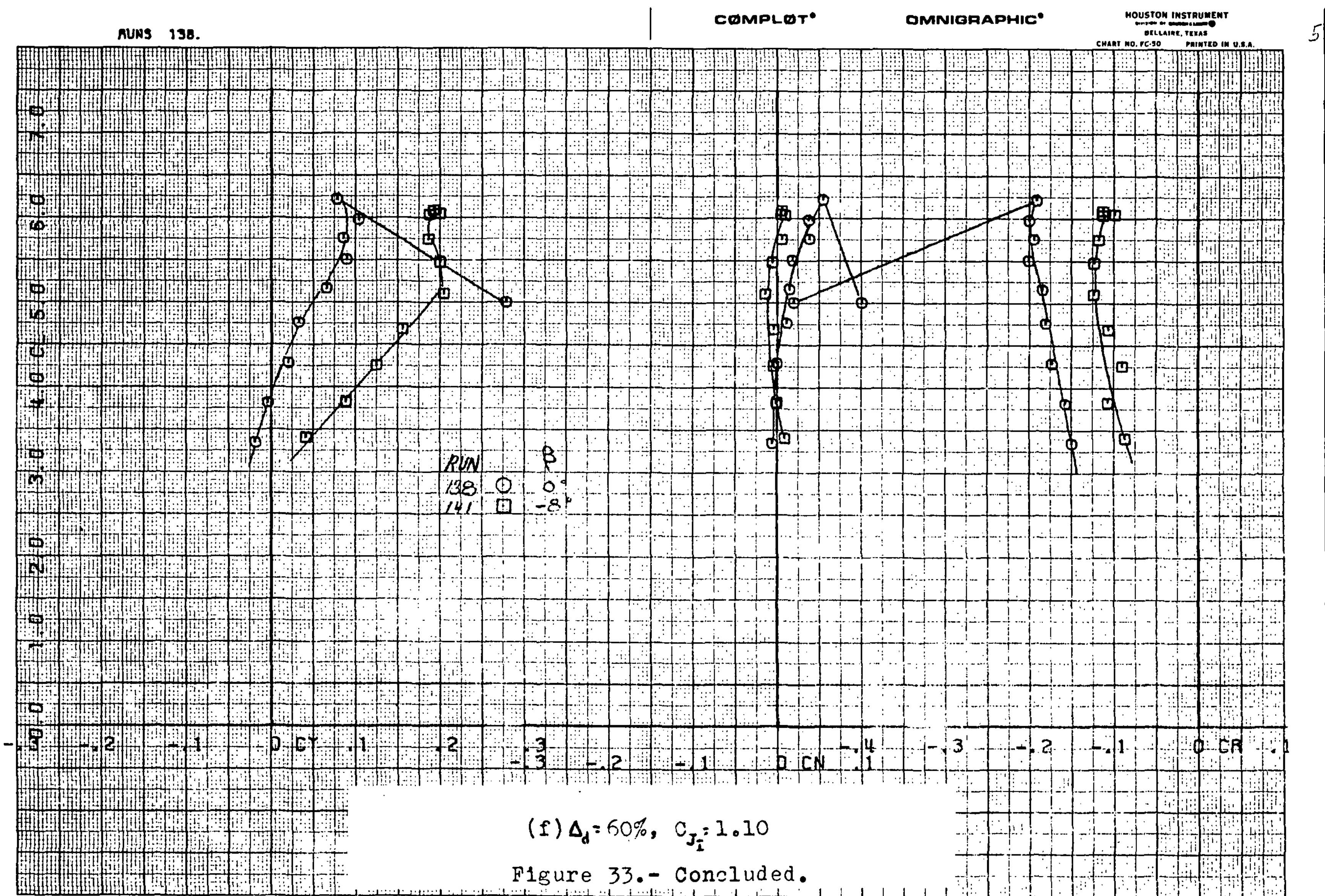

(f) $\Delta_d = 60\%$, $C_{J_T} = 1.10$

Figure 33.- Concluded.

RUNS 156.

COMPLOT® OMNIGRAPHIC® HOUSTON INSTRUMENT BELLAIRE, TEXAS CHART NO. PC-50 PRINTED IN U.S.A.

67

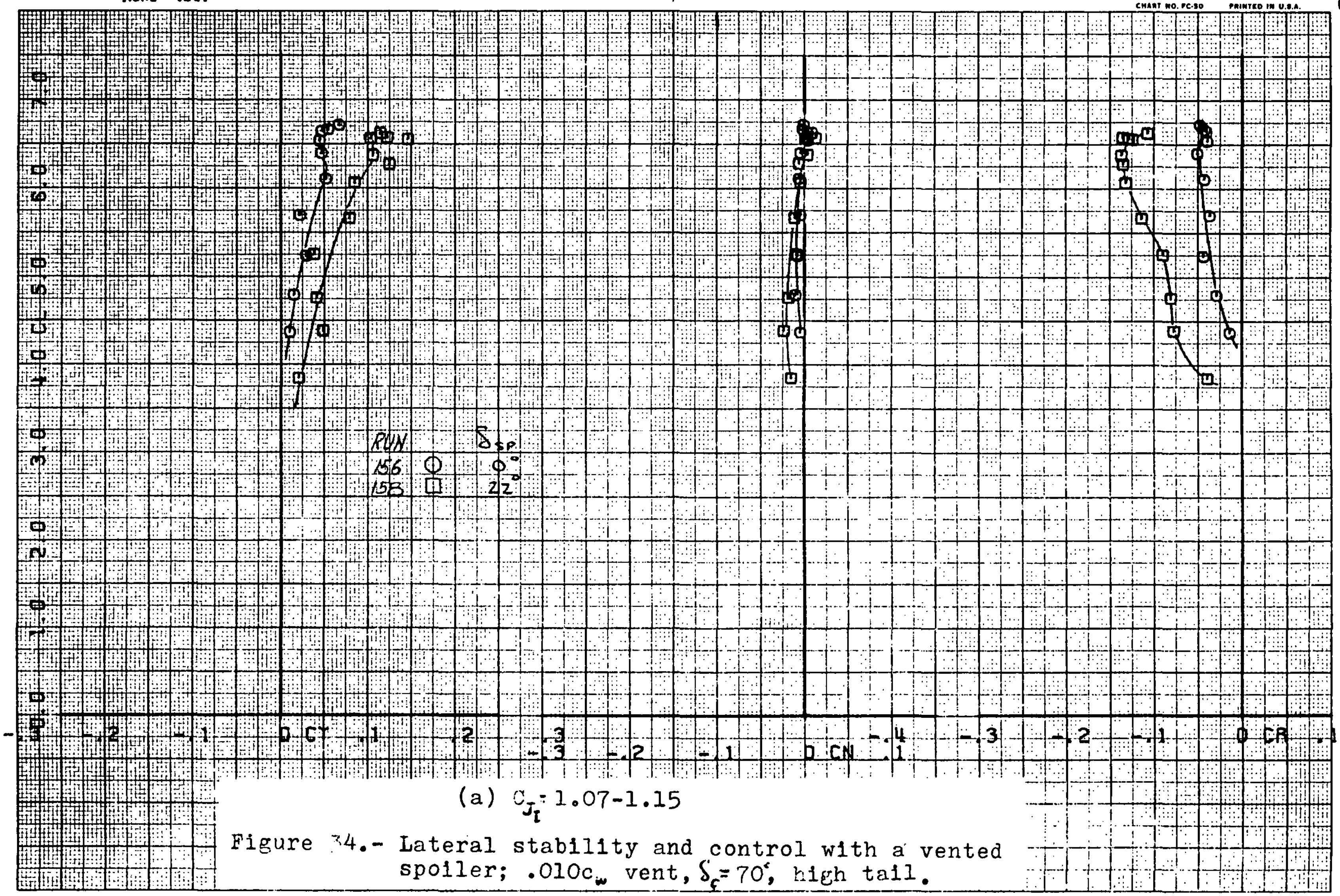

(a) C_{J_t} = 1.07-1.15

Figure 34.- Lateral stability and control with a vented spoiler; .010c_w vent, δ_f = 70°, high tail.

34a

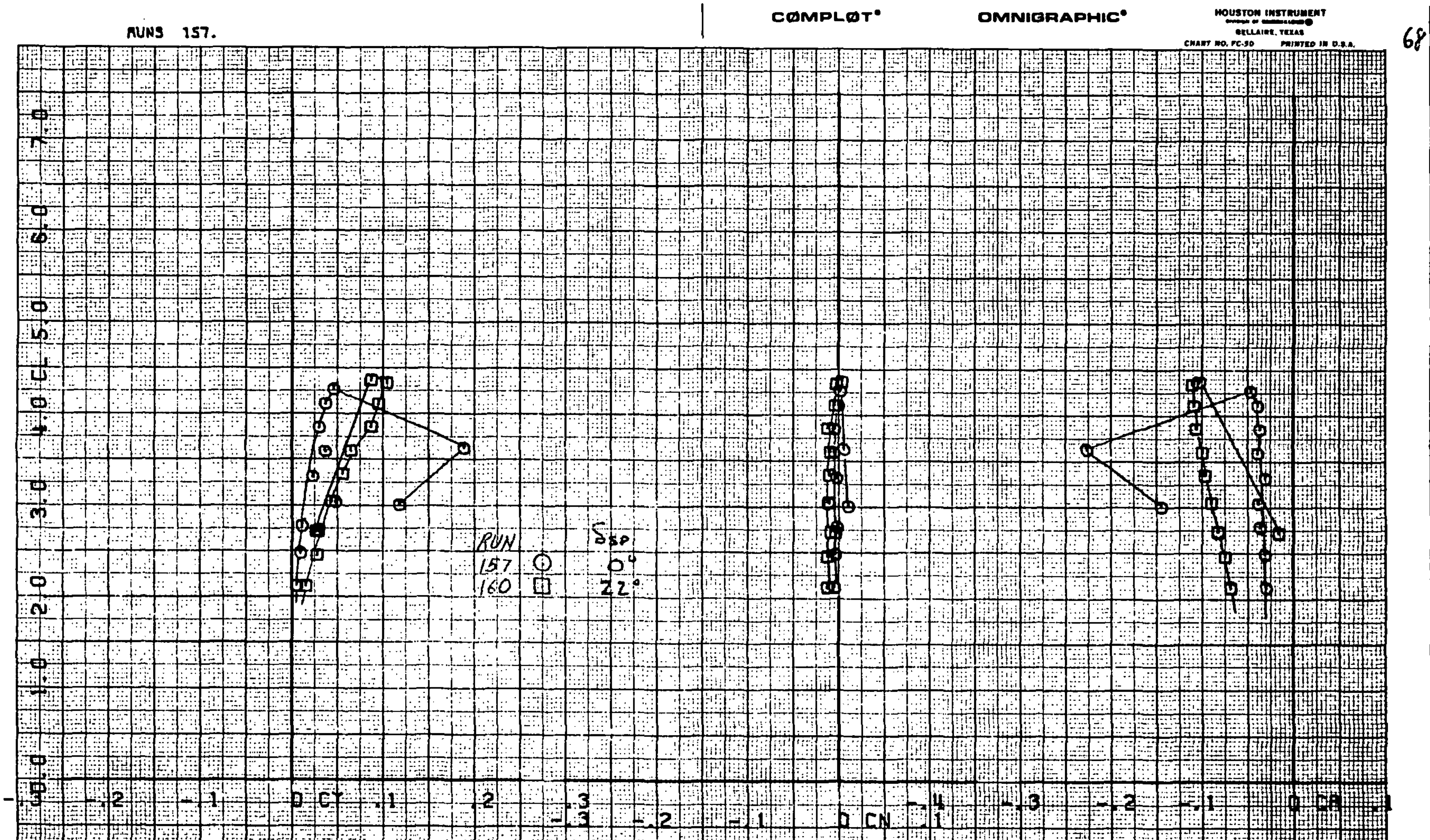

(b) $C_{J_I} = .36$

Figure 34.- Continued.

NASA
AMES RESEARCH CENTER

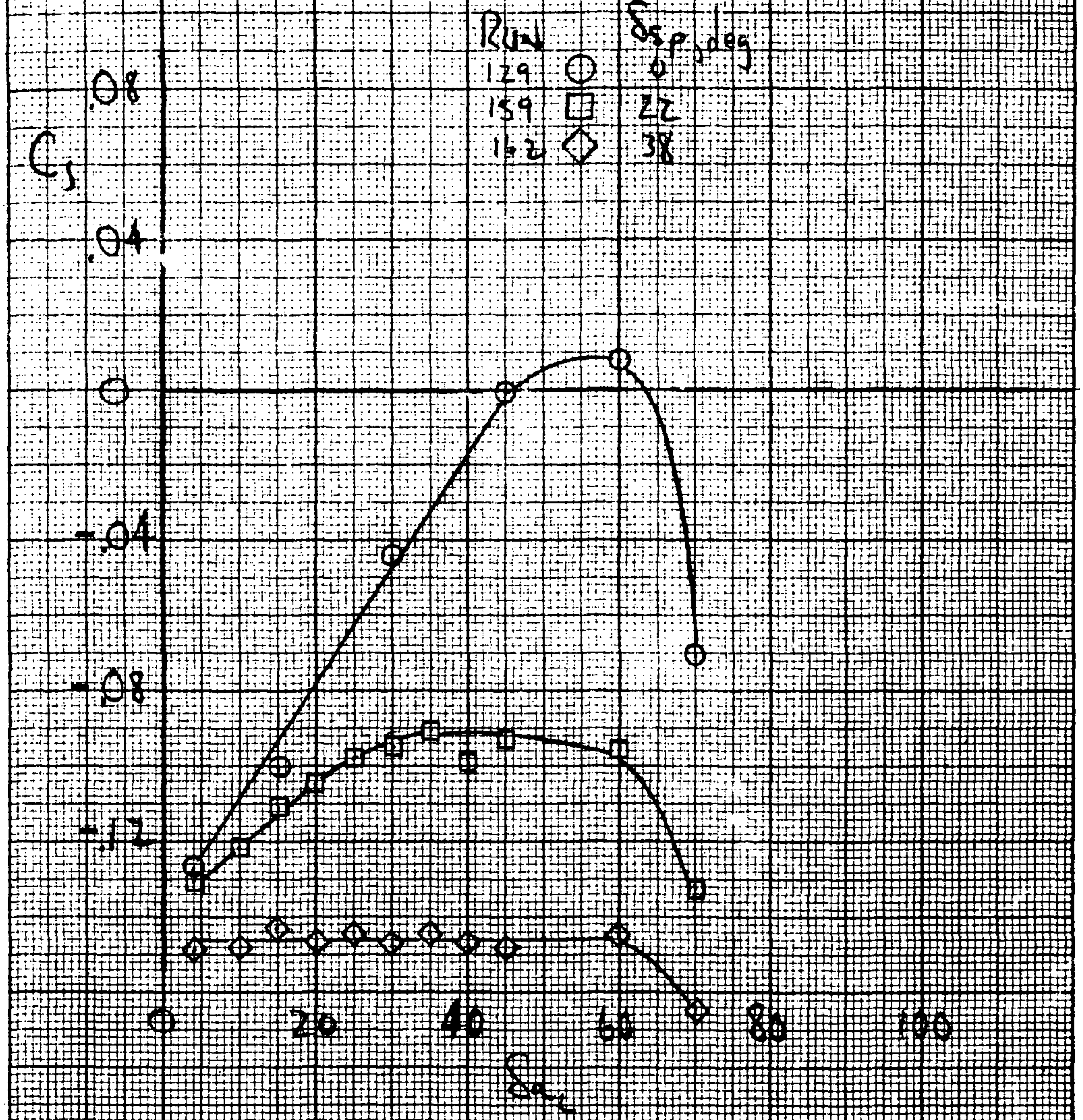

(c) Aileron control effectiveness; C_{J_1} = 1.1, α = 4°, δ_{a_R} = 30°

Figure 34.- Continued.

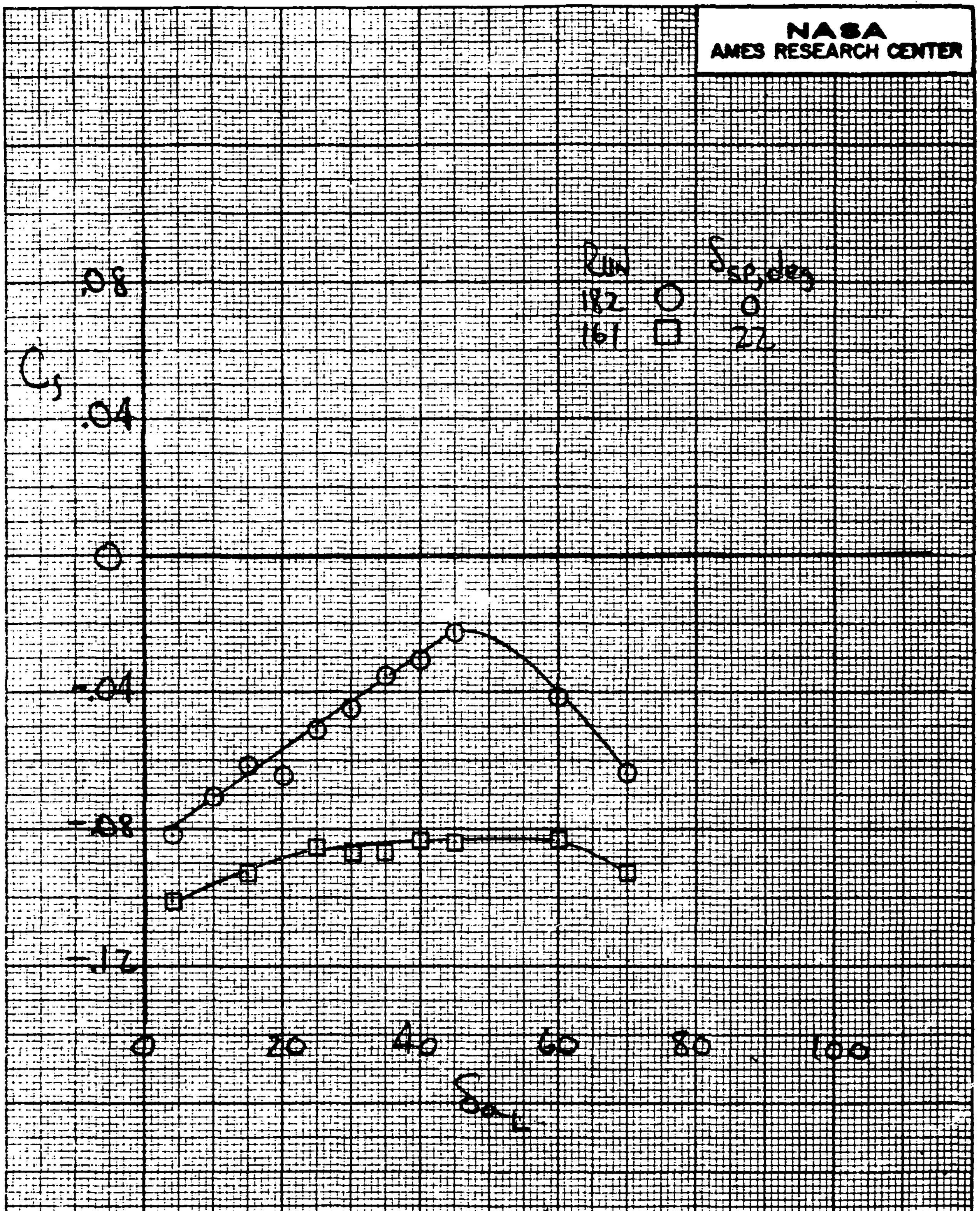

(d) Aileron control effectiveness; $C_{J_T} = .4$, $\alpha = 4°$, $\delta_{a_R} = 30°$

Figure 34.- Concluded.

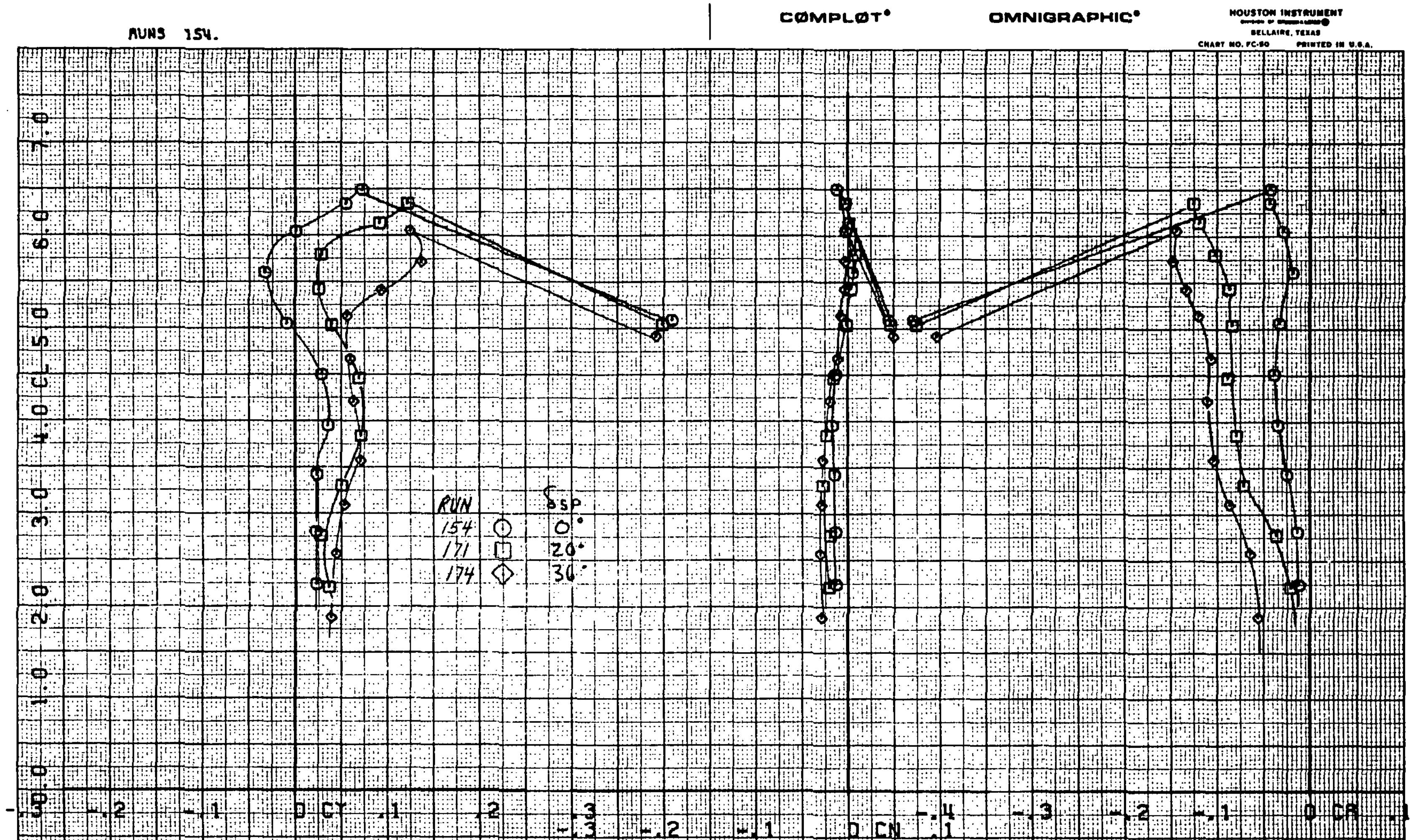

(a) C_{J_T} = 1.05-1.15

Figure 35.- Lateral stability and control with a vented spoiler; δ_f = 40°, high tail, .016c_w vent.

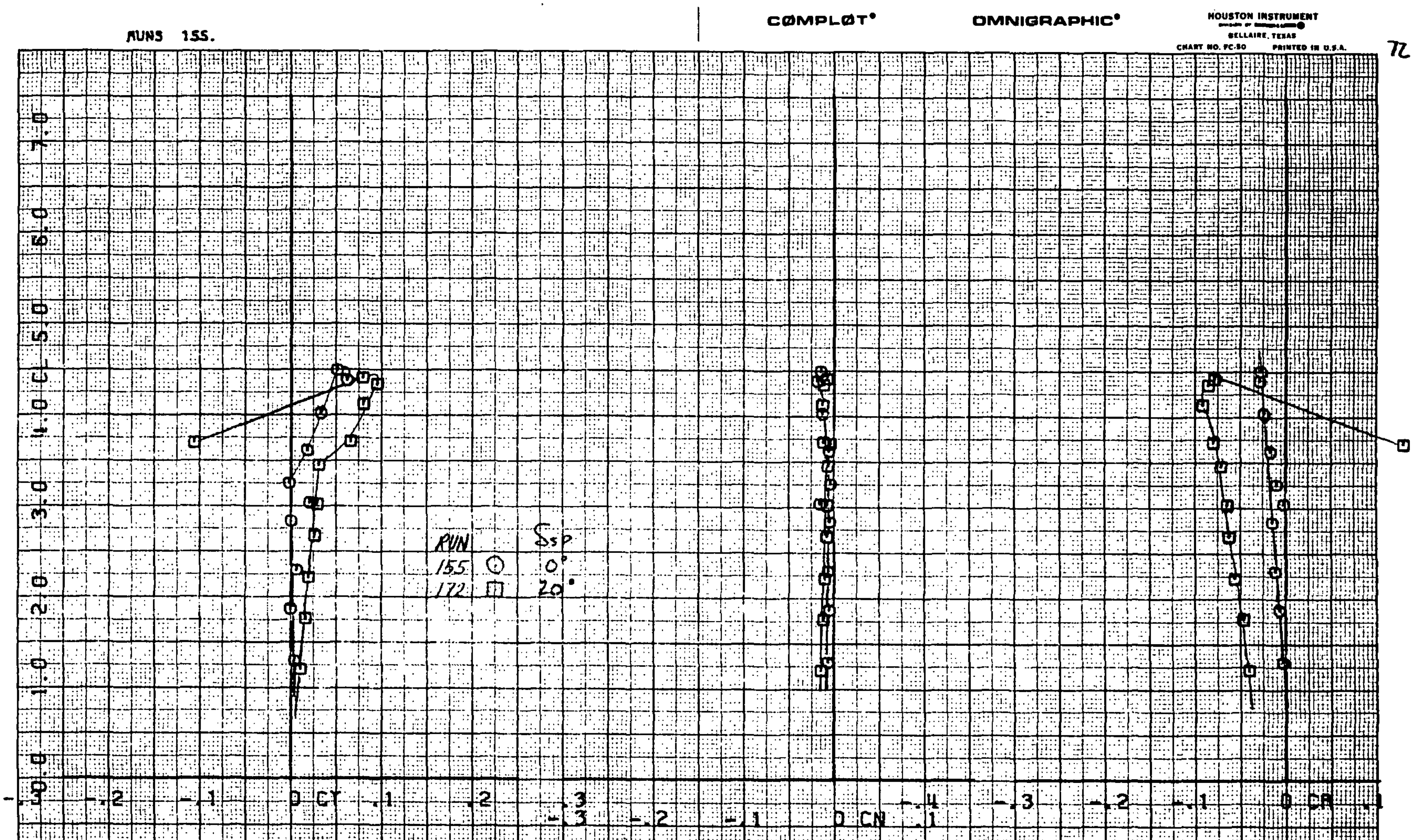

(b) $C_{J_T} = .36$

Figure 35.- Continued.

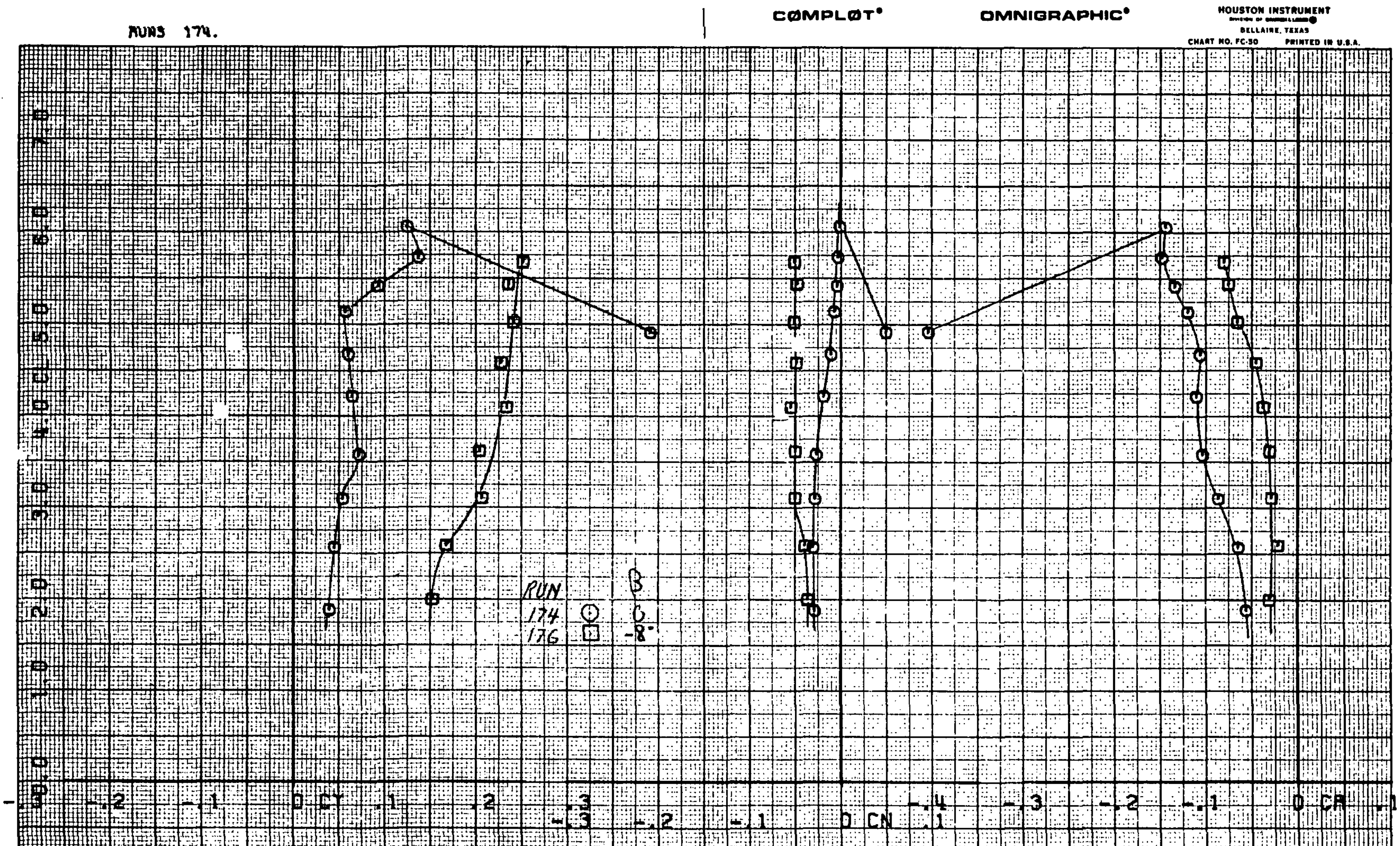

(c) $C_{J_I} = 1.06$, $\delta_{sp} = 36^\circ$

Figure 35.- Continued.

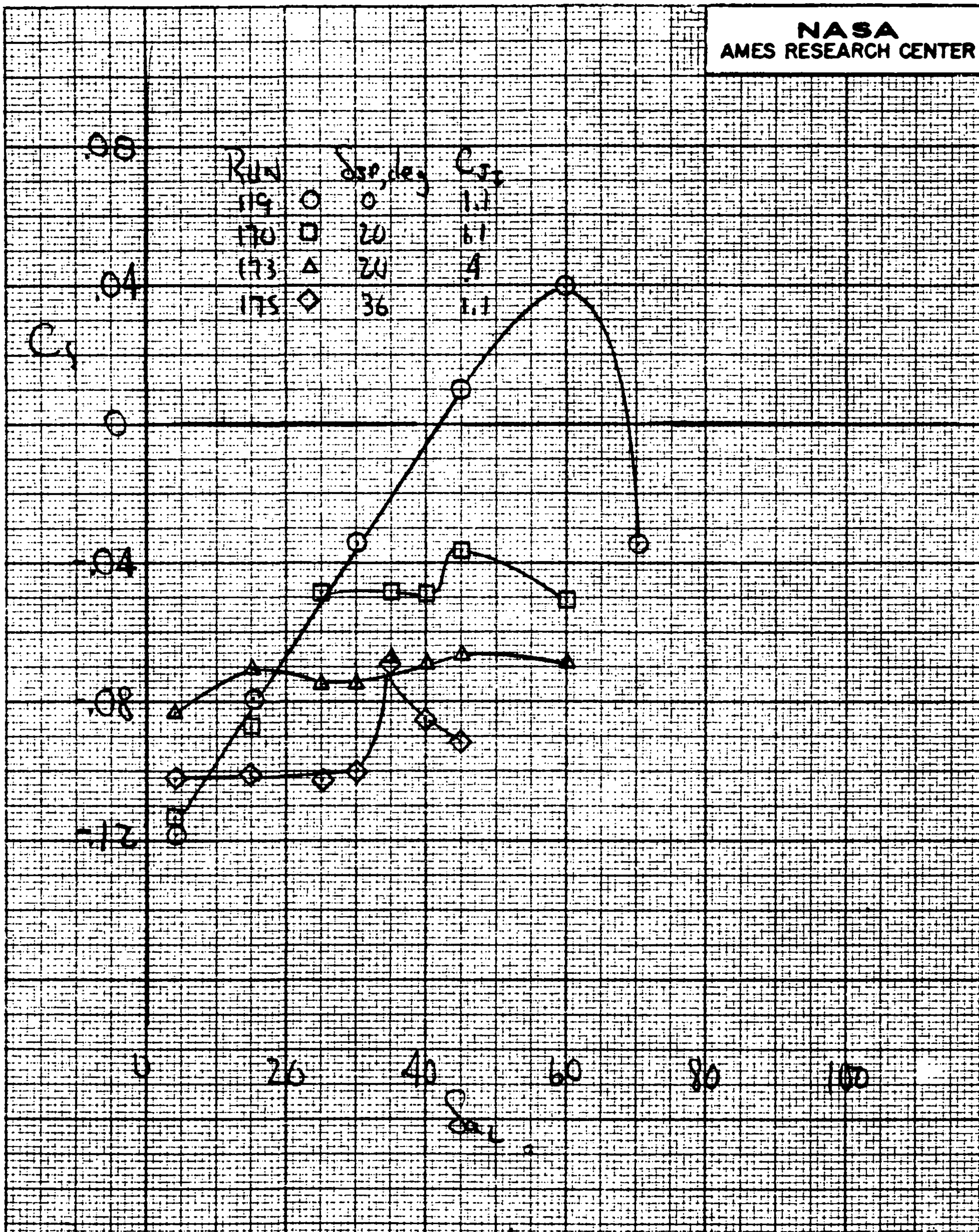

(d) Aileron control effectiveness; $\alpha = 4°$, $\delta_{a_R} = 30°$

Figure 35.- Concluded.

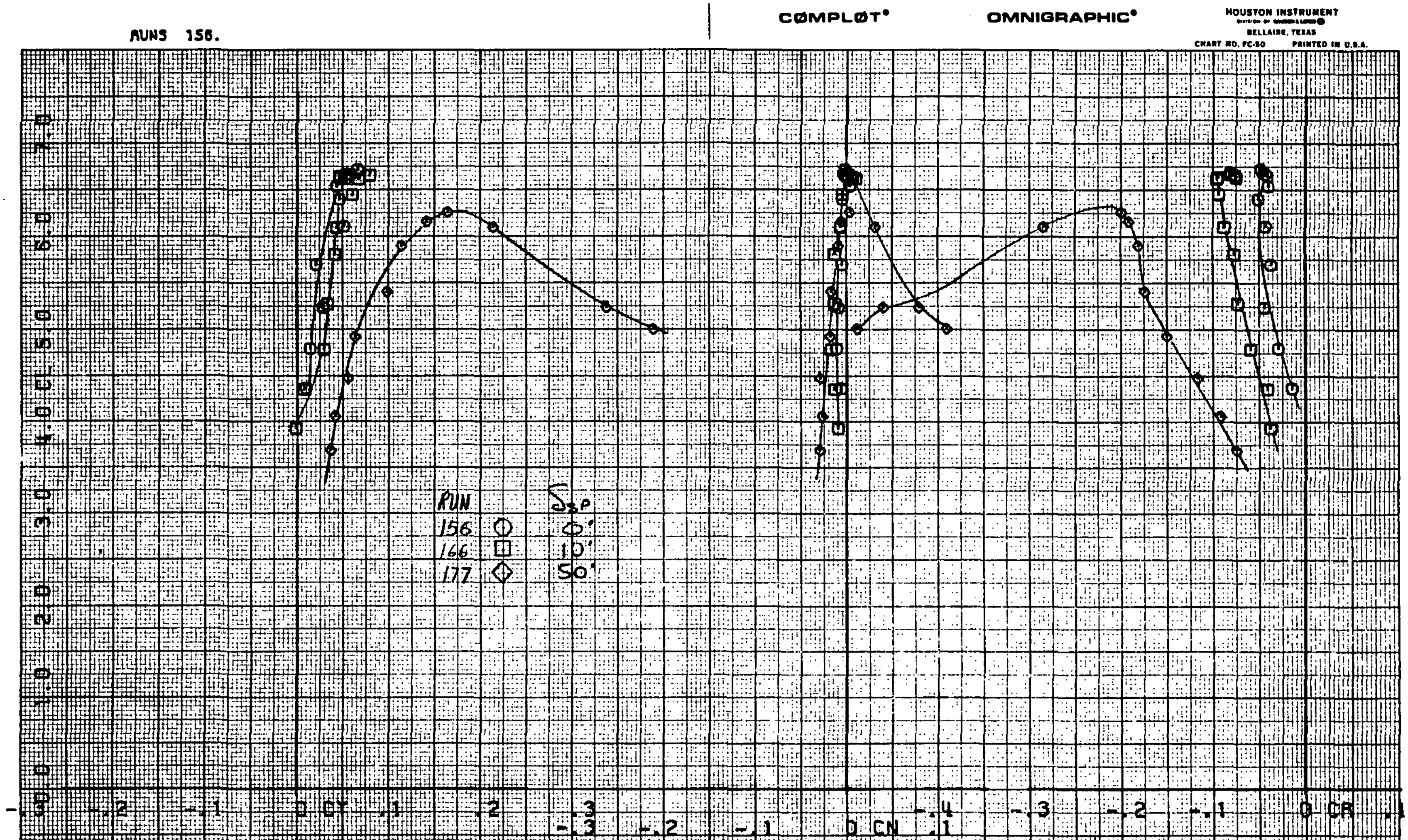

(a) C_{J_I}=1.07-1.15

Figure 36.- Lateral stability and control with a vented spoiler; δ_f=70°, high tail, .016c$_u$ vent.

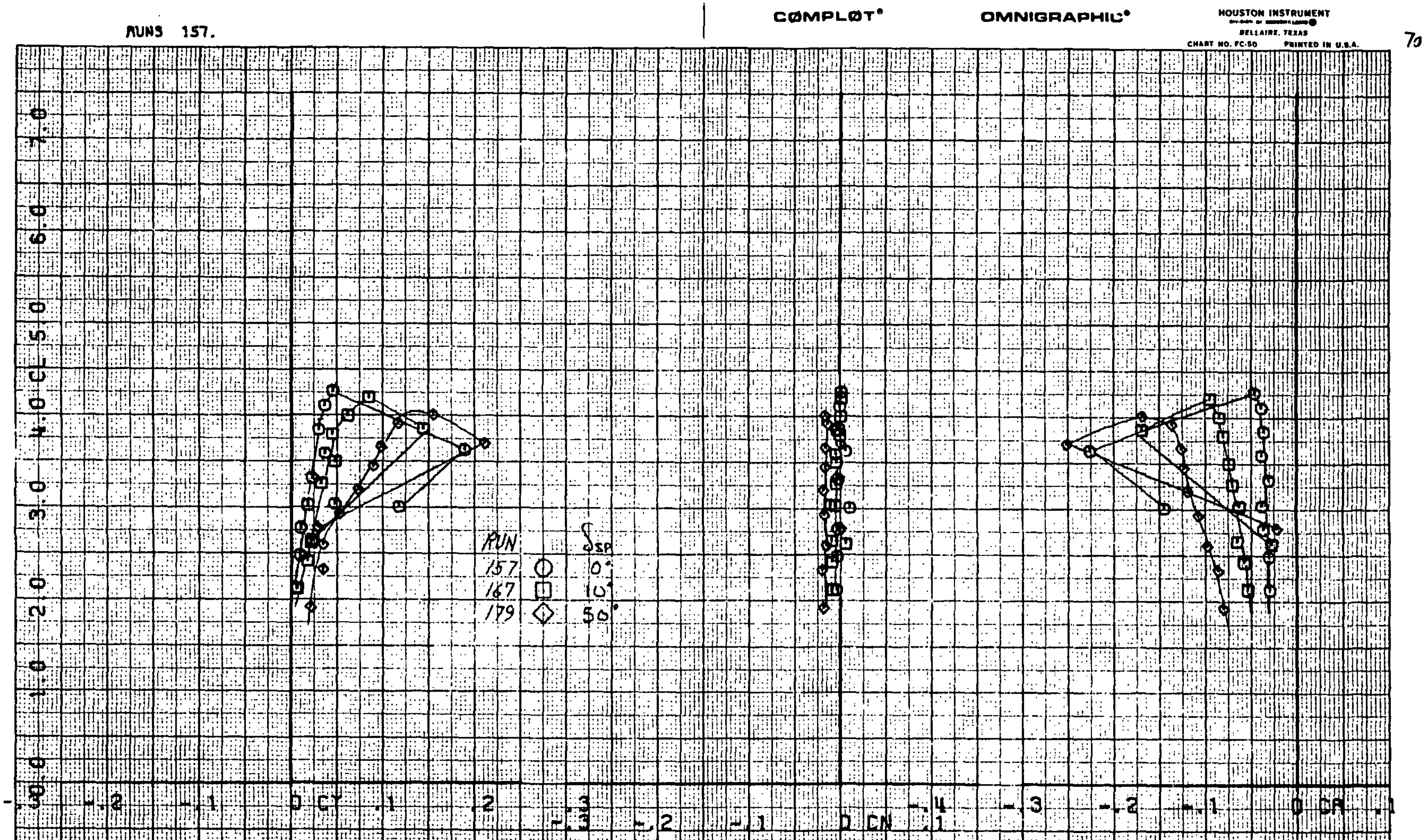

(b) $C_{J_T} = .36$

Figure 36.- Continued.

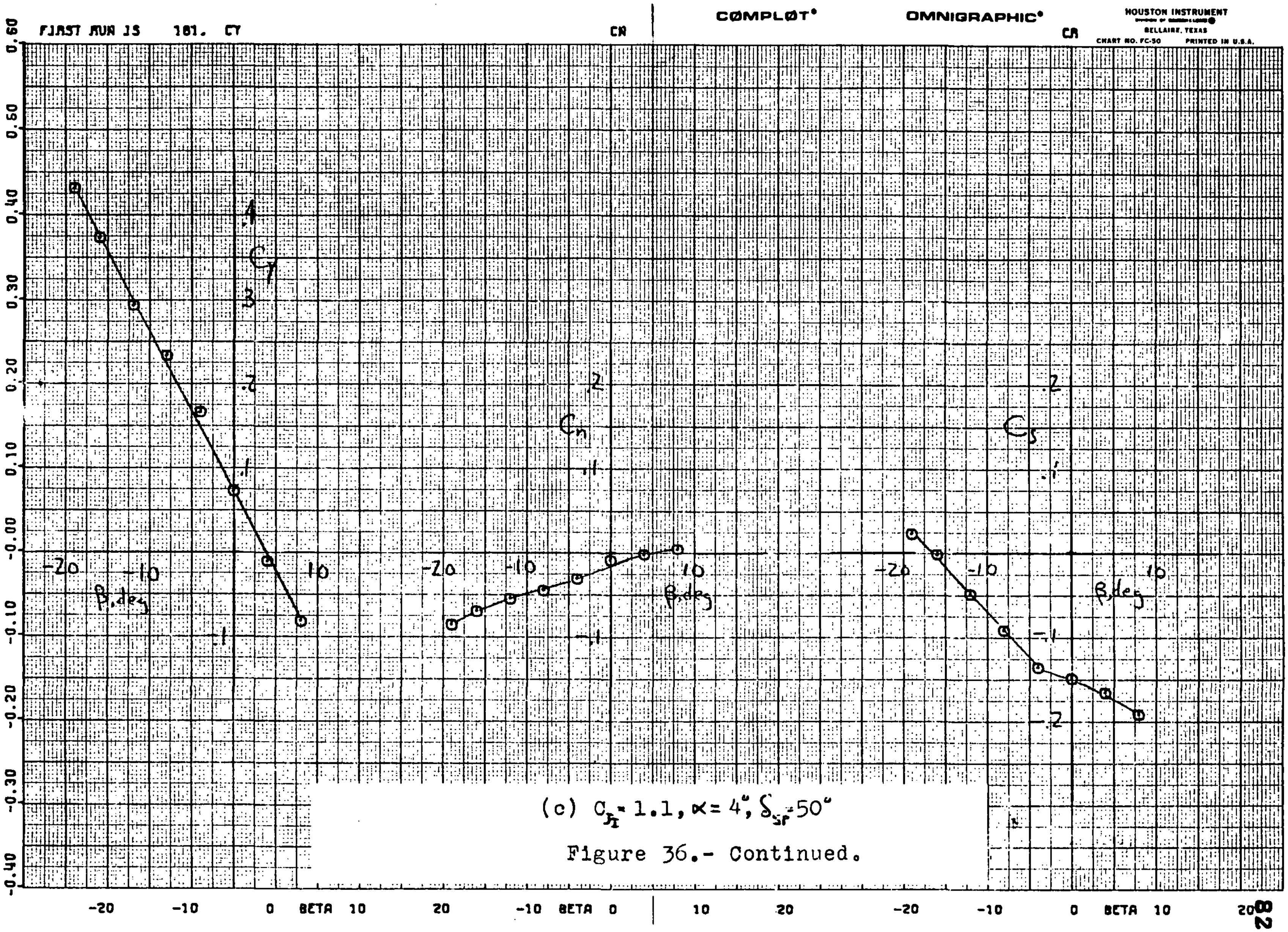

(c) $C_{T} = 1.1, \alpha = 4°, \delta_{sf} = 50°$

Figure 36.- Continued.

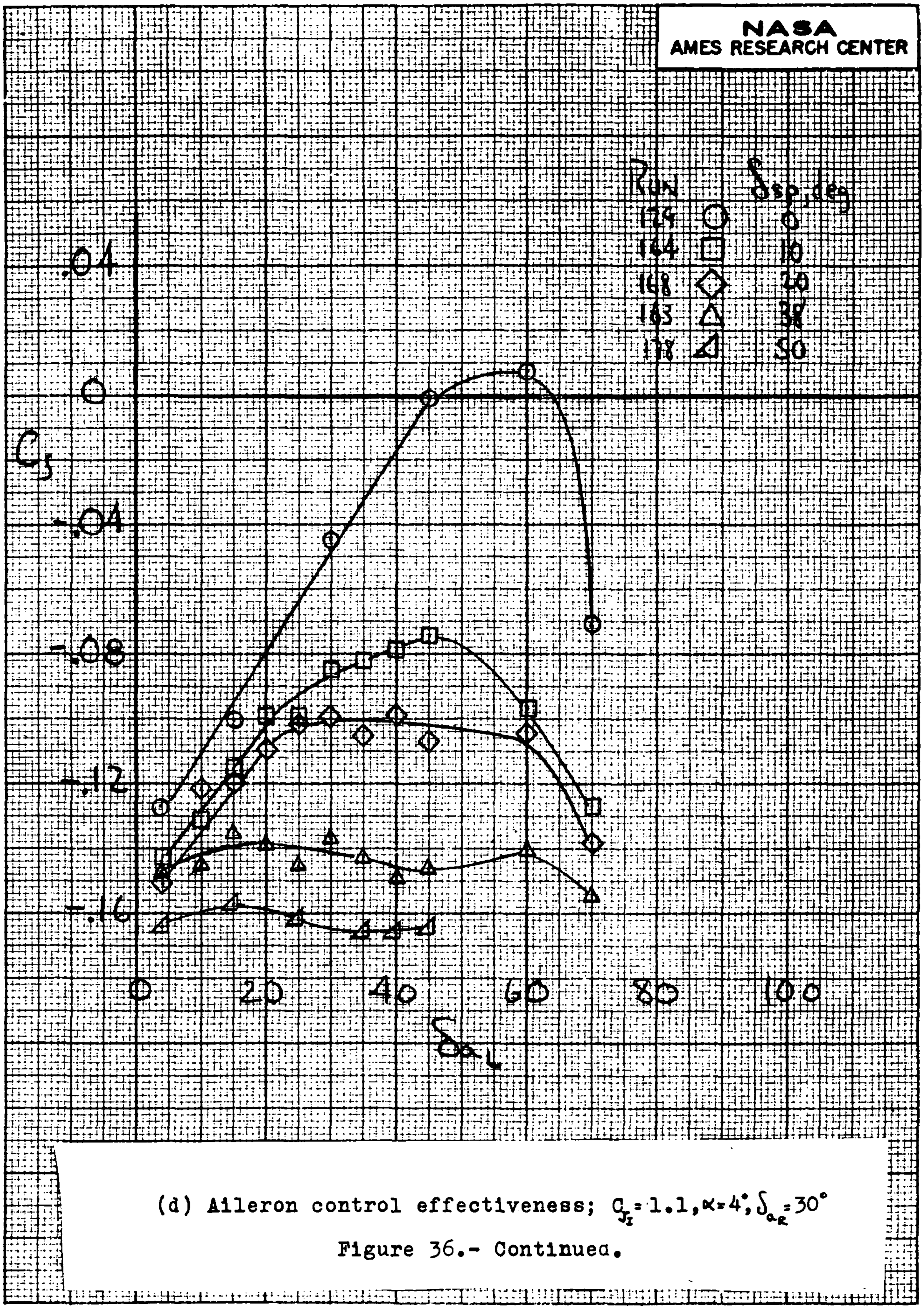

(d) Aileron control effectiveness; C_{J_I} = 1.1, α = 4°, δ_{a_R} = 30°

Figure 36.- Continued.

36d

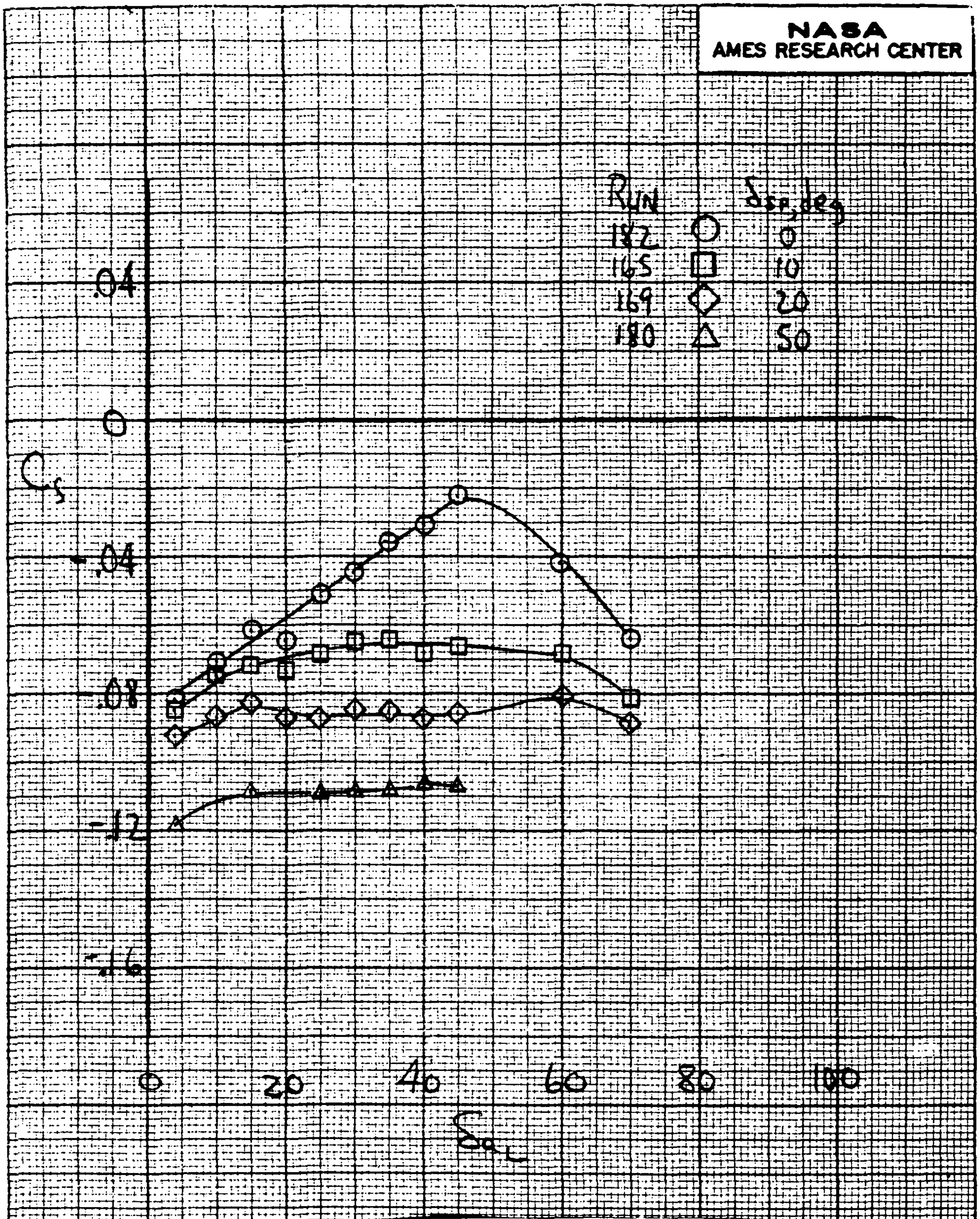

(e) Aileron control effectiveness; $C_{J_T} = .4$, $\alpha = 4°$, $\delta_{a_R} = 30°$

Figure 36.- Concluded.

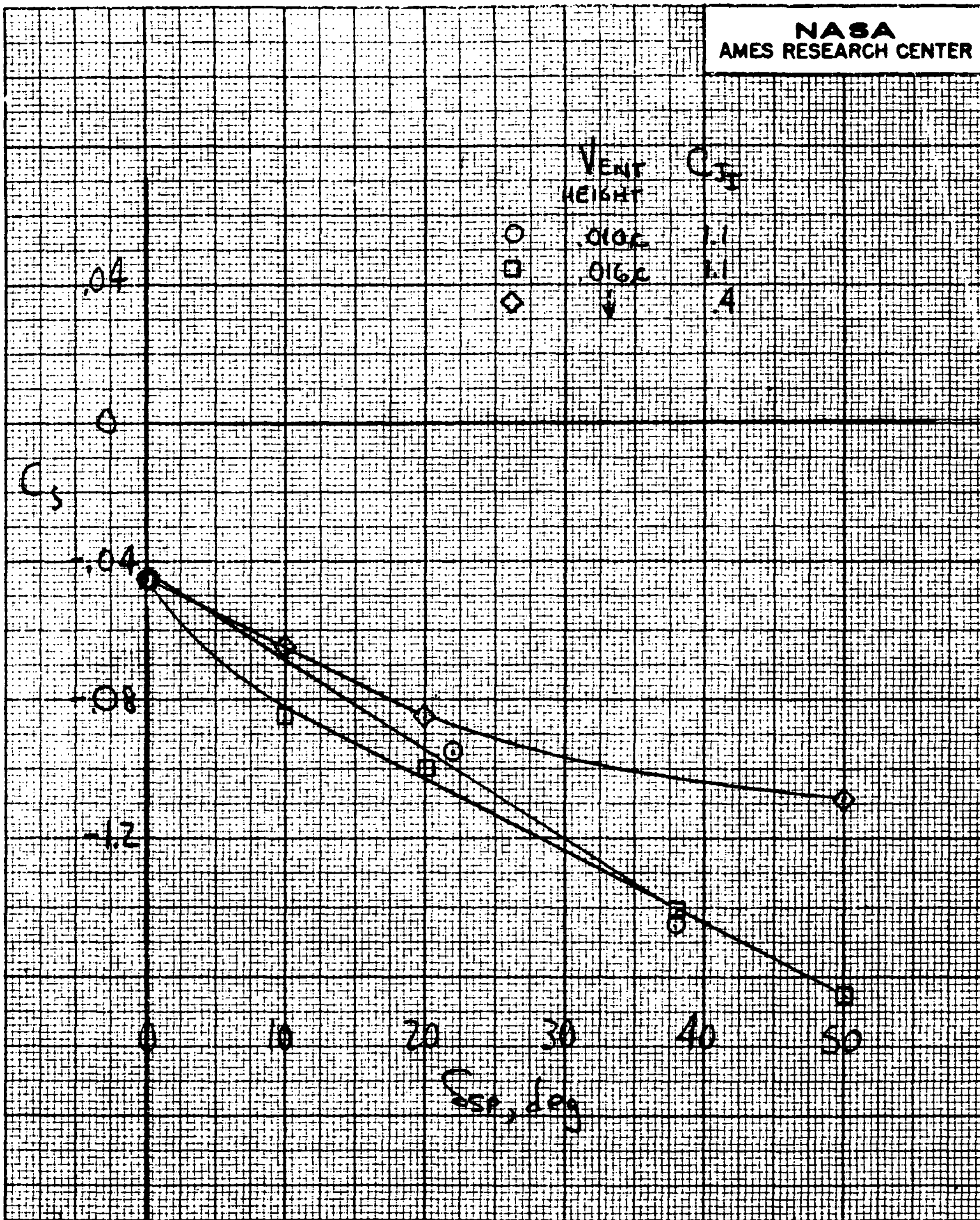

(a) $\delta_a = 30^\circ$

Figure 37.- Spoiler control effectiveness; $\delta_f = 70^\circ$, $\alpha = 4^\circ$.

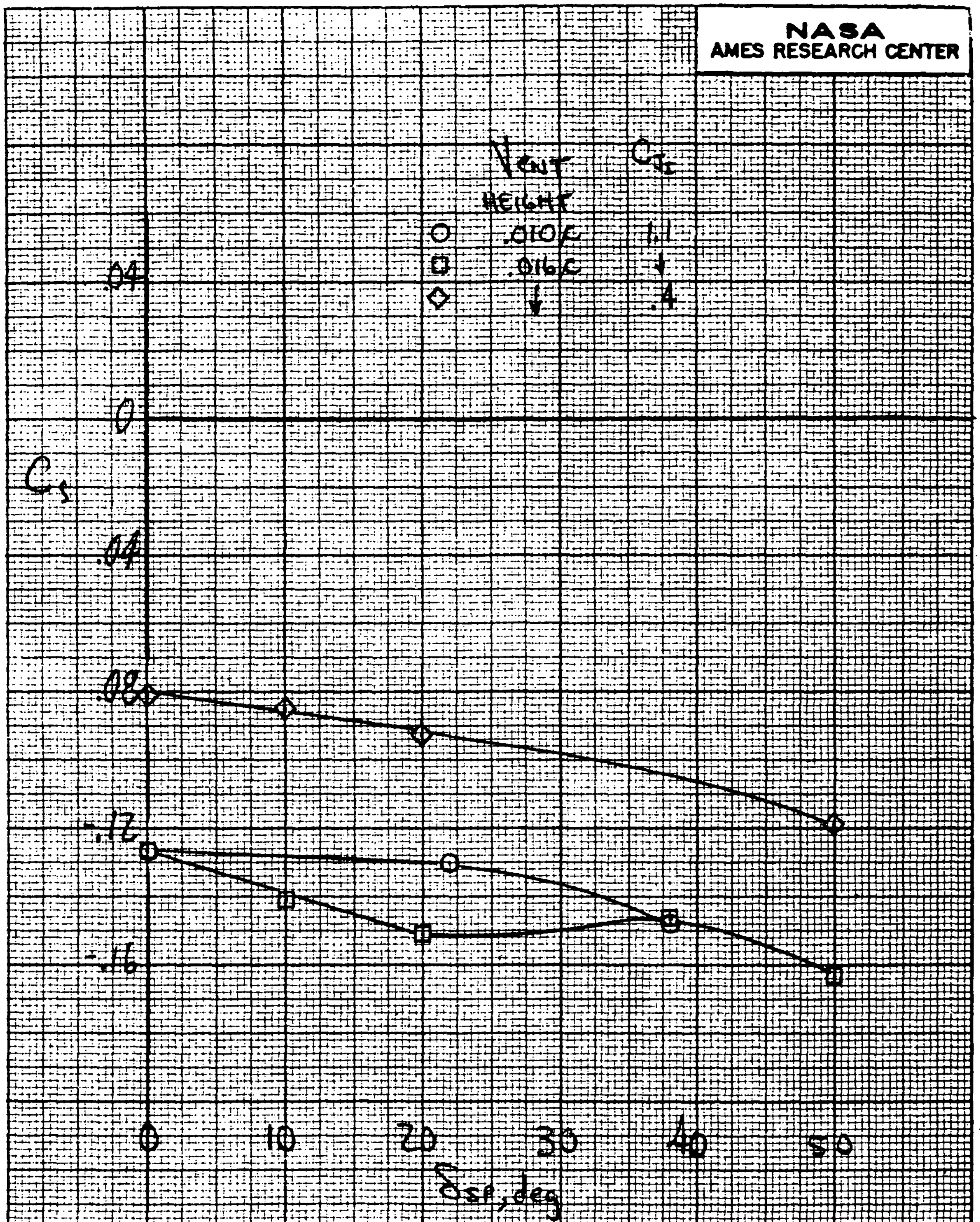

(b) $\delta_a = 4/30°$

Figure 37.- Concluded.

NASA--ARC- Coml., Calif